IL
NUOVO CIMENTO
ORGANO DELLA SOCIETÀ ITALIANA DI FISICA
SOTTO GLI AUSPICI DEL CONSIGLIO NAZIONALE DELLE RICERCHE

VOL. XIV, N. 6 *Serie decima* 16 Dicembre 1959

Momentum Spectrum and Positive Excess of μ-Mesons (*).

J. PINE (**), R. J. DAVISSON (***) and K. GREISEN
Laboratory of Nuclear Studies, Cornell University - Ithaca, N. Y.

(ricevuto il 17 Aprile 1959)

Summary. — The absolute spectrum and positive excess of cosmic-ray μ-mesons near sea level have been measured in the range 2 to 175 GeV/c. The magnetic spectrometer and the method of data reduction are described in detail. The integral spectrum has been compared with the range distribution in the earth, and the agreement indicates that there is no serious error in the theoretical expression for the rate of energy loss. The π-meson production spectrum has been computed and found to fit a power law with exponent −2.64. Also the spectrum of the pion positive excess has been obtained, which is related to the pion production by primary protons in their first collisions. It is concluded that at 10^{12} eV per nucleon, most of the primary cosmic-ray energy is carried by protons, and that the proportion of their energy given to pions in a single interaction is in the neighborhood of 10%.

1. – Introduction.

A magnetic spectrometer has been used to measure the momentum spectrum and the positive excess of cosmic-ray particles near sea level. The measurements extend from a momentum of about 2 GeV/c upward, the maximum measurable momentum being about 175 GeV/c. For this range of momenta the apparatus records only μ-mesons to all intents and purposes.

(*) Supported by the National Science Foundation.
(**) Now at Stanford University, Stanford, Cal.
(***) Now at the Hycon Eastern Corporation, Boston, Mass.

Results will be presented here for the momentum spectrum of μ-mesons incident in directions near the vertical. For the positive excess, measurements taken at various zenith angles have been combined.

Similar measurements of the momentum spectrum, extending to lower maximum momenta, have been made by OWEN and WILSON [1] and by CARO, PARRY and RATHGEBER [2]. The results of our experiment are in good agreement with OWEN and WILSON but not with CARO *et al.* The measured differential muon spectrum is used to calculate a spectrum of pions at production. The data have also been used to derive an integral momentum spectrum which is compared, via the range-energy relation of BARRETT *et al.* [3], with the measurements of cosmic-ray intensity underground. Reasonable agreement is obtained.

The measurements of the positive excess are consistent with those of other workers [4-7] and extend to somewhat higher energy. The statistical accuracy is unfortunately quite low. A crude analysis based on the positive excess and the spectrum of primary protons indicates low inelasticity for pion production in interactions of primaries with energy $\sim 10^{12}$ eV.

2. – Apparatus.

2·1. *General description.* – The measurements presented here represent the first results obtained with the large magnetic spectrometer now in use at Cornell. The magnet is shown in Fig. 1. The pole faces, 22 in. wide by 45 in. high, are separated by an $8\frac{1}{4}$ in. air gap. For this experiment the magnet was run at a field of about 13 kG. Power for the magnet is derived from a motor-generator set, and the magnet current is regulated to better than 0.1%. The magnet is mounted on a cradle which allows it to be rocked through zenith angles from 0° to 68°. The spectrometer is housed in a trailer with a roof consisting mainly of about 1 in. of wood.

Fig. 2 indicates schematically the instrumentation of the experiment. Six trays of Geiger counters, plus four single counters, are used. In addition,

---

(1) B. G. OWEN and J. G. WILSON: *Proc. Phys. Soc.*, A **68**, 409 (1955).

(2) D. E. CARO, J. K. PARRY and H. D. RATHGEBER: *Austral. Journ. Sci. Res.*, A **4**, 16 (1951).

(3) P. H. BARRETT, L. M. BOLLINGER, G. COCCONI, Y. EISENBERG and K. GREISEN: *Rev. Mod. Phys.*, **24**, 133 (1952).

(4) B. G. OWEN and J. G. WILSON: *Proc. Phys. Soc.*, A **64**, 417 (1951).

(5) E. BERETTA, I. FILOSOFO, B. SOMMACAL and G. PUPPI: *Nuovo Cimento*, **10**, 1354 (1953).

(6) I. FILOSOFO, E. POHL and J. POHL-RÜLING: *Nuovo Cimento*, **12**, 809 (1954).

(7) R. B. BRODE and M. J. WEBER: *Phys. Rev.*, **99**, 610 (1955).

there are three cloud chambers. Particles are recorded if they produce a six-fold coincidence in trays A, B, C, A', B' and C'. The particle momentum is inferred from the counters which are discharged in A, B and C. The counters discharged in A', B' and C' determine whether the trajectory of the particle was straight in a plane parallel to the magnetic field. This determination helps to rule out cases where a scattering occurs in the material at the center of the magnet gap, and more importantly, to reject particles which scatter off the magnet pole-faces or

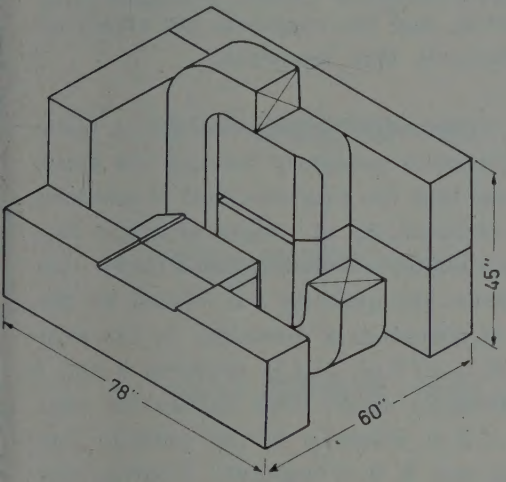

Fig. 1. – Cut-away view of magnet and coil assembly. For clarity, one of the two symmetrically placed coils is not shown in the Figure. Also removed are half of one side and pole-face, and one return leg of the magnet. The slot leading to the center of the magnetic field is used for illumination and photography of the central cloud chamber.

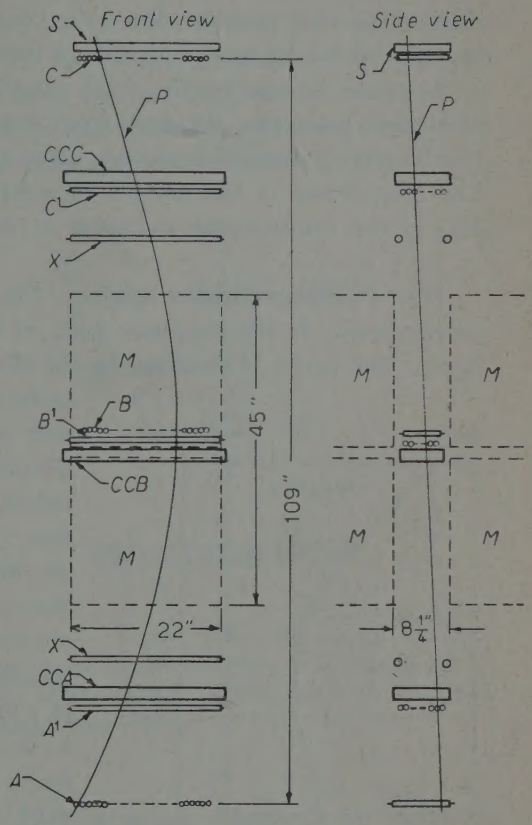

Fig. 2. – Arrangement of Geiger counters and cloud chambers, with illustrative particle trajectory.

the material of the coils. The coils extend near to the location of trays A' and C', and, because of the finite size of the Geiger counters, particles scattered off the coils in the vicinity of counters X can appear to have had a straight trajectory. Counters X are placed in anticoincidence to eliminate such cases.

The diameter of the Geiger counters determines the highest momentum which can be measured from a knowledge of the counters discharged in trays A, B and C. In order to increase the momentum resolution, the cloud cham-

bers *CCA*, *CCB* and *CCC* are utilized. Their purpose is to provide information analogous to that given by the *A*, *B* and *C* counters: *i.e.*, the lateral co-ordinate of the particle trajectory in each of three horizontal measuring planes. The added precision provided by the cloud-chamber measurements is needed for particles with momenta exceeding (15÷20) GeV/c. On the other hand, the cloud chambers are inefficient for measuring the spectrum at low momenta. Their dead-time reduces the rate at which data can be obtained, and the labor involved in analyzing the pictures would be excessive.

In order to reserve the cloud chambers for the small minority of particles of highest momenta, the data from the Geiger counters are electronically analyzed within a few microseconds after a particle passes through the apparatus. The momentum of the particle is computed, and the chambers are expanded only if the computation indicates a sufficiently high momentum.

2·2. *The Geiger counter system.* – Fig. 3 illustrates the projection, in a plane perpendicular to the magnetic field, of a particle trajectory through the apparatus. The figure is idealized to the extent that the magnetic field is assumed to be a constant, B_0, in a region of height $2d_1$, and zero outside of that region. Under this assumption, the quantity s is related to the radius of curvature R according to the relation $1/R = 2s/[d_1(d_1+2d_2)]$, provided θ and s are sufficiently small. This implies the relation $p = K/s$, where p is the particle momentum and K is a constant. Floating-wire measurements have shown that for the range of s and θ of interest here, p may be assumed to be proportional to $1/s$, with no significant error. These measurements have also been used to determine the constant of proportionality, K, which is 23.2 GeV cm/c for x_a, x_b and x_c measured in the planes of Geiger trays *A*, *B* and *C*. For convenience the distance s will be referred to as the « sagitta », although this is not strictly in keeping with the definition of the word. The sagitta is related to the lateral co-ordinates very simply: $x = x_a + x_c - 2x_b$.

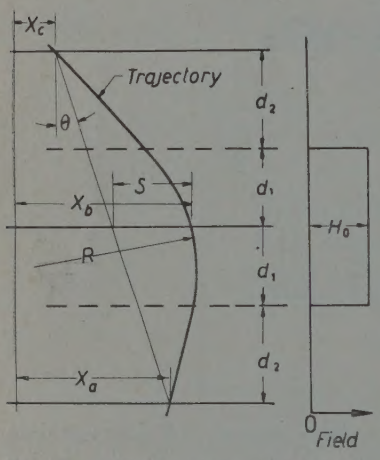

Fig. 3. – Illustration of idealized magnetic field and particle trajectory, defining quantities used in the momentum determinations.

Fig. 4*a* shows the numbering of the Geiger counters in trays *A*, *B* and *C*. They are $\frac{5}{8}$ in. in outer diameter, with 0.020 in. brass walls. After the passage of a particle through the apparatus, a small digital computer which is part of the electronics determines the sum $N = n_A + 2n_B + n_C$, where n_i denotes the number of the counter discharged in tray i. If the particle had passed

through the centers of the struck counters, its sagitta would be $63.5 - N$, measured in units of counter radii.

Depending on the value of N, a particle is assigned a sagitta channel. The channels are numbered $+0$, $+1$, $+2$, ..., corresponding to $N = 64, 65, 66, \ldots$, and -0, -1, -2, ..., for $N = 63, 62, 61, \ldots$. The absolute value of the channel number is $\frac{1}{2}$ unit less than its nominal sagitta, while the sign of the channel refers to the direction in which the particle is bent by the magnetic field, and hence determines the sign of its charge. Particles counted in a channel have a range of sagittas, and each channel may be characterized by a sagitta-acceptance function which can be calculated and must be used in the data reduction. Some acceptance functions $g(s)$ are indicated in Fig. 7.

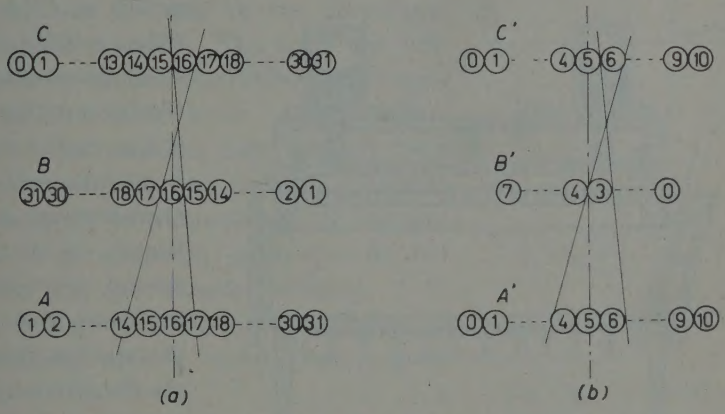

Fig. 4. – Lateral disposition and numbering of the Geiger counters in sagitta trays (*a*) and scattering trays (*b*). The straight lines illustrate the possible range of computer answers for straight trajectories.

Fig. 4*b* shows the numbering of the « scattering counters » of trays A', B' and C'. It can be seen that all straight trajectories produce a sum $N' = n_{A'} + 2n_{B'} + n_{C'}$ of 16, 17 or 18. This sum is performed electronically by the same circuitry as is used for computing the sum N. Memory circuits store the numbers $n_{A'}$, $n_{B'}$ and $n_{C'}$ until the computation of N is complete and the computer is free. If the result for N leads to a count in one of twelve preselected channels or groups of channels, that information is stored while the computer determines N'. Only if N' is 16, 17 or 18 is the count recorded on the channel register appropriate to the value of N. Counters X are placed in anticoincidence by allowing a pulse from any of them to add 32 to the sum N', which guarantees rejection. It should be noted that the electronics is incapable of dealing with events where more than one counter is discharged in any one tray, and hence such cases are rejected.

The circuitry used with the counters is rather complex, utilizing about 500 vacuum tubes and an equal number of semiconductor diodes. However, marginal-checking procedures have been developed which permit replacement of many components before they deteriorate enough to affect proper operation The result is that the circuitry is very reliable for long periods when properly maintained.

2.3. *The cloud chamber system.* – If the answer from the computation of N leads to a count in one of the channels -1, -0, $+0$, $+1$, then the cloud chambers are expanded. The equation $p = K'/s'$ holds, where s' is the sagitta measured with the cloud chambers, and K' is 13.75 GeV cm/c. Fig. 5 is a cross-section appropriate to *CCA* or *CCC*. (The middle chamber, *CCB*, is essentially identical except that its depth is 6 in. rather than 8 in.). Some aspects of the chambers are unconventional as a result of special problems resulting from their use with the spectrometer. They are illuminated and photographed through the tilted front glass, with one single-lens camera per chamber. Because of the rear mirror, two images are obtained of each track. Close to the bottom of the mirror a scale is engraved, extending across the 24 in. width of the chamber. The co-ordinates where both track images appear to intersect the bottom of the chamber are read on the mirror scale. Fig. 6 illustrates the geometry, P and P' being the points of intersection and x_1 and x_2 the measured quantities. The quantity of interest, x, is easily calculated from the expression $1/x = \frac{1}{2}((1/x_1)+(1/x_2))$. The distance d can be calculated from the relation $d = c(x_2 - x_1)/(x_2 + x_1)$. The two images of the track nearly coalesce for particles near the center-line of the system, and d is then impossible to determine with good accuracy. Determination of d is not of direct importance, but for the cases where d is well determined the information is used as part of a check procedure to be described.

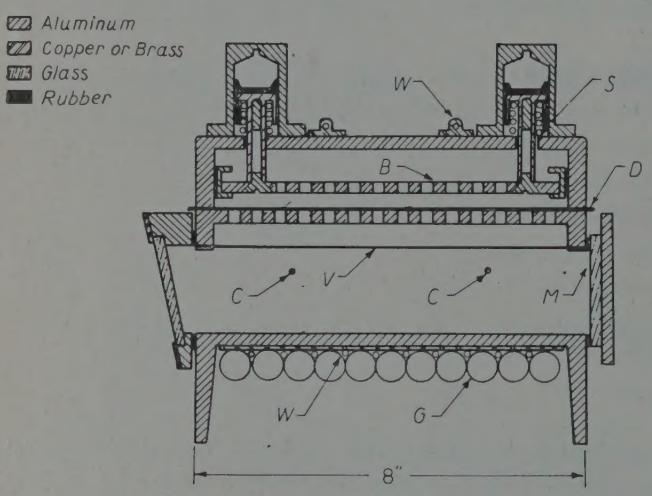

Fig. 5. – Cross-sectional view of one of the cloud chambers and scattering counter trays. B = backstop. C = clearing-field wires. D = diaphragm. G = Geiger counters. M = front-surface mirror. V = velvet. W = water tubes. S = coil spring.

Fig. 5 also illustrates several other aspects of the chambers. The tray of scattering counters is part of the chamber, water tubes are provided for temperature control, and the expansion is upward to produce minimum gas motion near the chamber bottom where measurements are made. The backstop is supported on rods attached to six hydraulically-activated pistons, two of which are shown in the figure. The hydraulic system allows the expansion ratio to be varied by adjusting a master plate located in an accessible place.

The chambers are expanded by opening two holes in the top of the chamber (not visible in the cross-section of Fig. 5), reducing the pressure on the rear of the diaphragm to atmospheric pressure. The holes are normally closed by balloon-like rubber diaphragms inflated so as to cover them. All six balloon valves, two per chamber, are inflated from a common manifold, the pressure in which can be reduced to atmospheric by opening a conventional magnetic pop-valve located away from the spectrometer magnet. Activating this pop-valve produces expansion of the chambers, with a speed that is quite adequate.

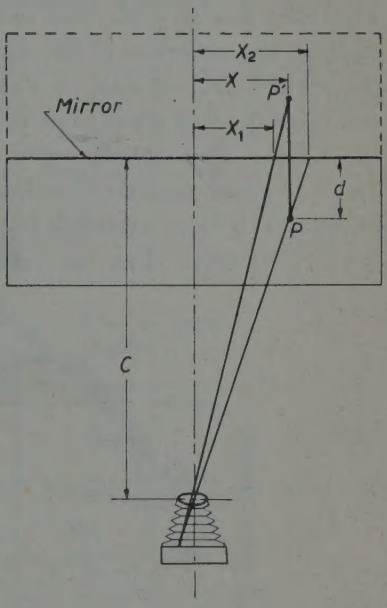

Fig. 6. – Illustration of the position measurement of one point on a cloud chamber track, photographed directly and in reflection.

Each chamber is illuminated by two small, circular G.E. FT 218 flash tubes at 150 joules per tube. The flash tubes are in lamp-houses about 5 ft. from the chambers. Each lamp-house contains a magnesium-carbonate housing for the flash tube, besides lenses and mirrors. A small opening in the magnesium-carbonate cavity is used as a virtual light source, and the lenses and mirror permit a reasonable fraction of the light to be focused at the front window of the chamber. The light is incident on each chamber from directions at 45° to either side of the camera axis. In the case of the central chamber, the narrow slot through which it is illuminated and photographed is lined with mirrors and acts as a light pipe.

Other aspects of the chamber operation are conventional. The dead-time is $2\frac{3}{4}$ min, the chambers are very well-behaved, and conditions for good track formation can easily be maintained. However, the front illumination requires extremely clean surfaces on both front windows and rear mirrors for good photography. The result is that rather frequent disassembly and cleaning of the chambers is necessary in order to maintain acceptable picture quality.

3. – The μ-meson momentum spectrum.

3·1. *Geiger-counter data.* – A histogram of the counting rates in the various Geiger counter sagitta channels is shown in Fig. 7. For the momentum spectrum, channels of opposite sign have been combined: *e.g.*, channel 0 is the sum of $+0$ and -0. The errors are statistical standard deviations. At large sagittas the aperture of the apparatus is reduced because of the curvature of the particle trajectories. A « magnetic cut-off correction » is applied to correct the rates for this effect, and the magnitude of the correction may be seen from the figure. The smooth curve $f(s)$ is a sagitta distribution inferred from the data. At small sagittas the cloud-chamber results are used (as described below in Section 3·2) to establish $f(s)$ with good accuracy. Also, it is necessary that $f(0) = 0$ in order that the total energy carried by the mesons remain finite.

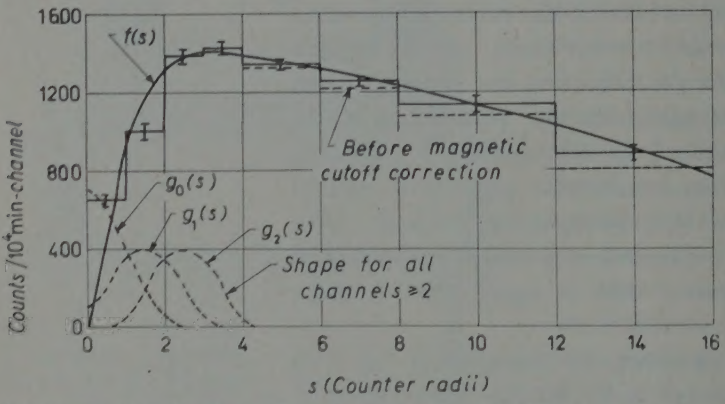

Fig. 7. – Histogram of sagitta spectrum determined with Geiger counters. The dashed curves $g_i(s)$ are the acceptance functions of the first three channels.

The procedure used in reducing the counter data is as follows: For each channel a sagitta-acceptance function is calculated. The functions $g_0(s)$, $g_1(s)$, and $g_2(s)$ shown in Fig. 7 are the sagitta acceptance of channels 0, 1 and 2. The shape of $g_2(s)$ is appropriate to all channels above 2. The acceptance functions express the relative aperture of a given channel for particles of various sagittas. These functions have been calculated on the assumption that the Geiger counters have uniform efficiency for particles which pass through the counter gas and zero efficiency for particles which pass only through the walls.

From $f(s)$ and $g_i(s)$ the median sagitta $s_i^{(m)}$ of particles counted in the i-th channel is calculated by numerical integration. For each channel a factor k_i is found such that

$$k_i \int_0^\infty f(s) g_i(s) = f[s_i^{(m)}] .$$

If the observed rate in a given channel is to be used to infer the rate appropriate to the median sagitta of that channel, it must be multiplied by the factor k_i appropriate to that channel. A method thus exists for converting the Geiger-counter data into points on a differential sagitta spectrum, the points being located at the median sagittas of the channels. The conversion of the differential sagitta spectrum into a differential momentum spectrum follows in a straightforward manner from the relation $p = K/s$. Point by point transformation of the sagitta data yields points on a momentum spectrum plotted at the median momenta of the various counter channels. Fig. 8 shows the results of this data reduction.

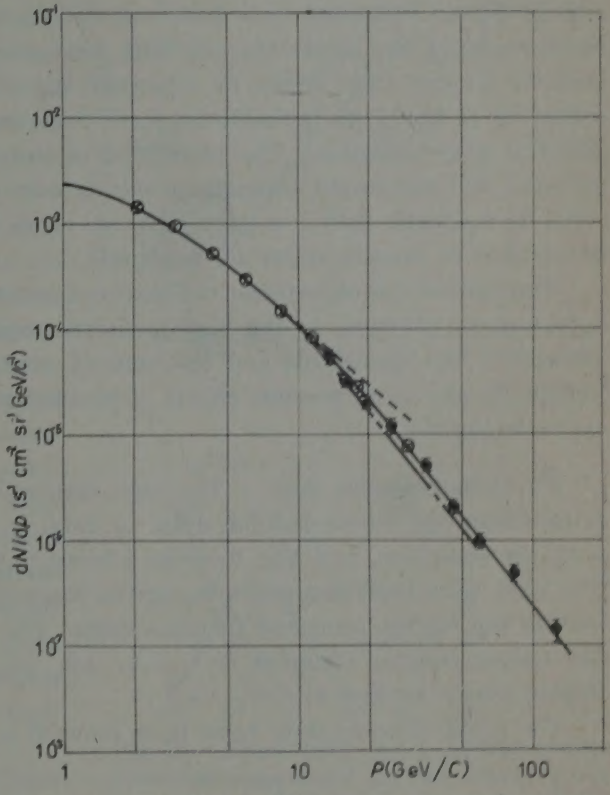

Fig. 8. – The differential μ-meson momentum spectrum. Key: ● This experiment, cloud chambers; ○ This experiment, Geiger counters; ---- Rossi [8]; —— Owen and Wilson [1]; – – – Caro *et al.* [2].

The « ideal » aperture of the spectrometer, assuming Geiger trays to be 100% efficient over their entire area, is 11.7 cm²-sr. In order to obtain the absolute spectrum from the data, this aperture has been reduced to account for the effects of counter walls and the requirement that one and only one counter be discharged in each of the six counter trays. Of particles which produce a six-fold coincidence, it is estimated from auxiliary measurements performed with the apparatus that $(12 \pm 5)\%$ are not analyzed because more than one counter is discharged in one or more trays. The counter walls result in a calculated efficiency of $(93.6 \pm 0.5)\%$ per tray, where the error is meant to include the effects of small air spaces between counters and variations in wall thickness. End effects are neglected because the ideal aperture is defined by the side walls of a series of crossed counter trays. A six-fold coincidence can be produced only by a particle which does not pass through the end region of any counter. The effective aperture of the apparatus

which results from consideration of the total efficiency is (6.9 ± 0.6) cm²-sr. This aperture has been used to obtain the spectrum of Fig. 8. The errors shown in the figure are purely statistical and do not include the uncertainty in the absolute normalization.

In evaluating the accuracy of the data several other factors have been considered. Coulomb scattering in the material of the apparatus will affect measurements at low momenta, but for the range of momenta considered here effects due to scattering have been calculated and found to be negligible. The inefficiency of the apparatus resulting from the discharge of more than one counter in any tray might be expected to be momentum-dependent. Calculations of knock-on probabilities have been made which indicate that this effect is also negligible. The alignment of the apparatus has been carefully checked and monitored throughout the data-taking. The sagitta distribution with no magnetic field is a very sensitive check of the alignment, and possible errors due to misalignment are negligible.

Throughout this experiment the observed counting rates are ascribed entirely to μ-mesons. Because of the high momenta required, the amount of material present in the apparatus, and the veto of events with multiple counter discharges in any tray, possible effects of protons, pions and electrons are thought to be negligible.

3·2. *Cloud-chamber data.* – The high momentum points of Fig. 8 are obtained from the cloud-chamber data. A total of 1089 particles were analyzed with the chambers, and Fig. 9 shows a histogram of the sagitta distribution. The data have been grouped into sagitta channels of width 0.8 mm, s' representing the sagitta measured in these units. The total acceptance function of the Geiger counter channels -1, -0, $+0$, $+1$, which trigger the chambers, is also shown in Fig. 9.

The cloud-chamber data have been reduced in a manner analogous to the handling of the counter data. Fig. 10 shows the sagitta distribution folded and corrected for the variation with s' of the acceptance of the counter channels which trigger the chambers. The acceptance func-

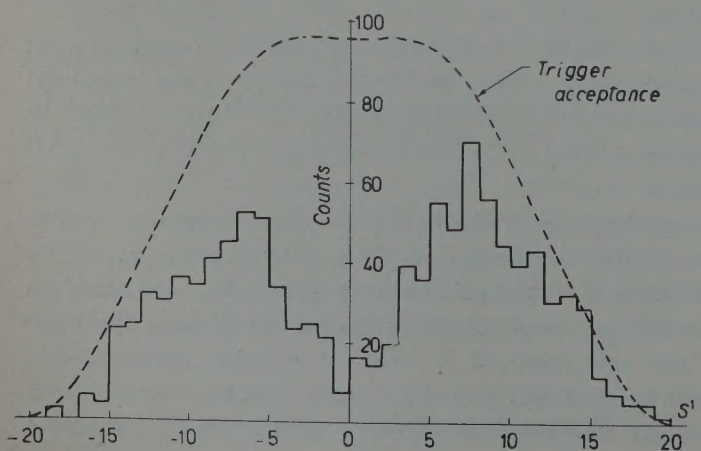

Fig. 9. – Histogram of cloud chamber sagitta measurements.

tions for the cloud chamber channels are also shown in Fig. 10. These functions cannot be derived from simple geometrical considerations, as for the counters, but depend on an evaluation of the measurement errors. The manner in which this is handled will be described later. The function $f(s')$ is a smooth fit to the sagitta histogram, subject to the condition that $f(0) = 0$. Using $f(s')$ and the acceptance functions, median sagittas have been calculated for each channel, correction factors analogous to the k_i for the counter data have been found, and the data from the various channels have been reduced to points on a differential momentum spectrum, plotted at the median momenta of the channels. (For these data, as well as the counter data, groups of the lower momentum channels are combined in the analysis).

From the cloud chamber data a relative spectrum is obtained. However, the fact that the chambers are triggered by counter channels 0 and 1 permits the data to be normalized to the absolute spectrum obtained with the counters.

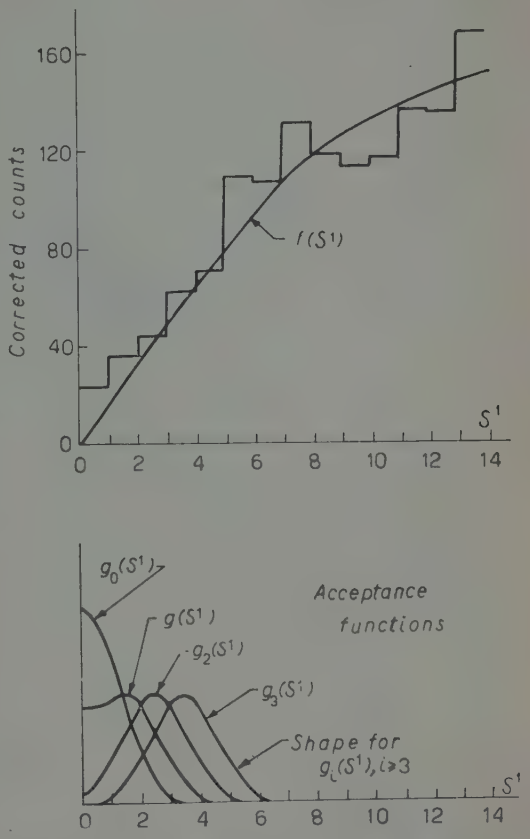

Fig. 10. – Upper part: cloud chamber sagitta distribution corrected for the effect of the Geiger counter trigger requirement. Lower part: acceptance functions for the cloud chamber sagitta channels.

The errors shown for the cloud chamber data of Fig. 8 are purely statistical standard deviations. The major factor which may introduce further uncertainty in the data is the establishment of the acceptance functions $g_i(s')$. Knowledge of these functions is equivalent to knowledge of the distribution of measurement errors and of any momentum-dependent biases.

The method by which the cloud-chamber data are processed provides great freedom from subjective bias and yields a method for estimating measurement errors. For each particle of high momentum, three cloud-chamber pictures are obtained. Each contains, coded on neon bulbs, the numbers of the counters discharged in the neighboring counter trays: *e.g.*, trays A and A' for chamber A.

This information helps in locating the track of interest. Each picture is scanned and the co-ordinates x_1 and x_2 (see Fig. 6) are recorded. In addition a register number and the Geiger counter numbers indicated by the neon bulbs are recorded. This information is transferred to a punched card for further analysis using an IBM Card-Programmed Computer (CPC). As a specific example, consider a « run » consisting of 300 particles. All the pictures of *CCA* are first scanned. In about 240 pictures tracks of sufficiently good quality are found and the reduced data recorded. Then the pictures from *CCB* are scanned, ignoring those 60 corresponding to the rejects of *CCA* in order to save scanning time. The requirement of good track quality may result in 180 particles now accepted in *CCA* and *CCB*. Then pictures from the last chamber are scanned, and the final yield may be about 150 particles analysed in all three chambers.

At no time during the scanning is there any knowledge of particle momentum, so that the typical rejection rate cited above is free of any subjective bias which is momentum-dependent. Further reduction of the data is done with the CPC and IBM card-sorting equipment. The three data cards for a given particle are combined for the first time when they are fed to the computer. From x_1 and x_2 the lateral co-ordinate x and the depth co-ordinate d are computed for each chamber. The three lateral co-ordinates are combined to obtain a sagitta. From the lateral and depth co-ordinates in each chamber the particle trajectory is reconstructed and the point of intersection with the plane of each counter tray is computed. From this information the distance of the trajectory from the center-line of each of the six struck Geiger counters is computed. These distances we shall call Y values: Y_A, Y_B and Y_C refer to trays A, B and C, while $Y_{A'}$, $Y_{B'}$ and $Y_{C'}$ refer to trays A', B' and C'.

For Y measured in units of counter diameters, it is evident that perfect measurement accuracy would lead to Y values uniformly distributed from -0.5 to $+0.5$. A typical Y distribution for a « run » of about 120 particles is shown in Fig. 11.

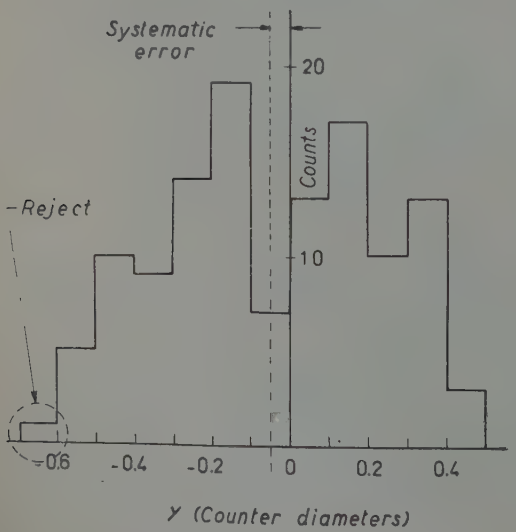

Fig. 11. – Distribution of points at which tracks cross a Geiger counter, as determined by extrapolation of trajectories on the basis of co-ordinates measured in the cloud chambers. The data shown here refer to a single run taken within a short time. Distributions like this are used to infer systematic and random errors in the cloud chamber measurements.

The distribution is principally useful for three purposes. First, gross errors, due to mistaken identification of a track in one of the chambers, or to faulty recording of the co-ordinates x_1 and x_2, are likely to yield impossibly large Y values. Particles for which such a Y value exists are rejected. Fig. 11 shows the limiting case of this criterion, in which a particle has been rejected, perhaps unnecessarily. The general attitude has been to reject in case of doubt. The total number rejected on this basis remains exceedingly small, and no momentum-dependent bias is introduced. Second, the existence of uniform sideways gas motion in the chambers results in a systematic shift of the center of gravity of the distribution. This shift measures a systematic error which is subtracted out. Third, the shape of the tail of the distribution provides a measure of the small random errors of measurement. For the last purpose, the statistical accuracy of a single Y distribution is inadequate. However, a composite distribution for all the particles measured provides better statistical accuracy.

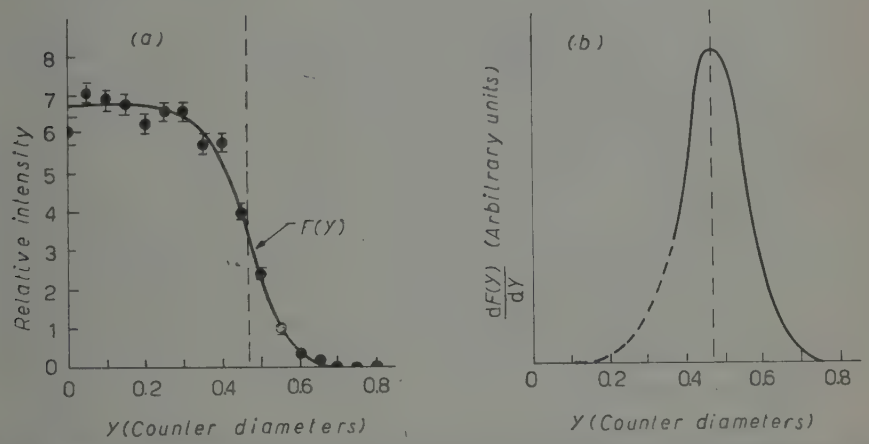

Fig. 12. – (*a*) Combined distribution of inferred distances from the center of a Geiger counter, at which the recorded tracks crossed the counter. (*b*) Derivative of curve drawn in Fig. 12 (*a*). This is a geometrically magnified error distribution.

Fig. 12*a* shows the composite distribution of the Y_A and Y_C data for the entire experiment, while Fig. 12*b* shows the derivative of the distribution. From the second curve the error distribution for measurements of lateral co-ordinates in chambers A and C can be derived. Errors in these chambers are magnified similarly in projecting the trajectory to the planes of trays A and C, respectively. Errors in chamber B show up in the composite Y_B distribution, unmagnified. (There is negligible coupling of errors in a given chamber to Y distributions in Geiger trays other than the nearest.) From the measurement errors derived from the composite Y distributions the sagitta acceptance

functions $g_i(s')$ are derived. The over-all precision of the cloud-chamber system corresponds to a standard error of 1.0 units of s' which corresponds to a momentum of 176 GeV/c. This corresponds to a standard error of about $\pm$ 0.75 mm in the lateral co-ordinate measurements in each chamber. Such a value is consistent with subjective estimates, but the fact that it is derived from an objective analysis of the actual data should be emphasized.

The Y' distributions, those of $Y_{A'}$, $Y_{B'}$ and $Y_{C'}$, are also examined as a further check on errors. In this case the precision with which the depth d is measurable in the chambers varies greatly with the location of the track (see Fig. 6), and the data are analysed in such a way that this is accounted for. The net result of the Y and Y' analysis is to reject 2.5% of the particles on the basis of the Y analysis and 10% on the basis of the Y' analysis. These numbers are as large as this because of extreme conservatism in the rejection criteria and do not truly reflect the incidence of really gross errors. The entire process uses one minute per particle of computer time and is completely independent of particle momentum.

After the Y and Y' analyses are concluded the particle momenta are read off the punched cards and recorded. No further evaluation is performed. As a result of the data-reduction procedure, it is felt that the cloud-chamber data are more free of bias and unexpected error than is usual in such measurements. The effect of a 50% error in the estimate of the resolution of the apparatus would be small except in the highest momentum channels. Even there, it would not be important in comparison with the statistical uncertainties. The composite Y distributions are inconsistent with such a large change in the resolution. It is felt, therefore, that the statistical errors of Fig. 8 accurately specify the reliability of the data over the entire range of measured momenta, except for the uncertainty in absolute normalization.

3·3. *Comparison with other measurements.* – The full line of Fig. 8 fits the data of this experiment and of OWEN and WILSON ([1]), whose measurements extend to 20 GeV/c. The data summarized by ROSSI ([8]) and the measurements of CARO *et al.* ([2]) agree with the full line at low momenta and deviate at high momenta in the manner shown. CARO *et al.* and OWEN and WILSON have obtained their absolute normalizations from ROSSI at momenta of 2 GeV/c and 1 GeV/c respectively.

The deviation of the Rossi curve at high momenta is perhaps plausible in view of the fact that it depends in this region on early cloud chamber data which might have had lower resolution than was estimated. We can see no sufficient explanation for the disagreement between our results and those of CARO *et al.*

([8]) B. ROSSI: *Rev. Mod. Phys.*, **20**, 537 (1948).

3.4. *The pion spectrum at production.* – It is possible to derive from the sea-level muon spectrum the spectrums of pions at production. The analysis of BARRETT *et al.* [3] provides the expression

$$(3.1) \qquad M(E) = \frac{F(E/r)}{r} \frac{\lambda_\pi}{\lambda_p} \frac{B}{E} \left[\frac{1}{1+(B/E)} - \frac{\lambda_\pi/\lambda'}{2+(B/E)} + \frac{(\lambda_\pi/\lambda')^2}{3+(B/E)} - \cdots \right],$$

where $M(E)$ is the muon differential spectrum, $r=m_\mu/m_\pi=0.76$, and $F(E/r)$ is the pion differential spectrum. (The π-μ decay kinematics are simplified to the extent that E_π is assumed equal to E/r.) The quantities λ_π and λ_p are the absorption mean free paths of pions and of non-pion producers of pions respectively; B is a constant equal to $0.90 \cdot 10^{11}$ eV; and λ' is defined by $1/\lambda' = \lambda_p^{-1} - \lambda_\pi^{-1}$. The formula is derived from a one-dimensional differential equation which neglects any angular spread in pion production and decay, and also neglects ionization losses and μ-decay.

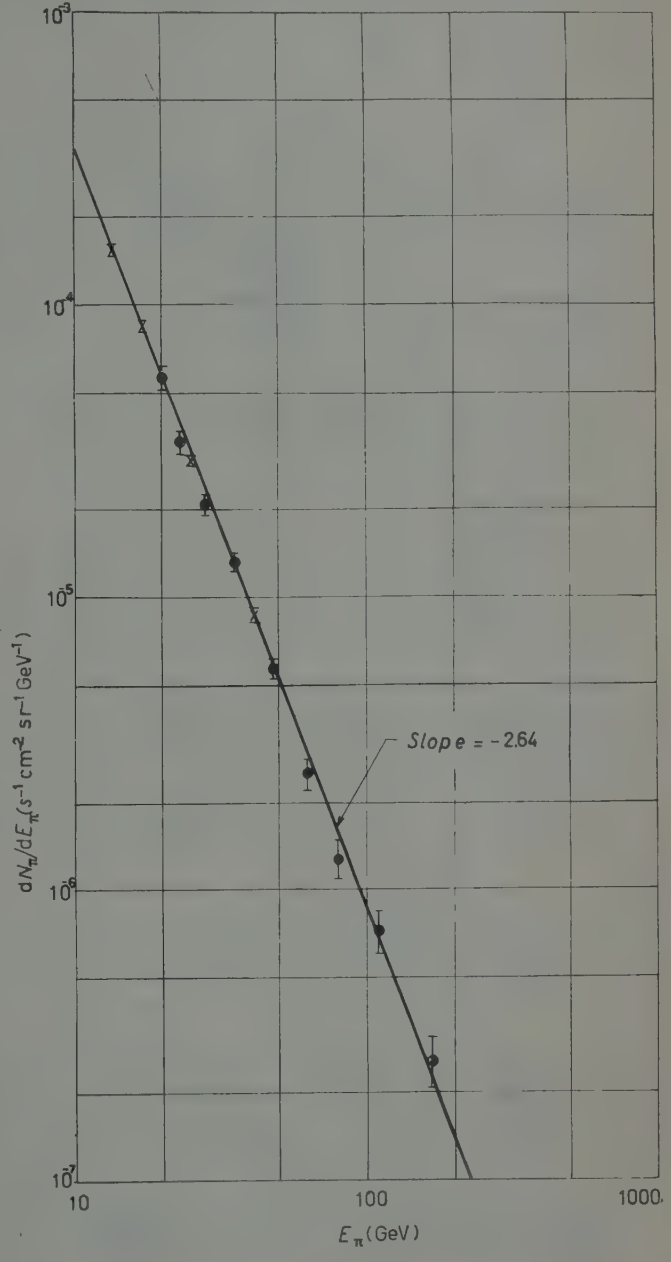

Fig. 13. – Inferred differential spectrum of pions at production. Cloud chamber data are indicated by •, Geiger counter data by x.

In addition, λ_p and λ_π are assumed small compared with the thickness of the atmosphere.

The assumptions should be valid in the present application if corrections are made for muon ionization loss and decay. Because both effects are small, the corrections have been made under the assumption that all the high-energy muons observed at sea level are produced at a depth of about 100 g/cm² from the top of the atmosphere. If $\lambda_p = \lambda_\pi$, Eq. (3.1) simplifies to the form

$$M(E) = \frac{F(E/r)}{r} \frac{1}{1+(E/B)}. \tag{3.2}$$

For $\frac{1}{2} < \lambda_\pi/\lambda_p < 2$ this equation is correct to within about 30%. Assuming $\lambda_\pi/\lambda_p \approx 1$, we have used Eq. (3.2) to reduce the muon momentum spectrum at sea level, corrected for ionization loss and μ-decay, to a pion spectrum at production, $F(E_\pi)$. The data of this experiment have been carried through the analysis point by point and the resultant pion spectrum is shown in Fig. 13. The straight line which is shown on the figure represents the relation $F(E_\pi) = 0.156\,(E_\pi)^{-2.61}$ s^{-1} cm^{-2} sr^{-1} GeV^{-1}. PUPPI [9] has performed a similar analysis based on the data of OWEN and WILSON [1] and of CARO *et al.* [2]. The difference between his result and that found here reflects the discrepancy between our spectrum and that of CARO *et al.*

3·5. *Comparison with underground measurements.* – Many workers have measured the variation with depth underground of the vertical intensity of penetrating radiation, the observed particle flux being ascribed to cosmic-ray μ-mesons. The data of this experiment have been used to derive an integral momentum spectrum at sea level. This spectrum has been compared with the underground measurements by means of an energy-range relation derived from the energy loss formula for earth given by BARRETT *et al.* [3]:

$$\frac{\mathrm{d}E}{\mathrm{d}h} = a + k \ln \frac{E'_m}{mc^2} + bE\,,$$

where: $a = 1.88 \cdot 10^6$ eV cm²/g,

$k = 0.0766 \cdot 10^6$ eV cm²/g,

$b = 3.5 \cdot 10^{-6}$ cm²/g,

$E'_m = E^2/(E+A)$,

$A = 1.13 \cdot 10^{10}$ eV,

m = mass of μ-meson.

(9) G. PUPPI: *Progress in Cosmic Ray Physics*, vol. 1 (New York, 1956), p. 341.

Fig. 14 illustrates the comparison. The data of EHMERT [10], CLAY [11] and V. C. WILSON [12] are normalized to the results from this experiment near 10^4 g/cm^2. The data of AVAN and AVAN [13], RANDALL and HAZEN [14], BOL-

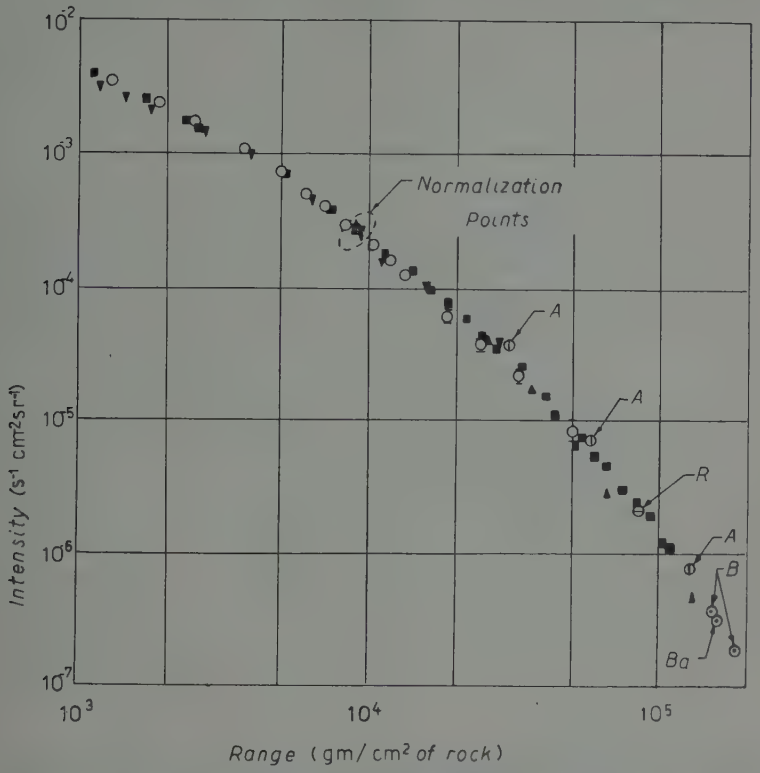

Fig. 14. – Integral muon range spectrum in earth. Points derived from this experiment are compared, via an assumed range-energy relation, with direct measurements made underground. Key: ▼ Ehmert [10]; ▲ Clay [11]; ■ Wilson [2]; A Avan and Avan [13]; R Randall and Hazen [14]; B Bollinger [15]; Ba Barrett *et al.* [3]; ⊙ this experiment.

LINGER [15], and BARRETT *et al.* [3] are absolute measurements. The data of EHMERT, taken under water, have been corrected to rock by multiplying the depth in g/cm^2 by 1.19, a conversion factor consistent with measurements

---

[10] A. EHMERT: *Zeits. f. Phys.*, **106**, 751 (1937).
[11] J. CLAY: *Rev. Mod. Phys.*, **11**, 128 (1939).
[12] V. C. WILSON: *Phys. Rev.*, **53**, 337 (1938).
[13] L. AVAN and M. AVAN: *Compt. Rend.*, **241**, 1122 (1955); also, private communication.
[14] C. A. RANDALL and W. E. HAZEN: *Phys. Rev.*, **81**, 144 (1951).
[15] L. M. BOLLINGER: *Cornell University Thesis* (1951); *Phys. Rev.*, **79**, 207 (1950).

of Clay. Statistical errors are shown for our data where the errors are significant on the scale of the graph. These errors were computed from the total number of counts used to obtain each point. However, in converting the differential spectrum data to an integral spectrum, neighbouring points are not statistically independent. Fig. 14 differs in one respect from a similar graph given by BARRETT *et al.* ([3]) in which the relative measurements were normalized to an absolute intensity of $3.6 \cdot 10^{-4}$ s^{-1} cm^{-2} sr^{-1} at a depth of 10^4 g/cm^2. This normalization, from the older work quoted by ROSSI ([8]), is in disagreement with our data. The normalization used here is $2.7 \cdot 10^{-4}$ s^{-1} cm^{-2} sr^{-1}.

The comparison afforded by Fig. 14 illustrates only fair consistency between the results from this experiment and the underground data. Among some of the underground measurements there is also only rough agreement, reflecting some of the difficulties in such measurements. The comparison of magnetic spectrometer measurements at sea level with underground intensity data should be useful in checking the assumptions underlying the range-energy relation. On the basis of the available data one may say that it is verified that mainly μ-mesons are detected in both cases and that no important energy-loss mechanism for muons of energy up to 100 GeV has been neglected. If anything, the theoretical expression for $\mathrm{d}E/\mathrm{d}h$ seems high. The systematic errors which may be present in the available underground data and the poor statistical accuracy of the momentum spectrum at the highest momenta do not appear to justify a stronger conclusion or a more detailed analysis at this time.

4. – The positive excess.

4·1. *Experimental data.* – The data obtained with the spectrometer provide a determination of the positive excess as a function of momentum. In Fig. 15 measurements of the relative positive excess η obtained in this and other experiments ([4-7]) are shown. We define $\eta = (\mu^+ - \mu^-)/(\mu^+ + \mu^-)$, where μ^- and μ^+ are the intensities of negative and positive μ-mesons.

In the highest momentum channels of the Geiger counter system of the apparatus, the sagitta acceptance functions allow some particles of negative charge to appear in channels which nominally count positive particles, and vice versa. Correction for this effect can be made from a knowledge of the sagitta spectrum and the acceptance functions. However, in this experiment the high resolution cloud chamber data provide a direct measure of this contamination; hence the necessary corrections to the Geiger counter data have been calculated from the direct observations with the chambers.

The statistical accuracy of the highest momentum cloud chamber channels is so low that a significant determination of the positive excess cannot be made. For the cloud-chamber data only channels free from contamination of oppo-

site-sign particles have been used. Misalignment of the apparatus can introduce error in the determination of η. However, the standards maintained during the experiment permit only negligible errors to arise from this cause. In addition, data were taken with frequent reversal of the direction of magnetic field.

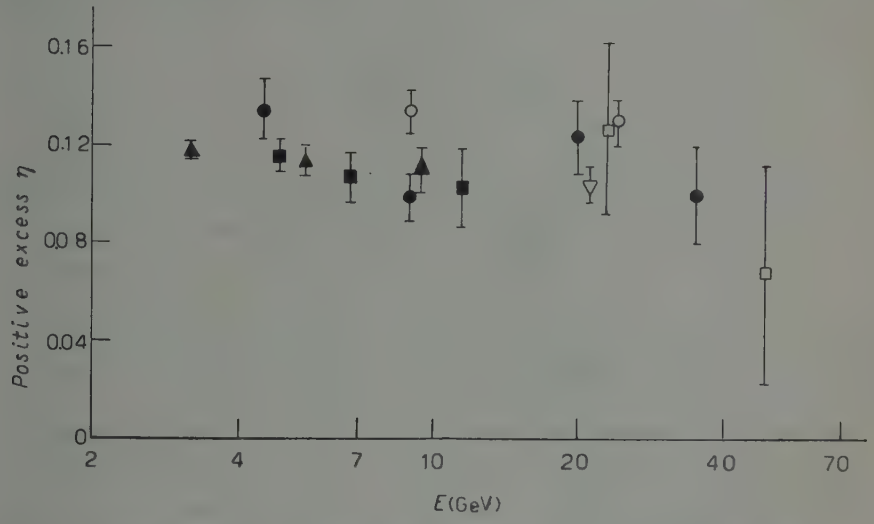

Fig. 15. – Positive excess of μ-mesons at sea level, $(\mu^+ - \mu^-)/(\mu^+ + \mu^-)$. Key: • This experiment, Geiger counter data; □ This experiment, cloud chamber data; ■ Owen and Wilson [4]; ▲ Beretta *et al.* [5]; ▽ Filosofo *et al.* [6]; ○ Brode and Weber [7].

The results of this experiment shown in Fig. 15 represent, in general, combinations of counts in several channels in order to obtain average points with better statistics. The procedure has been continued of plotting points at the median energy of the measured particles. In addition, data taken at zenith angles of 45° and 68° have been combined with the 0° data to obtain better statistical accuracy. No significant zenith angle variation of η was found nor is any expected. The data from this experiment are in general agreement with the other measurements shown in the figure.

4·2. *Interpretation of the positive excess.* – Let it be assumed that on the average equal numbers of protons and neutrons emerge from interactions of high-energy protons with air nuclei. A positive excess of average value $\frac{1}{2}$ the proton charge is then carried off by other particles emerging from the interactions. Let the other particles be mainly π-mesons, and also assume that π-decay is the major source of muons. These assumptions, although oversimplified, may represent a useful first approximation for purposes of drawing rough conclusions from the positive-excess data.

Within the framework of these assumptions, the muon positive excess can

be ascribed largely to the decay of first-generation pions: *i.e.*, those produced in interactions of primary protons. The equal numbers of protons and neutrons emerging from the primary interactions will produce no further positive excess. It is true that at high energies some first-generation pions will interact rather than decay, thereby contributing their excess to second-generation pions. However, the energy dependence of the primary spectrum tends to make unimportant the positive excess propagated by pion interactions compared to that generated at the same energy by primary protons.

We thus ascribe the observed positive excess to the decay of pions resulting from the interaction of primary protons. Then, in principle, a rather direct connection can be made between the positive excess and the properties of high-energy primary interactions. The program is as follows: from the relative muon positive excess the absolute momentum spectrum of positive excess muons can be derived, via the measured muon momentum spectrum. From these muon data, the spectrum of positive excess pions at production can be derived. From this spectrum and that of primary protons, conditions can be found which the high-energy interactions must fulfill. This program is illustrated by the very approximate analysis which follows.

From the positive excess data, it appears that the relative excess η is approximately invariant and equal to about 0.11 from 5 to 40 GeV. To derive the positive excess pion spectrum at production, D_π, the analysis of Section 3·4 can be used. Now λ_p and λ_π should be identified with the interaction mean free paths of primary protons and pions, and again we assume $\lambda_p \approx \lambda_\pi$. The immediate result is that for the range of energies over which $\eta \approx 0.11$, $D_\pi \approx 0.11\ F(E) = 0.017\,1\ (E)^{-2.64}\ \mathrm{s^{-1}\ sr^{-1}\ cm^{-2}\ GeV^{-1}}$.

We now consider a phenomenological model of the interaction of a primary proton of energy E_p with an air nucleus. Let M charged pions be produced with an average positive excess of $\frac{1}{2}$. We further assume this excess charge is distributed among the mesons without regard to their energies or directions of emission. We recognize neutral mesons and admit inelasticity by assuming that the charged pions carry off a fraction $\frac{2}{3}f$ of E_p. In order to account crudely for the energy distribution among the mesons in the laboratory system, it is assumed that a fraction g of the charged mesons carry off most of the energy $\frac{2}{3}f\,E_p$, and share this energy equally. The fraction $(1-g)$ of the mesons, having lower energy, is ignored in comparison with the mesons of that energy produced by other primaries.

First generation pions of energy E_π are thus ascribed to interactions where $E_p = (3gM/2f)E_\pi$. The first-generation charged pion spectrum $\mathrm{d}\pi_1/\mathrm{d}E_\pi$ can now be expressed in terms of the primary proton spectrum $\mathrm{d}N/\mathrm{d}E_p$:

$$\left.\frac{\mathrm{d}\pi_1}{\mathrm{d}E_\pi}\right|_{E_\pi} = \frac{3(gM)^2}{2f}\left.\frac{\mathrm{d}N}{\mathrm{d}E_p}\right|_{E_p=(3gM/2f)E_\pi}. \tag{4.1}$$

From the positive excess spectrum the first-generation pion spectrum follows:

$$\frac{\mathrm{d}\pi_1}{\mathrm{d}E_\pi} = 2MD_\pi \,. \tag{4.2}$$

The experimental data on the differential spectra may be expressed by two power laws:

$$\begin{cases} D_\pi = AE_\pi^{-\beta} \,, \\ \mathrm{d}N/\mathrm{d}E_p = CE_p^{-\gamma} \,. \end{cases} \tag{4.3}$$

Combining Eqs. (4.1), (4.2) and (4.3), we obtain the result:

$$g^{(\gamma-2)}(3M/2f)^{(\gamma-1)} = (C/2A)E_\pi^{(\beta-\gamma)} \,. \tag{4.4}$$

For the differential spectra in particles-s^{-1}-cm^{-2}-sr^{-1}-GeV^{-1}, we have found previously $A = 0.017$ and $\beta = 2.64$. Values of C and k are derived from data presented by BARRETT *et al.* [3]. The choice $C = 3.0$ and $\gamma = 2.48$ is in good agreement with the curve of their Fig. 19 over a broad region centered at about $3 \cdot 10^{11}$ eV. This choice of C and γ involves the tacit assumption that α-particles and heavier nuclei, which would contribute no positive excess, are a small fraction of the primaries. The available data suggest that the spectra of protons and heavy nuclei are nearly parallel, hence the presence of heavy nuclei does not contribute much uncertainty to γ, but it is possible that for the proton spectrum the value of C should be reduced by about 30%.

It should be emphasized that the values of C, A, β, and γ have significant experimental uncertainties. Therefore, we can only infer that the right-hand side of Eq. (4.4) is slowly varying with E_π, and has a value perhaps known to within a factor of 2. Taking $E_\pi = 30$ GeV, substituting the values of the parameters, and solving for f, the result is

$$f = 0.050\, Mg^{\frac{1}{2}} \,. \tag{4.5}$$

This relation refers to interactions with $E_p \approx (3gM/2f)E_\pi$: *i.e.*, $E_p \approx 9g^{0.7} \cdot 10^{11}$ eV. The estimated factor two of uncertainty in the right-hand side of Eq. (4.4) implies a factor 1.6 for the uncertainty in f. If the constant C is reduced by 30% to allow for the primary nuclei which contain both protons and neutrons, f is increased by a factor 1.27. g must be less than unity and is likely to be $\frac{1}{2}$ or less, purely on the basis of kinematics. With these allowances, we find

$$f \approx M \cdot (0.05^{+0.03}_{-0.02}) \,. \tag{4.6}$$

A value for M can be estimated from the observed positive excess. An upper limit is immediately obvious: if all the primaries were protons and all the observed muons came from decay of first-generation pions, the positive excess of 0.11 would indicate $M = 4.5$. The effect of heavy primaries and second-generation pion production is to reduce this value. Hence an upper limit of f can be given: $f \lesssim 0.3$.

The trend of the positive excess data with energy, exhibited in Fig. 15, is well understood qualitatively. At low energies, primary protons produce single mesons with a very large positive excess ($\eta \approx 0.7$), but μ-e decay prevents the majority of the first-generation mesons from reaching sea level, and the positive excess is therefore greatly diluted by symmetrically charged mesons, produced by secondary protons and neutrons at lower altitudes. As the energy increases, first-generation mesons become a larger proportion of all the mesons reaching sea level, but multiple production becomes more important in the primary interactions. These two effects tend to compensate for each other, and account for the small variation of the positive excess at sea level. At extremely high energies, not only is muon decay negligible, but also muon production from late generations of pions is ultimately inhibited by the improbability of π-μ decay in the lower atmosphere. The positive excess is therefore expected to diminish in inverse proportion to the average multiplicity of meson production in the primary collision: *i.e.*, as $E_\mu^{-\frac{1}{4}}$ if the multiplicity is proportional to the $\frac{1}{4}$ power of the primary energy. The points at the highest energies in Fig. 15 suggest that this decrease may begin to be appreciable at energies E_μ exceeding 50 GeV. That the decrease is not observed below 50 GeV indicates qualitatively that until this energy at least, the pions produced by secondary nucleons are a considerable proportion of those produced in the primary encounters: *i.e.*, that the primary interactions are highly elastic. This conclusions agrees qualitatively with eq. (4.6).

In order to estimate M and hence f a little more precisely, one may make use of the observation that the absorption mean free path in the atmosphere for the producers of meson showers is about twice the length corresponding to a geometric cross section ([16]). This suggests that succeeding generations of pions have progressively smaller amplitudes by a factor of about 2. By taking into account also the diminishing probability of π-μ decay for succeeding generations, one computes for a pion energy of 30 GeV (muon energy 23 GeV) that about $\frac{4}{7}$ of the muons reaching sea level are products of the first generation. Assuming that 30% of the first-generation muons are produced by primary nuclei of $Z > 1$ and 70% by protons, one estimates $M = 1.8$ for the effective multiplicity of production of charged pions of ~ 30 GeV by protons of ~ 600 GeV.

([16]) See, *e.g.*, H. K. Tichо: *Phys. Rev.*, **88**, 236 (1952).

It should be emphasized that the actual multiplicity, inelasticity, and division of energy among the produced mesons fluctuate widely from one event to another, and that the quantities M, f and g used in our simplified model must represent suitably weighted averages. In particular, because of the steepness of the energy spectra involved, great weight is given to those fluctuations which result in a high-energy meson being created by a primary whose energy is lower than the normal value for such a process. Thus, the fluctuations exaggerate the importance of events with low M and high f. Our rather low value of M is therefore not directly comparable with values obtained by other methods of observation; but it is the right kind of weighted average to use in eq. (4.6).

Finally, we are led to an extremely low estimate for the proportion of the primary proton energy given to pions in a collision with a nucleus of nitrogen or oxygen: namely,

$$f \approx 0.09^{+0.03}_{-0.01} \quad \text{at} \quad E_p \approx 600 \text{ GeV} . \tag{4.7}$$

It is believed that the fluctuations would not make this result too low. It should be pointed out, however, that primary protons may lose energy to other particles as well as pions; our value of f does not include the energy given to recoil nucleons, nor the possible energy absorbed in the creation of K-mesons and nucleon-antinucleon pairs.

It can easily be verified that if the estimated proportion of primary nuclei with $Z > 1$ had not been taken into account, we would have been led to slightly greater values of the multiplicity, M, and the inelasticity, f. Conversely, the assumption of a much larger proportion of heavy nuclei would indicate values of M and f that are quite impossibly small. Thus, the high value of the relative positive excess of 50 GeV muons seems to constitute a proof that at 10^{12} eV/nucleon, most of the primary cosmic ray energy is still carried by protons.

Although the analysis carried out above is over-simplified and some of the input data are rather crude, it is felt that the qualitative conclusions are reliable and that this method of approach is useful in the study of high energy interactions. Here the individual interactions are not observed in detail, but average characteristics can be inferred which complement the results obtained from detailed measurements such as those made with emulsions.

RIASSUNTO

Si sono misurati lo spettro dell'impulso assoluto e l'eccesso positivo di mesoni μ da raggi cosmici presso il livello del mare nel campo fra 2 e 175 GeV/c. Si descrivono dettagliatamente lo spettrometro magnetico ed il metodo per la riduzione dei dati. Lo spettro completo è stato confrontato alla distribuzione dei valori dell'impulso nella terra, e l'accordo indica che non vi è errore importante nella espressione teorica per l'ammontare della perdita di energia. Lo spettro di produzione dei mesoni π è stato analizzato e si è trovato che segue una legge esponenziale con esponente -2.64. Si è ottenuto anche lo spettro dell'eccesso positivo di pioni, che è in relazione alla produzione di pioni da protoni primari nelle loro prime collisioni. Si conclude che a 10^{12} eV per nucleone, la maggior parte della energia dei raggi cosmici primari è portata dai protoni, e che la percentuale della loro energia conferita ai pioni in una sola interazione è approssimativamente del 10%.

IL NUOVO CIMENTO Vol. XIV, N. 6 16 Dicembre 1959

The Study of Cosmic Ray Variations with Nuclear Emulsions.

C. J. Waddington

H. H. Wills Physical Laboratory - University of Bristol

(ricevuto l'8 Giugno 1959)

Summary. — It is shown that the density of ending particles observed in nuclear emulsions exposed at high altitudes is related to the primary cosmic ray flux. Because this is a parameter which is readily determined it is suggested that its use is particularly appropriate for studying temporal variations of the primary radiation. The necessary corrections for background particles are established, and preliminary applications illustrated. A value is obtained for the exponent of the primary energy spectrum during solar maximum, and relations derived relating this parameter to the flux of primary cosmic ray α-particles.

Introduction.

During the last decade much of our detailed knowledge of the composition and characteristics of the primary cosmic radiation has been derived from measurements made in nuclear emulsions. In general the information obtained has been on the chemical composition of the primary radiation, the form of the energy spectrum over a limited range of energy ($(0.1 \div 4)$ GeV per nucleon) and the flux variations over the surface of the earth. It is a consequence of the nature of these measurements that we know rather less about the protons of the primary beam than about almost any other component, even though they are both by number and by mass the most abundant. The properties of the α-particle component, on the other hand, are the best known of all, and most of this information has been obtained from nuclear emulsion detectors, although recently composite Čerenkov-scintillator counter arrays have assumed increasing importance.

As a result, when it was realized that it would be desirable to monitor the long term temporal variations, such as that with the solar cycle, using equipment giving detailed information of the effects being produced on the various components, nuclear emulsions were the obvious choice. Thus, as part of the

IGY, several laboratories, in particular the University of Minnesota, have made fairly frequent exposures of small emulsion stacks on high altitude balloons. These stacks have been designed to have sufficient collecting area to allow an α-particle flux to be measured, and the energy spectrum of these α-particles investigated.

The determination of such an α-particle flux value is not a negligible undertaking, involving as it does several man-months of effort. As a consequence it is desirable to select those stacks which have recorded the flux during a period when there has been a significant change from the value previously measured. Obviously external measurements may indicate which stacks can be most profitably analysed. For example, neutron monitors at sea level are sensitive indicators of changes in the total cosmic ray flux above a fairly low energy. However, they will not indicate changes in the low energy component. Alternatively, counting equipment flown together with the emulsion stacks can indicate those of particular interest.

Nevertheless, it is undoubtedly desirable to have some internal parameter which can be readily determined, which will indicate whether a stack is of particular interest. It has been found that the density of ending particles in these stacks is a parameter which is capable of revealing the presence of temporal variations and of permitting a comparison of the energy spectra of the primary cosmic ray particles. Values of the density of ending particles, ε, can be determined with an accuracy of better than $\pm 10\%$ in only a few man-hours, appear to be a sensitive indication of the cosmic ray exposure and, furthermore, reflect the behaviour of the proton component rather than that of the α-particles. This may be particularly important if recent evidence that the proton and α-particle components sometimes vary in a different manner, MEYER [1], FREIER *et al.* [2] is confirmed.

In this paper the necessary corrections for the production of ending particles during the lifetime of the emulsions are established, and the implications and limitations on the use of this parameter are discussed with relation to nine separate high altitude exposures made under widely differing conditions.

1. – Experimental procedure.

In order to assist other workers who may wish to compare their own measurements with those reported in this paper the experimental procedures adopted will be given in some detail.

The emulsions were searched for the tracks of ending particles by an ob-

[1] P. MEYER: preprint (University of Chicago, 1959).

[2] P. S. FREIER, E. P. NEY and J. R. WINCKLER: Report to the 1959 IUPAP Moscow Conference.

server using a microscope having a ×10 objective and ×16 binocular eyepieces. Under these conditions an eyepiece graticule defined a square field of view of side 310 μm. In order to reduce the effects of blemishes on the surfaces of the emulsions being searched a thin film of microscope oil was always placed on the surface of the emulsion.

In each stack of emulsions considered, an emulsion at the centre of the stack was selected for scanning in order to ensure that the distribution of the local matter should be roughly symmetrical. Later it was found that this was a relatively unimportant precaution.

Each of the emulsions selected for measurement was scanned along a line parallel to the top edge and 1 cm below it, for not more than 2 mm further into the stack. This criterion was designed to reduce any effects due to differing amounts of overlying local matter. Once again, it was later found that the results were not critically dependent on this factor.

In selecting the types of particles whose ending tracks were to be recorded it was at first hoped that there might exist certain classes of ending particles whose densities varied more sensitively with the primary radiation than did the overall density. Experience appears to suggest that although such classes might exist, for example those ending particles which have charges of six or greater, they are of such low frequency that the information content of a given period of observation is very small. For this reason only one limitation was placed on the selection of ending particles. To eliminate the α-particles produced by radioactive decays in the emulsion; which reflect only the total age of the emulsion; tracks were not included if they had a total projected range in the emulsion of less than 62 μm.

2. – Experimental material.

Measurements were made on emulsions from 13 different stacks. Details of these stacks and of their exposures are shown in Table I.

3. – The production of ending particles.

An examination of the disintegrations produced by cosmic ray particles in emulsions flown at high altitudes shows that the majority of the primary particles are singly charged, and furthermore, that the majority of the emitted particles have relatively low energies. Thus, it would appear that most of the ending particles observed in any region of an emulsion stack should be produced locally, and that the number of these particles should be a function of the primary proton flux.

TABLE I. – *Details of the emulsion stacks and of their exposures.*

Stack	Volume (litre)	Place	Cut-off (GeV/c)	Date	Rate of ascent (ft/min)	Mean ceiling (g/cm²)	Time at ceiling altitude (h)	Corrected time (h)
O	10	Manitoba	0.6	3- 8-58	815	4.5	8.68	10.40
M	22.3	Minnesota	1.0	18- 9-56	950	6.7	8.13	9.30
N	3.73	Minnesota	1.0	14- 6-58	1000	4.1	9.75	11.08
B	1.86	S. England	2.4 ± 0.1	9- 7-54	700	10.0	4.15	5.65
D	0.12	S. England	2.4 ± 0.1	20-11-58	840	25.0	4.50	6.23
E	1.44	N. Italy	4.6 ± 0.2	14- 9-54	880	8.0	5.83	6.75
G	13.5	N. Italy	4.6 ± 0.2	12-10-54	870	23.0	5.67	6.42
T	1.3	Texas	4.5 ± 0.2	8- 2-59	850	3.6	16.67	20.08 (*)
S	0.56	Sardinia	5.6 ± 0.4	29- 7-53	520	18.0	6.77	8.00
P	1.80	Guam	14.9	12- 2-57	800	10.0	7.10	8.27
C	27 (**)	London-Beirut	~ 4.6	1958	—	310	600	—
J	11.0	Jungfraujoch	~ 4.0	1956	—	680	5000	—
X	0.08 (***)	S. England	2.4 ± 0.1	1957-58	—	1000	13000	—

(*) Stack also flew to 80000 feet and fell again.
(**) Composite emulsion and lead.
(***) Surrounded by local matter during sea level exposure.

The first of these conclusions may have to be modified in stacks exposed under conditions of very low geomagnetic cut-off energy, since then primary protons can, in principle, contribute directly to the density of ending particles. In practice the number of such particles must generally be negligible compared with the number of particles produced locally. For stacks flown in localities with higher cut-off energies the primary protons can hardly be brought to rest within a stack by ionization loss before interacting. In stack *E*, for example, it was found that only $(17 \pm 3)\%$ of the ending particles were produced more than 6 mm away from the point at which they came to rest. One important consequence of this localized production of particles is that any stacks having linear dimensions greater than a few cm can be safely compared, and it is unimportant precisely where in a stack the density of ending particles is measured; provided, only that there is not so much overlying matter that the flux of star producing particles is seriously changed. However, it has been shown by ANDERSON [3] and FREIER *et al.* [2] that occasionally the flux of low energy protons may be greatly enhanced, and it is therefore desirable to make measurements under as little residual matter as possible. As an example of the usual independence of density measurements with depth,

[3] K. A. ANDERSON: *Phys. Rev. Lett.*, **1**, 335 (1958).

measurements made at 1 mm, 1 cm, and 38 cm from the top edge of stack M gave values for ε, in enders/cm^3, of $(9.50 \pm 0.48)\cdot 10^3$, $(9.96 \pm 0.37)\cdot 10^3$ and $(11.5 \pm 0.8)\cdot 10^3$ respectively. It should be noticed, however, that the D stack gives results which are incompatible with those obtained from the other stacks considered, and that it was also the smallest. On the other hand, this discrepancy may be due, not to the size of the stack, but to an incorrectly determined flight curve, since this is not well known.

Since the protons of the primary radiation make up at least 86% of the total incident particle flux, and since the rate of production of low energy fragments from disintegrations is hardly dependent on the nature of the primary particle, the density of ending particles should be a measure of the primary proton flux. It will be a function of the other components of the primary radiation only in so far as they have similus energy spectra. Thus, in Section **5**·2 these measurements are compared with the α-particle flux values only because these are in general better known than the proton flux values; the linear relationship found between these two quantities can be most easily explained by suggesting that the proton and α-particle fluxes have a simple relationship over the range of energies considered.

4. – Analysis of results.

4·1. *The correction for background particles.* – In addition to those particles which end in the stack during the exposure there will be a background of ending particles produced throughout the sensitive life-time of the emulsions. These background particles may be separated into those particles produced while the stack is stored at or near sea level, and those produced during transportation by air. In order to compare the results obtained in different stacks a correction must be applied for these background particles since different stacks may have had very different histories. This correction can best be made by having a control emulsion which has the same history as the stack but is not flown. Unfortunately, this eventuality was not foreseen at the time of exposure of the material being considered here, and so it is necessary to attempt to determine the correction directly. For this reason values of ϱ, the rate of production of ending particles, were successively determined in a stack that was kept at sea level, the X-stack, a stack exposed on the Jungfraujoch, the J-stack, and one exposed on a Comet aircraft, the C-stack. These data, taken in conjunction with values of ϱ (see Section **4**·2) obtained from emulsions exposed by balloon over Northern Italy, the E and G stacks, have been used to construct a curve of the variation of ϱ with altitude, Fig .1. This curve must be regarded as tentative since not all the exposures were made at the same latitude, nor were they contemporaneous, and both the X and C stacks

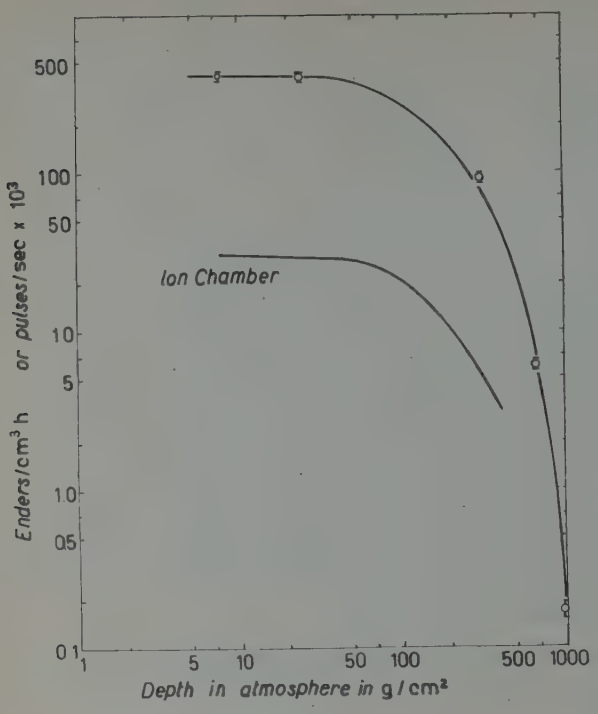

were exposed after the decrease in cosmic ray intensity associated with the recent period of solar maximum.

A further difficulty in making these corrections is that the precise history of many of these stacks is not known. Thus while an uncertainty in

Fig. 1. – The variation of the rate of production of ending particles, ϱ, in enders/cm³ h, with the depth in the atmosphere expressed in g/cm². The experimental points shown are, from left to right, taken from the *E*, *G*, *C*, *J* and *X* stacks respectively. Also shown is the pulse rate obtained with an ionization chamber over Minnesota by WINCKLER and PETERSON (4).

TABLE II. – *Details of the correction of the observed values of ε for background particles, the values of ϱ obtained, and the comparable α-particle fluxes.*

Stack	No. of enders	ε enders/cm³	Corrections		ε_{corr} enders/cm³	ϱ enders/cm³ h	$J\alpha_0$ α-part./m² sr s
			sea level	air			
O	364	$6.5 \cdot 10^3$	200	750	5550	532 ±37	160—130
M	743	$10.0 \cdot 10^3$	170	1000	8830	950 ±35	280± 20 (*)
N	454	$6.1 \cdot 10^3$	190	1000	4910	435 ±21	160—130
B	303	$3.26 \cdot 10^3$	58	—	3200	567 ±33	162± 19 (*)
D	210	$2.82 \cdot 10^3$	130	—	2690	432 ±30	—
E	330	$2.95 \cdot 10^3$	255	—	2700	400 ±22	89± 8 (*)
G	211	$2.84 \cdot 10^3$	200	—	2640	396 ±27	89± 8
T	517	$6.95 \cdot 10^3$	368	1000	5582	277 ±15	65^{+7}_{-5}
S	253	$2.72 \cdot 10^3$	254	—	2480	309 ±20	70± 9 (*)
P	228	$2.45 \cdot 10^3$	340	1000	1110	134 ±50	15± 5
C	199	$53.5 \cdot 10^3$	—	—	53200	89 ± 6	—
J	211	$30.0 \cdot 10^3$	—	—	30000	6.0 ± 0.4	—
X	163	$2.19 \cdot 10^3$	—	—	2190	0.17± 0.02	—

(*) α-particle flux determined in same stack.

(4) J. R. WINCKLER and L. PETERSON: *Nature*, **181**, 1317 (1958).

the total sensitive lifetime of each stack is not very important due to the small magnitude of the sea level correction, the correction for air transportation is not negligible and depends on the duration and mean altitude of the flights. For the purposes of this paper it has been assumed that all aeroplane flights were at a mean depth in the atmosphere of 470 g/cm² (20 000 feet) and that at such a depth in the atmosphere temporal variations are negligible. The estimated corrections due to such flights are shown in Table II. It may be noted that while these corrections are as little as 10% for a stack such as the *M* stack they are nearer 50% for the *P* stack. Control emulsions are essential for such large corrections.

4·2. *Derivation of* ϱ *from the corrected density.* – It can be seen from Fig. 1 that for depths in the atmosphere of less than about 30 g/cm² (78 000 feet) the rate of production of ending particles is independent of altitude and is presumably closely similar to that value which would be observed at the top of the atmosphere. In order to calculate the value of ϱ from a value of ε_h corrected for background obtained in a stack exposed on a high altitude balloon, an additional correction must be made for the effects of the relatively slow rate of ascent to the ceiling altitude. This correction has been made by calculating an effective total time of exposure by giving each 10 min interval a weight proportional to the value of ϱ at that altitude. While a diagram such as that shown in Fig. 1 could have been constructed by successive approximation, the procedure actually adopted was to predict that ϱ should vary with altitude similarly to the known variation shown by an ionization chamber, WINCKLER and PETERSON [4], and to use this variation. From Fig. 1 it can be seen that the shapes of the two curves are in sufficient agreement to justify this procedure.

5. – Applications.

5·1. *Latitude effect.* – Since values of ϱ have been measured in stacks exposed at a number of different localities it is possible to investigate the variation of ϱ with geomagnetic cut-off rigidity, *R*. Fig. 2 shows the variation of ϱ, expressed in enders/cm³·hour, with the magnetic cut-off rigidity expressed in GeV/c. The values used for these rigidities are somewhat uncertain, although in a number of cases the experimentally determined values have been used. The values calculated by QUENBY and WEBBER [5] are also shown for comparison. The marked difference between observations made at sunspot

---

[5] J. J. QUENBY and W. R. WEBBER: *Phil. Mag.*, **4**, 90 (1959).

minimum and sunspot maximum is clearly illustrated in this figure, as it is in Fig. 3, which shows ϱ as a function of the total geomagnetic cut-off energy, T.

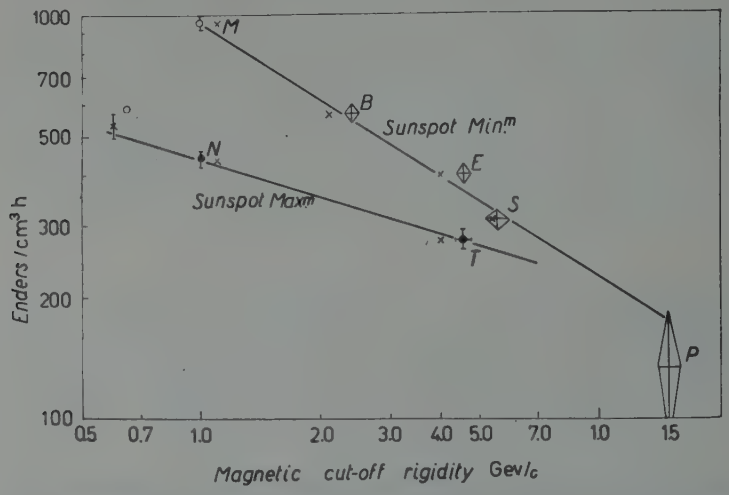

Fig. 2. – The variation of ϱ, expressed in enders/cm³ h, with R, the magnetic cut-off rigidity in GeV/c. Crosses mark the rigidity values calculated by QUENBY and WEBBER (5).

That ϱ is overwhelmingly a reflection of the primary proton flux is shown by the increased value obtained in the O stack relative to that in the N stack.

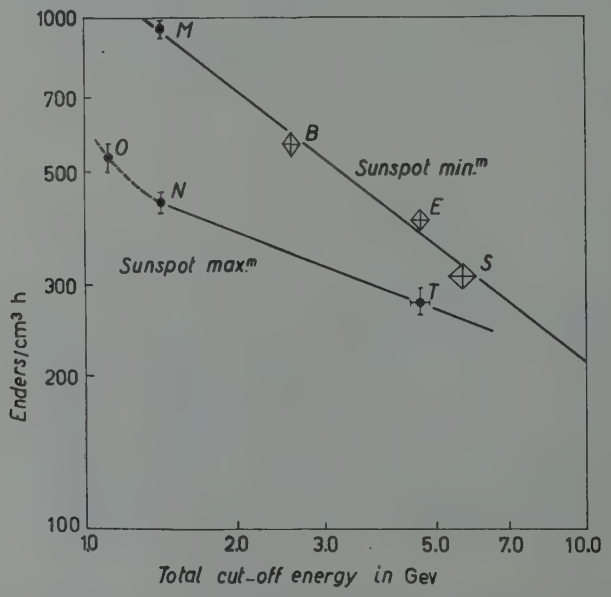

Fig. 3. – The variation of ϱ, expressed in enders/cm³ h, with T, the total cut-off energy in GeV.

No *additional* primary particles with charges greater than those of the protons could have entered the O stack, since even for the N stack the observation of helium and heavier nuclei is limited by their absorption in the overlying atmospheres rather than by geomagnetic effects.

Between the energy limits of $(1.4 \div 6)$ GeV it can be seen that both at sunspot minimum and sunspot maximum the relation between ϱ and T can be expressed in the form $\varrho = C \cdot T^n$ where C and n are constants. While these constants cannot be well determined from this somewhat sparse data it is interesting to note that n apparently changes from 0.76 at sunspot minimum to 0.38 at sunspot maximum. This is an appreciably greater relative change than that observed previously for the primary α-particle energy spectrum, FREIER *et al.* [6], suggesting that these measurements of ϱ provide a sensitive method of measuring changes in the energy spectrum of the primary radiation.

Unfortunately it does not appear feasible to calculate the true primary spectrum directly from the observed variation of ϱ. An attempt was made by assuming that ϱ should be proportional to the product of the flux and the mean value of N_h, the number of « black » and « grey » tracks originating from nuclear disintegrations in emulsion. This mean value of N_h can be calculated from the values observed in emulsions exposed to monoenergetic protons from accelerating machines and the assumed primary energy spectrum. Such calculations result in a variation of ϱ with energy considerably greater than that observed, when any reasonable form of the primary energy spectrum is used. In view of the fact that cosmic ray data, CAMERINI *et al.* [7], show that the average energy of the « grey » particles emitted from disintegrations is essentially independent of the primary energy above about 1 GeV, the above discrepancy is not understood. It is possible that the situation is obscured by the presence of an appreciable number of relatively low energy albedo particles.

However, if the form of the energy spectrum of the primary particles at sunspot minimum is assumed, then it is possible to use these data to obtain the energy spectrum at sunspot maximum. For, let the spectrum at sunspot minimum be of the form $\mathrm{d}N_{\min} \propto T^{-\gamma}\,\mathrm{d}T$ and that at sunspot maximum be $\mathrm{d}N_{\max} \propto T^{-\beta}\,\mathrm{d}T$. Now experimentally we have $\mathrm{d}\varrho_{\min} \propto T^{-1.76}\mathrm{d}T$ and $\mathrm{d}\varrho_{\max} \propto T^{-1.38}\mathrm{d}T$. Also it is apparent that $\mathrm{d}N_{\min}/\mathrm{d}\varrho_{\min} = \mathrm{d}N_{\max}/\mathrm{d}\varrho_{\max}$. Thus if a value for either γ or β is assumed, the other can be calculated. If γ is assumed to be 2.5, MCDONALD [8], then $\beta = 2.12$ which is in good agreement with the value of

---

[6] P. S. FREIER, E. P. NEY and C. J. WADDINGTON: *Phys. Rev.*, **114**, 365 (1959).

[7] U. CAMERINI, J. H. DAVIES, P. H. FOWLER, C. FRANZINETTI, H. MUIRHEAD, W. O. LOCK, D. H. PERKINS and G. YEKUTIELI: *Phil. Mag.*, **42**, 1241 (1951).

[8] F. B. MCDONALD: *Phys. Rev.*, **109**, 1367 (1958).

2.17 obtained by FREIER *et al.* (6) for the α-particle energy spectrum at solar maximum. Too great a reliance should not be placed on this value for β due to the uncertainties, in the determination of $d\varrho_{min}$ and $d\varrho_{max}$, but it is interesting to note that the primary energy spectrum can apparently be determined by making such simple measurements on emulsions exposed at not more than two localities.

5·2. *Variation of ϱ with primary α-particle flux.* – The primary α-particle flux has been determined in the *B*, *E*, *S* and *M* stacks, and is known from measurements made from presumably comparable exposures for the *N*, *O*, *T* and *P* stacks. Since measurements of primary α-particle fluxes have been used to monitor the cosmic radiation it is instructive to compare these flux values with the values obtained for ϱ. Such a comparison is shown in Fig. 4

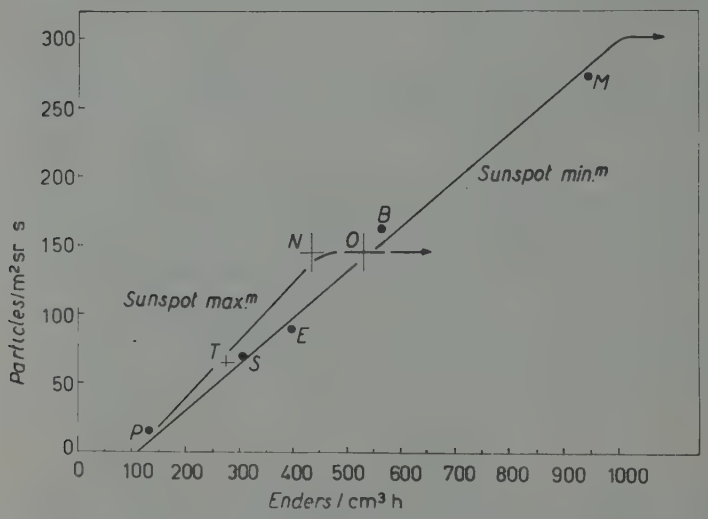

Fig. 4. – The relationship between the flux of primary α-particles and ϱ, the rate of production of ending particles.

from which it can be seen that there exists a linear relationship between the α-particle flux J_{α^0} and ϱ. It should be noted that this relationship must fail for exposures made under conditions of lower magnetic rigidity than 1 GeV/c where the α-particle flux ceases to increase at lower rigidities, unlike the proton flux.

At sunspot minimum the relation between J_{α^0} and ϱ is:

$$J_{\alpha^0} = 0.34\,\varrho - 38 \text{ α-particles/m}^2 \text{ sr s}$$

for ϱ between 150 and 1000 enders/cm^3·hour while at sunspot maximum it is

$$J_{\alpha^0} = 0.42\,\varrho - 45 \ \alpha\text{-particle/m}^2\cdot\text{sr}\cdot\text{s}$$

for ϱ between 150 and 450 enders/cm^3·hour.

6. – Conclusions.

The density of ending particles in nuclear emulsions appears to be a parameter which is a sensitive indication of the total flux of primary cosmic ray particles. Of all the observed parameters in nuclear emulsion which are related to the primary cosmic radiation it is probably the easiest to determine and it is thus particularly suited to studying temporal variations. Furthermore, it is primarily a function of the proton component of the radiation, which is not customarily studied with emulsions.

The density of these ending particles is such that it should be possible to expose very small stacks of emulsions, a few cm^3 in volume, on ordinary meteorological sounding balloons, and thus obtain a detailed coverage of the temporal variations. It should be appreciated, however, that these measurements are not readily able to provide detailed information on the characteristics of the particles producing these changes. The information provided is in many ways analogous to that provided by an ion chamber, without the advantage of time resolution during the exposure. This disadvantage, while not serious in many cases, may result in misleading conclusions if there is a large flux variation during the course of the exposure, such as that recently reported by FREIER *et al.* [2], who observed a large enhancement of the low energy proton flux during a period of decreased total intensity.

* * *

The author thanks Professor C. F. POWELL R.F.S. for the hospitality and facilities of his laboratory, Dr. A. ENGLER for the opportunity to make measurements on the *O* stack, and Drs. MEYER, FREIER, NEY and WINCKLER for the communications of results prior to publication. He also thanks the Royal Society for the award of a Mackinnon Research Studentship.

RIASSUNTO (*)

Si dimostra che la densità di particelle a fine percorso osservate in emulsioni nucleari esposte ad altitudini elevate è proporzionale al flusso dei raggi cosmici primari. Poichè questo parametro è facilmente determinabile si suggerisce il suo uso per lo studio delle variazioni temporanee della radiazione primaria. Si indicano le correzioni necessarie per le particelle di fondo, e si illustrano alcune applicazioni preliminari. Si ricava un valore dell'esponente dello spettro dell'energia primaria durante un massimo solare e si derivano espressioni che mettono questo parametro in relazione col flusso delle particelle α della radiazione cosmica primaria.

(*) *Traduzione a cura della Redazione.*

IL NUOVO CIMENTO Vol. XIV, N. 6 16 Dicembre 1959

Mesonic Decays of Hyperfragments.

G. C. Deka

H. H. Wills Physical Laboratory - University of Bristol

(ricevuto il 2 Luglio 1959)

Summary. — A search for hyperfragments emitted from the nuclear interactions of 4.5 GeV π^--mesons and 300 MeV/c K^--mesons provided twenty-one decays of hyperfragments. Nine of these have been identified as specific hypernuclei from the momentum balance of the decay particles; their binding energies have been measured and found to be in good agreement with the results obtained by other authors.

1. – Results.

A systematic scan was made to observe double stars which could be possible examples of the decay of hyperfragments. An Ilford G-5 emulsion stack exposed to an intense beam of 4.5 GeV π^--mesons and a K-5 emulsion stack exposed to 300 MeV/c K^--mesons were area scanned under low magnification. Double stars were picked up and selected for analysis using the criteria as described by Filipkowski [1]. In examining 51 000 stars in the π-stack 98 double stars were found, 6 of which were mesonic decays; also among 1 300 K-stars 61 double stars were found, 15 of which decayed mesonically.

Three decays in flight, one mesonic and two non-mesonic, were also observed. In 4 cases, two decay pions disappeared in flight and the other two left the stacks. Of the 17 mesonic decays in which the pions were followed to rest and identified, 9 were analysed as specific hypernuclei and their binding energies were measured from the momentum balance of the decay products; whereas the rest do not permit complete analysis. The observed data relevant to these events have been represented in Tables I and II.

---

[1] A. Filipkowski, J. Gierula and P. Zielinski: *Acta Phys. Polon.*, **16**, 139 (1957).

TABLE I. – « *Uniquely* » *defined mesonic decays of Hfs.*

Event no.	Parent star	Decay at rest or in flight	Time of flight (10^{-11} s)	Coplanarity or Colinearity	Track	Range of tracks (μm)	Identity	Decay scheme	B_Λ (MeV)	Remarks
1	3+0, K^-	R	5.8	Copl.	Hf	245	He	$^5He_\Lambda \rightarrow {}^4He+p+\pi^-$	2.92±.6	—
					1	8.5	He			
					2	35.4	p			
					3	15.38 mms	π^-			
2	4+0, K^-	F	4.5	Col.	Hf	131	H	$^4H_\Lambda \rightarrow {}^4He+\pi^-$	1.84±.5	—
					1	298	He			
					2	33.24 mms	π^-			
3	4+0, K^-	R	0.3	Copl.	Hf	99	He	$^5He_\Lambda \rightarrow {}^4He+p+\pi^-$	2.8 ±.6	—
					1	34	p			
					2	5.5	He			
					3	15.8 mms	π^-			
4	3+I, K^-	R	0.4	Copl.	Hf	138	He	$^5He_\Lambda \rightarrow {}^4He+p+\pi^-$	2.44±.6	—
					1	6	He			
					2	56	p			
					3	15.54	π^-			
6	2+0, K^-	R	0.07	Copl.	Hf	5		$^8Be_\Lambda \rightarrow {}^7Be+p+\pi^-$	5.8 ±.8	—
					1	3.5	r			
					2	699	p			

7 (*)	4+1, K	R	0.4	Copl.	Hf	32.5	H			
					1	33	He			
					2	22.5	He			
4123					3	10.06 mms	π^-			
8	3+1, K^-	R	0.08	no	Hf	6.0	H	$^4H_\Lambda \rightarrow {}^3He+n+\pi^-$	$1.89 \pm .8$	—
					1	8.75	He			
					2	16.69 mm	π^-			
10	4+0, K^-	R	0.12	Col.	Hf	41.2	H	$^4H_\Lambda \rightarrow {}^4He+\pi^-$	$2.2 \pm .6$	—
					1	8.3	He			
					2	38.4 mms				
15	3+0, K^-	R	0.1	no	Hf	7.0	He	$^5He_\Lambda \rightarrow {}^3He+p+n+\pi^-$	1.7 ± 1.1	—
					1	9.6	He			
					2	72.5	p			
					3	1.8 mm	π^-			
16	17+2, π^-	R	0.2	Copl.	Hf	45	He	$^5He_\Lambda \rightarrow {}^4He+p+\pi^-$	$3.2 \pm .8$	—
					1	23	p			
					2	6.5	He			
					3	15.5 mms	π^-			

(*) This event has already been published by P. H. Fowler: *Phil. Mag.* **36**, 1460, (1958).

TABLE II. — « *Non uniquely* » *defined mesonic decays.*

Event no.	Parent star	Decay at rest or in flight	Time of flight (10^{-11} s)	Coplanarity or Colinearity	Track	Range of tracks (μm)	Identity	Decay scheme	B_Λ (MeV)	Remarks
5	4+0, K^-	R	8.0	Copl.	Hf	365	He	$^5He_\Lambda \rightarrow {}^4He+p+\pi^-$	2.37 ± 3	π^- disappears in flight
					1.	7	He	or		
					2	77	p	$^4He_\Lambda \rightarrow {}^3He+p+\pi^-$	2.2 ± 3	
					3	> 2.8 mms	π^-			
9	3+0, K^-	R	0.64	Col.	Hf	86		$^4H_\Lambda \rightarrow {}^4He+\pi^-$	1.9 ± 2	Do.
					1	8.4	He	or		
					2	> 0.8 mm	π^-	$^3H_\Lambda \rightarrow {}^3He+\pi^-$		
11	2+1, K^-	R	0.12	Copl.	Hf	26	He	$^4He_\Lambda \rightarrow {}^3He+p+\pi^-$	$3.4 \pm .8$	—
					1	3	He	or		
					2	591	p	$^5He_\Lambda \rightarrow {}^4He+p+\pi^-$		
					3	9.47 mm	π^-			
12	3+0, K^-	(?)	—	no	Hf	11.2		—	—	No scheme fits
					1	2.5	recoil			
					2	7.9 mm	π^-			
13	3+0, K^-	R	—	no	Hf	5.2		$^{7,8}Li_\Lambda \rightarrow {}^{6,7}Li+p+\pi^-$	~ 7	Assumed recoil range
					1	77.5	p	or		
					2	13.65 mms	π^-	$^{8,10}B_\Lambda \rightarrow {}^{7,9}B+p+\pi^-$		

					1	3	r	or		
					2	1.35 mms	p	$^{8,10}Be_{\Lambda} \rightarrow {}^{7,9}Be + p + \pi^-$	~ 6	
					3	2.35 mms	π^-			
17	21+1, π^-	R	1.05	Copl.	Hf	82	H	$jH_{\Lambda} \rightarrow d + p + \pi^-$	$0.12 \pm .5$	—
					1	3.5	d, t	or		
					2	94	p	$^4H_{\Lambda} \rightarrow t + p + \pi^-$	$0.11 \pm .5$	
					3	17.79 mms	π^-			
18	10+2, π^-	R	0.13	Copl.	Hf	23	He	$^4He_{\Lambda} \rightarrow {}^3He + p + \pi^-$	$2.34 \pm .6$	—
					1	3	He	or		
					2	2407	p	$^5He_{\Lambda} \rightarrow {}^4He + p + \pi^-$	$2.5 \pm .6$	
					3	2501	π^-			
19	18+2, π^-	R	0.33	Copl.	Hf	76		$^4He_{\Lambda} \rightarrow {}^3He + p + \pi^-$	2.78 ± 2	π is not
					1	10	Heff	or		stopped
					2	450	p	$^5He_{\Lambda} \rightarrow {}^4He + p + \pi^-$	2.6 ± 2	
					3	> 2 mms	π^-			
20	22+2, π^-	R	0.12	Copl.	Hf	28		$^4He_{\Lambda} \rightarrow {}^3He + p + \pi^-$	2.8 ± 3	Do.
					1	5	r	or		
					2	1.51 mms	p	$^5He_{\Lambda} \rightarrow {}^4He + p + \pi^-$	2.7 ± 3	
					3	> 1.5 mms	π^-			
21	13+2, π^-	(?)	—	no	Hf	17		—	—	No scheme
					1	5.5	r			fits
					2	7.2 mms	π^-			

2. – Description of a few specific hyperfragments.

Events 9 and 10 have their secondary tracks colinear within limits of errors. The pion of the event 9 disappears in flight. The other pion has been followed to rest and identified as a negative pion captured at rest. Its energy and momentum obtained from the range are (52.5 ± 0.5) MeV and (133 ± 2) MeV/c respectively.

Assuming that there was no neutral particle involved in the decay, the pion momentum has been given to the recoil nucleus. The recoil range for ^{4}He calculated from this momentum is found to be 9 μm whereas the observed range is $(8.5 \pm .6)$ μm. The binding energy B_Λ which has been found to be $\sim (2.2 \pm .6)$ MeV assuming a decay scheme as $^4H_\Lambda \to {}^4He + \pi^-$ is in good agreement with other results. Event 2 has its two secondary tracks non colinear, but the three tracks, including the parent track are coplanar. The pion has been followed to rest and its energy and momentum are found to be 48.8 MeV and (127 ± 2) MeV/c respectively. If one assumes the other secondary track is due to ^{4}He there is a good balance of the transverse momentum and the momentum in the direction of the parent particle gives an energy of (28.5 ± 0.6) MeV for $^4H_\Lambda$. The binding energy B_Λ calculated for the decay scheme $^4H_\Lambda \to {}^4He + \pi^-$ decaying in flight has been found to be $\sim (1.85 \pm 0.7)$ MeV, which is in good agreement with other results. Another feature in support of this decay scheme is that the secondary track of range ~ 298 μm has δ-ray density of an α-particle whereas the parent particle appears to be singly charged. The time of flight has been found to be $4.0 \cdot 10^{-12}$ s. A photograph of the event ([2]) is reproduced.

Events 1, 3, 4, 15, 16 are examples of $^5He_\Lambda$. One of the pions disappears in flight, the rest have been followed to rest and identified. In the case of event 15 the tracks are non-coplanar whereas in the others they are found to be coplanar within the limits of errors. The secondaries have been identified from the momentum balance and the binding energies have been found to be in good agreement with the results of other authors (Levi-Setti *et al.* ([2])).

3. – A possible example of $^8Be_\Lambda$.

A photograph of the event (6) is reproduced. A K^--meson captured at rest by an emulsion nucleus gives rise to a star of type $2+1$ K^-. One of the secondary particles produces a short track (~ 5 μm) and gives rise to another three prong star at rest. One of the three particles has been followed to rest and identified as a negative pion, the second one is possibly a proton and the

([2]) R. Levi Setti, W. E. Slater and V. L. Telegdi: *Suppl. Nuovo Cimento*, **1**, 10 (1958).

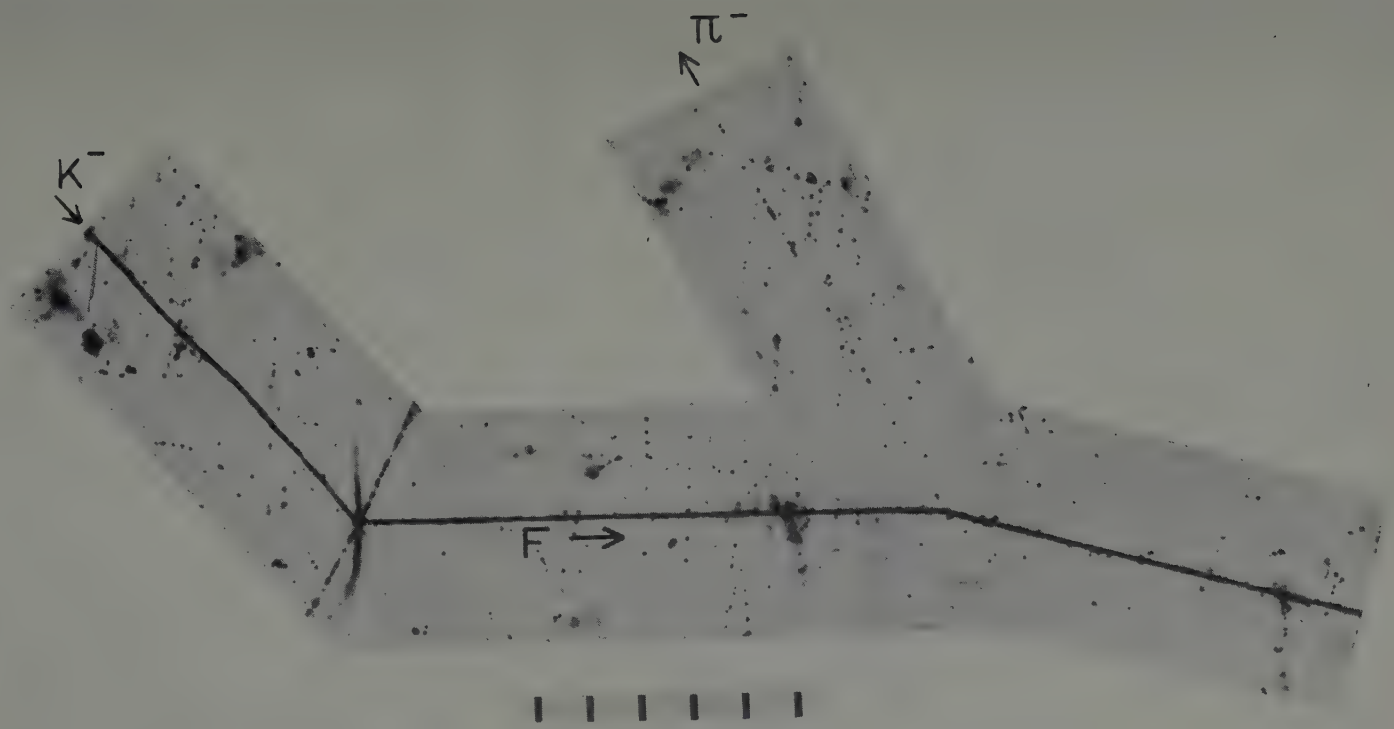

Fig. 1. – Event 2. A ^4H hyperfragment, produced by the absorption of a stopped K^--meson, decayed in flight according to the relation $^4H_\Lambda \rightarrow {}^4He + \pi^-$.

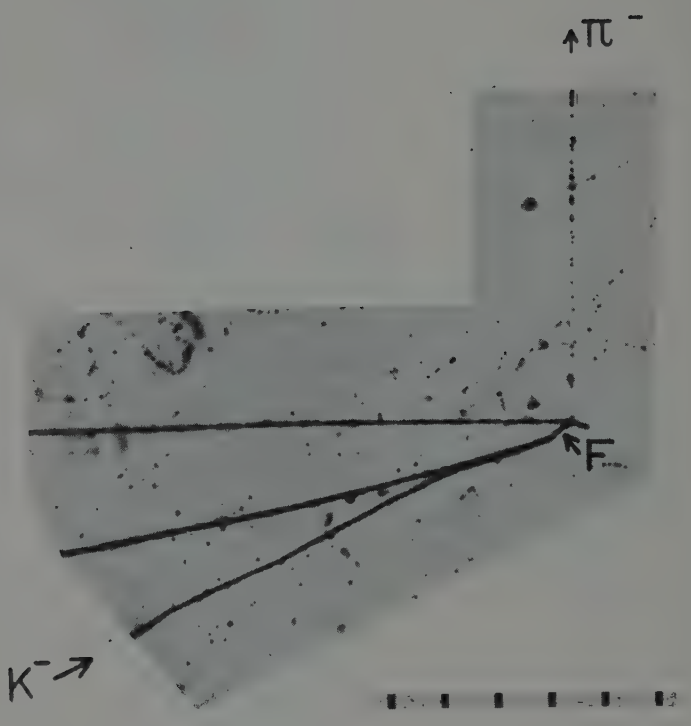

Fig. 2. – Event 6. A ^{8}Be hyperfragment, produced by the absorption of a stopped K^--meson, decayed at rest into three coplanar particles according to the relation: $^{8}Be_{\Lambda} \rightarrow {}^{7}Be + p + \pi^-$.

third one is a short recoil. The three tracks are coplanar, but the precision of measurements of angles is not high because of the short recoil. The energy and momentum of the pion are obtained from its range. The angle between the proton and the pion is $(90.5 \pm 1)°$. The vector sum of their momenta is (163 ± 2) MeV/c, which has been attributed to the third particle. The expected ranges for ^{6}Li, ^{7}Li and ^{7}Be of this momentum are found to be 4.8, 4.4 and 2.9 μm. The range for ^{7}Be seems to be more close to the observed recoil range $\sim (3.5 \pm .5)$ μm. It has been assumed, therefore, that the event was due to $^8\mathrm{Be}_\Lambda$ decaying in the following mode:

$$^8\mathrm{Be}_\Lambda \rightarrow {}^7\mathrm{Be} + \mathrm{p} + \pi^- + Q \ ,$$

which gives $B_\Lambda = (5.8 \pm 0.6)$ MeV, assuming that the ^{7}Be nucleus was formed in the ground state. Details of the event have been given in Table III.

TABLE III. – *Details of the event.*

Track	Identification	Dip angle deg.	Plane angle deg.	Range in (μm)	Energy (MeV) from range	Momentum (MeV/c) from range
Hf	—	$0 \pm .1$	—	5	—	—
1	π^-	$2 \pm .5$	$90.5 \pm .5$	6451	$18.2 \pm .5$	73.5 ± 2
2	p	17	154 ± 1	699	11.1	148
3	^{7}Be (?)	0 ± 1	116 ± 1	$3.5 \pm .5$	2.1	164

4. – Two unidentified events.

In event 14, a nuclear particle of range 5 μm emitted from a Σ^--capture star gives rise to a three prong star. One of them is identified as due to a π^--meson, one is due to a singly charged particle, the other is a 3 μm recoil. Three tracks are coplanar within the errors of measurements; precise measurements are impossible due to the short recoil. The residual momentum of the pion and the other particle, assuming it to be a proton is found to be (135 ± 3) MeV/c. This corresponds to ranges for ^{6}Li, ^{7}Li, ^{7}Be and ^{9}Be 4, 3.8, 2.5, and 2.0 μm respectively. The B_Λ values are found be ~ 8 MeV for ^{7,8}Li and ~ 7 MeV for ^{8,10}Be hypernuclei, assuming that these were formed in the ground states. The possibility that these were formed in the excited states cannot be excluded.

In event 13, a 5.2 μm range particle emitted from a K^--star gives rise to a two prong star. One of the particles is identified as a π^--meson and the other is a singly charged particle. The event cannot be interpreted in terms of these two particles alone, because the visible energy is too high to allow

the emission of a neutron which makes the B_Λ values for any hypernuclei improbable. A plausible interpretation can be obtained by assuming a recoil of range $< 1\ \mu$m which is not possibly detected due to the fact that the recoiling nucleus may be moving in the direction opposite to the parent particle. The resultant momentum of the pion and the other particle as a proton is (42 ± 3) MeV/c in the direction of the parent particle. If one assumes a ^{6,7}Li or a ^{7,9}Be nucleus carries this momentum then their ranges will be less than 1 μm and reasonable B_Λ values are also obtained, whereas such values for heavier hypernuclei are too low as compared to the values observed by others.

5. – Analysis of events involving a short recoil.

The three body decays of hydrogen, helium and lithium hyperfragments which can be represented by $F^A \to F^{A-1} + p + \pi^-$ are frequently found to be associated with a short recoil due to F^{A-1} which makes its identification difficult. For example, there is often little difference between the ranges of ^{3}He and ^{4}He recoils resulting from ^{4}He$_\Lambda$ and ^{5}He$_\Lambda$ decays. In such cases, however, the proton and pion momenta can be measured with a greater accuracy from their ranges which are generally long. The recoil nucleus in a few favourable cases, could be identified from its range and the momentum it absorbs in the following way. The expected range for an assumed nucleus is calculated from the pion proton residual momentum which should have the same direction as the recoil. An identification of the hyperfragment could be made from a comparison of the expected and observed ranges of the recoil and from an acceptable binding energy obtained thereof. Results of such an analysis have been shown in Table IV.

TABLE IV. *Distinguishing* He-*hyperfragments* (*decay*: ^{4,5}He$_\Lambda \to {}^{3,4}$He$+p+\pi^-$) *from the range of the recoil.*

Event no.	Residual momentum of $p+\pi$ (*a*)	Calculated range from (*a*) for		Observed range (μm)	B_Λ in MeV for		Remarks
		^{3}He	^{4}He		^{4}He$_\Lambda$	^{5}He$_\Lambda$	
1	133.5 ± 5	12	9	$8.5 \pm .5$	2.27	2.9	^{5}He$_\Lambda$
3	111.5 ± 4	8.8	6.5	$5.5 \pm .6$	2.67	2.8	^{5}He$_\Lambda$
4	121.5 ± 5	10	7.5	$6.1 \pm .5$	2.05	2.44	^{5}He$_\Lambda$
11	68 ± 3	3.0	2.3	$3 \pm .5$	3.0	3.2	(?)
16	122.5 ± 5	10.2	7.8	$6.5 \pm .5$	2.57	3.2	^{5}He$_\Lambda$
18	70.5 ± 4	4.2	2.5	$3.8 \pm .5$	2.34	2.57	(?)

TABLE V. – *Average B_Λ-values of the uniquely defined hyperfragments.*

Hf.	No. observed	Decay scheme	B_Λ (MeV)	Average B_Λ (MeV)
^{4}H	3	^{4}He+π^-	1.84±0.6 1.89±0.6 2.2 ±0.8	1.97±0.4
^{5}He	4	^{4}He+p+π^-	2.92±0.5 2.8 ±0.6 2.44±0.6 3.2 ±0.8	2.84±0.44
^{8}Li	1	^{4}He+^{3}He+π^-	5.2 ±0.5	5.2 ±0.5
^{7}Be	1	^{7}Be+p+π^-	5.8 ±0.8	5.8 ±0.8

For momentum balance and for computing binding energies use of the following was made.

1) Barkas range energy tables, Report U. C. R. L. 2426 Rev, 1957 ([3]).

2) Wilkins range energy curves, 1951 ([4]).

3) Mass defects of isotopes given by AJZEMBERG and LAURISTSEN, 1955 ([5]).

* * *

I am very grateful to Professor C. F. POWELL for the hospitality of his laboratory, and various members of the department, in particular to Dr. P. H. FOWLER and Dr. D. EVANS for their valuable suggestions and helpful discussions. The author wishes to thank the Government of Assam (India) for granting him study leave.

([3]) W. H. BARKAS: Report UCRL-2426 Rev (1957).
([4]) J. J. WILKINS: Atomic Energy Research Est., Harwell Rept. G/R 664 (1951).
([5]) F. AJZUNBERG and T. LAURISTSEN: *Rev. Mod. Phys.*, **27**, 77 (1955).

RIASSUNTO (*)

Un esame degli iperframmenti emessi dalle interazioni nucleari di mesoni π^- di 4.5 GeV e di mesoni K$^-$ di 300 MeV/c ha fornito ventun decadimenti di iperframmenti. Basandoci sulla conservazione del momento d'impulso delle particelle di decadimento, nove di essi sono stati identificati come ipernuclei specifici; si sono misurate le loro energie di legame e si è trovato che esse sono in buon accordo con i risultati ottenuti dagli altri autori.

(*) *Traduzione a cura della Redazione.*

IL NUOVO CIMENTO Vol. XIV, N. 6 16 Dicembre 1959

Hyperfragments Produced by K^- Capture in Nuclear Emulsion: π^0 Decay Modes (*) (**).

R. G. Ammar

Department of Physics and The Enrico Fermi Institute for Nuclear Studies The University of Chicago - Chicago, Ill.

(ricevuto il 17 Luglio 1959)

Summary. — This is a systematic study of the π^0-decays of light hypernuclei ($A \leqslant 5$) produced by K^- capture in nuclear emulsion. Approximately $3 \cdot 10^4$ K^- stars were examined, yielding a total of 94 1-prong events satisfying the following conbitions: $R_c \geqslant 5$ μm, 8 μm $\leqslant R_0 \leqslant 50$ μm, $\theta \geqslant 66°$, where R_c is the range of the primary (connecting track), R_0 that of the secondary (recoil) and θ the angle between their directions at their point of intersection. Of the 69 events which could be charge (Z) identified, 55 had $Z=1$ and 14 $Z=2$. In the $Z=1$ category the true π^0-events could not be separated from 1-prong Σ^--events because of the overwhelming ($\gtrsim 90\%$) contribution of the latter. It is concluded that probably all the 14 $Z=2$ events represent true He_Λ decays (~ 10 $^4He_\Lambda$ and ~ 4 $^5He_\Lambda$). In addition, three 2-prong events were consistent with the interpretation as $^4He_\Lambda$ decays. One can define for the π^0-decays of $^4He_\Lambda$ the ratio: $R'(^4He_\Lambda)$ = (two-body decays)/(all decays − «unobservable» ones); the «unobservable» ones being π^0-neutron-recoil decays with recoil momenta < 110 MeV/c and other modes with $\geqslant 1$ neutron. A value $R'(^4He_\Lambda) = 0.82^{+.15}_{-.18}$ is found here. The analogous quantity for $^4H_\Lambda$ was computed from the data of ref. [10] and yields $R'(^4H_\Lambda) = 0.88^{+0.07}_{-0.06}$. These two numbers are equal within their experimental errors. This equality is consistent with the assumption $|p_-/s_-| = |p_0/s_0|$ as predicted by the $\Delta T = \frac{1}{2}$ rule. The ratio, ϱ, of two body π^0-decays of $^4He_\Lambda$ to the total number of π^--decays of $^4He_\Lambda$ was determined to be 0.7 ± 0.4. Accordingly as the spin of $^4He_\Lambda$ is 0 or 1, ϱ is a measure of the strength either of the s- or of the p-wave channel in the neutral mode of the free Λ decay.

(*) Research supported by the U. S. Air Force Office of Scientific Research, Contract no. AF 49(638)-209.

(**) A thesis submitted to the Department of Physics, the University of Chicago, in partial fulfilment of the requirements for the Ph. D. degree.

1. – Introduction.

A convenient means for the study of the properties of the Λ is the hyperfragment, in which the Λ hyperon is bound to a nuclear fragment. Such hyperfragments may be classified according to their decay modes, of which there are three prominent ones. The first

$$\Lambda + \mathcal{N} \to n + \mathcal{N} \tag{1}$$

can occur only in the presence of nucleons, while the remaining two modes

$$\Lambda \begin{cases} \nearrow p + \pi^- & (2) \\ \searrow n + \pi^0 & (2') \end{cases}$$

are also observed with the free Λ's. SILVERSTEIN [1] and SLATER [2] investigated systematically in this laboratory the non-mesic decays (1) and the charged mesic decays (2). Recently, LEVI SETTI and SLATER [3] described a hyperfragment decaying by process (2′) in which the subsequent π^0-decay involved the emission of an electron-positron pair by internal conversion (Dalitz pair), but to date no systematic investigation of process (2′) appears to have been carried out.

The purpose of the present work is to fill this gap in our knowledge. The π^0 hyperfragments studied here were produced by K^--captures in nuclear emulsion.

2. – Formulation of the problem.

2·1. *General.* – The basic similarity of the mesic modes (2), (2′) makes it natural to first discuss briefly the charged mode (2) which has already been investigated extensively. It is known [4] that in K^- captures in nuclear emulsion hypernuclides with mass number $A \leqslant 5$ constitute $\sim 80\%$ of the total yield of hyperfragments decaying by (2). Consequently we shall confine ourselves to the π^0 decays of such light hypernuclides.

(1) E. M. SILVERSTEIN: *Suppl. Nuovo Cimento*, **10**, 41 (1958).
(2) W. E. SLATER: *Suppl. Nuovo Cimento*, **10**, 1 (1958).
(3) R. LEVI SETTI and W. E. SLATER: *Phys. Rev.*, **111**, 1395 (1958).
(4) R. AMMAR, R. LEVI SETTI, W. E. SLATER, S. LIMENTANI, P. E. SCHLEIN and P. H. STEINBERG: *Mesic decays of hypernuclei from K^- capture - I: Binding energies.* to be published in *Nuovo Cimento*. See also report submitted by the same authors to the *Annual International Conference on High Energy Physics at CERN* (1958).

2·2. *Kinematics of decay.* – The decay configurations may be classified as to whether one or two visible (charged) particles are emitted.

2·2.1. One-prong events. – Table I gives the main kinematic quantities associated with some π^0-decays of $^3H_\Lambda$, $^4H_\Lambda$, $^4He_\Lambda$, and $^5He_\Lambda$ which lead to such events; these quantities have already been given by FRANZINETTI and MORPURGO (5). This table shows that the energy of the visible prong, the recoil, is always quite small.

TABLE I. – *Kinematics for π^0-neutron-recoil and π^0-recoil decay modes of light hypernuclei.*

Hypernuclide	π^0-neutron-recoil mode		π^0-recoil mode	
	Maximum recoil energy (MeV)	Maximum recoil range (μm) (*)	Recoil energy (MeV)	Recoil range (μm) (*)
$^3H_\Lambda$	13.4	560	2.44	35
$^4H_\Lambda$	9.8	256	—	—
$^4He_\Lambda$	11.2	78	2.47	8.9
$^5He_\Lambda$	7.6	37	—	—

(*) In nuclear emulsion at standard density. For the range-energy relations used, see ref. (4).

Fig. 1, a photomicrograph, shows a typical one-prong event (« hook ») found in the course of the present work. The micron scale in this figure illustrates the inconspicuous nature of such events. This « hook » could possibly be identified with the two-body decay of $^4He_\Lambda$ listed in Table I; it is produced at point O by K^--capture and presumably decays at point O' yielding a recoil R of ~ 9 μm range.

In this work, we confined ourselves to « hooks » having recoils with a range R_0 lying between 8 and 50 μm. The lower limit was chosen so as not to exclude the $^4He_\Lambda$ decay just referred to, while the upper limit was chosen so as to include the two-body decays of $^3H_\Lambda$ ($R_0 = 35$ μm) as well as on the basis of our knowledge of recoil spectra in π^--mesic decays (4).

The true π^0-decays were distinguished from Coulomb scatterings on the basis of the angle, θ, between the directions of the connecting track (OO')

(5) C. FRANZINETTI and G. MORPURGO: *Suppl. Nuovo Cimento*, **6**, 469 (1957).

in Fig. 1 and of the recoil ($O'R$) at their point of intersection. Since most ($\sim 99\%$) of the hyperfragments produced in K^--capture decay at rest (4), their recoils should be isotropically distributed, while Coulomb scattering is very strongly peaked forward. One obviously has to choose a cut-off angle θ such that most of the true π^0-events are retained while at the same time discriminating as well as possible against scatterings. This cut-off angle was estimated to lie between 60° and 70°; a value $\theta = 66°$ was ultimately adopted. The effectiveness of this discrimination will be discussed in Section 4·1.

2·2.2. Two-prong events. – Events in this category are analysed by momentum balance in the same manner as non-mesic hyperfragments (1), with the help of an electronic computer. The code is so set up that at most one neutral particle, *e.g.* the π^0, is considered in making a momentum balance.

Fig. 1. – Photomicrograph of a typical « hook ». This event is consistent with the interpretation $^4He_\Lambda \to \pi^0 + {}^4He$.

2·3. *Theoretical background.* – The study of hypernuclei decaying by π^0-emission may be expected to shed light on the neutral decay mode (2′) of the free Λ. Of particular interest is the extent of parity non-conservation (6) in this process. Assuming the Λ to have spin $\frac{1}{2}$ (6,7), its decay may involve s and p waves (8); we denote the amplitudes for these channels in the neutral mode by s_0 and p_0 respectively. The corresponding amplitudes in the charged mode will be called s_- and p_-. While

(6) R. Plano, A. Prodell, N. Samios, M. Schwartz, J. Steinberger, P. Bassi, V. Borelli, G. Puppi, H. Tanaka, P. Waloschek, V. Zoboli, M. Conversi, P. Franzini, I. Mannelli, R. Santangelo, V. Silvestrini, D. A. Glaser, C. Graves and M. L. Perl: *Phys. Rev.*, **108**, 1353 (1957); F. S. Crawford jr., M. Cresti, M. L. Good, K. Gottstein, E. M. Lyman, F. T. Solmitz, M. L. Stevenson and H. K. Ticho: *Phys. Rev.*, **108**, 1102 (1957).

(7) M. Ruderman and R. Karplus: *Phys. Rev.*, **102**, 247 (1956).

(8) T. D. Lee and C. N. Yang: *Phys. Rev.*, **109**, 1755 (1958).

rather extensive data ([6,7,9]) bearing on $|s_-/p_-|$ are available, very little is known experimentally about s_0 and p_0.

DALITZ ([9]) has pointed out that ${}^4\mathrm{He}_\Lambda$ provides a favorable case for gaining such knowledge. Thus, for example, the decay mode

$$(3) \qquad {}^4\mathrm{He}_\Lambda \to \pi^0 + {}^4\mathrm{He}$$

can proceed only through either the s or p channel, according as to whether the spin of ${}^4\mathrm{He}_\Lambda$, $J({}^4\mathrm{He}_\Lambda)$, is 0 or 1. Hence the ratio $R({}^4\mathrm{He}_\Lambda)$ of mode (3) with respect to all other π^0-modes of ${}^4\mathrm{He}_\Lambda$ is a measure of either $|s_0|^2$ or $|p_0|^2$ if $J({}^4\mathrm{He}_\Lambda)$ were known. However, as a consequence of charge independence (or symmetry), which is well borne out by the equality of their binding energies ([4]), ${}^4\mathrm{H}_\Lambda$ and ${}^4\mathrm{He}_\Lambda$ have the same spin. The analogous branching ratio, $R({}^4\mathrm{H}_\Lambda)$ for the mode

$$(3') \qquad {}^4\mathrm{H}_\Lambda \to \pi^- + {}^4\mathrm{He}$$

of ${}^4\mathrm{H}_\Lambda$ is governed by entirely similar considerations, and has already been investigated experimentally ([10]). Thus it becomes possible, at least in principle, to compare the p/s ratios in the neutral and charged modes without a knowledge of the spin of the two $A = 4$ hypernuclei. Indeed, $R({}^4\mathrm{H}_\Lambda) = R({}^4\mathrm{He}_\Lambda)$ implies $|p_0/s_0| = |p_-/s_-|$, as long as one neglects departures from charge symmetry.

3. – Experimental procedure.

3·1. *Emulsion stacks.* – The majority of the events reported here ($\sim 80\,\%$) were located in the EFINS stack of the EFINS-NU collaboration experiment ([4]). In addition, data from $\sim 40\,\%$ of the NU stack as well as from a Berkeley stack (1U) (*) were included to increase the statistics.

These emulsion stacks were all exposed to enriched K^- beams from the Berkeley Bevatron. The number of K^- stars examined (at least one charged prong) was found to be $(1.9 \pm 0.3)\cdot 10^4$ for the EFINS stack and was estimated to be about the same for the entire NU stack, while the Berkeley stack 1U contained only $\sim 2\cdot 10^3$ K^- stars. Further details of exposure and calibration of the stacks are discussed elsewhere ([4]).

([9]) R. H. DALITZ: *Phys. Rev.*, **112**, 605 (1958).

([10]) R. AMMAR, R. LEVI SETTI, W. E. SLATER, S. LIMENTANI, P. E. SCHLEIN and P. H. STEINBERG: *Mesic decays of hypernuclei from* K^- *capture - II: Branching ratios in the mesic decay modes of* ${}^3\mathrm{H}_\Lambda$ *and* ${}^4\mathrm{H}_\Lambda$. Report submitted to the *Annual International Conference on High Energy Physics at Kiev* (1959).

(*) We are greatly indebted to Dr. W. H. BARKAS for the loan of this stack.

3·2. *Scanning of the stacks.* – The stacks were area-scanned with 10× oculars and 12× air objectives. When a K^- star was located, it was examined under 53× oil objective and each non-minimum track was followed to the end of its path in one given pellicle. In the scanning, no attempt was made to trace the prongs from the K^- stars into neighbouring pellicles. All connected stars found in this manner were then recorded.

With respect to the « hooks », the scanners were instructed to record all events with $R_0 \geq 5$ μm and $\theta \geq 45°$. The cut-offs $R_0 \geq 8$ μm and $\theta \geq 66°$ were imposed on the data only later. This procedure was intended to eliminate subjective bias.

The EFINS and NU stacks had previously been scanned in a less thorough manner, primarily to detect π^--mesic hyperfragments; at that time, an attempt to record « hooks » was made only in about 50% of the EFINS stack. Ultimately, we wish to compare our results with those of the EFINS-NU collaboration ([4,10]) which to date includes only events from that previous scan. Thus the efficiency ε for detecting « retained hooks » (see Section 3·3) relative to π^--events in that scan was evaluated from the number of coincidences in the two scans of the EFINS stack. A value $\varepsilon = 1.38 \pm 0.09$ was found for this stack, which, as noted, yielded ~ 80% of our « hooks ». For the NU stack, which was scanned only once for « hooks » (as compared with ~ 1.5 scans for the EFINS stack), $\varepsilon = 1.26$ was inferred from the EFINS data. Since the Berkeley stack contributed negligibly to our final results, its scanning efficiency is not discussed. The absolute detection efficiency for « retained hooks » in the EFINS stack was 0.86 ± 0.04.

3·3. *Measurement of ranges and angles.* – The range R_c of the connecting track, together with the recoil range R_0 and the angle θ (see Section 2·2) were measured for all « hooks ». Only events satisfying the following three conditions were retained:

$$R_c \geq 5 \text{ μm},$$

$$8 \text{ μm} \leq R_0 \leq 50 \text{ μm},$$

$$\theta \geq 66°.$$

For each such event, all grey and black prongs, of the parent K^- star were followed (through several pellicles if necessary) to their ends. This was done to check whether any other prongs of the K^- were due to strange particles. Since only one such particle (charged or neutral) can result from K^--absorption, such an observation would automatically rule out the « hook » as a possible hyperfragment. About 1% of the events in question were discarded on the basis of this check. A comparable number of events were also discarded be-

cause the event was obviously a 1-prong Σ^--star (*e.g.* it showed unmistakably an Auger electron). A « hook » was retained if all the above conditions were met.

For the two-prong events, we measured R_c, the ranges R_1, R_2 of the two prongs, and the space angle φ between them. We considered only those 2-prong events with R_1, $R_2 \geqslant 5$ μm and with connecting tracks suitable for making a determination of charge (see Section 3·4).

3·4. *Charge identification.* – In order to extract the π^0 decays from among the retained « hooks », it is necessary to determine the mass and/or charge of the events. These parameters can, at least for favorable cases, be deduced from ionization measurements on the connecting track.

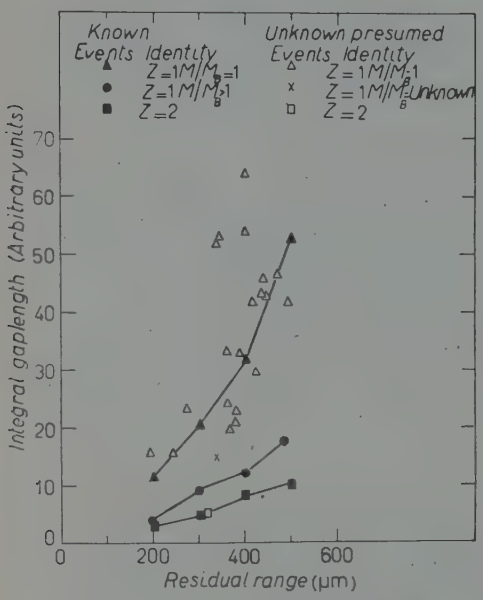

Fig. 2. – Integral gap length for the EFNIS stack. The curve for $Z=1$, $M/M_B=1$ is the average of results from two known events (protons from the decay of Σ^+). The curve for $Z=1$, $M/M_B>1$ is the average result from 4 H_Λ events (4), (two each of $^3H_\Lambda$ and $^4H_\Lambda$). The curve for $Z=2$ is the average of the results from 2 He_Λ events (4). The results of measurements on the unknown events are also shown together with their presumed identity. Only tracks with dips $\leqslant 30°$ are shown here.

The type and scope of these measurements were dictated primarily by the properties of the emulsion stacks as well as by the fraction of events that each contributed to the total. The three stacks were calibrated as follows:

i) EFINS stack. – Since ~80% of the events came from this stack, extensive calibration was performed on it. For $R_c \geqslant 300$ μm, *integral gap length* was generally sufficient as a sensitive parameter without normalizing the gap lengths observed within each pellicle. It was possible, with tracks of such lengths, to distinguish particles of baryonic mass M_B from the known hyperfragments with mass $\geqslant 3M_B$. The various calibration points for this gap-length measurement are shown in Fig. 2, together with points corresponding to unknown events. Profile measurements (11) were performed for each

(11) G. Alvial, A. Bonetti, C. Dilworth, M. Ladu, J. Morgan and G. Occhialini: *Suppl. Nuovo Cimento*, **4**, 244 (1956).

track with $R_c \lesssim 300$ μm. The thickness of the track T_n was measured at each residual range nt. The cell length t was chosen as ≈ 0.57 μm while n ranged from about 2 to about 100. Considerable difficulties were encountered in using the mean $\overline{T}$ of the distribution $\{T_n\}$ as a charge (Z) sensitive parameter. In the thick pellicles used, $\overline{T}$ was observed to vary with depth by about 30% from top to bottom. This may have been caused by a temperature gradient in the unmounted pellicles during the hot « stage » of development. $\overline{T}$ was normalized to account for this gradient as well as for variations (of order 2%) in the lateral shrinkage. The resulting mean normalized track thickness, $\overline{T}_0$, is plotted in Fig. 3*a*, giving (79 ± 7)% discrimination between $Z = 1$ and $Z = 2$.

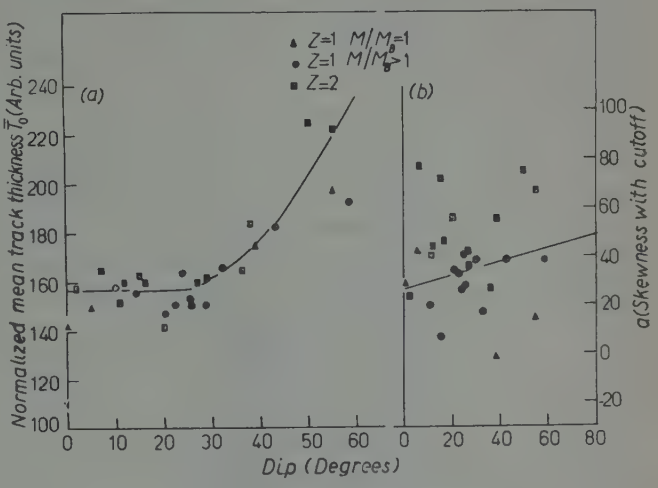

Fig. 3. – *a*) Mean normalized track thickness $\overline{T}_0$ *vs.* dip for EFINS stack using events with previously determined identity [4]. *b*) Skewness α [12] with 3.75 σ cutoff and replacement, *vs.* dip for EFINS stack using the same events as *a*).

In addition, the skewness of the distribution $\{T_n\}$, is found to be a charge sensitive

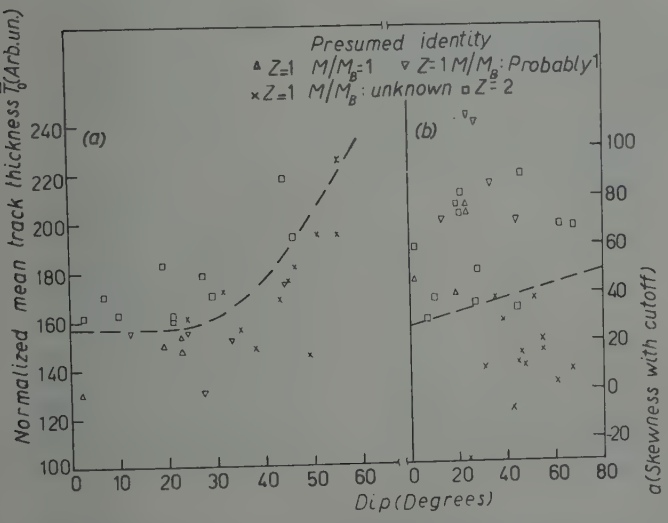

Fig. 3'. – This shows the results of measurements on the unknown tracks together with their assigned identity. In most cases several parameters have gone into the assignment of an identity. (One of the two prong $^4He_\Lambda$ events with a steep connecting track is not shown in the figure. It gave a value $\overline{T}_0$ which is off scale and clearly $Z = 2$; the projected range was too short to give a meaningful α).

parameter, probably related to the presence of sub-δ-rays, and the tendency to form gaps. Details of this method have been described elsewhere [12]. The calibration based on events of independently known identity is shown in Fig. 3*b*. All the measured « hooks » of the present experiment are plotted together with their presumed identities in Fig. 3′. In most cases several ionization parameters were used for the identification of a given event.

It is worth pointing out that for flat tracks ($\leqslant 30°$ dip) this profile technique may also give some information concerning the masses of the particles. At the same residual range, particles of baryonic mass may be expected to yield more δ-rays (and sub-δ-rays) than for example ${}^{3}H_{\Lambda}$ or ${}^{4}H_{\Lambda}$. Consequently the simultaneous determination of both the thickness $\bar{T}_0$ and the skewness α may enable one to discriminate between ${}^{4,5}He_{\Lambda}$, ${}^{3,4}H_{\Lambda}$, and Σ (or p) according as to whether $\bar{T}_0$ and α are 1) both large, 2) both small, or 3) $\bar{T}_0$ small and α large, essentially confirming a trend noted earlier [12]. However due to the poor statistics available on flat tracks with $M_B \geqslant 3$, one cannot exclude the possibility that for $Z = 1$ both the events with $M_B = 1$ and $M_B \geqslant 3$ belong to a single population which is not well delineated from that of $Z = 2$ for dips $\leqslant 30°$. Even the realization of this possibility is not expected to alter the presumed identities of the « hooks » significantly, since a variety of ionization parameters were used. For large dips the discrimination appears to be adequate and not very sensitive to M_B.

ii) NU stack. – In these pellicles which were thinner and showed less gradient than i), the unnormalized *mean track thickness* $\bar{T}$ was found adequate as the primary means of charge iden-

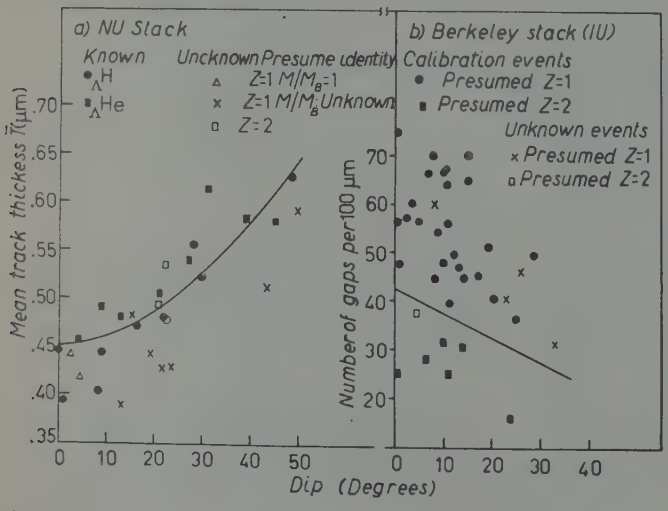

Fig. 4. – *a*) Mean track thickness $\bar{T}$ for NU stack. The known events are those of ref. [4]. The presumed identities of the unknown events are also indicated. *b*) Number of gaps/100 μm for Berkeley stack. See Sect. **3**·**4** for details of calibration.

[12] R. G. AMMAR: *A possible method of specific charge identification from profile measurements in nuclear emulsions*, to be published in *Nuovo Cimento*.

tification ([13]). The cell length t was here chosen to be ~ 0.45 μm and n ranged approximately between 60 and 80. The calibration used is reproduced in Fig. 4*a*. The discrimination between $Z=1$ and $Z=2$ is $(89 \pm 7)\%$ effective. For longer tracks ($R_r \geqslant 300$ μm), the *number of gaps* was used as a subsidiary means of identification. The corresponding calibration is not reproduced here.

iii) Berkeley stack 1U. – This stack was very underdeveloped and hence singularly suited for charge determinations based on the *number of gaps*. With a view towards obtaining as a by-product a rough estimate of the charge spectrum of the prongs from K^- stars, the corresponding calibration was performed in the following manner: All prongs from K^--captures with ranges $\geqslant 80$ μm and with dips $\leqslant 30°$ were gap-counted. For any given pellicle, this separates the prongs into two groups which presumably represent $Z=1$ and $Z=2$. This procedure was carried out for two pellicles. A difference of about 8% was observed between the mean gap-counts for either pellicle and the mean of both. This may be taken as a rough measure of the development fluctuations from pellicle to pellicle. To obtain the calibration shown in Fig. 4*b*, the gap-counts from the two pellicles were normalized to their mean and combined.

3·5. *Background events.*

3·5.1. Σ^--captures. – 1-prong Σ^- stars constitute the major contaminant of the retained « hooks », and are moreover isotropically distributed in θ like true π^0-hyperfragments. In addition 2-prong Σ^- stars may also simulate true π^0 decays involving 2 charged particles. Hence it is useful to know both the range and prong number distributions for Σ^- stars. Fig. 5

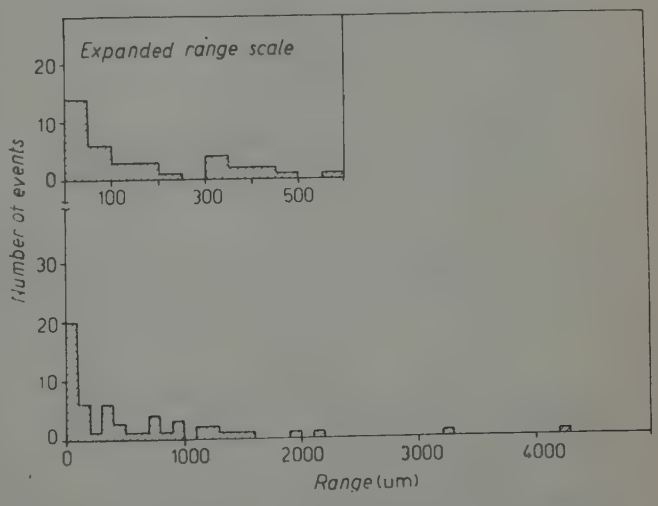

Fig. 5. – Range distribution of connecting tracks for secondary stars ($\geqslant 2$ prongs) from K^--captures. Only tracks with range $\geqslant 5$ μm and which stop in a single (~ 1200 μm thickness) are considered.

([13]) S. Limentani, P. E. Schlein and P. H. Steinberg: private communication. I am greatly indebted for this information which simplified the calibration of the NU stack.

shows the range distribution of the connecting tracks of a representative sample (~ 50) of stars with two or more prongs. Where the connecting tracks are long ($\geqslant 200$ μm), one can easily establish that they are indeed due to Σ's. For shorter ranges this is, however, no longer possible in general: hence the distribution of Fig. 5 undoubtedly includes some hyperfragments. This percentage may be estimated by comparing a subset of the distribution of Fig. 5, *viz.* that of connecting tracks of stars with three or more prongs, with the grand distribution. In this manner the hyperfragment component due to two prong non-mesic He_Λ was estimated to be $\sim 20\%$ of the events with connecting tracks < 200 μm. The range distribution in Fig. 5 is influenced by the particular thickness (~ 1200 μm) of the pellicles used, since only connected stars contained in the same pellicle were scanned for. This distribution may be compared with the range distribution independent of pellicle thickness ([14]).

The prong number distribution of 150 Σ^--stars (see also ([15])) having at least one prong, is shown in Fig. 6-1. There may have been a bias against the detection of certain one-prong configurations, *e.g.* those in which one short prong is emitted forward. For our purposes there was no need to correct for this possible bias, for reasons which will become apparent subsequently (See Sect. 4·1.1).

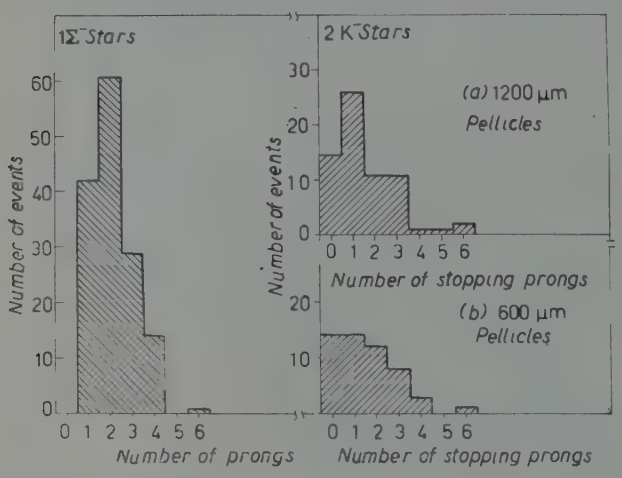

Fig. 6. – 1) Prong number distribution of presumed Σ^--stars. Only those stars were selected for which the connecting track was sufficiently long ($\geqslant 200$ μm) to permit identification as Σ^-. 2) Distribution of the number of stopping prongs per K^--capture in which no charged strange particle comes to rest in the original pellicle for (*a*) 1200 μm pellicles and (*b*) 600 μm pellicles. Only prongs with range $\geqslant 13$ μm are included.

3·5.2. Coulomb scatterings. – To assess the magnitude of the contamination contributed by Coulomb scatterings we need to know the flux of particles and the scattering cross-section as a function of residual range.

([14]) F. Gilbert, C. Violet and R. White: *University of California Rad. Lab., Report* UCRL-4814 (1957).

([15]) N. N. Biswas and M. Ceccarelli: *Nuovo Cimento*, **8**, 599 (1958).

In estimating the flux, we confine ourselves to events capable of simulating acceptable « hooks ». Hence, in exploring the prong number and range distributions, we retain only K^--stars in which no charged strange particles (stopping in the original pellicle) were emitted. This set undoubtedly includes some events in which the strange particle stops in a neighbouring pellicle; no attempt was made to eliminate these events from the distribution. However, the number is expected to be less than the frequency ($\sim 21\%$) of charged strange particles emitted from K^--stars ([16]). In addition, since our criteria (see Section 3·3) require events with $R_0 \geqslant 8$ μm, and ranges $R_c \geqslant 5$ μm, we include only prongs with ranges $\geqslant 5 + 8 = 13$ μm. Fig. 6-2 shows the resulting distributions for the number of stopping prongs from K^- stars, both for the 1200 and the 600 μm pellicles. Figs. 7 and 8 show the range distributions of these prongs, again separately for the two thicknesses. Fig. 8 also illu-

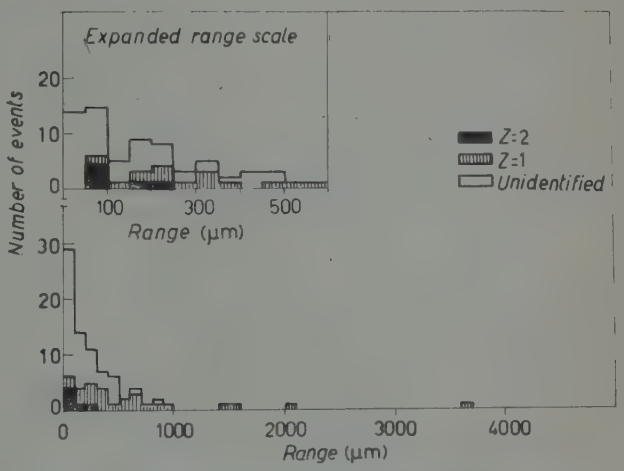

Fig. 7. Range distribution of stopping prongs from K^--capture in which no charged strange particle comes to rest in the original pellicle (1200 μm thick). Only prongs with range $\geqslant 13$ μm are included.

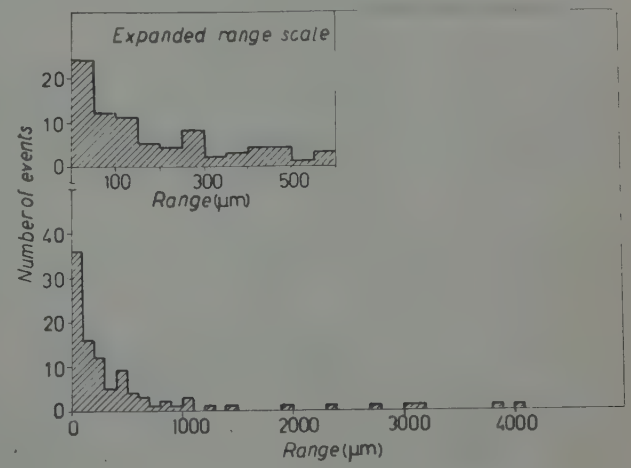

Fig. 8. – Similar to Fig. 7 but for 600 μm pellicles. In addition the charge spectrum of those prongs with range $\geqslant 80$ μm and dip $\leqslant 30°$ are also indicated.

([16]) G. L. Bacchella, A. Berthelot, A. Bonetti, O. Goussu, F. Lévy, M. René, D. Revel, J. Sacton, L. Scarsi, G. Tagliaferri and G. Vanderhaeghe: *Nuovo Cimento*, **8**, 215 (1958).

strates the charge spectrum of flat prongs with ranges $\geqslant 80\ \mu m$ (see Section 3·4).

Fig. 9 shows graphs of the differential scattering probability dP/dR for Coulomb scattering through angles $\theta \geqslant 66°$ as a function of residual range,

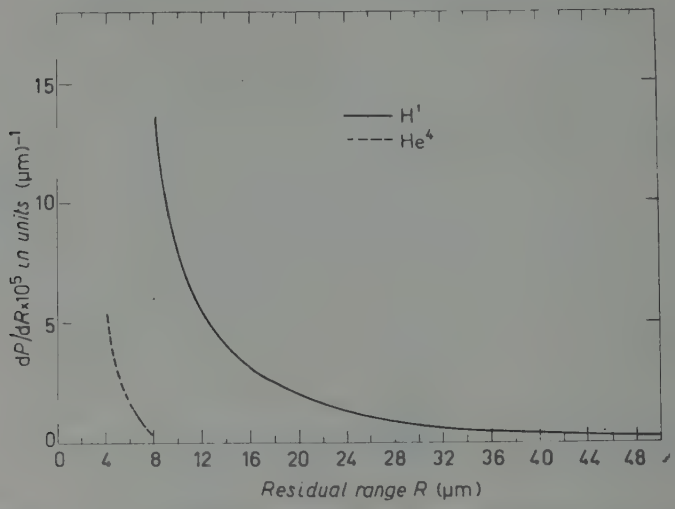

Fig. 9. – Differential probability dP/dR for Coulomb scattering through an angle $\geqslant 66$ as a function of residual range. This was calculated using Williams' cross section ([16]) and appropriate emulsion quantities.

for protons and for α-particles. These graphs were computed from the formulae given by Williams ([17]) using the constants appropriate to nuclear emulsion.

Scatterings may also lead to two charged prongs in a configuration simulating a true π^0 decay. This possibility was assessed on an individual basis for those events either assigned to $Z = 2$ from ionization measurements or which were not Σ^- captures (see Section 4·2).

4. – Results discrimination between true π^0-events and background.

4·1. *Acceptable one-prong events or « hooks ».* – A total of 94 acceptable « hooks » were found. Of these, 69 had sufficiently long and/or flat connecting tracks to permit a charge assignment, *e.g.* a minimum projected range of $\sim 50\ \mu m$ was necessary to permit charge identification in the EFINS stack.

([17]) E. S. Williams: *Proc. Roy. Soc.* (*London*), A **169**, 531 (1939); *Phys. Rev.*, **58**, 292 (1940).

The remaining 25 events could not be identified. The range (R_c) distributions of the connecting tracks for all the 1-prong events are shown in Fig. 10 separately for the 1200 μm and the 600 μm pellicles. The charge and mass of each primary track are indicated wherever they could be determined.

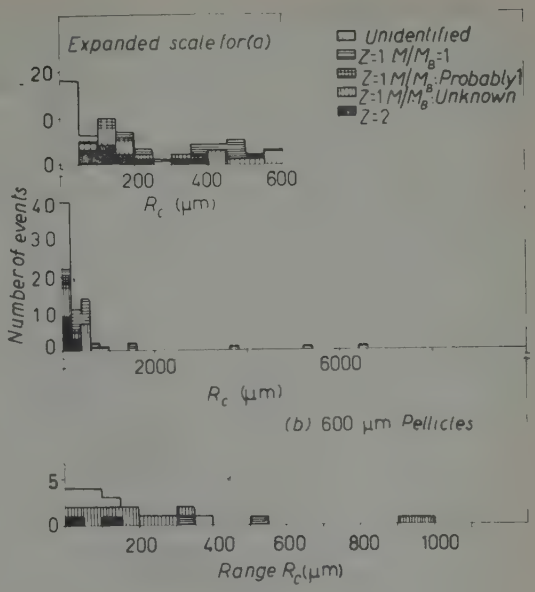

Fig. 10. – Range distribution of connecting tracks for all 1-prong events. The charge and mass character of the connecting track is indicated when known.

4·1.1. Identified charge $Z = 1$. – Fig. 11 shows the distribution of the ranges R_0 of these « hooks » of which the primary (connecting) track was assigned to *charge* 1. To provide the basis for an estimate of the number of Coulomb scatterings present, the distributions over θ, in intervals of equal solid angle, are also shown in this figure. These distributions include altogether 55 events, and are displayed separately for the two pellicle thicknesses used. Specific symbols are used in this figure to represent the various categories of events distinguished by the information available about their masses: i) $M/M_B = 1$ with fair certainty; ii) M/M_B probably 1, on the basis of small $\bar{T}_0$ and large α (see Section 3·4)

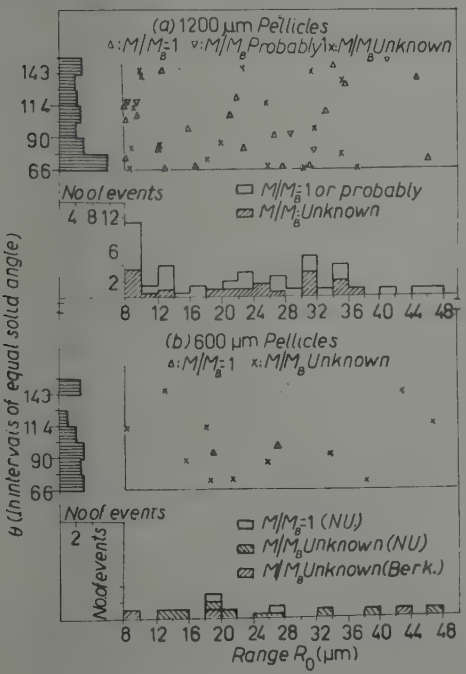

Fig. 11. – Joint distribution of R_0 and θ for 1-prong events for (*a*) 1200 μm and (*b*) 600 μm pellicles. The mass of the particle is also indicated where known.

but without recourse to gap lengths; and iii) M/M_B unmeasurable. Categories ii) and iii) consist of short and/or steep events. For such events even the assignment of $Z = 1$ is made with less confidence than for group i).

In the range of interest, the scattering is most probable for ranges between 8 and 10 μm, where the probability is about $2 \cdot 10^{-4}$. The « flux » is estimated from the number of observed K^- stars (see Section 3·1), the number of stopping prongs/star longer than 50 μm (from Figs. 6-2, 7 and 8), and from the charge spectrum of the stopping prongs (Fig. 8). An upper limit for the total number of scatterings expected is about 6, distributed 4:2 between the events from the 1200 μm and the 600 μm emulsions, respectively. The data of Fig. 11 (θ-distributions) are quite consistent with this estimate. The effect of nuclear scattering has been estimated to be negligible.

Very simple order-of-magnitude estimates already indicate that the relative proportion of one-prong Σ^--stars among the 55 events here considered could be overwhelming. For this reason it appears preferable to analyse the data internally, *i.e.* to use our partial knowledge of the mass spectrum of these events as well as of the range distribution of $^{3,4}H_\Lambda$ hypernuclei (4). According to Fig. 5, about $\frac{1}{2}$ of the Σ^--stars have ranges greater than 300 μm. On the other hand, only about $\frac{1}{3}$ of the $^{3,4}H_\Lambda$ go beyond this range. For the EFINS stack 17 of the $Z = 1$ events with connecting tracks longer than 300 μm received a unique mass assignment; *none* had a mass different from M_B. Consequently the number of $^{3,4}H_\Lambda$ events with $R_r \geqslant 300$ μm relative to that of the Σ^--events is less than 1/17. To extrapolate into the remaining range between 50 and 300 μm, we note that about $\frac{1}{3}$ of the Σ^--events (Fig. 5) and roughly $\frac{1}{2}$ of $^{3,4}H_\Lambda$ hypernuclei (Ref. (4)) lie in this range. Hence the probable fraction of true π^0-decays in this range is less than about 12%. Thus the present experiment can contribute little to the study of $^{3,4}H_\Lambda$ decaying by π^0-emission. One can perhaps infer an upper limit for the frequency of the decay mode

$$^3H_\Lambda \rightarrow \pi^0 + {}^3H \tag{4}$$

as follows. In Fig. 11 four events are located with $R_0 \approx 35$ μm, the predicted R_0 for (4). Of these two are ruled out as having baryonic mass. Considering that only 70% of the full solid angle has been retained for the acceptable « hooks », not more than 3 ± 2 decays (4) were contained in the total volume scanned as compared to 5 ± 3 2-body π^- decays of $^3H_\Lambda$. In computing this latter number from the data of Ref. (4), due account has been taken of relative and absolute scanning efficiencies.

4·1.2. Identified charge $Z = 2$. – The conditions which must be fulfilled for charge assignment ($R_r \geqslant 50$ μm) automatically rule out the presence of hyperfragments with $Z > 2$ since the range spectrum of such events is

known to cut-off sharply beyond this range (4). For this reason no direct discrimination of $Z = 2$ from higher charges was undertaken. There are a total of 14 events of this kind. The distribution of the recoils R_0 is shown in Fig. 12. A very marked peak for R_0 between 8 and 10 μm emerges. A comparison with Fig. 11 indicated not only that our methods of charge discrimination are effective, but also that the « hooks » of charge 2 have an R_0 spectrum very different from that of $Z=1$ events. The probability of collecting, in a purely random manner, a population so alien in character to the distribution of the dominant $Z = 1$ events, is vanishingly small.

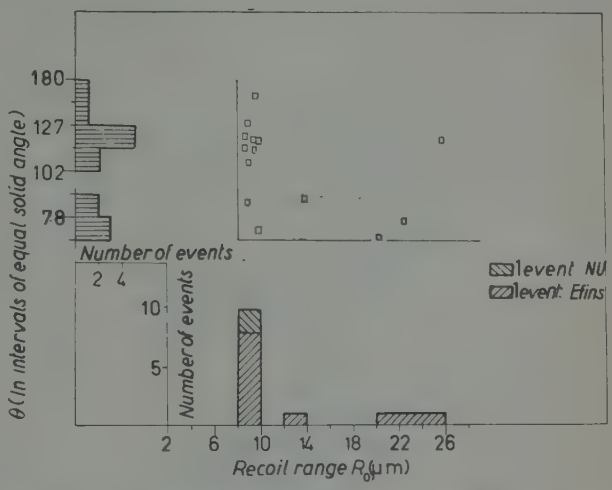

Fig. 12. – Joint distribution of R_0 and θ for $Z=2$ events.

The main contaminants of this class of events could be Coulomb scatterings and non-mesic hyperfragments. Since both the cross-section (Fig. 9) and the « flux » are an order of magnitude smaller here than for $Z = 1$, scatterings may be neglected.

As far as the non-mesic hyperfragment contamination is concerned, it may with fair confidence be ruled out on the basis of the following argument: As seen from Fig. 12, our distribution contains no events with R_0 between 26 and 50 μm. The range spectrum of non-mesic one-prong hyperfragments extends up to rather high values (1,18), and should contribute to the empty interval just mentioned. Thus, unless there were a peculiar mechanism to enhance the range spectrum of one-prong non-mesic He_Λ events in the region between 8 and 26 μm, the contribution of such events to this region should be comparable to that in the region (26÷50) μm, *viz.* essentially nil.

Thus we conclude that probably all 14 events are genuine π^0-decays of $^{4,5}He_\Lambda$. The position of the prominent peak in Fig. 12 corresponds exactly to the predicted R_0 for the two-body decay of $^4He_\Lambda$ (see Table I). The more complex π^0-decays of $^{4,5}He_\Lambda$ may of course contribute to this peak and can account, as will be shown, for the rest of the observed distribution.

---

(18) S. Limentani, P. E. Schlein, P. H. Steinberg and J. Roberts: *Bull. Am. Phys. Soc.*, **4**, 289 (1959).

4·1.3. Unidentified charge. – In all, 25 acceptable « hooks » fall into this category. Fig. 13 shows the R_0 distribution of the 18 events in the EFINS stack with $R_c \leqslant 50$ μm. No attempt was made to utilize these events, primarily because at such short ranges R_c the contribution from hyperfragments with $Z > 2$ can neither be ruled out nor assessed at present.

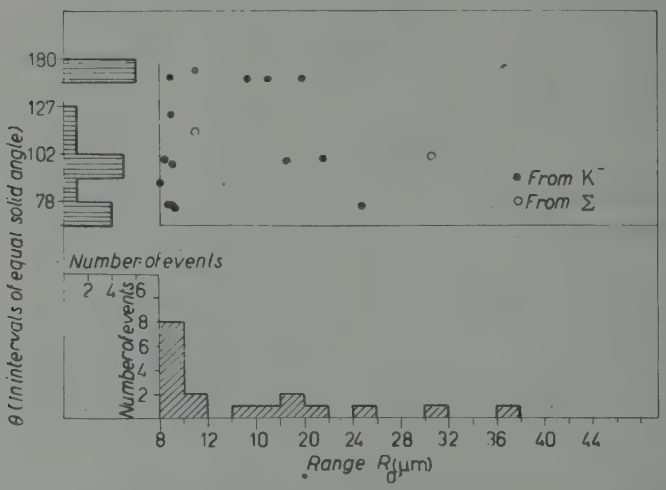

Fig. 13. Joint distribution of R_0 and θ for unidentified events with 5 μm $\leqslant R_c \leqslant$ 50 μm. Only events from the EFINS stack are included.

4·2. *Two-prong events.* – Silverstein's [1] code, restricted to search for He_Λ decays, was the primary means of kinematic analysis. We did not look for the decay modes

$$(5) \qquad {}^4He_\Lambda \begin{cases} \nearrow \pi^0 + p + d + n \\ \searrow \pi^0 + p + p + 2n \end{cases}$$

involving more than one neutral particle. Also, we did not attempt to interpret the results of the code analysis in terms of ${}^5He_\Lambda$ π^0-decays, because the most abundant π^0-decay of ${}^5He_\Lambda$ is probably

$$(6) \qquad {}^5He_\Lambda \to \pi^0 + n + {}^4He$$

which yields only *one* visible prong. This expectation assumes charge independence and is based on the fact that for ~ 60 uniquely identified examples of the π^--decay of ${}^5He_\Lambda$ (Ref. [4]) no mode other than

$$(6') \qquad {}^5He_\Lambda \to \pi^- + p + {}^4He$$

has been reported. We are thus confined to detecting the decays

$$(5') \qquad {}^4\mathrm{He}_\Lambda \begin{cases} \nearrow \pi^0 + \mathrm{d} + \mathrm{d} \\ \searrow \pi^0 + \mathrm{p} + \mathrm{t} \end{cases} .$$

In selecting the events for analysis it is useful to refer to Fig. 14 where the kinematics for the decays (5′) are translated into the observable ranges and angle; in this manner events clearly inconsistent with (5′) may be rejected at the outset. These possible background events are 2-prong Σ^--stars, scat-

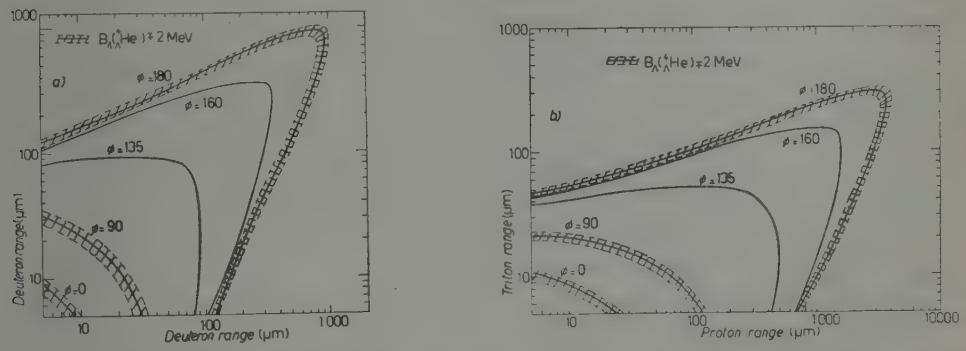

Fig. 14. – Possible configurations for the charged particles from the decays: *a*) ${}^4\mathrm{He}_\Lambda \to \pi^0 + \mathrm{d} + \mathrm{d}$ and *b*) ${}^4\mathrm{He}_\Lambda \to \pi^0 + \mathrm{p} + \mathrm{t}$. Relativistic kinematics were used for the π^0 only. φ is the space angle between the two prongs. Ranges refer to nuclear emulsion at standard density.

terings with visible recoils, and 2-prong hyperfragments. For the EFINS stack it was found that $\sim 10\,\%$ of all 2-prong events with R_r (projected in the plane of the emulsion) $\geqslant 50$ μm were able to simulate the decays (5′) giving « acceptable » binding energies comprised between -2.5 and 6.5 MeV centered around the approximate binding energy (B_Λ) of ${}^4\mathrm{He}_\Lambda$. Not all events received a code analysis. Since only decays (5′) are sought, the code analysis is equivalent to assuming only 3 sets of identities for the two prongs, viz. (dd), (pt), and (tp). These permutations were sometimes performed manually. A total of 13 events, satisfying the criteria for charge identification in their respective stacks, gave « acceptable » binding energies. Of these, 2 were identified as $Z = 2$ from ionization measurements, and for each of these, scattering was ruled out on the basis of the observed configuration (*e.g.* low cross-section, lack of coplanarity, etc.). Non mesic He_Λ with 2-prongs and low visible energy release is probably rare (no such case was found in 33 2-prong

He_Λ events analyzed in the NU stack ([19]). Since, in order to simulate a π^0-event, the prongs must also be favourably oriented, we conclude that the contribution of non mesic He_Λ to the present statistics (2 events) is not significant. The events are summarized in Table II.

TABLE II. – *2-prong events which have been interpreted as* $^4He_\Lambda$.

Parent	Connecting track		Ranges of prongs (μm)	Spaceangle between prongs	Probable decay mode	$\sim B_\Lambda$ (MeV)
	range (μm)	charge				
K^-	293	2	13.9 9.7	61.5°	$^4He_\Lambda \to \pi^0+p+t$	4.3
K^-	74	2	97.2 45.0	130.5°	$^4He_\Lambda \to \pi^0+d+d$	3.2
Σ^-	12	—	25.0 172.6	147.5°	$^4He_\Lambda \to \pi^0+d+d$	— 2.4

The remaining 11 events were either recognized as being interactions in flight or were assigned to $Z=1$ and are presumably those events capable of simulating true π^0-events. In Table II, a third event (emitted from a Σ^--star) is included for completeness; although neither a Σ nor a scattering R_c is too short to rule out hyperfragments with $Z>2$ and the identification is less certain than for the others.

5. – Discussion and conclusions.

5·1. *Events with* $Z=1$. – The considerations of Section 4·1 lead us to conclude that K^--captures are rather poorly suited for isolating definite cases of π^0-decays of $^{3,4}H_\Lambda$; this is due to the unavoidable presence of an overwhelming background of one-prong Σ^--stars. The mass measurements required are tedious and frequently altogether impossible. Given a sufficiently high flux of K^--particles, Σ^--induced hyperfragments may provide a more convenient way for studying this problem.

([19]) P. E. SCHLEIN: *Phys. Rev. Lett.*, **2**, 220 (1959).

5·2. *π^0-decays of* He_Λ. – As pointed out in Section 2·3 it is important to establish the frequency of decay mode (3) which gives rise to the peak in Fig. 12. In order to do this we must be able to separate the events which represent the decay of $^5He_\Lambda$ from those of $^4He_\Lambda$.

To accomplish this, we adopt the following general procedure: i) assume $|p_0/s_0| = |p_-/s_-|$ *i.e.* the validity of the $\Delta T = \frac{1}{2}$ rule, T being the isotopic spin. (Some relation of this kind is necessary for the separation.) ii) Test the experimental conclusions for consistency with this specific assumption.

5·2.1. $^5He_\Lambda$-events. – Apart from modifying Coulomb effects, the ratio of π^0 modes to π^- modes of $^5He_\Lambda$ should be exactly the same as in the free Λ-decay ([9]), *viz.*, 1 to 2 (from the $\Delta T = \frac{1}{2}$ rule). This, together with the recoil momentum (P_{rec}) spectrum for π^--decays of $^5He_\Lambda$ will be used to subtract the contribution of π^0-decays of $^5He_\Lambda$ from the distribution ot Fig. 12.

The spectrum of the recoil momenta, in the π^--decays, shows the effect of a strong final state interaction ([20]) resulting in a peaked distribution at $P_{rec} \sim 130$ MeV/c. This spectrum can be understood in terms of a simple model in which $^5He_\Lambda$ is assumed to decay into $\pi^- + {}^5Li^*$, with the $^5Li^*$ in the unbound $p_{\frac{3}{2}}$ state. The main peak in the P_{rec} distribution corresponds to those configurations in which the proton is emitted backward in the (p-^{4}He) c.m. system. This is predicted to occur at $P_{rec} = 131.2$ MeV/c, while the corresponding peak for the π^0-decay mode is predicted at $P_{rec} = 121.1$ MeV/c.

To obtain the expected π^0-recoil distribution, for $P_{rec} \geqslant 130$ MeV/c, the empirical distribution for the π^- mode was taken and the momentum scale contracted by 121.1/131.2, *i.e.* the two distributions were normalized to the positions of their peaks. Actually one may in addition expect that the distribution for the π^0 case should be narrower ([21]) than for the π^- since the (^{4}He-n) resonance is sharper than the (^{4}He-p) resonance, (0.95 *vs.* 1.8 MeV relative energy). This may well introduce a small systematic error.

On this basis one finds that the total number of $^5He_\Lambda$ events with $P_{rec} \geqslant 130$ MeV/c (corresponding to $R_0 \geqslant 8$ μm) is 4.2 ± 1.1. This error contains only the various statistical uncertainties, and makes no allowance for systematic errors. Of these events, 1.7 ± 0.7 occur in the region of the peak ($(8 \div 10)$ μm) and 2.5 ± 1.1 in the region $R_0 > 10$ μm.

5·2.2. $^4He_\Lambda$ events. – In order to compare $R(^4He_\Lambda)$ with $R(^4H_\Lambda)$ (cf. Section 2·3), it is necessary to include π^0-neutron-recoil (πnr) decays of $^4He_\Lambda$

([20]) R. G. Ammar, R. Levi Setti, W. E. Slater, S. Limentani, P. E. Schlein and P. H. Steinberg: *Nuovo Cimento*, **13**, 1118 (1959).

([21]) N. Byers and W. N. Cottingham: private communication, to appear in *Nucl. Phys.*

which yield recoil ranges less than 8 μm. These are not retained in the present experiment, and neither are the decays (5). It is hence convenient to define ratios $R'(^4\mathrm{He}_\Lambda)$ and $R'(^4\mathrm{H}_\Lambda)$ in which one excludes from the total those (πnr) decays which yield recoils with less than some momentum P^*_{rec} and those of (5), as well as the π^- counterparts for $^4\mathrm{H}_\Lambda$. The value of P^*_{rec} was chosen as 110 MeV/c which corresponds to ^{3}He recoils with 8 μm range.

It follows from the discussion of DALITZ and LIU [22] and subject to the limitations outlined there that $|p_-/s_-| = |p_0/s_0|$ implies $R'(^4\mathrm{He}_\Lambda) = R'(^4\mathrm{H}_\Lambda)$. Imposing these cut-offs on the data of Ref. [10] one obtains

$$R'(^4\mathrm{H}_\Lambda) = 0.88^{+0.07}_{-0.06}\,, \tag{7}$$

while this experiment yields the value

$$R'(^4\mathrm{He}_\Lambda) = 0.82^{+.15}_{-.18}\,. \tag{7'}$$

The value (7') has been corrected for the systematic error introduced in extracting a small signal from a large background when the probability of making a correct charge identification is less than one. Such a situation indeed exists for He_Λ decays with $R_0 > 10$ μm. For recoil ranges between 8 and 10 μm, this correction is negligible, since the population is evenly distributed between $Z = 2$ and $Z = 1$, as can be seen from a comparison of Figs. 11 and 12. In addition, allowance has been made for the loss of two-body modes in which the recoil is less than 8 μm ($\sim 10\%$) [4]. Finally in computing (7') we used only those 2-prong events which had R_c greater than the minimum range necessary to permit charge identification in a given stack. Thus the 2-prong event from the Σ^--capture with $R_c = 12$ μm was excluded.

The values (7) and (7') are equal within their errors and hence are consistent with the initial hypothesis that $|p_0/s_0| = |p_-/s_-|$. With some qualifications, this consistency lends added support to the $\Delta T = \frac{1}{2}$ rule.

A further useful parameter is ϱ, the ratio of the 2-body π^0-modes to the total number of $^4\mathrm{He}_\Lambda$ π^--decays. The corresponding number of π^--decays were computed from Ref. [4] and [20], taking into account the relative yield of π^- and π^0-decays and the fraction of $^4\mathrm{He}_\Lambda$ which can be charge identified ($\sim 2/3$). One obtains

$$\varrho = 0.7 \pm 0.4\,. \tag{8}$$

---

[22] R. H. DALITZ and L. LIU: to be published in *Phys. Rev.* I am greatly indebted to Prof. DALITZ for a preprint of this article.

Approximately half the contribution to this error comes from the τ^--decays where there is a large uncertainty in determining the fraction of $^4He_\Lambda$ decays amongst the ambiguous events, *i.e.* essentially those with recoils $\lesssim 3$ μm.

This ratio ϱ essentially is a measure of the amount of s or p wave amplitude (accordingly as $J(^4He_\Lambda)$ is 0 or 1) in the neutral mode of the free Λ-decay, and has been calculated by DALITZ and LIU (22). Assuming the $\Delta T = \frac{1}{2}$ rule to hold and taking say $|p_-/s_-| = 1$ for definiteness one obtains from his expressions $\varrho = 0.95$ for $J(^4He_\Lambda) = 0$ and $\varrho = 0.67$ for $J(^4He_\Lambda) = 1$. A far better accuracy than given in (8) is needed before stringent conclusions can be drawn from ϱ.

* * *

I am indebted to Professors V. L. TELEGDI and R. H. DALITZ for much helpful assistance and criticism. In particular I should like to thank Professor DALITZ for many helpful discussions concerning the theoretical aspects of the problem and Professor V. L. TELEGDI for suggesting the problem and for help with the writing of the manuscript. In addition I am grateful for the aid of Professor R. LEVI SETTI in various stages of the experimental investigation.

I should like to thank the following at the Enrico Fermi Institute for Nuclear Studies for their help in scanning the stack: J. BAPTIST, T. BARTHA, W. BEECHER N. CRAYTON, J. CRONIN, C. DOLNICK, R. DOWNEY, H. FINE, D. KENNEDY, P. KLIAUGA, J. MARKIN, M. MCCOY, J. MCQUAID, E. MOORE, J. MOTT, B. POLNY, P. SATTERBLOM, P. SIEVERT, and D. WHITE.

In addition it is a pleasure to thank J. MOTT for help with the measurements, N. CRAYTON for help with the calculations, and P. GYGI for technical aid in setting up the profile microscope and its immediate environs.

I should like to thank Professor J. H. ROBERTS and Dr. S. LIMENTANI for making available the events in the NU stack together with the facilities for making the measurements *in situ*. I should also like to thank the entire NU group for their co-operation.

Finally we wish to extend our appreciation to Dr. E. J. LOFGREN and the Bevatron staff for providing us with the K^- exposure, without which this experiment would not have been possible.

RIASSUNTO (*)

In questo articolo si fa uno studio sistematico dei decadimenti π^0 di ipernuclei leggeri ($A \leqslant 5$) prodotti da cattura K^- in emulsione nucleare. Si sono esaminate approssimativamente $3 \cdot 10^4$ stelle K^- producenti in totale 94 eventi con l rami, eventi che soddisfano le seguenti condizioni: $R_c \geqslant 5$ μm, 8 μm $\leqslant R_0 \leqslant 50$ μm, $\theta \geqslant 66°$, dove R_c è il percorso del primario (traccia di collegamento), R_0 è il percorso del secondario (rinculo) e θ è l'angolo compreso fra tali direzioni nel loro punto di intersezione. Dei 69 eventi di cui si è potuta identificare la carica (Z), 55 hanno $Z=1$ e 14 $Z=2$. Nella categoria $Z=1$ non si sono potuti separare gli eventi π^0 veri dagli eventi Σ^- con l rami a causa del preponderante contributo ($\gtrsim 92\%$) di questi ultimi. Si conclude che con ogni probabilità tutti i 14 eventi con $Z=2$ rappresentano decadimenti He_Λ veri (~ 10 $^4He_\Lambda$ e ~ 4 $^5He_\Lambda$). Oltre a ciò, tre eventi con 2 rami potevano interpretarsi come decadimenti $^4He_\Lambda$. Per i decadimenti π^0 del $^4He_\Lambda$ si può definire il seguente rapporto: $R'(^4He_\Lambda)$=(decadimenti a due corpi)/(tutti i decadimenti — quelli osservabili); in esso i decadimenti «inosservabili» sono decadimenti di rinculo neutronico π^0 con impulsi di rinculo < 110 MeV/c ed altri modi di decadimento con uno o più neutroni. Si trova qui. un valore $R'(^4He_\Lambda)=0.82^{+.15}_{-.18}$. La grandezza analoga per $^4H_\Lambda$ è stata calcolata con i dati di cui alla nota ([10]); si ha $R'(^4H_\Lambda)=0.88^{+0.06}_{-0.05}$. Questi due numeri sono uguali entro i limiti dei rispettivi errori sperimentali. Tale uguaglianza è coerente con l'ipotesi $|p^-/s^+| = |p_0/s_0|$ prevista dalla regola $\Delta T = \frac{1}{2}$. Si è trovato che il rapporto ϱ_4 fra i decadimenti π^0 di due corpi del $^4He_\Lambda$ ed il numero totale dei decadimenti π^- del $^4He_\Lambda$ è uguale a 0.7 ± 0.4. A seconda che lo spin del $^4He_\Lambda$ è 0 o 1 ϱ è una misura dell'intensità dei canali d'onda s o p nel modo neutro del decadimento del Λ libero.

(*) *Traduzione a cura della Redazione.*

IL NUOVO CIMENTO Vol. XIV, N. 6 16 Dicembre 1959

Investigation of a High Energy Electron-Photon Cascade in Emulsion.

E. Fenyves, A. Frenkel and F. Telbisz

Central Research Institute of Physics, Departement for Cosmic Rays - Budapest

J. Pernegr, V. Petržílka, J. Sedlák and J. Vrána

Physical Institute of the Czechoslovak Academy of Sciences
Faculty of Technical and Nuclear Physics of the Charles' University - Praha

(ricevuto il 30 Luglio 1959)

Summary. — A photon initiated high energy electron-photon cascade was investigated. The energy of the primary photon was determined from the longitudinal development and the lateral distribution of the cascade to be about $2 \cdot 10^{12}$ eV. The energy spectrum of electron pairs generated on the first 1.5 cascade units was measured. The spectrum obtained does not deviate significantly from either the spectrum calculated by the Bethe-Heitler theory or from that calculated by Migdal extending the Landau-Pomerančuk-Ter-Mikaelyan theory.

1. – Introduction.

We have investigated a high energy electron-photon cascade found in the plates of the I-stack exposed in the Po-Valley Expedition, 1955 (*). The cascade was originated by a high energy electron pair produced by a photon coming from outside the stack.

The electron-photon cascade lays rather flat in the emulsion (its projection length is about 6.5 mm in one plate) and could be followed in our plates up to a depth of 5 cascade units (1 c.u. = 2.83 cm). We have investigated the primary energy of the photon producing the cascade and the energy spectrum of pairs generated from the origin of the first pair up to a depth of 1.5 c.u.

(*) The authors are indebted to Dr. Lanius for his kind lending them several plates from the Berlin part of the I-stack.

The energy spectrum obtained was compared with the distribution based on the Bethe-Heitler theory ([1]) and with that calculated by MIGDAL ([2]) extending the Landau-Pomerančuk-Ter-Mikaelyan theory ([2-4]) where the influence of the medium on the bremsstrahlung process was taken into account.

2. – Determination of the primary energy.

The energy of the primary photon (E_0) was determined from the Čudakov-Perkins effect ([5-8]) and from the longitudinal and lateral development of the cascade ([9-11]) at depths of 2.8, 4 and 5 c.u.

From the decrease of the ionization up to the distance of 250 μm from the origin of the first pair the energy of the primary photon was evaluated using the Čudakov formula ([5]) and was found to be equal or higher than about $2 \cdot 10^{12}$ eV.

The primary energy of the cascade was determined also following the method of PINKAU ([9]) for longitudinal development of the cascade and using the numerical tables of cascade curves computed bu BUTCHER, CHARTRES and MESSEL ([12]) under approximation A. The error of the primary energy was estimated according to the calculations on the fluctuations of cascades by JÁNOSSY and MESSEL ([13]) (see Table I).

The values of primary energy obtained from the lateral distribution of the cascade at the depths of 2.8, 4 and 5 c.u. are given on Table I; for their determination the total number of electrons (N) inside a circle of radius R around the core was plotted against R for different depths. By fitting these lateral distribution to the N *vs.* $E_0 R$ curves calculated by PINKAU ([10]) on the basis of the expressions given by NISHIMURA and KAMATA ([14]) for the lateral spread of electrons under approximation B, the primary energy (E_0) could be estimated.

([1]) W. HEITLER: *The Quantum Theory of Radiation* (Oxford, 1954).
([2]) A. B. MIGDAL: *Phys. Rev.*, **103**, 1811 (1956).
([3]) L. L. LANDAU and I. A. POMERANČUK: *Dokl. Akad. Nauk SSSR*, **92**, 535, 735 (1953).
([4]) M. L. TER-MIKAELYAN: *Dokl. Akad. Nauk SSSR*, **94**, 1033 (1954).
([5]) A. E. ČUDAKOV: *Izv. Akad. Nauk SSSR*, **19**, 651 (1955).
([6]) D. H. PERKINS: *Phil. Mag.*, **46**, 1146 (1955).
([7]) W. WOLTER and M. MIĘSOWICZ: *Nuovo Cimento*, **4**, 648 (1956).
([8]) K. VLACHOVSKÝ: *Czechosl. Journ. Phys.* (in press).
([9]) K. PINKAU: *Nuovo Cimento*, **3**, 1283 (1956).
([10]) K. PINKAU: *Phil. Mag.*, **2**, 1389 (1957).
([11]) A. A. VARFOLOMEEV and I. A. SVETLOLOBOV: preprint (1959).
([12]) J. C. BUTCHER, B. A. CHARTRES and H. MESSEL: *Nucl. Phys.*, **6**, 241 (1958).
([13]) L. JÁNOSSY and H. MESSEL: *Proc. Phys. Soc.*, A **63**, 1110 (1950).
([14]) J. NISHIMURA and K. KAMATA: *Progr. Theor. Phys.*, **7**, 185 (1952).

TABLE I. – *Energy of the primary photon (in units of* 10^{12} eV).

Method / Depth in c.u.	Longitudinal development: under Approx. A [9-12]	Lateral distribution under Approx. B [10]	Longitudinal development Monte-Carlo calc. [11]	Čudakov-Perkins effect [5]
Origin	—	—	—	$\geqslant 2$
2.8	2.0 ± 0.7	~ 1.9	~ 3.1	—
4	1.0 ± 0.2	~ 1.2	—	—
5	1.1 ± 0.1	~ 0.9	—	—

The above energy values obtained from the longitudinal development and lateral distribution, under approximations A and B respectively, are, however, systematically underestimated because in both approximations not all possible interactions of cascade particles are taken into account and the asymptotic Bethe-Heitler formulas for radiation processes and pair production are used.

A more correct estimation of the primary energy can be obtained using the graphs of VARFOLOMEEV and SVETLOLOBOV [11]. From these data we have obtained a higher value for the energy of the primary photon (see Table I).

For the further considerations the primary energy $2 \cdot 10^{12}$ eV is taken as an accepted value.

3. – Investigation of the spectrum of pairs.

The energies of individual electron pairs generated from the origin of the first pair up to a depth of 1.5 c.u. were determined by the method of Lohrman [15] or from (relative as well as single) scattering measurements. In some cases both methods were used; the results are given in Table II [16].

The histogram on Fig. 1 corresponds to the measured data given in Table II; the scale of the y-axis is reduced by a factor 2 because of the comparison with the theoretical curves drawn for 1 electron with energy $1 \cdot 10^{12}$ eV. The curves B-H and M correspond to the spectrum of pairs calculated by the Monte-Carlo [11] method using Bethe-Heitler formulas [1] and those of MIGDAL [2].

The limits of errors were taken according to the cascade fluctuations given by VARFOLOMEEV and SVETLOLOBOV [11].

---

[15] E. LOHRMAN: *Nuovo Cimento*, **2**, 1029 (1955).

[16] J. PERNEGR, V. PETRŽÍLKA, J. SEDLÁK and J. VRÁNA: *Czechosl. Journ. Phys.* (in press).

TABLE II.

No. of pair	Distance from the origin (c. u.)	Distance from the core (μm)	E (GeV)	No. of pair	Distance from the origin (c. u.)	Distance from the core (μm)	E (GeV)
1	0	—	—	18	0.98	core	0.14
2	0.2	core	160	19	0.98	»	5.8
3	0.2	»	500	20	1.06	»	38
4	0.38	»	2.5	21	1.11	7	1.90
5	0.51	»	30	22	1.22	7	2.0
6	0.57	»	1.16	23	1.22	16	0.21
7	0.60	»	0.32	24	1.23	15	0.11
8	0.64	»	23	25	1.25	130	0.064
9	0.69	»	17	26	1.26	8	3.3
10	0.76	260	0.18	27	1.30	4	0.98
11	0.86	135	0.030	28	1.32	11	0.42
12	0.89	core	1.30	29	1.32	9	1.20
13	0.92	18	0.21	30	1.40	20	5.9
14	0.92	5.5	7.1	31	1.41	18	4.55
15	0.92	core	0.6	32	1.41	8	14.9
16	0.93	340	0.013	33	1.45	9	2.2
17	0.95	9	3.1	34	1.47	9	2.2

From Fig. 1 we can see that due to the large statistical fluctuations the measured spectrum is difficult to be related with either the B-H or M curve.

Similar conclusions can be drawn from the energy spectrum of the first generation of bremsstrahlung photons (Fig. 2) using the method of Mięsowicz and his co-workers ([17,18]). The electron pairs corresponding to the first generation of photons are identified as apparent tridents which originate at distances from the axis of the core not exceeding about 1 μm. The theoretical spectra B-H and L-P-T, calculated on the basis of the Bethe-Heitler ([1]) and the Landau-Pomerančuk-Ter-Mikaelyan ([3,4]) theories, respectively, were drawn according to reference ([18]) taking into account the energy dependence of the cross-section for pair production.

From the above discussion it is clear that no definite conclusion about the validity of the B-H or L-P-T and M theories can be drawn from one or only a few cascades. Our results should be therefore considered as a contribution

([17]) M. MIĘSOWICZ, O. STANISZ and W. WOLTER: *Nuovo Cimento*, **5**, 513 (1957).
([18]) J. BENISZ, Z. CHYLINSKI and W. WOLTER: *Nuovo Cimento*, **11**, 525 (1959).

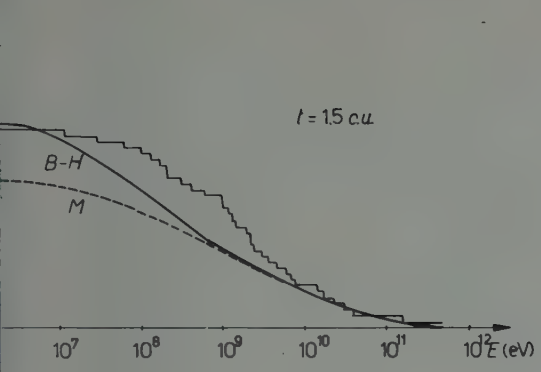

Fig. 1. – Integral energy spectrum of pairs up to 1.5 c.u. The histogram corresponds to the measured data; the curves B-H and M calculated by the Monte Carlo method using Bethe-Heitler and Migdal formulas for a primary electron energy of 10^{12} eV were taken from ref. [11].

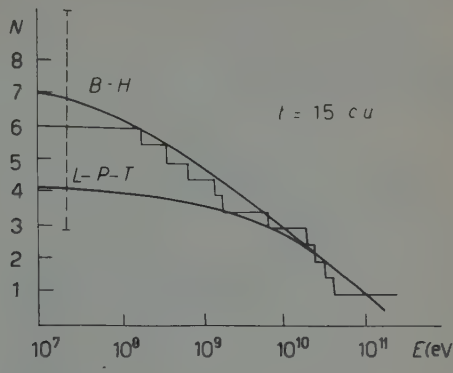

Fig. 2. – Integral energy spectrum of electron-pairs produced by the first generation of bremsstrahlung photons. The histogram corresponds to the measured data of pairs; the curves B-H and L-P-T are calculated on the basis of the Bethe-Heitler and Landau-Pomerančuk-Ter-Mikaelyan theories.

to a much larger statistics of similar events and any definitive conclusions can not be drawn until several laboratories will collect a sufficient number of cascades.

* * *

The authors are indebted to Prof. JÁNOSSY for valuable discussions and to Mr. FARKAS for assistance in the measurements. We wish to express our thanks to Prof. DANYSZ who has kindly provided the emulsion plates for the present investigation.

RIASSUNTO (*)

È stata studiata una cascata di elettroni-fotoni ad alta energia iniziata da un fotone Si è determinata in circa $2 \cdot 10^{12}$ eV l'energia del fotone primario in base allo sviluppo longitudinale ed alla distribuzione laterale della cascata. È stato misurato lo spettro di energia delle coppie di elettroni generate nelle prime 1.5 unità della cascata. Lo spettro ottenuto non differisce in maniera significativa sia dallo spettro calcolato con la teoria di Bethe-Heitler sia da quello calcolato con l'estensione di Migdal della teoria di Landau-Pomerančuk-Ter-Mikaelyan.

(*) *Traduzione a cura della Redazione.*

IL NUOVO CIMENTO Vol. XIV, N. 6 16 Dicembre 1959

Lee Model with Complex Energy Eigenvalues.

R. Ascoli

Istituto di Fisica dell'Università - Torino
Istituto Nazionale di Fisica Nucleare - Sezione di Torino (*)

E. Minardi

Società Nazionale Cogne - Aosta
Istituto Nazionale di Fisica Nucleare - Sezione di Torino (**)

(ricevuto il 21 Agosto 1959)

Summary. — The Lee model with fixed point particles is investigated when complex energy eigenvalues appear in the subspace $(V, N+\theta)$. It is proved that in general such a model has no physical interpretation, at least in the usual framework. Indeed a problem in the subspace $(2V+\theta, V+N+2\theta, 2N+3\theta)$ is considered, and it is shown that expressions which are usually interpreted as probabilities become negative. Such difficulties do not appear in simpler problems.

1. – Introduction.

We know that the following three cases may occur in the Lee model without form factor (1), depending on the values of the masses and of the coupling constant:

1) For sufficiently small values of the coupling constant there are two real discrete eigenvalues of the energy in the subspace $(V, N+\theta)$, the corresponding eigenvectors having opposite norms.

(*) Now at C.E.R.N., Genève.
(**) Now at EURATOM, Bruxelles.
(1) We remember that such a model is consistent only using indefinite metric.

2) One particular value of the coupling constant exists, for which the two real eigenvalues of the energy coincide (so called dipole ghost case).

3) For larger values of the coupling constant two complex conjugate energy egenvalues occur in the same subspace (V, N+0), the corresponding eigenvectors being of zero norm and non-orthogonal.

Till now only the first two cases had been investigated to see whether a physical interpretation is possible at least in the simplest non trivial problem. The first case has been investigated by KÄLLÉN and PAULI [2] in the subspace (V+0, N+2θ) with the conclusion that a physical interpretation is not possible (at least in the usual framework) [3]. The second case has been investigated in the same subspace by W. HEISENBERG [4] with the conclusion that a physical interpretation is possible (at least with some departures from the usual framework [5]).

The purpose of the present paper is to investigate whether a physical interpretation of the theory is possible in the third case.

In this case the problem in the subspace (V+0, N+2θ) is rather simple, and it may be concluded that a physical interpretation in this subspace is possible [6].

The first non trivial problem occurs in the subspace (2V+0, V+N+2θ 2N+3θ). So we are led to a problem with two heavy particles and in particular we need to know the properties of the eigenvectors of the energy in the subspace (2V, V+N+0, 2N+2θ). We shall limit ourselves to the case in which the distance between the two heavy particles is large, because the examination of this case is sufficient to answer the question on the possibility of giving the theory a physical interpretation.

2. – Bound stationary states in the subspace (2V, V+N+0, 2N+2θ).

We investigate here the properties of the bound stationary states in the subspace (2V, V+N+0, 2N+2θ), by supposing the N- or V-particles to be fixed at two points $\boldsymbol{x} = -\boldsymbol{l}$ and $\boldsymbol{x} = \boldsymbol{l}$; let us call them points 1 and 2. Using

---

[2] G. KÄLLÉN and W. PAULI: *Mat. Fys. Medd. Dan. Vid. Selsk.*, **30**, no. 7 (1955).

[3] A physical interpretation also in this case may however be possible by changing the connection between S matrix and Hilbert space (private communication of B. FERRETTI; see also R. J. N. PHILLIPS: *Nuovo Cimento*, **1**, 823 (1955)).

[4] W. HEISENBERG: *Nucl. Phys.*, **4**, 532 (1957).

[5] V. GLASSER: *Proc. of the Annual Int. Conf. on High Energy Phys. at CERN* (1958), p. 132.

[6] R. ASCOLI and E. MINARDI: *Nuovo Cimento*, **8**, 951 (1958) and *Nucl. Phys.*, **9**, 242 (1958-59).

Heisenberg's notation (4), the Hamiltonian in this subspace may be written ($\hbar = c = 1$)

$$(1) \qquad H = \int \mathrm{d}^3k\,\omega a^*(\boldsymbol{k})a(\boldsymbol{k}) + m_{\mathrm{V}}(\psi^*_{\mathrm{V}_1}\psi_{\mathrm{V}_1} + \psi^*_{\mathrm{V}_2}\psi_{\mathrm{V}_2}) - \\ - g_0\pi\sqrt{2}\,[\psi^*_{\mathrm{V}_1}\psi_{\mathrm{N}_1}a(-\boldsymbol{l}) + \psi^*_{\mathrm{V}_2}\psi_{\mathrm{N}_2}a(\boldsymbol{l}) + \psi^*_{\mathrm{N}_1}\psi_{\mathrm{V}_1}a^*(-\boldsymbol{l}) + \psi^*_{\mathrm{N}_2}\psi_{\mathrm{V}_2}a^*(\boldsymbol{l})]\,,$$

where ψ_{V_1}, ψ_{N_1}, ψ_{V_2}, ψ_{N_2} are the destruction operators of the V- and N-particles at the points 1 and 2 respectively; m_{V} is the mass of the V-particle, the origin of the scale of the energies being chosen so that the mass of the N-particle is 0,

$$(2) \qquad a(\boldsymbol{x}) = (2\pi)^{-\frac{3}{2}}\int \mathrm{d}^3k\,\frac{a(\boldsymbol{k})\exp[i\boldsymbol{k}\cdot\boldsymbol{x}]}{\sqrt{2\omega}}\,,$$

$a(\boldsymbol{k})$ and its complex conjugate are the destruction and creation operators for a θ-particle of momentum $\boldsymbol{k}$ and energy $\omega = \sqrt{\boldsymbol{k}^2 + \mu^2}$, μ being the mass of the θ-particle.

The state of the considered system is given by the following expression

$$(3) \qquad |\Phi\rangle = \Big[A\psi^*_{\mathrm{V}_1}\psi^*_{\mathrm{V}_2} + \psi^*_{\mathrm{N}_1}\psi^*_{\mathrm{N}_2}\iint \mathrm{d}^3k_1\,\mathrm{d}^3k_2\varphi(\boldsymbol{k}_1, \boldsymbol{k}_2)a^*(\boldsymbol{k}_1)a^*(\boldsymbol{k}_2) + \\ + \psi^*_{\mathrm{V}_1}\psi^*_{\mathrm{N}_2}\int \mathrm{d}^3k\varphi_2(\boldsymbol{k})a^*(\boldsymbol{k}) + \psi^*_{\mathrm{V}_2}\psi^*_{\mathrm{N}_1}\int \mathrm{d}^3k\varphi_1(\boldsymbol{k})a^*(\boldsymbol{k})\Big]|0\rangle\,,$$

where we choose $\varphi(\boldsymbol{k}_1, \boldsymbol{k}_2) = \varphi(\boldsymbol{k}_2, \boldsymbol{k}_1)$ and $|0\rangle$ is the vacuum.

From the Schrödinger equation of a stationary system

$$(4) \qquad H|\Phi\rangle = E|\Phi\rangle\,,$$

the following system of integral equations is obtained:

$$(5) \qquad (-E + 2m_{\mathrm{V}})A = \frac{g_0}{\sqrt{4\pi}}\int \frac{\mathrm{d}^3k}{\sqrt{2\omega}}\,(\varphi_2(\boldsymbol{k})\exp[i\boldsymbol{k}\boldsymbol{l}] + \varphi_1(\boldsymbol{k})\exp[-i\boldsymbol{k}\boldsymbol{l}])\,,$$

$$(6) \qquad (-E + \omega_1 + \omega_2)(\varphi(\boldsymbol{k}_1, \boldsymbol{k}_2) + \varphi(\boldsymbol{k}_2, \boldsymbol{k}_1)) = \\ = \frac{g_0}{2\sqrt{4\pi}}\left[\exp[i(\boldsymbol{k}_1 + \boldsymbol{k}_2)\boldsymbol{l}]\left(\frac{\varphi_2(\boldsymbol{k}_2)}{\sqrt{2\omega_1}} + \frac{\varphi_2(\boldsymbol{k}_1)}{\sqrt{2\omega_2}}\right) + \right. \\ \left. + \exp[-i(\boldsymbol{k}_1 + \boldsymbol{k}_2)\boldsymbol{l}]\left(\frac{\varphi_1(\boldsymbol{k}_1)}{\sqrt{2\omega_2}} + \frac{\varphi_1(\boldsymbol{k}_2)}{\sqrt{2\omega_1}}\right)\right],$$

(7) $$(-E+m_V+\omega)\varphi_2(\boldsymbol{k}) = \\ = \frac{g_0}{\sqrt{4\pi}}\left(\frac{\exp[-i\boldsymbol{k}\boldsymbol{l}]}{\sqrt{2\omega}}A + 2\int \mathrm{d}^3k_1 \frac{\exp[-i\boldsymbol{k}_1\boldsymbol{l}]}{\sqrt{2\omega_1}}\varphi(\boldsymbol{k}_1, \boldsymbol{k})\right),$$

(8) $$(-E+m_V+\omega)\varphi_1(\boldsymbol{k}) = \\ = \frac{g_0}{\sqrt{4\pi}}\left(\frac{\exp[i\boldsymbol{k}\cdot\boldsymbol{l}]}{\sqrt{2\omega}}A + 2\int \mathrm{d}^3k_2 \frac{\exp[i\boldsymbol{k}_2\cdot\boldsymbol{l}]}{\sqrt{2\omega_2}}\varphi(\boldsymbol{k}, \boldsymbol{k}_2)\right),$$

where $\omega_1 = \sqrt{\boldsymbol{k}_1^2+\mu^2}$, $\omega_2 = \sqrt{\boldsymbol{k}_2^2+\mu^2}$.

Now we eliminate $\varphi(\boldsymbol{k}_1, \boldsymbol{k}_2)$ with use of eq. (6) taking into account the symmetry between the arguments $\boldsymbol{k}_1$ and $\boldsymbol{k}_2$; thus the following system of integral equations is obtained:

(5) $$(-E+2m_V)A = \frac{g_0}{\sqrt{4\pi}}\int \frac{\mathrm{d}^3k}{\sqrt{2\omega}}(\varphi_2(\boldsymbol{k})\exp[i\boldsymbol{k}\cdot\boldsymbol{l}] + \varphi_1(\boldsymbol{k})\exp[-i\boldsymbol{k}\cdot\boldsymbol{l}]),$$

(9) $$\varphi_1(\boldsymbol{k})h(E-\omega) = \\ = -\frac{A\exp[-i\boldsymbol{k}\cdot\boldsymbol{l}]}{g_0\sqrt{4\pi}\sqrt{2\omega}} - \frac{\varphi_2(\boldsymbol{k})}{4\pi}\int \frac{\mathrm{d}^3k_2 \exp[2i\boldsymbol{k}_2\cdot\boldsymbol{l}]}{2\omega_2(\omega+\omega_2-E)} - \frac{1}{4\pi\sqrt{2\omega}}\int \frac{\mathrm{d}^3k_2}{\sqrt{2\omega_2}(\omega_2+\omega-E)}\cdot \\ \cdot(\exp[i(\boldsymbol{k}+\boldsymbol{k}_2)\cdot\boldsymbol{l}]\varphi_2(\boldsymbol{k}_2) + \exp[i(-\boldsymbol{k}+\boldsymbol{k}_2)\cdot\boldsymbol{l}]\varphi_1(\boldsymbol{k}_2)),$$

(10) $$\varphi_2(\boldsymbol{k})h(E-\omega) = \\ = -\frac{A\exp[i\boldsymbol{k}\cdot\boldsymbol{l}]}{g_0\sqrt{4\pi}\sqrt{2\omega}} - \frac{\varphi_1(\boldsymbol{k})}{4\pi}\int \frac{\mathrm{d}^3k_1 \exp[-2i\boldsymbol{k}_1\cdot\boldsymbol{l}]}{2\omega_1(\omega+\omega_1-E)} - \frac{1}{4\pi\sqrt{2\omega}}\int \frac{\mathrm{d}^3k_1}{\sqrt{2\omega_1}(\omega_1+\omega-E)}\cdot \\ \cdot(\exp[-i(\boldsymbol{k}+\boldsymbol{k}_1)\cdot\boldsymbol{l}]\varphi_1(\boldsymbol{k}_1) + \exp[-i(-\boldsymbol{k}+\boldsymbol{k}_1)\cdot\boldsymbol{l}]\varphi_2(\boldsymbol{k}_1)),$$

where

(11) $$h(E) = \frac{E-m_V}{g_0^2} + \int \frac{k^2\,\mathrm{d}k}{2\omega(\omega-E)}.$$

We note that this system of equations is invariant with respect to the transformation $\boldsymbol{l}\to-\boldsymbol{l}$, $\varphi_1\to\varphi_2$, $\varphi_2\to\varphi_1$. Thus if $\varphi_1 = f_1(\boldsymbol{l})$, $\varphi_2 = f_2(\boldsymbol{l})$ is a solution of the system, $\varphi_1 = f_2(-\boldsymbol{l})$, $\varphi_2 = f_1(-\boldsymbol{l})$ is also a solution of the system. Now, as it happens for any symmetry with respect to a group of two elements, two cases are possible: either one has degenerate solutions: this case occurs if the transformation $\boldsymbol{l}\to-\boldsymbol{l}$, $\varphi_1\to\varphi_2$, $\varphi_2\to\varphi_1$, gives rise to a new linearly independent solution, or one has $f_1(\boldsymbol{l}) = cf_2(-\boldsymbol{l})$, $f_2(\boldsymbol{l}) = cf_1(-\boldsymbol{l})$. In this case one obtains from the preceding equalities $f_1(\boldsymbol{l}) = c^2 f_1(\boldsymbol{l})$, so that $c = \pm 1$ and the solutions have the property:

(12) $$f_1(\boldsymbol{l}) = \pm f_2(-\boldsymbol{l}).$$

Let us first consider the system of eqs. (5), (9) and (10) in the limit $l \to \infty$. In this case it is satisfied by the energy $E_0 = E_V + E_V^*$ and by the functions φ_{10} and φ_{20} describing the state of two non interacting V-particles with complex conjugated energies E_V and E_V^* at the points 1 and 2 respectively. Indeed the functions φ_{10} and φ_{20} are, as is known,

$$\varphi_{10} = \frac{A g_0 \exp[i\boldsymbol{k}\cdot\boldsymbol{l}]}{\sqrt{4\pi}(\omega - E_V)\sqrt{2\omega}}, \qquad \varphi_{20} = \frac{A g_0 \exp[-i\boldsymbol{k}\cdot\boldsymbol{l}]}{\sqrt{4\pi}(\omega - E_V^*)\sqrt{2\omega}}. \tag{13}$$

When these φ_{10} and φ_{20} functions are substituted in eqs. (9) and (10) one finds that the first integral and the second term of the second integral in the right hand sides of eqs. (9) and (10) tend to zero in the limit $l \to \infty$ and it is easy to verify that the equations are satisfied using (11).

In the limit $l \to \infty$ the system is equally satisfied by the solution

$$\varphi_{10} = \frac{A g_0 \exp[i\boldsymbol{k}\cdot\boldsymbol{l}]}{\sqrt{4\pi}(\omega - E_V^*)\sqrt{2\omega}}, \qquad \varphi_{20} = \frac{A g_0 \exp[-i\boldsymbol{k}\cdot\boldsymbol{l}]}{\sqrt{4\pi}(\omega - E_V)\sqrt{2\omega}}, \tag{14}$$

obtained from (13) applying the transformation $\boldsymbol{l} \to -\boldsymbol{l}$, $\varphi_1 \to \varphi_2$, $\varphi_2 \to \varphi_1$. This solution is linearly independent from (13), so that there is degeneration. It must be noted that both solutions (13) and (14) give rise to two non orthogonal states with zero norm; thus the states obtained with a superposition of them may have any norm different from zero, positive or negative.

Let us now consider the case in which $\boldsymbol{l}$ is finite, but still large. Then we can consider the effect of the first integral and of the second part of the second integral in eqs. (9) and (10), which we have neglected when $l \to \infty$, as a perturbation. In both the cases in which the perturbation destroyes the degeneration or not, we will obtain the solutions of the system by assuming as a zero approximation those linear combinations of the solutions (13) and (14) (corresponding to two non interacting V-particles) which satisfy the symmetry property expressed by the relation (12):

$$\begin{cases} \varphi_{10} = \dfrac{A g_0 \exp[i\boldsymbol{k}\cdot\boldsymbol{l}]}{\sqrt{4\pi}\sqrt{2\omega}}\left(\dfrac{1}{\omega - E_V^*} \pm \dfrac{1}{\omega - E_V}\right) = \dfrac{A g_0 \exp[i\boldsymbol{k}\cdot\boldsymbol{l}]}{\sqrt{4\pi}\sqrt{2\omega}} B_\pm(\omega), \\ \varphi_{20} = \dfrac{A g_0 \exp[-i\boldsymbol{k}\cdot\boldsymbol{l}]}{\sqrt{4\pi}\sqrt{2\omega}}\left(\dfrac{1}{\omega - E_V} \pm \dfrac{1}{\omega - E_V^*}\right) = \dfrac{A g_0 \exp[-i\boldsymbol{k}\cdot\boldsymbol{l}]}{\sqrt{4\pi}\sqrt{2\omega}} B_\pm^*(\omega). \end{cases} \tag{15}$$

We now put $\varphi_1 = \varphi_{10} + \varphi_1'$, $\varphi_2 = \varphi_{20} + \varphi_2'$, $E = E_0 + E'$, where φ' and E' are supposed to be small, and we subtract from eqs. (9) and (10) the corresponding unperturbed equations (*i.e.* eqs. (9) or (10) with the first integral and the second part of the second integral omitted and $E = E_0$). In the case of equation (9)

the following expression is obtained:

$$(16)\qquad \varphi_1'(\boldsymbol{k})h(E_0-\omega)+\varphi_{10}(\boldsymbol{k})h'(E_0-\omega)E'=$$
$$=-\frac{\varphi_{20}(\boldsymbol{k})}{4\pi}\int\frac{\mathrm{d}^3k'\exp[2i\boldsymbol{k}'\cdot\boldsymbol{l}]}{2\omega'(\omega+\omega'-E)}-\frac{1}{4\pi\sqrt{2\omega}}\int\frac{\mathrm{d}^3k'\exp[i(\boldsymbol{k}+\boldsymbol{k}')\cdot\boldsymbol{l}]}{\sqrt{2\omega'}(\omega+\omega'-E)}\varphi_2'(\boldsymbol{k}')-$$
$$-\frac{1}{4\pi\sqrt{2\omega}}\int\frac{\mathrm{d}^3k'\exp[i(\boldsymbol{k}+\boldsymbol{k}')\cdot\boldsymbol{l}]}{\sqrt{2\omega'}}\left(\frac{1}{\omega+\omega'-E}-\frac{1}{\omega+\omega'-E_0}\right)\varphi_{20}(\boldsymbol{k}')-$$
$$-\frac{1}{4\pi\sqrt{2\omega}}\int\frac{\mathrm{d}^3k'\exp[-i(-\boldsymbol{k}+\boldsymbol{k}')\cdot\boldsymbol{l}]}{\sqrt{2\omega'}(\omega+\omega'-E)}\varphi_{10}(\boldsymbol{k}')\,.$$

Remembering that φ' and E' are small, we can solve this equation with respect to $\varphi_1'(\boldsymbol{k})$ by an iteration procedure, neglecting in a first approximation the second term in the right hand side and introducing the approximation $(\omega+\omega'-E)^{-1}\simeq(\omega+\omega'-E_0)^{-1}[1+E'(\omega+\omega'-E_0)^{-1}]$. Thus by using the expressions (15) for φ_{10} and φ_{20} and by taking into account the spherical symmetry of the integrals, one obtains (dropping the indices of B):

$$(17)\qquad \varphi_1'(\boldsymbol{k})=\frac{-Ag_0}{h(E_0-\omega)\sqrt{4\pi}\sqrt{2\omega}}\Bigg[B(\omega)h'(E_0-\omega)E'\exp[i\boldsymbol{k}\cdot\boldsymbol{l}]+$$
$$+\exp[-i\boldsymbol{k}\cdot\boldsymbol{l}]\int\frac{\mathrm{d}k'k'\sin 2k'l}{4\omega' l(\omega+\omega'-E_0)}\left(1+\frac{E'}{\omega+\omega'-E_0}\right)B(\omega)+$$
$$+E'\exp[i\boldsymbol{k}\cdot\boldsymbol{l}]\int\frac{\mathrm{d}k'k'^2B^*(\omega')}{2\omega'(\omega+\omega'-E_0)^2}+$$
$$+\exp[-i\boldsymbol{k}\cdot\boldsymbol{l}]\int\frac{\mathrm{d}k'k'\sin 2k'l}{4\omega' l(\omega+\omega'-E_0)}B(\omega')\left(1+\frac{E'}{\omega+\omega'-E_0}\right)\Bigg].$$

With the same procedure, starting from eq. (10), one obtains:

$$(18)\qquad \varphi_2'(\boldsymbol{k})=\frac{-Ag_0}{h(E_0-\omega)\sqrt{4\pi}\sqrt{2\omega}}\Bigg[B^*(\omega)h'(E_0-\omega)E'\exp[-i\boldsymbol{k}\cdot\boldsymbol{l}]+$$
$$+\exp[i\boldsymbol{k}\cdot\boldsymbol{l}]\int\frac{\mathrm{d}k'k'\sin 2k'l}{4\omega' l(\omega+\omega'-E_0)}\left(1+\frac{E'}{\omega+\omega'-E_0}\right)B^*(\omega)+$$
$$+E'\exp[-i\boldsymbol{k}\cdot\boldsymbol{l}]\int\frac{\mathrm{d}k'k'^2B(\omega')}{2\omega'(\omega+\omega'-E_0)^2}+$$
$$+\exp[-i\boldsymbol{k}\cdot\boldsymbol{l}]\int\frac{\mathrm{d}k'k'\sin 2k'l}{4\omega' l(\omega+\omega'-E_0)}B^*(\omega')\left(1+\frac{E'}{\omega+\omega'-E_0}\right)\Bigg].$$

The quantity E' is calculated by using the eigenvalue equation (5), which

gives:

$$-E'A = \frac{g_0}{\sqrt{4\pi}} \int \frac{\mathrm{d}^3 k}{\sqrt{2\omega}} (\varphi_2' \exp[i\boldsymbol{k}\cdot\boldsymbol{l}] + \varphi_1' \exp[-i\boldsymbol{k}\cdot\boldsymbol{l}]). \tag{19}$$

By substituting eqs. (17) and (18) into eq. (19) one obtains:

$$E' = \frac{g_0^2}{2\pi} \int \frac{\mathrm{d}^3 k}{2\omega h(E_0 - \omega)} \Big[h'(E_0 - \omega) E' \operatorname{Re} B(\omega) + \operatorname{Re}\,(B(\omega) \exp[2i\boldsymbol{k}\cdot\boldsymbol{l}]) \cdot \int \frac{\mathrm{d}k' k' \sin 2k'l}{4l\omega'(\omega + \omega' - E_0)} \left(1 + \frac{E'}{\omega + \omega' - E_0}\right) + E' \int \mathrm{d}k' \operatorname{Re} B(\omega') \frac{k'^2}{\omega'(\omega + \omega' - E_0)} + \operatorname{Re}\left(\exp[2i\boldsymbol{k}\cdot\boldsymbol{l}] \int \frac{\mathrm{d}k' k' \sin 2k'l}{2\omega' l(\omega + \omega' - E_0)} \left(1 + \frac{E'}{\omega + \omega' - E_0}\right) B(\omega')\right)\Big]. \tag{20}$$

This is a linear algebraic equation with respect to the unknown E', having real coefficients. Thus it gives a real value for E', at least if l is sufficiently large. Moreover, remembering eqs. (15), one must expect different values of E' corresponding to the different signs appearing in these equations and thus one expects the degeneration to be removed when l is decreased starting from infinity (7). Therefore in the limit $l \to \infty$ the present solutions must go in the degenerate solutions (15) implying a norm of the state which is different from zero, positive for one of the solutions, negative for the other. Thus one can conclude from continuity that the norms of the states remain different from zero at least for a sufficiently large l, positive for one state, negative for the other.

So we have in the subspace (2V, V+N+0, 2N+2θ) at least for sufficiently large l, two eigenvectors of norm different from zero (one with positive norm, the other with negative norm) belonging to real discrete energy eigenvalues. Moreover the inspection of eq. (20) leads to the conclusion that $|E'|$ decreases for increasing l more rapidly than any power of l^{-1}.

3. – Scattering states in the subspace (2V+θ, V+N+2θ, 2N+3θ).

We are now in position to discuss problems of scattering states in the subspace (2V+θ, V+N+2θ, 2N+3θ).

---

(7) Actually this conclusion is based on the first term of the iterative solution of the system of eqs. (8)-(10). However we expect the ratio of the remaining terms of such an expansion to the first one to tend to zero nearly exponentially, as $l \to \infty$ owing to the structure of the integrals appearing in the system. So the conclusion is justified at least for sufficiently large values of l.

Let us consider the scattering of 3θ-particles on 2N-particles. The total energy of the system is then real. Thus, owing to the conclusions of the preceding Section the situation is similar to the one discussed by KÄLLÉN and PAULI (2): in general the outgoing waves will consist of a superposition of states of 3θ- and 2N-particles and states of one θ-particle, leaving a bound state of real energy of the subspace (2V, $V+N+\theta$, $2N+2\theta$); in general a superposition of both kinds of such states with positive or negative norm, will be produced.

Such a process cannot be physically interpreted, at least in the usual framework, for two different reasons:

1) It is not possible to give a probabilistic interpretation to the theory, because the expression which usually gives the probability of emission of one θ-particle with formation of the bound state of negative norm would be negative.

2) Both bound states of real energy of the subspace (2V, $V+N+\theta$, $2N+2\theta$) may hardly be physically interpreted. Indeed, at least for large l, even if the total energy is real, such states would describe a superposition of states of two weakly interacting systems (V-particles) of complex conjugate energies.

More simply and exactly it is sufficient to apply the theorems of Section 4.1 of our work (6) to conclude that the model cannot be probabilistically interpreted in this case.

4. – Discussion.

The results may be better understood taking into account some general properties of spaces with indefinite metric.

Let us first consider the subspace (V, $N+\theta$). In this subspace there is one axis of negative norm, the V-axis. Then for any selfadjoint operator one of the following cases may occur:

1) There are complex eigenvalues. In this case they must be in pairs of complex conjugates, the corresponding pairs of eigenvectors being of norm zero and not orthogonal (4). Only one pair may occur in this subspace because otherwise we could construct more then one linearly independent vector of negative norm.

2) There are only real eigenvalues and no eigenvector has zero norm; then they form a complete orthogonal set and therefore one of them and only one has negative norm.

3) There are only real eigenvalues with one and only one eigenvector of zero norm. In this case (dipole ghost) the system of eigenvectors is not complete.

4) There are only real eigenvalues and there is a subspace of degenerate eigenvectors with one axis of negative norm: in the simplest case there are only two independent degenerate eigenvectors so that the subspace is a plane and there are two degenerate eigenvectors of zero norm.

As HEISENBERG [4] has shown in the subspace (V, N + θ) of the Lee model with indefinite metric only cases 1, 2, 3 may occur. The limiting case between 1 and 2 is 3.

Now we have assumed to be in case 1. So we have two discrete non orthogonal eigenstates of zero norm and energies E_{V} and E_{V}^*:

For a particle fixed at point 1 they are given by:

$$(21)\qquad \begin{cases} |\psi_1\rangle = \left(c\psi^*_{\mathrm{V}_1} + \psi^*_{\mathrm{N}_1}\int \mathrm{d}^3k\,\psi_1(\boldsymbol{k})\,a^*(\boldsymbol{k})\right)|0\rangle = O_1^*|0\rangle\,, \\ |\tilde{\psi}_1\rangle = \left(c\psi^*_{\mathrm{V}_1} + \psi^*_{\mathrm{N}_1}\int \mathrm{d}^3k\,\tilde{\psi}_1(\boldsymbol{k})\,a^*(\boldsymbol{k})\right)|0\rangle = \tilde{O}_1^*|0\rangle\,, \end{cases}$$

$$(22)\qquad \psi_1(\boldsymbol{k}) = \frac{cg_0\exp[-i\boldsymbol{k}\cdot\boldsymbol{l}]}{\sqrt{4\pi}\sqrt{2\omega}\,(\omega - E_{\mathrm{V}})}\,, \qquad \tilde{\psi}_1(\boldsymbol{k}) = \frac{cg_0\exp[-i\boldsymbol{k}\cdot\boldsymbol{l}]}{\sqrt{4\pi}\sqrt{2\omega}\,(\omega - E_{\mathrm{V}}^*)}\,.$$

For a particle fixed at point 2 we have corresponding formulae with the index 2 instead of 1 and $\boldsymbol{l}$ instead of $-\boldsymbol{l}$.

We have, with an appropriate choice of the normalization:

$$(23)\qquad \begin{cases} \langle 0|O_1O_1^*|0\rangle = 0\,, & \langle 0|\tilde{O}_1\tilde{O}_1^*|0\rangle = 0\,, \\ \langle 0|O_2O_2^*|0\rangle = 0\,, & \langle 0|\tilde{O}_2\tilde{O}_2^*|0\rangle = 0\,, \\ \langle 0|O_2O_1^*|0\rangle = 0\,, & \langle 0|\tilde{O}_2O_1^*|0\rangle = 0\,, \quad \text{etc.}, \\ \langle 0|\tilde{O}_1O_1^*|0\rangle = \langle 0|\tilde{O}_2O_2^*|0\rangle = 1\,. \end{cases}$$

Let us now pass to the subspace (2V, V + N + θ, 2N + 2θ).

We assume l to be large and we neglect at first the interaction between the particles at point 1 and at point 2. Then we may construct the eigenstates in this subspace starting from the eigenstates in the subspace (V, N + 0). We have besides a continuum of energy eigenstates a system of discrete eigenstates. This system may be obtained from the discrete eigenstates of the subspace (V, N + 0). These span a two dimensional space with one axis of negative norm. So the subspace spanned by the discrete eigenstates of the system of two non-interacting V-particles will be with two axes of negative norm. Many cases may occur in general for the eigenvectors of a selfadjoint operator in such a space: the one which occurs here is a combination of cases 1 and 4 considered above. Indeed the energy eigenvectors may be obtained, when the interaction is neglected, from:

$$(24)\quad |1\rangle = O_1^* O_2^* |0\rangle\,, \quad |2\rangle = O_1^* \tilde{O}_2^* |0\rangle\,, \quad |3\rangle = \tilde{O}_1^* O_2^* |0\rangle\,, \quad |4\rangle = \tilde{O}_1^* \tilde{O}_2^* |0\rangle\,.$$

Now $|1\rangle$ and $|4\rangle$ belong to complex energies $2E_V$ and $2E_V^*$ respectively, have zero norm and are not orthogonal, owing to eqs. (23).

On the contrary $|2\rangle$ and $|3\rangle$ belong to the same real energy $E_V + E_V^*$. Using eqs. (23) we see that they have norm zero and are not orthogonal (but orthogonal to $|1\rangle$ and $|4\rangle$). So they belong to a plane of indefinite metric of eigenvectors of real energy $E_V + E_V^*$ (see Fig. 1).

If we introduce the interaction between the particles at points 1 and 2 we expect in general the degeneration to be removed. Moreover we were dealing with two equal systems. So we know that the perturbed eigenfunction has to be either symmetric or antisymmetric against permutation of the two systems. So the unperturbed eigenfunctions to which the perturbed eigenfunctions approach when the interaction is removed, will be the symmetric and the antisymmetric combinations of the eigenfunctions $|2\rangle$ and $|3\rangle$:

$$(25)\quad \begin{cases} |s\rangle = \dfrac{1}{\sqrt{2}} (O_1^* \tilde{O}_2^* + \tilde{O}_1^* O_2^*) |0\rangle\,, \\ |A\rangle = \dfrac{1}{\sqrt{2}} (O_1^* \tilde{O}_2^* - \tilde{O}_1^* O_2^*) |0\rangle\,. \end{cases}$$

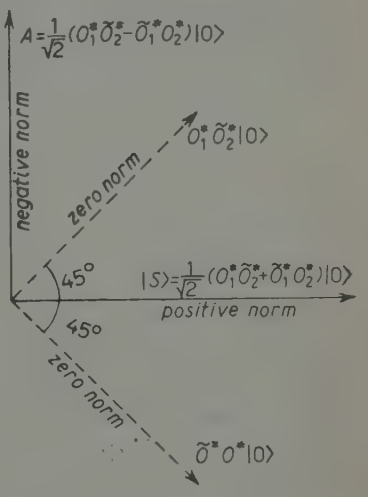

Fig. 1. – The plane of degenerate eigenvectors belonging to the real discrete energy eigenvalues in the subspace (2V, V + N + θ, 2N + + 2θ), when the interaction between particles 1 and 2 is neglected. When a symmetric perturbation is removed the eigenvectors tend to $|A\rangle$ and $|S\rangle$.

Now using eqs. (23) we have for the norm of $|S\rangle$:

$$\langle S|S\rangle = \tfrac{1}{2}\langle 0|(\tilde{O}_2 O_1 + O_2\tilde{O}_1)(\tilde{O}_1^* O_2^* + \tilde{O}_1^* O_2^*)|0\rangle = \tfrac{1}{2}(\langle 0|\tilde{O}_2\tilde{O}_2^*|0\rangle\langle 0|O_1 O_1^*|0\rangle + \tag{26}$$

$$+ \langle 0|O_2 O_2^*|0\rangle\langle 0|\tilde{O}_1\tilde{O}_1^*|0\rangle + \langle 0|\tilde{O}_2 O_2^*|0\rangle\langle 0|O_1\tilde{O}_1^*|0\rangle +$$

$$+ \langle 0|O_2\tilde{O}_2^*|0|\rangle\langle 0|\tilde{O}_1 O_1^*|0\rangle) = 1\,.$$

Analogously we obtain

$$\langle A|A\rangle = -1\,. \tag{27}$$

When the degeneration is removed from a sufficiently weak interaction, we expect from continuity that the complex eigenvalues remain complex, so that the corresponding eigenvectors will remain of zero norm and not orthogonal; again from continuity we expect that the norm of the two further eigenstates will remain different from zero, positive for one, negative for the other; so the corresponding eigenvalue must be real. These conclusions are sufficient for the discussion or the application of the theorems of our previous work ([6]): the eigenstates of complex energy do not give rise to troubles for the physical interpretation, because they cannot be produced, owing to energy conservation. On the contrary the eigenstates of real energy may be produced, and they may have negative norm so that we have the already discussed troubles.

5. – Conclusions.

In conclusion we see that in the case of complex energy eigenvalues the Lee model with fixed point particles and indefinite metric cannot be physically interpreted at least using the usual framework or also the method proposed by HEISENBERG in the case of the dipole ghost. No difficulty occurs in the subspace $(V+\theta,\ N+2\theta)$, but the first troubles arise in the subsapce $(2V+\theta,\ V+N+2\theta,\ 2N+3\theta)$, that is in the scattering of $3\,\theta$ particles on 2 N-particles.

It is natural to ask wether similar conclusions hold for any theory with indefinite metric in which complex energy eigenvalues occur. In our opinion it is not possible to extend the results obtained here to the case in which all the particles have a kinetic energy. Indeed an essential part of the argument is based on the symmetry properties of the wave function of two equal interacting systems, when the interaction destroyes the degeneration. In the case of the Lee model with fixed particles the degeneration is destroyed because the particles do not go away one from the other, so that the interaction between

them remains also when $t \to \pm\infty$. The situation seems to be different in the case of moving particles, so that in this latter case it could be possible to choose asymptotic states of the type of the non symmetrized states $|2\rangle$ and $|3\rangle$ (formula (24)) which have zero norm (and are not orthogonal) so that they could be treated with the method used by HEISENBERG in the case of the dipole ghost.

RIASSUNTO

Si studia il modello di Lee con particelle puntiformi fisse nel caso in cui si hanno autovalori complessi dell'energia nel sottospazio $(V, N+\theta)$. Si dimostra che in generale tale modello non è fisicamente interpretabile, almeno nel quadro dell'usuale schema interpretativo. Infatti si considera un problema nel sottospazio $(2V+\theta, V+N+2\theta, 2N+3\theta)$ e si mostra che espressioni usualmente interpretate come probabilità divengono negative. Tali difficoltà non si presentano in problemi più semplici.

IL NUOVO CIMENTO Vol. XIV, N. 6 16 Dicembre 1959

Search for the Decay $\mu \to e + \gamma$ and Observation of the Decay $\mu \to e + \nu + \bar{\nu} + \gamma$.

J. Ashkin (*), T. Fazzini, G. Fidecaro, N. H. Lipman, A. W. Merrison and H. Paul (**)

CERN - Genève

(ricevuto il 23 Agosto 1959)

Summary. — This paper reports a search for the $\mu \to e + \gamma$ mode of decay. The result is negative within the sensitivity of the experiment: the branching ratio we find is $(1.2 \pm 1.5) \cdot 10^{-6}$. We present also evidence for the existence of the decay process $\mu \to e + \nu + \bar{\nu} + \gamma$.

1. – Introduction.

One of the most interesting problems in the field of weak interactions is the experimental fact that certain processes which would obey well established conservation laws are, nevertheless, not observed. Such processes are, for example, $\mu \to e + \gamma$, $\mu \to 3e$, $\mu + p \to e + p$. It is clearly important in these circumstances to establish the degree of « forbiddenness » of these unobserved processes with as great an experimental accuracy and reliability as possible. With this in mind we have searched for the decay $\mu^+ \to e^+ + \gamma$.

This decay has an added interest in that several recent attempts to account for the universality of weak interactions [1] have made use of the idea, first proposed by Ogawa [2], that the weak interactions are transmitted by a charged vector boson. However, as Ogawa pointed out, if this is so then the decay

(*) Ford Foundation Fellow, on leave from Carnegie Institute of Technology, Pittsburgh.

(**) Ford Foundation Fellow, on leave from Institut für Radiumforschung, Vienna.

(1) See, for example, J. J. Sakurai: *Nuovo Cimento*, **7**, 649 (1958); N. Byers and R. E. Peierls: *Nuovo Cimento*, **10**, 520 (1958).

(2) S. Ogawa: *Prog. Theor. Phys.*, **15**, 487 (1956). A discussion of this idea can be found in the *Proceedings of the 1958 Annual Conference on High Energy Physics* (*CERN*), p. 253, by L. Michel.

$\mu \to e+\gamma$ should be observable. An explicit calculation of the branching ratio $(\mu \to e+\gamma)/(\mu \to e+\nu+\bar{\nu})$ was first made by FEINBERG ([3]), with the result that it should be $\simeq 10^{-3}$ ([*]). This conclusion has recently been re-examined by EBEL and ERNST ([4]), who studied also the effect of an anomalous magnetic moment of the boson, and by MEYER and SALZMAN ([5]) in the accompanying paper.

The first experiment to search for this decay mode was that of HINCKS and PONTECORVO ([6]) and since then the experiment has been repeated several times ([7]). The experiment is made difficult, as has been recently realized, by the existence of the decay $\mu \to e+\nu+\bar{\nu}+\gamma$ which provides a background of e, γ pairs. The branching ratio of this process compared with the normal decay mode of the muon has been calculated by FRONSDAL and ÜBERALL ([8]) and KINOSHITA and SIRLIN ([9]). The $\mu \to e+\gamma$ mode, however, can be distinguished because, firstly, the *whole* rest energy of the muon goes into the electron and the γ-ray so that one should observe, as it is a two-body decay, a mono-energetic electron and a mono-energetic γ-ray each of about 53 MeV. Secondly, the electron and γ-ray will be emitted at 180° to each other. The bremsstrahlung process, on the other hand, gives continuous spectra for both the electron and γ-ray which are heavily weighted towards low energies, and the angular correlation does not favour 180° emission. So, by searching for high energy electrons and γ-rays at 180° we discriminate strongly against this process.

Of course the principal difficulty in searching for rare decay modes is to be sure that nothing has been introduced into the design of the apparatus which would obscure the effect one is looking for. For this reason the apparatus was not designed with the idea of rejecting electronically as many unwanted events as possible. We preferred to record during the run also events to be re-examined later, which would show that the apparatus was working properly. This was obtained with a low energy discrimination in the electron and γ-ray telescopes and by not rejecting electronically events in prompt coincidence with an incoming pion. The e-γ coincidences triggered the 5 oscilloscope traces on which we displayed pulses from most of the counters used in the experiment, and these traces were photographed. The measurement of

---

([3]) C. FEINBERG: *Phys. Rev.*, **110**, 1482 (1958).

([*]) Actually FEINBERG obtained 10^{-4} but he was apparently in error ([4,5]).

([4]) M. E. EBEL and F. J. ERNST: to be published.

([5]) PH. MEYER and G. SALZMAN: *Nuovo Cimento*, in press.

([6]) E. P. HINCKS and B. PONTECORVO: *Phys. Rev.*, **73**, 257 (1948).

([7]) For a complete list of references, see the report on *Weak Interactions* by A. I. ALIHANOV to the 9-th International Conference on High Energy Physics, Kiev (1959).

([8]) C. FRONSDAL and H. ÜBERALL: *Phys. Rev.*, **113**, 654 (1959).

([9]) T. KINOSHITA and A. SIRLIN: *Phys. Rev. Letters*, **2**, 177 (1959).

the electron and γ-ray energies as well as the rejection of unwanted events was done later on the photographs. The experiment relies entirely on the analysis of these photographs.

Earlier this year we carried out a preliminary experiment as a guide in designing the final experiment. This experiment showed for the first time the existence of the decay $\mu \to e + \nu + \bar{\nu} + \gamma$, and that the rate of this decay agrees with the theoretical prediction. This experiment showed also the importance of this process as a background in searching for $\mu \to e + \gamma$. We describe this experiment briefly in Section **4**, together with some computations we have made on the internal bremsstrahlung process.

2. – Description of the apparatus.

The layout of the experiment is shown in Fig. 1. The 65 MeV positive pion beam of the 600 MeV CERN Synchro-cyclotron was first filtered by

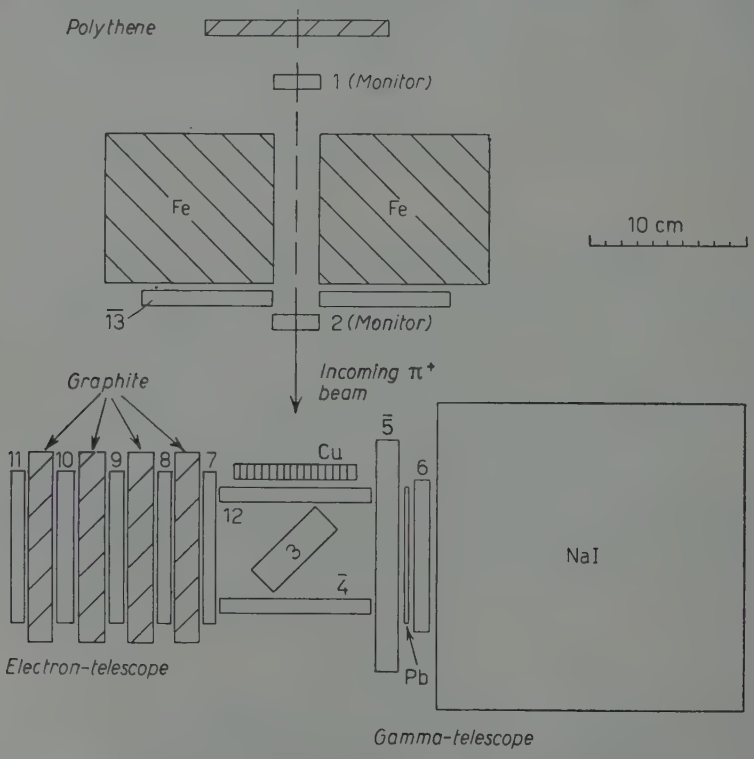

Fig. 1. – Schematic diagram of the apparatus.

2 cm polythene to remove protons of the same momentum. It then passed through the monitor counters 1 and 2, which were 5 cm high, 3 cm wide and

1 cm thick, mounted on either side of a thick steel collimator. The pions were then slowed down in a block of copper and about 50% came to rest in counter 3. Counter 3 was 5 cm high, 6 cm wide and 2 cm thick. It was inclined at an angle of about 45° to the beam, in this way presenting an effective thickness of about 3 cm to the beam. To identify particles stopping in counter 3, 123 were in fast (about 20 ns ($= 2\tau$)) coincidence, with counter 4 in anti-coincidence. About 3 000 pions/s were stopped in counter 3. Nearly all these pions decayed and gave a muon which stopped in 3.

Electrons were detected in the range telescope formed of counters 7, 8, 9, 10, 11. The dimensions of each of these counters was 10 cm × 10 cm × 1 cm, and between the counters were four graphite absorbers each of thickness 3.49 g/cm². The γ-ray telescope consisted of counter 5 (in anticoincidence), a lead converter of thickness 3.4 g/cm² and counter 6. Behind counter 6 there was a large cylindrical NaI(Tl) counter 20 cm in diameter and 20 cm long. Counter 5 was 15 cm × 15 cm × 1.5 cm and counter 6 was circular with diameter 9.5 cm and thickness 1 cm. Counter 12, which was interposed between the stopping counter and the copper moderator to recognize spurious events involving the copper moderator itself, was 10 cm × 10 cm × 1 cm. Counter 13 was a large counter 30 cm × 30 cm × 1 cm with a hole 5 cm × 3 cm.

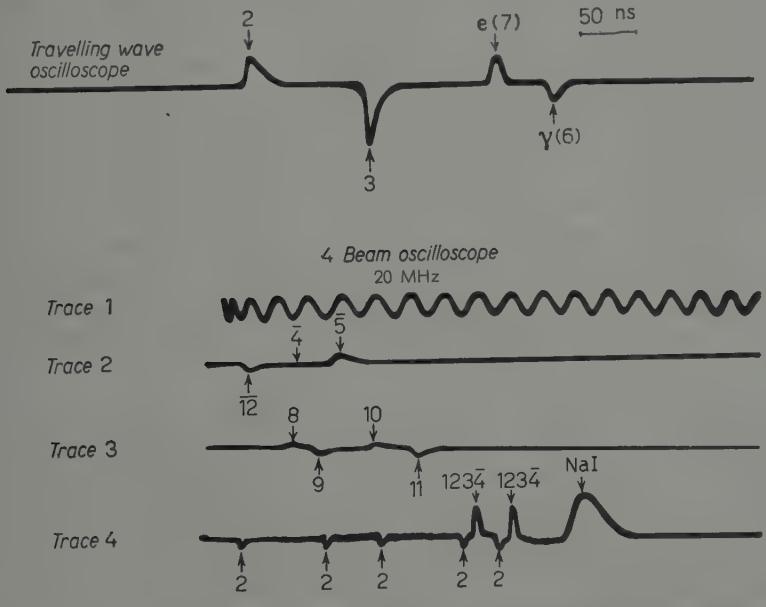

Fig. 2. – Examples of traces from the travelling wave and four-beam oscilloscopes.

This hole was made to coincide with the input counters 1 and 2 and the hole through the collimator. We recorded an e-γ coincidence whenever we had a coincidence $\bar{5}\,6\,7\,8\,\overline{13}$. The resolving time of this coincidence circuit was

19 ns ($= 2\tau$). Whenever there was such a coincidence we recorded on a fast oscilloscope the pulses from counters 2, 3, 6 and 7. This was a travelling wave oscilloscope with a band-witdh of 2 000 MHz made by EDGERTON, GERMESHAUSEN and GREER. A typical trace from this oscilloscope with pulses from all four counters present is shown in the top trace of Fig. 2. At the same time we displayed (shown also in Fig. 2) on a four-beam oscilloscope pulses from counters 4, 5, 12 (on trace 2); from counters 8, 9, 10 and 11 (on trace 3); from counter 2, the NaI counter, and the coincidence pulse $1\,2\,3\,\overline{4}$ (on trace 4). On trace 1 we displayed a 20 MHz calibration signal. Traces 1 2 and 3 were all run from the same time base. Trace 4 was run from an independent time base having a speed of 2 μs/cm. Every 15 minutes a 100 MHz sine wave was displayed on the fast oscilloscope, along with a 1 MHz sine wave on trace 4 of the slow oscilloscope.

A simplified block diagram is shown in Fig. 3, and this is for the most part self-explanatory. For the sake of clarity many components have been omitted. In order to reduce the number of photographs we introduced an energy cut on the γ-ray side; not with absorbers, which would have led to a loss of resolution in the NaI counter, but electronically. We arranged that the fast and slow oscilloscopes were triggered only if the pulse in the NaI counter was sufficently large (corresponding to a γ-ray of initial energy of about 15 MeV). The pulse from the NaI counter was amplified and then passed to a discriminator, which essentially set the triggering level. The output from the discriminator was then put in double coincidence with the pulse from $\overline{5}\,6\,7\,8\,\overline{13}$, suitably delayed. The output from this coincidence circuit then triggered the fast and slow oscilloscopes. All this entailed delaying the pulses which were to be displayed on the oscilloscopes, for considerable times, but this was accomplished without any serious loss in pulse shape. The pulses displayed on the fast oscilloscope were transmitted through low-attenuation cables, type HM7Al made by Telcon. As the length of these cables could not be easily changed we adjusted the delay of the trigger with the delay shown in Fig. 3 after the mixer.

Another point to be mentioned is that, in order to recognize the various types of random events the apparatus would record, we displayed genuine random events defined by the fast coincidence circuit D in which counters 7 and 8 were delayed by 1 radio-frequency period (60 ns). Both the coincidence circuits C and D triggered the oscilloscopes and there was no problem in distinguishing the resultant pictures on the oscilloscopes.

We reduced the background from cosmic ray events by displacing the whole of trace 1 on the slow oscilloscope while the cyclotron was on. This was done by taking a signal from the cyclotron R.F. just before the protons hit the internal target and using it to generate a square wave of 1 ms duration which was applied to the trace 1 Y-plates (the pulse from the cyclotron has

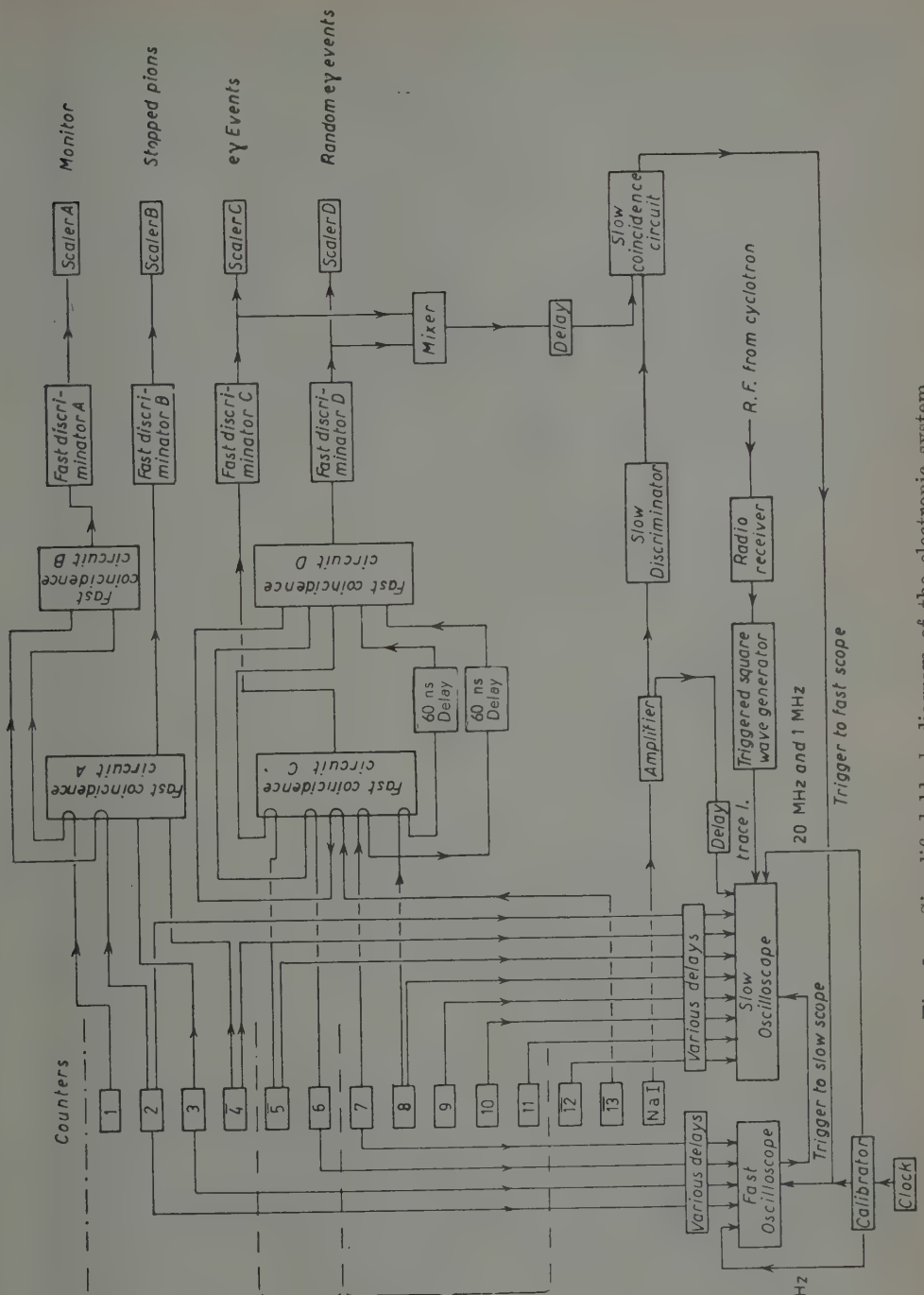

Fig. 3. – Simplified block diagram of the electronic system.

a duration of about 300 μs). In this way we could recognize events which were not correlated with cyclotron pulses.

Because of the very low sensitivity of the 4-beam oscilloscope (about 40 V/cm) and the reduction in pulse amplitudes due to the large delays we used, we ran the photomultipliers (RCA 6810A's) in such a condition that they gave as large a pulse as possible. We were able to do this safely by providing each multiplier with an electrostatic shield, formed by painting the glass envelope with aquadag, putting this at photocathode potential, and by using a specially designed photomultiplier chain which we have previously described ([10]). In these conditions the photomultipliers were operated at fairly high voltage around and over 3 000 V and we obtained output current pulses of over 1 A into the 125 Ω coaxial cable without any breakdown.

The resolution of the NaI(Tl) counter was measured in a separate experiment as follows.

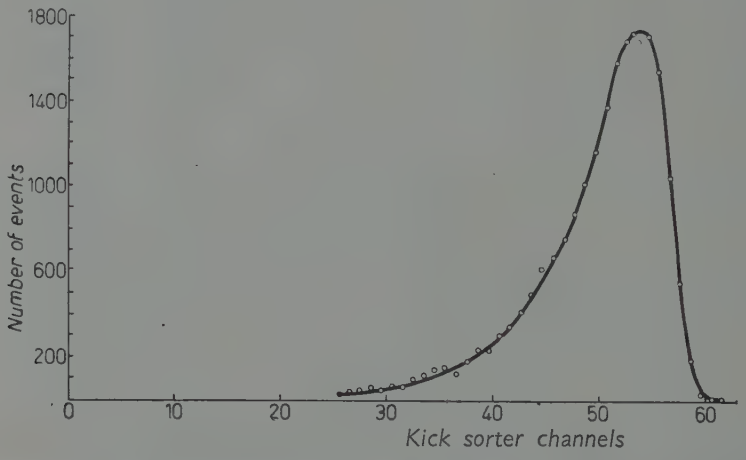

Fig. 4. – Measured pulse height spectrum from the NaI(Tl) counter for mono-energetic 53 MeV positrons incident.

The external proton beam of the CERN Syncro-cyclotron was allowed to fall upon a thick lead target. Many of the γ-rays from the decay of neutral pions, produced by p-p and p-n interactions were converted to positrons in the target. A mono-energetic positron beam was obtained by magnetic selection. The pulse height spectrum shown in Fig. 4 was obtained from the NaI(Tl) counter in gated coincidence with counter 6 (No. 6 of the present

([10]) J. ASHKIN, T. FAZZINI, G. FIDECARO, A. W. MERRISON, H. PAUL and A. V. TOLLESTRUP: *Nuovo Cimento*, **13**, 1240 (1959).

experiment) for a 53 MeV positron beam incident; the resolution (full width at $\frac{1}{2}$ height) is 17%. The resolution curves obtained at 25 MeV and 110 MeV are essentially the same as above. The stability of the NaI(Tl) counter was verified with a ^{22}Na source both at the time the calibration was made and during the experiment, and was found satisfactory.

3. – Experimental results and analysis.

The event we searched for was a high-energy electron coming from counter 3, in time coincidence with a high energy γ-ray. This would be characterized by a pair of photographs showing:

a) pulses from counters 3, 6 and 7, on the fast oscilloscope present with the proper time relationship for a coincident event, but with either no pulse from counter 2, or with a pulse from counter 2 not in the right position for an incoming pion coincident with the e-γ coincidence;

b) pulses from counters 7-11 in the electron telescope (trace 3 of 4-beam oscilloscope, see Fig. 2);

c) no pulse present from counter $\bar{5}$ (trace 2). We should also expect no pulses present from counters $\bar{4}$ and $\overline{12}$, because an event originating in the source counter should not trigger these (trace 2).

d) a large pulse from the NaI(Tl) counter (trace 4).

For example, the event in Fig. 2 would be accepted as an e-γ event if the time relationship of the pulses in the fast and slow oscilloscopes were correct and if there were no pulses present in counter $\bar{5}$ and $\overline{12}$. Because of the high input rate of pions, many counter 2 and $1\,2\,3\,\bar{4}$ pulses were present on trace 4 of the slow oscilloscopes. When the experiment was run at much lower rates there was rarely more than one $1\,2\,3\,\bar{4}$ pulse present, which thus could be associated with a single muon decay event. The time analysis of these $1\,2\,3\,\bar{4}$ pulses was important in the observation of the process $\mu \to e + \nu + \bar{\nu} + \gamma$ described in the next Section.

We ran the experiment in its final version for about 50 hours and in this time stopped $7.35 \cdot 10^8$ pions in counter 3, taking a total of 5394 pairs of photographs on the oscilloscopes. We scanned the films first for events with a high energy electron (*i.e.*, pulses from counters 8, 9, 10, 11 present on trace 3 of the slow oscilloscope). Examining the fast oscilloscope, the events which were left could be classified into the following categories:

a) *Prompts*: These are events with pulses from counters 2, 6 and 7 in prompt coincidence. Such an event could arise from the decay of a neutral pion produced by a charge exchange interaction of an incoming positive pion.

Of the resulting two γ-rays, one is converted and triggers the electron telescope, and the other triggers the γ-ray telescope. In most of the prompt events a pulse from counter 12 was present on trace 2 of the 4-beam oscilloscope.

b) e(7) γ(6) *events*: Pulses from counters 6 and 7 are present but not from counter 3. This could be a muon decaying with emission of a γ-ray in some place other than counter 3. Some of these events are random; for example the electron from one muon triggers the electron telescope in random coincidence with a γ-ray from another muon.

c) « 3e(7) γ(6) » *events*: These are the same as *b*) but with a pulse from counter 3. They are essentially the events we are searching for and will be analysed in detail. They will, of course, include random events similar to those described in *b*).

d) « 3e(7) 3γ(6) » *events*: These are a class of random events which contain two separate pulses from counter 3, one in coincidence with a pulse in counter 6 and the other with a pulse in counter 7.

e) *Random events*: Triggered by the random coincidence circuit (circuit *D* of Fig. 3) and clearly recognizable. We recorded these for the purpose of comparison. These also could be classified into the categories *b*), *c*), *d*) and a few into category *a*).

After this analysis we were left with 184 events of the first four categories (associated with a high-energy electron) as shown in Table I.

TABLE I.

Prompt	e (7) γ (6)	3e (7) γ (6)	3e (7) 3 γ (6)
65	26	72	21

On examination of trace 2 of the slow oscilloscope it was necessary to reject a further 50 of the 72 events 3e(7) γ(6), because of the presence of $\overline{4}$, $\overline{5}$ or $\overline{12}$ pulses. 31 of the rejections were due to a $\overline{5}$ pluse being present. We did not expect the apparatus to record any such events, and in fact it was verified that these were random events which could be recorded only because the time interval for which the anticoincidence counter $\overline{5}$ was rejecting events was not wide enough to cover the whole acceptance time interval of the coincidence circuit.

The remaining 22 events were then subjected to a careful time analysis, and the associated NaI pulse heights were measured in order to select those events which had the correct e(7) γ(6) time delay, defined to the closest possible limits, and a γ-ray energy lying within the small range defined by the apparatus.

The measurements of distance between pulses on the fast oscilloscope film were made with I.E.P. (Instrument for the Evaluation of Photographs) [11], which is a projector having digitized micrometer movements to read X and Y co-ordinates and recording data directly on punched tape. We measured always the position of the peak of the pulse.

The resolution of the time measuring system, fast oscilloscope film + I.E.P. + + operator, was determined by asking the operator to make repeated measurements of the same event (event 17). The result is shown in the form of a histogram in Fig. 5. It is seen that the resolution (full width at $\frac{1}{2}$ height) is of the order of $\frac{1}{2}$ ns. Since in the final analysis of the 3e(7) γ(6) events each measurement was made at least three times, the uncertainty in the average distances would be only 2 or 3 tenths of a nanosecond. This uncertainty gives a negligible contribution to the overall resolution width for e(7) γ(6) coincidences on the fast oscilloscope.

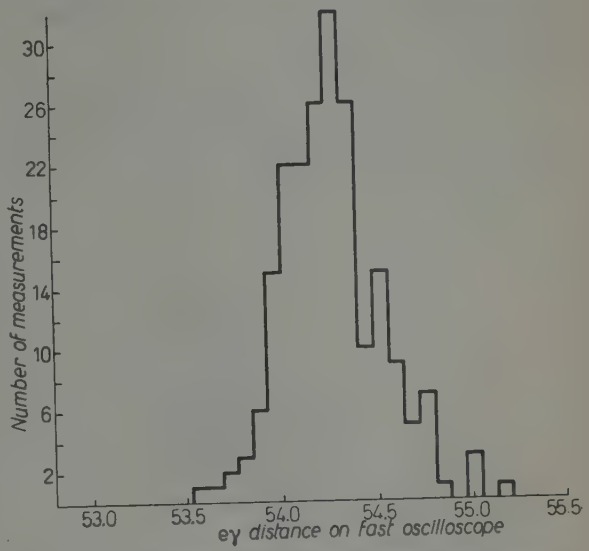

Fig. 5. - Histogram of time delays for repeated measurements on a single 3e(7) γ(6) event.

The total time resolution of the system, scintillators + photomultipliers + + fast oscilloscope film I.E.P. + operator, was determined by measuring 133 « prompt » events (for which one knows that particles went through counters 6 and 7 in exact coincidence). The result obtained is shown in the top part of Fig. 6. The best-fit Gaussian to the histogram has a standard deviation $\sigma = 0.70$ ns. This has been used as the defining time resolution curve in the analysis of the 3e(7) γ(6) events. (*).

---

(11) Y. Goldschmidt-Clermont, G. von Dardel, F. Iselin, L. Kowarski and C. Peyrou: *Nucl. Instr.*, **2**, 146 (1959).

(*) Measurements made in the past wtih the fast oscilloscope have shown that resolutions a factor two better than that discussed above, may be obtained. It may be claimed that by using the poorer time resolution curve defined by the « prompt » events in the analysis of the 22 events 3e(7) γ(6) we have certainly not underestimated the number of « reals ».

Plotted also in Fig. 6 is the expected pulse height distribution from the NaI(Tl) counter for 53 MeV γ-rays emitted from counter 3, and converted within the 3 mm Pb converter. The energy loss distribution of the electron-positron pair in the Pb converter and counter 6 has been taken into account, together with the experimentally determined NaI(Tl) resolution curve for mono-energetic particles.

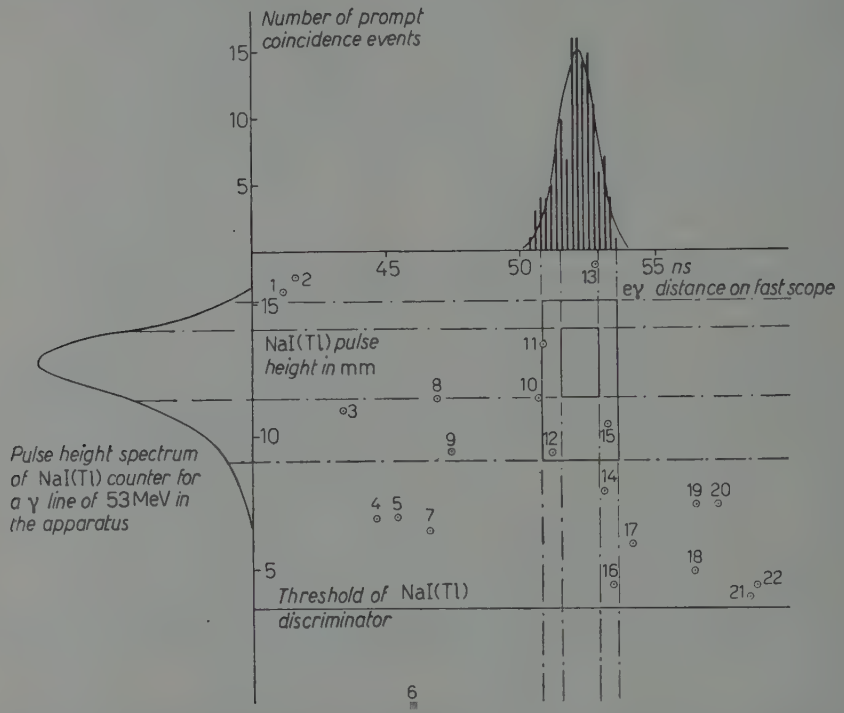

Fig. 6. – Time delay and pulse height analysis of the 22 observed e-γ events. Abscissa gives the time delay between the e(7) and γ(6) pulses; comparison is made with the measured resolution curve for « prompt » events. The ordinate gives the NaI(Tl) pulse height; comparison is made with a computed curve of the expected pulse height distribution for 53 MeV γ-rays incident on the Pb converter.

The final analysis of the 22 events which had an energetic electron, in terms of the time resolution between electron and γ-ray events and in terms of γ-ray energy, is shown in Fig. 6. We have drawn in this figure the threshold for the NaI discrimination and we would expect to see no events below this. One event (6) has, however, been recorded, and this could be due perhaps to « pile up » in the slow coincidence circuit or discriminator.

We have drawn on Fig. 6 « boxes » which correspond to 68% of the area under each of the resolution curves and 95% of the area under each curve. It can be seen that no events survive the first criteria and 3 events (11, 12, 15)

the second. It is clear from the number of events falling outside the time resolution curve that we can attribute a certain number of events in the « boxes » to random events, and this we evaluated to be one event for the larger box.

We have another criterion which we must take into account, and that is the time coincidence between the « 3 » and the « e » pulses for our 22 events. The « 3-e » and the « e-γ » time distributions are plotted in Fig. 7. It is at once clear from this figure that the « 3-e » distribution is considerably narrower than the « e-γ » distribution; but, nevertheless, those events which survived the criteria applied in Fig. 6 (11, 12, 15) survive also this further test.

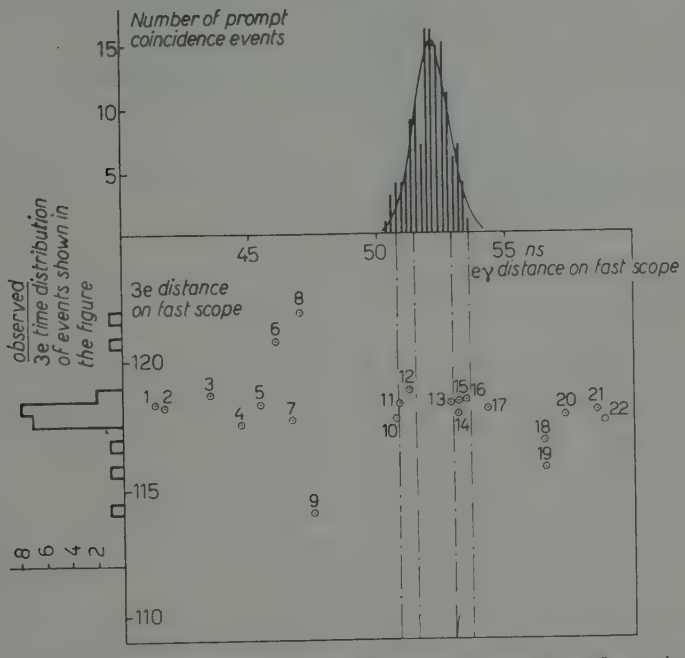

Fig. 7. – Analysis of the 22 3eγ events in terms of the 3e end eγ time delays.

From these results we can deduce the branching-ratio for

$$(\mu \to e + \gamma)/(\mu \to e + \nu + \bar{\nu})$$

once we know the detection efficiency of the apparatus. This we calculated, taking the following factors into account.

a) The geometry of the apparatus. With a Monte Carlo calculation we were able to calculate the probability that an electron and a γ-ray emitted at 180° to each other from any point in counter 3 should enter the solid angles subtended by their respective telescopes. This probability was $1.94 \cdot 10^{-2}$.

b) The detection efficiency of the electron telescope for 53 MeV electrons. For this we used the results of the Monte Carlo calculations of LEISS, PENNER and ROBINSON [12] which led to an efficiency for our telescope of 57%.

c) The conversion efficiency of the lead converter. For this we used the pair production cross-sections of DAVIES, BETHE and MAXIMON [13], which gave a conversion efficiency of 22%.

If we use the number of events observed in the smaller box of Fig. 6, the efficiency of the apparatus is reduced by $(0.68)^2 = 0.46$. If we use the larger box containing 95% of the area of each of the resolution curves, it is reduced by $(0.95)^2 = 0.90$. No correction is necessary for internal bremsstrahlung, as the apparatus was expressly designed to rule out this process, as may be seen in Fig. 8. In this figure the predicted pulse height spectrum for internal bremsstrahlung (based on the calculations of FRONSDAL and ÜBERALL [8]), with all the experimental efficiencies folded in, is compared with the expected spectrum for $\mu \to e + \gamma$ for a branching ratio $(\mu \to e + \gamma)/(\mu \to e + \nu + \bar{\nu})$ of 10^{-6}. This value of the branching ratio was assumed only for the purpose of designing the apparatus. It is seen that the overlap of the two curves is negligible.

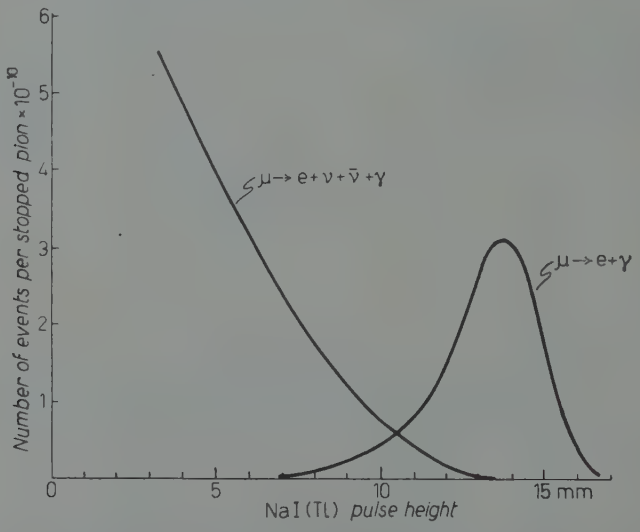

Fig. 8. - Predicted pulse height spectra from the NaI(Tl) counter for the two processes $\mu \to e + \gamma$ and $\mu \to e + \nu + \bar{\nu} + \gamma$ (both curves have a class interval of 0.5 mm).

Taking into account all the factors mentioned above and using the results defined by the larger box, *viz.* 3 events minus one random, we obtained the

---

[12] J. E. LEISS, S. PENNER and C. S. ROBINSON: *Phys. Rev.*, **107**, 1544 (1957), and private communication.

[13] H. DAVIES, H. A. BETHE and L. C. MAXIMON: *Phys. Rev.*, **93**, 788 (1954).

branching ratio

$$\frac{\mu \to e + \nu}{\mu \to e + \nu + \bar{\nu}} = (1.2 \pm 1.2) \cdot 10^{-6}.$$

The error given is essentially the statistical error on 3 events, as the error on the subtracted random event is much smaller.

We also applied the maximum likelyhood method to separate the reals from the randoms, assuming a flat time distribution for the randoms and the known « prompts » Gaussian distribution (of Fig. 6) for the real events. Considering the events lying within the 95% acceptance limit for the NaI(Tl) pulses we obtained essentially the same branching ratio as that given above, *viz.*

$$\frac{\mu \to e + \gamma}{\mu \to e + \nu + \bar{\nu}} = (1.2 \pm 1.5) \cdot 10^{-6}.$$

We will take the second result with the larger error as our final branching ratio.

4. – The internal bremsstrahlung process and a preliminary experiment.

Because we ran the experiment with a very high rate of incoming pions, the rate of random events made it very difficult to make a good analysis of the process $\mu \to e + \nu + \bar{\nu} + \gamma$. However, a preliminary experiment which we made early this year at a much lower beam rate gave the first clear evidence that this process existed. We give in this section a brief account of the experiment and of some computations which we have made using the theory of Fronsdal and Überall ([8]). In the experiment described below we have identified coincidences of electrons and γ-rays and we have shown that they have an exponential time distribution, measured from the entry of the pion into the apparatus, with the known mean life of the muon. The computations show, firstly, that the process occurs at the rate required by the theory and, secondly, that it makes a negligible contribution to the background in our final experiment.

The apparatus we used was essentially similar to that described above. The principal differences were that the electron telescope had only two counters with a graphite absorber of thickness 3.49 g/cm² between them, and that there was an additional counter in the γ-ray telescope with 3.49 g/cm² of graphite absorber between it and counter 6. The NaI(Tl) counter was smaller, 12.5 cm diameter and 10 cm long. We used also a water Čerenkov counter behind the electron telescope, which with the maximum energy available from the beam was sensitive only to electrons. The electron and γ-ray telescopes had effective

energy cut-offs of 15 MeV and 22 MeV respectively, ignoring the information from the Čerenkov and NaI(Tl) counters.

A total of $149 \cdot 10^6$ π-mesons were stopped in counter 3, and the analysis of the films gave 25 real $3e\gamma$ events, which had a preceding $1\,2\,3\,\bar{4}$ pulse (π-μ decay) on the slow oscilloscope. This last requirement was introduced as a condition against cosmic ray background. An integral decay curve of these events is shown in Fig. 9 where the straight line represents the known mean life of the muon. The mean life computed from our 25 events after correcting for the finite length of the time base is (2.5 ± 0.5) μs. The correction to take into account random $1\,2\,3\,\bar{4}$ pulses was negligible because of the low counting rate. The fact that the observed events follow an exponential having the known muon mean life proves that the observed e-γ coincidences came from the decay of the muon.

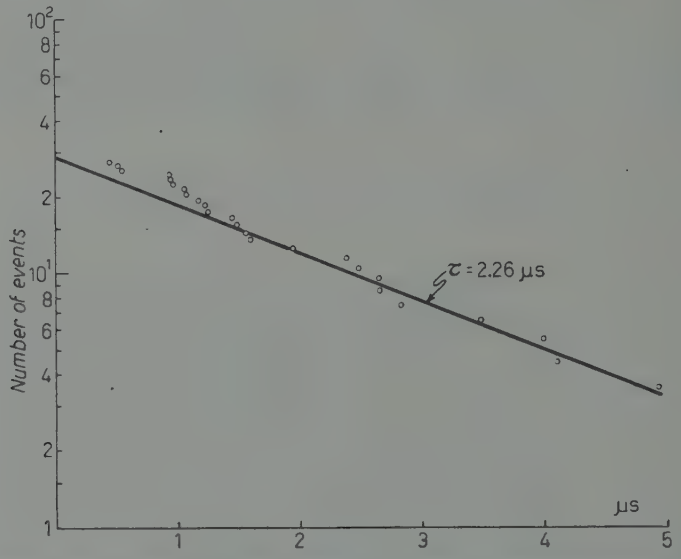

Fig. 9. – Integral decay curve for the observed internal bremsstrahlung events of the early CERN experiment.

The Čerenkov counter was used only to prove that the particles seen by the electron telescope were, in fact, electrons. It was also verified that the γ-ray telescope was detecting γ-rays by means of a run with the lead converter removed.

The pulse height information from the NaI(Tl) counter was not used, as the small size of this counter together with the large absorber thickness between it and the lead converter made its effective energy resolution very poor.

A calculation was made of the expected internal bremsstrahlung rate on the basis of the theory of Fronsdal and Überall ([8]), for the special conditions

considered by them of a 2-component neutrino theory with $V-A$ coupling. With the geometry of the apparatus, and the telescope efficiencies as a function of energy folded into the calculation, the expected number of internal bremsstrahlung events was found be to 40. It is difficult to estimate the error in this figure as this depends on uncertainties in calculating the electron and γ-ray efficiencies, but the computed figure of 40 is certainly quite compatible with the experimental result of 27 ± 5 which is obtained after correcting for the finite length of the time base available for the observation of the incoming pion.

It may be suggested that the agreement between the predicted and measured $\mu \to e + \nu + \bar{\nu} + \gamma$ rate has served as a useful check on the reliability of the apparatus.

* * *

We should like to thank Mr. M. FELL and Mr. M. RENEVEY who were responsible for most of the construction of the apparatus and who helped us considerably in the running of the experiment.

* * *

We should like also to thank Dr. Y. GOLDSCHMIDT-CLERMONT for extending to us the facilities of I.E.P., and M.me H. HEYDER for her helpful and efficient running of our programmes on the Mercury computer. We should like to thank the Harshaw Chemical Company, and in particular Dr. E. C. STEWART, for supplying us at short notice with the very large NaI(Tl) counter.

RIASSUNTO

Il presente lavoro descrive una ricerca del decadimento $\mu \to e + \gamma$. Il risultato è negativo entro la sensibilità dell'esperimento: il rapporto $(\mu \to e + \gamma / \mu \to e + \nu + \bar{\nu})$ è stato trovato $= (1.2 \pm 1.5) \cdot 10^{-6}$. Viene descritta anche la rivelazione del processo $\mu \to e + \nu + \bar{\nu} + \gamma$.

IL NUOVO CIMENTO Vol. XIV, N. 6 16 Dicembre 1959

Analysis of K^- Absorption in Deuterium (*).

T. Kotani (**) and M. Ross

Department of Physics, Indiana University - Bloomington, Ind.

(ricevuto il 31 Agosto 1959)

Summary. — We have examined theoretically the capture of K^- at rest by deuterium, principally in terms of final state $Y\pi$ interactions. In particular we calculated total rates, the momentum spectra associated with the production of $\Sigma^-+n+\pi^+$ and $\Lambda^0+p+\pi^-$, and the corresponding angular correlation. (The latter are not found to be useful except perhaps as a check). On the basis of total rates it is known that capture from the P Bohr orbit through the s wave $K\pi$ channel probably dominates. This assignment is reinforced by the spectrum of the low momentum Λ peak (Λ's converted from Σ's). A definitive check can be made when a somewhat better converted Λ spectrum is measured, since one should observe a double peak (with a cusp at the maximum pion momentum associated with production) if this assignment is correct. Analysis of the high pion momentum Λ peak (directly produced Λ's), using this assignment reveals that the spectrum is insensitive to the $Y\pi$ interaction and yet does not seem to agree with the data. This spectrum shape (and that for $\Sigma^-n\pi^+$) depends significantly on the $K\pi \to Y\pi$ absorption process off the energy shell, which in turn depends on the $K\pi$ scattering lengths. Preliminary comparison of data and theory indicates a large negative real part for the isotopic spin one $K\pi$ scattering length. Finally, from the relative rate for conversion of Σ's into Λ's, we deduce a minimum value for the imaginary part of the isotopic spin $\frac{1}{2}p$ wave $\Sigma\pi$ scattering length. The result, larger than the pion Compton wavelength, indicates a very strong potential in the $\Sigma\pi$ channel and/or coupling $\Sigma\pi$ and $\Lambda\pi$ channels, a potential much stronger than indicated by the universal pion baryon interaction. Capture from the S Bohr orbit is also extensively discussed. In this case, the spectra associated with Σ^- and direct Λ production are sensitive to the final $Y\pi$ interaction.

(*) Supported in part by the National Science Foundation.

(**) Present address: Department of Physics, Tokyo Metropolitan University, Setagaya, Tokyo.

1. – Introduction.

It is the purpose of this paper to show that a study of the reactions of K^- stopped in deuterium may be useful to obtain information on the hyperon-nucleon interaction and may have bearing on the pion-hyperon interaction. Specifically we want to consider the reactions:

$$(1) \qquad K^- + d \to n + \Sigma^- + \pi^+ , \qquad p_\pi^{max} = 177.8 \text{ MeV/c} ,$$

$$(2) \qquad K^- + d \to p + \Lambda + \pi^- , \qquad p_\pi^{max} = 264.5 \text{ MeV/c} .$$

We will consider the momentum spectra (the maximum pion momenta are shown in (1) and (2)) and the angular distributions.

The pion momentum spectra have recently been reported [1]. The spectrum associated with (2) shows two peaks, near 250 MeV/c and 185 MeV/c (see Fig. 5*a*). These are just the pion momenta expected if the K^- were absorbed by a single nucleon to produce $\Lambda+\pi$ and $\Sigma+\pi$, respectively. The higher momentum peak can be explained by direct production of Λ's associated with K^- absorption by one of the nucleons in the deuteron. The lower peak can be interpreted as production of $\Sigma+\pi$:

$$(3) \qquad \left.\begin{matrix} p + (n + K^-) \\ n + (p + K^-) \end{matrix}\right\} \to \left\{\begin{matrix} p + \Sigma^0 + \pi^- \\ n + \Sigma^+ + \pi^- \end{matrix}\right. , \qquad p_\pi^{max} = 186.7 \text{ MeV/c} ,$$

followed by the reaction on the second nucleon:

$$(4) \qquad \left.\begin{matrix} p + \Sigma^0 \\ n + \Sigma^+ \end{matrix}\right\} \to p + \Lambda^0 .$$

(We neglect the $p+\Sigma^0$ and $n+\Sigma^+$ mass difference). The $\Sigma\Lambda$ conversion (4) competes with « elastic » isotopic spin $1=\frac{1}{2}$ Σ-nucleon scattering. This competition has been considered independently by KARPLUS and RODBERG [2].

---

[1] N. HORWITZ, D. MILLER, J. J. MURRAY, M. SCHWARTZ and H. D. TAFT: *Bull. Am. Phys. Soc.*, **3**, 363 (1958), and private communication.

[2] R. KARPLUS and L. S. RODBERG: *Phys. Rev.*, **115**, 1058 (1959). We would like to thank Drs. KARPLUS and RODBERG for communicating their results before publication. See also L. B. OKUŃ and M. I. ŠMUŠKEVIČ: *Žurn. Eks. Teor. Fiz.*. (*U.S.S.R.*), **30**, 979 (1956) [translation: *Sov. Phys.*, **3**, 792 (1956)].

4187

We will emphasize certain features of the process which do not receive emphasis in their work. For example we will discuss the cusplike behavior [3] which should appear in the pion distribution of (2) at the threshold momentum (3) of the Σ production. We will also try to draw some conclusion concerning the universal pion-baryon interaction which predicts a small $\Sigma\Lambda$ conversion cross-section.

The strong interaction of the low momentum $\Sigma\mathcal{N}$ pair can modify the spectrum of their relative momentum k_Σ, and the angular correlation between $\boldsymbol{k}_\Sigma$ and $\boldsymbol{p}_\pi$. If this final state interaction is attractive without a bound state, for instance, a lower relative momentum will be favored and the total reaction rate will be increased. Assuming, as we do, that isotopic spin is conserved in the reactions, since the process (1) involves no $\Sigma\Lambda$ conversion, it depends on fewer unknown parameters and may be convenient for obtaining information on the $\Sigma\mathcal{N}$ ($I=\frac{3}{2}$) interaction.

We shall employ an impulse approximation in which the K^- absorption is by a single nucleon, so it can be specified in terms of the $\overline{K}\mathcal{N}$ T-matrix. This assumption is probably not unreasonable, the reaction range for K^- absorption being small compared to the size of the deuteron. There will be an additional amplitude associated with specifically K^--2$\mathcal{N}$ absorption. The probability for finding the two nucleons within the K-particle Compton wave length of each other in the deuteron is less than 1%. Correspondingly, we may anticipate an average K-2$\mathcal{N}$ amplitude about 10% of the magnitude of the amplitude calculated. The amplitude associated with the K$\mathcal{N}$ process is, however, strongly peaked while the K-2$\mathcal{N}$ amplitude should give rise to a very broad pion momentum distribution. A further simplification can be made since the pion nucleon states which occur are principally isotopic spin $\frac{1}{2}$ states and the corresponding probability for a $\pi\mathcal{N}$ final state interaction is very small. We will neglect $\pi\mathcal{N}$ scattering. For the direct Λ production the $\pi\mathcal{N}$ system is in $I=\frac{1}{2}$ state. In the case of $\Sigma^-\pi^+$n production (1), the probability for this system in the state $[\Lambda(\pi\mathcal{N})_{I=\frac{1}{2}}]$ is eight times the probability in the state $[\Sigma(\pi\mathcal{N})_{I=\frac{3}{2}}]$. The situation is more complicated for the $\Sigma\Lambda$ conversion process. There is large overlap between states $[\Sigma(\pi\mathcal{N})_{I=\frac{3}{2}}]$ and $[\pi(\Sigma\mathcal{N})_{I=\frac{1}{2}}]$, in which we are interested. The main effect of the $\pi\mathcal{N}$ scattering in this case will be distortion of the spectrum shape and not a change in the conversion ratio. We will not try to make quantitative interpretation of the conversion spectrum shape, although we will show that its qualitative features are very interesting. A simple examination shows that significant amplitudes associated with $\pi\mathcal{N}$ scattering will exist for pion momenta in the region of

---

[3] G. BREIT: *Phys. Rev.*, **107**, 1612 (1958); R. G. NEWTON: *Ann. Phys.*, **4**, 29 (1958); A. M. LANE and R. G. THOMAS: *Rev. Mod. Phys.*, **30**, 257 (1958).

the $\Sigma\Lambda$ conversion peak (these momenta can be compared with 230 MeV/c, the relative $\pi\mathcal{N}$ momentum at the $\frac{3}{2}$, $\frac{3}{2}$ resonance), but that these contributions are not large enough to change the qualitative features of the conversion spectrum peak. The neglection of the $\pi\mathcal{N}$ interaction may also be supported by the small production rate, for example, $K^- + d \to \Sigma^- + p$, which is less than 1% of the total (1). In performing our calculation we keep in mind that amplitudes of order 1/10, on the average, of those we are considering, are being neglected.

2. – Formalism.

2·1. *The matrix element.* – We want to assume that the K^- is absorbed by the same mechanism as in the case of a free nucleon. The matrix element can be put in the form,

$$M_{fi} = \langle \psi_f^{(-)} | T_{K\mathcal{N}} | \varphi_i \rangle \,. \tag{5}$$

This form is convenient for the further assumption that the pion does not interact with the nucleon (the π-Y interaction on emission is accounted for in the T-matrix element) (4) (*). Thus, for the final state,

$$\psi_f^{(-)} = g_{Y\Upsilon'}^{(-)}(\boldsymbol{r}) \exp\left[i\boldsymbol{p}_\pi \cdot (\boldsymbol{r}_\pi - \boldsymbol{R})\right], \tag{6}$$

where $\boldsymbol{r}$ is the relative co-ordinate and R the co-ordinate of the center of mass of the $Y\mathcal{N}$ system. We can write

$$\boldsymbol{r}_\pi - \boldsymbol{R} = \boldsymbol{\rho}_{\pi Y} + [M_{\mathcal{N}}/(M_{\mathcal{N}} + M_Y)]\boldsymbol{r} \,.$$

For the initial state,

$$\varphi_i = \Phi_K(\boldsymbol{\rho}_{K\mathcal{N}} + \tfrac{1}{2}\boldsymbol{r}_{12})\, \Phi_d(\boldsymbol{r}_{12}) \,, \tag{7}$$

where $\boldsymbol{r}_{12}$ and ϱ_{ij} are relative co-ordinates of the indicated particles, Φ_d and Φ_K are the deuteron and Bohr orbit wave functions respectively, and the labels 1 and 2 refer to initial nucleons, nucleon « 1 » being assumed to absorb the K. $T_{K\mathcal{N}}$ is the T-matrix for hyperon production in K absorption by a single nucleon.

---

(4) G. F. Chew and G. C. Wick: *Phys. Rev.*, **85**, 636 (1952); G. F. Chew and M. L. Goldberger: *Phys. Rev.*, **87**, 778 (1952); M. Gell-Mann and M. L. Goldberger: *Phys. Rev.*, **91**, 398 (1953).

(*) We shall use the unit $\hbar = c = 1$.

We find the momentum relations among k_{ij}'s, which are relative momenta of the indicated particles;

$$\begin{cases} \boldsymbol{k}_{\mathrm{K}\mathcal{Q}} = \dfrac{2M_{\mathcal{Q}} + M_{\mathrm{K}}}{2(M_{\mathcal{Q}} + M_{\mathrm{K}})}\, \boldsymbol{k}_{\mathrm{kd}} - \dfrac{M_{\mathrm{K}}}{M_{\mathcal{Q}} + M_{\mathrm{K}}}\, \boldsymbol{k}_{12}\,, \\ \boldsymbol{k}_{\pi\mathrm{Y}} = \dfrac{M_{\mathrm{Y}}(M_{\mathrm{Y}} + M_{\mathcal{Q}} + \omega_\pi)}{(\omega_\pi + M_{\mathrm{Y}})(M_{\mathrm{Y}} + M_{\mathcal{Q}})}\, \boldsymbol{p}_\pi - \dfrac{\omega_\pi}{(\omega_\pi + M_{\mathrm{Y}})}\, \boldsymbol{k}_{\mathrm{Y}\mathcal{Q}}\,, \end{cases} \tag{8}$$

where $\omega_\pi^2 = (p_\pi^2 + M_\pi^2)$ is the total pion energy.

The general form of the matrix element is then

$$M_{fi} = \int \mathrm{d}\boldsymbol{r}\, T(\boldsymbol{k}_{\mathrm{K}\mathcal{Q}}, \boldsymbol{k}_{\pi\mathrm{Y}})\, g^{(-)*}(\boldsymbol{r}) \exp[-i\boldsymbol{q}\cdot\boldsymbol{r}]\, \Phi_{\mathrm{K}}\left(\frac{1}{2}\boldsymbol{r}\right) \Phi_{\mathrm{d}}(\boldsymbol{r})\,. \tag{9}$$

The $\boldsymbol{k}_{ij}$'s are now represented by Eq. (8) with $i\boldsymbol{k}_{12}$, $i\boldsymbol{k}_{\mathrm{Kd}}$ and $i\boldsymbol{k}_{\mathrm{Y}\mathcal{Q}}$ replaced by gradients operating on Φ_{d}, Φ_{K}, and $g_{\mathrm{YY}'}$, respectively. Also.

$$\boldsymbol{q} \equiv [M_{\mathcal{Q}}/(M_{\mathcal{Q}} + M_{\mathrm{Y}})]\boldsymbol{p}_\pi\,. \tag{10}$$

We feel that it is justified to approximate the momenta (8) so that

$$\begin{cases} i\boldsymbol{k}_{\mathrm{K}\mathcal{Q}} \to [(2M_{\mathcal{Q}} + M_{\mathrm{K}})/(M_{\mathcal{Q}} + M_{\mathrm{K}})]\boldsymbol{\nabla}', \\ \boldsymbol{k}_{\pi\mathrm{Y}} \to \dfrac{M_{\mathrm{Y}}(M_{\mathrm{Y}} + M_{\mathcal{Q}} + \omega_\pi)}{(\omega_\pi + M_{\mathrm{Y}})(M_{\mathrm{Y}} + M_{\mathcal{Q}})}\, \boldsymbol{p}_\pi\,, \end{cases} \tag{11}$$

where $\boldsymbol{\nabla}'$ operates only on the argument $\boldsymbol{r}$ of Φ_{K} in the matrix element. The angular momentum analysis of T is straightforward, while the energy dependence may be complicated. Since only a narrow range of small $|k_{\mathrm{K}\mathcal{Q}}|$ values are available, we can assume the usual $|k_{\mathrm{K}\mathcal{Q}}|$ threshold dependence for T. The $\pi\mathrm{Y}$ energy dependence of this T-matrix off the energy shell, may however be rapid. It has been suggested that information on the $\pi\mathrm{Y}$ system can be obtained this way [5]. Thus we want to consider the dependence of T on $|k_{\pi\mathrm{Y}}|$ as an unknown of interest.

---

[5] R. H. DALITZ and S. F. TUAN: *Phys. Rev. Lett.*, **2**, 425 (1959); M. ROSS: *Phys. Rev.*, **112**, 986 (1958).

2·2. *The wave functions.* – For the deuteron wave function we use the Hulthén function:

$$\Phi_d = n_d \varphi_d(r) = n_d(\exp[-\alpha r] - \exp[-\beta r])/r , \tag{12}$$

$$n_d = [\alpha\beta(\alpha+\beta)/2\pi(\alpha-\beta)^2]^{\frac{1}{2}}, \tag{13}$$

$$\alpha = 45.7 \text{ MeV} , \qquad \beta = 6.2\,\alpha . \tag{14}$$

Although KARPLUS and RODBERG (2) omit the β term ($\beta \to \infty$), we consider it to be quantitatively significant and will keep it. (See Figs. 1*b*, 5*a* and 6*a*). The neglect of the deuteron D-state will be considered in Section 4. The wave function of the K^- meson is needed in the $1S(L_{Kd}=0)$ and $2P(L_{Kd}=1)$ orbits. Since the Bohr radius, $a_K = (1/\alpha\mu_{Kd})$ is nearly fifteen times the size of the deuteron, we will consider only the value of Φ_K at the origin:

$$1S \text{ orbit:} \qquad \Phi_K(\tfrac{1}{2}\boldsymbol{r}) = n_S = 1/(\pi\alpha_K^3)^{\frac{1}{2}} , \tag{15}$$

$$2P \text{ orbit:} \qquad \Phi_K(\tfrac{1}{2}\boldsymbol{r}) = n_P \tfrac{1}{2}\boldsymbol{e}_i\cdot\boldsymbol{r} , \tag{16}$$

where

$$n_P = 1/(2^5\pi a_K^5)^{\frac{1}{2}} , \tag{17}$$

and $\boldsymbol{e}_i$ specifies the P orbit orientation.

In the final state we treat the baryons non-relativistically. The final energy is given by

$$E_K + M_d - M_{\mathcal{Q}} - M_Y = \omega_\pi + \varepsilon_Y + p_\pi^2/2(M_{\mathcal{Q}} + M_Y) , \tag{18}$$

where ε_Y is the center of mass energy of the $Y\mathcal{Q}$ pair, namely

$$\varepsilon_Y = k_Y^2/2\mu_{Y\mathcal{Q}} , \tag{19}$$

with k_Y, again, the relative momentum in the $Y\mathcal{Q}$ center of mass system. In the intermediate states, or for a bound state, ε_Y may be negative. This situation must be considered when $\Sigma\Lambda$ conversion occurs and $p_\pi > 186.7$ MeV/c. In this case k_Σ goes over to, say, $i\varkappa$, *i.e.*:

$$k_\Sigma \to i\varkappa , \qquad \varkappa > 0. \tag{20}$$

The function $g^{(-)}_{YY'}(\boldsymbol{r})$ of the $Y\mathcal{Q}$ system is readily written down outside the range of the $Y\mathcal{Q}$ interaction. To describe production of Λ's for example, we should consider the direct component:

$$g^{(-)}_{\Lambda\Lambda}(\boldsymbol{r}) = \exp[i\boldsymbol{k}_\Lambda\cdot\boldsymbol{r}] + \Sigma_l f^*_{\Lambda\Lambda,l} g^*_{\Lambda,l}(\boldsymbol{k}_\Lambda, \boldsymbol{r}) , \tag{21}$$

and the conversion component:

$$g^{(-)}_{\Sigma\Lambda}(\boldsymbol{r}) = \Sigma_l f^*_{\Lambda,l} g^*_{\Sigma,l}(\boldsymbol{k}_\Sigma, \boldsymbol{r}) , \tag{22}$$

and similarly for production of Σ's (in practice we do not need to consider production of Σ's via intermediate Λ's). Here the various f_l's are the non-angular parts of the scattering or absorption amplitudes. The symbol f_l itself will be reserved for $\Sigma \to \Sigma$ scattering. We are neglecting non-central forces and do not exhibit the spin function explicitly. We have defined:

$$g_{\Sigma,l} = (-i)^l (2l+1) P_l(\hat{\boldsymbol{k}}\cdot\hat{\boldsymbol{r}}) i k_\Sigma h^{(1)}_l(k_\Sigma r) , \tag{23}$$

where $h^{(1)}_l$ is the spherical Hankel function ([6]). Since the deuteron is large compared to the range of forces the use of h_l is a fairly good approximation, except very near the origin where $h_l \sim (k_\Sigma r)^{-(l+1)}$. Depending on the rate at which the rest of the matrix element vanishes, we sometimes need to improve the behavior of h_l by introducing a term like the β term in the deuteron function (12). So we may use, for example,

$$g'_{\Sigma,0} = (\exp[ik_\Sigma r] - \exp[-\varepsilon r])/r . \tag{24}$$

The use of such a modification will be discussed in each case.-

The total cross-section for $\Sigma\mathcal{N}$ elastic scattering is:

$$\sigma_{\Sigma\Sigma} = \Sigma_l 4\pi (2l+1) |f_l|^2 , \tag{25}$$

and for $\Sigma + \mathcal{N} \to \Lambda + \mathcal{N}$ is

$$\sigma_{\Lambda\Sigma} = \Sigma_l 4\pi (2l+1)(\mu_{\Lambda\mathcal{N}} k_\Lambda / \mu_{\Sigma\mathcal{N}} k_\Sigma) |f_{\Lambda,l}|^2 . \tag{26}$$

The elastic scattering and absorption amplitudes are given in terms of the phase shift:

$$f_l = (\exp[2i\delta_l] - 1)/2ik_\Sigma , \tag{27}$$

$$f_{\Lambda,l} = (\mu_{\Sigma\mathcal{N}}/\mu_{\Lambda\mathcal{N}} k_\Lambda k_\Sigma)^{\frac{1}{2}} \tfrac{1}{2} (1 - \exp[-4 \operatorname{Im} \delta_l])^{\frac{1}{2}} \exp[i \operatorname{Re}(\delta + \delta')] . \tag{28}$$

where δ' is the phase shift in the corresponding Λ-$\mathcal{N}$ channel. We wish to use the scattering length formalism:

$$\operatorname{tg} \delta_l = - k_\Sigma^{2l+1} [A_l(k_\Sigma) - iB_l(k_\Sigma)] , \tag{29}$$

([6]) L. I. SHIFF: *Quantum Mechanics* (New York, 1955), pp. 77 and 79.

where A and B are real and $B > 0$. If there is only elastic scattering, $B = 0$. We have

$$f_l = k_\Sigma^{2l}\{-A_l + i[B_l + k_\Sigma^{2l+1}(A_l^2 + B_l^2)]\}/\Delta_l \,, \tag{30}$$

$$|f_{\Lambda,l}|^2 = |k_\Sigma|^{2l}(\mu_{\Sigma\mathcal{N}}/\mu_{\Lambda\mathcal{N}}\, k_\Lambda)\, B_l/\Delta_l \,, \tag{31}$$

where

$$\Delta_l = (1 + k_\Sigma^{2l+1} B_l)^2 + (k_\Sigma^{2l+1} A_l)^2 \,. \tag{32}$$

For imaginary k_Σ, (20) we have a different definition for Δ_l, namely,

$$\Delta_l' = [1 - (-1)^l \varkappa^{2l+1} A_l]^2 + (\varkappa^{2l+1} B_l)^2 \,. \tag{33}$$

The entire final state wave function formalism above is independent of the relative Σ-Λ parity. One merely needs to keep in mind that l refers to the Σ-$\mathcal{N}$ orbital angular momentum in the final state.

3. – Angular momentum states.

3·1. *Matrix elements for S and P Bohr orbits.* – In addition to analyzing the final state in terms of the $Y\mathcal{N}$ orbital angular momentum, l, we need to consider two different orbital angular momenta in the initial state. We denote by $L_{K\mathcal{N}}$ the channel in which the $K^-\mathcal{N}$ interaction takes place. (Lower case s and p will be used.) It is sufficient to consider s and p channels so that

$$T(k_{K\mathcal{N}}, k_{\pi Y}) = T_0(\boldsymbol{k}_{Y\pi}, \boldsymbol{\sigma}) + \boldsymbol{T}_1(\boldsymbol{k}_{Y\pi}, \boldsymbol{\sigma})\cdot \boldsymbol{k}_{K\mathcal{N}} \,. \tag{34}$$

(See the discussion of Section 2·1). If the K is pseudoscalar with respect to $\mathcal{N}\Sigma$, T is scalar and $\boldsymbol{T}_1$ vector. Otherwise, for scalar K, T_0 is pseudoscalar and T_1 pseudovector. All but the first T_0 will have some spin dependence. We are not prepared, however, to separately examine the triplet and singlet $Y\mathcal{N}$ interaction in the final state. We will not evaluate the spin matrix element of the l.h.s. of (36) and (37) below for general spin dependent T_I. Instead the results will apply directly to the non-spin-dependent T-matrix possible for pseudoscalar K^-:

$$T_0 = T_0(k_{Y\pi}^2) \,, \qquad \boldsymbol{T}_1 = T_1(k_{Y\pi}^2)\, \boldsymbol{k}_{Y\pi} \,, \tag{35}$$

which leaves the two baryons in the triplet state. In the case of spin dependence the results will apply to some average over singlet and triplet final states.

Aside from affecting the polarization (which we now ignore) the parity of the K-particle does not influence the formalism or results significantly. We will use the form (35) in following sections.

We denote by L_{Kd}, or capital S, and P, the K^- Bohr orbit of interest. Then we write the matrix element (9):

$$M_{fi}(S) = 4\pi n_{\mathrm{d}} n_s T_0 \mathscr{M}_{0Y} , \tag{36}$$

$$M_{fi}(P) = 4\pi n_{\mathrm{d}} n_P \left[T_0 \mathscr{M}_{1Y} - i \boldsymbol{T}_1 \cdot \boldsymbol{e}_i \frac{(2M_{\mathcal{N}} + M_{\mathrm{K}})}{2(M_{\mathcal{N}} + M_{\mathrm{K}})} \mathscr{M}_{0Y} \right] , \tag{37}$$

where

$$\mathscr{M}_{0Y} = \frac{1}{4\pi} \int \mathrm{d}\boldsymbol{r}\, g_Y^{(-)*}(\boldsymbol{r}) \exp[-i\boldsymbol{q}\cdot\boldsymbol{r}] \varphi_{\mathrm{d}} , \tag{38}$$

$$\mathscr{M}_{1Y} = \frac{1}{4\pi} \int \mathrm{d}\boldsymbol{r}\, g_Y^{(-)*}(\boldsymbol{r}) \exp[-i\boldsymbol{q}\cdot\boldsymbol{r}] \frac{1}{2} \boldsymbol{r}\cdot\boldsymbol{e}_i \varphi_{\mathrm{d}} . \tag{39}$$

The interpretation of (37) is that although $L_{\mathrm{Kd}} \quad 1$, absorption can take place through the s wave $\mathrm{K}^-\mathcal{N}$ channel, because of the finite deuteron size. This is the T_0 term. There is also p wave absorption from the P Bohr orbit as represented by the $\boldsymbol{T}_1$ term.

3·2. *Total capture rates.* – The capture rate for given L_{Kd} and $L_{\mathrm{K}\mathcal{N}}$ has the form:

$$\Gamma(L_{\mathrm{Kd}}, L_{\mathrm{K}\mathcal{N}}) = 2\pi \int \frac{\mathrm{d}\boldsymbol{k}_Y \, \mathrm{d}\boldsymbol{p}_\pi}{(2\pi)^6 \, \mathrm{d}E_{\mathrm{d}}} |M_{fi}|^2 . \tag{40}$$

If we assume that the k_Y integration limits can be extended over all space and if we neglect the final state $\Sigma\mathcal{N}$ interaction, then we can use closure, and we see from (38) and (39) for s and p wave $\mathrm{K}\mathcal{N}$ absorption, respectively:

$$\Gamma(P, s) \approx \frac{\pi}{3} n_P^2 \left(\frac{1}{2} b_{0,s} + \frac{3}{2} b_{1,s} \right) r_{\mathrm{d}}^2 / \mu_{\mathrm{K}\mathcal{N}} , \tag{41}$$

$$\Gamma(P, p) \approx \pi n_P^2 \left(\frac{1}{2} b_{0,p} + \frac{3}{2} b_{1,p} \right) \left(\frac{2M_{\mathcal{N}} + M_{\mathrm{K}}}{M_{\mathcal{N}} + M_{\mathrm{K}}} \right)^2 \Big/ \mu_{\mathrm{K}\mathcal{N}} , \tag{42}$$

where we have identified our $T_{L(\mathrm{K}\mathcal{N})}$ matrix element as the sum of Kn and Kp contributions near zero momentum:

$$\frac{\mathrm{d}^3\boldsymbol{k}_\pi}{(2\pi)^3 \, \mathrm{d}E_p} |T_{L(\mathrm{K}\mathcal{N})}|^2 = 2(2L_{\mathrm{K}\mathcal{N}} + 1) \left(\frac{1}{2} b_{0,L} + \frac{3}{2} b_{1,L} \right) \Big/ \mu_{\mathrm{K}\mathcal{N}} , \tag{43}$$

where $b_{I,L}$ is the imaginary part of the scattering length for $K\pi$ scattering with isotopic spin I. The closure approximation overestimates Γ by about 20% (neglecting final state interaction). Eqs. (41) and (42) become,

$$\Gamma(P, s) \approx 8.5(\tfrac{1}{2}b_{0,s} + \tfrac{3}{2}\, b_{1,s})\cdot 10^{12}\ \mathrm{s}^{-1}\,, \tag{44}$$

$$\Gamma(P, p) \approx 9.2\,(\tfrac{1}{2}b_{0,p} + \tfrac{3}{2}\, b_{1,p})\cdot 10^{12}\ \mathrm{s}^{-1}\,, \tag{45}$$

where the b's are expressed in units of 10^{-13} cm. Analysis of K-p reactions yields ([7,8])

$$0.5 \leqslant \tfrac{1}{2}b_{0,s} + \tfrac{3}{2}b_{1,s} \leqslant 1.0 \quad \text{in units of } 10^{-13}\ \mathrm{cm}\,. \tag{46}$$

By subtracting an estimated s wave absorption cross-section from the K^--p data at 400 MeV/c ([9]), we find a value for p wave absorption (which is essentially an upper limit). Thus,

$$\tfrac{1}{2}b_{0,p} + \tfrac{3}{2}b_{1,p} \leqslant 0.1 \quad \text{in units of } (10^{-13}\ \mathrm{cm})^3. \tag{47}$$

Meanwhile the γ-ray transition to the $1S$ state has the rate $4.8\cdot 10^{11}\ \mathrm{s}^{-1}$. We are merely confirming the results of DAY and SNOW that $\Gamma(P, s)$ probably dominates ([10]).

There is sufficient uncertainty, however, to make it worthwhile to calculate $\Gamma(P, p)$ and $\Gamma(S, s)$ as well as $\Gamma(P, s)$. The former two rates have the same structure as seen from (36) and (37), except for the possibility of interference in (37). We will not explicitely discuss $\Gamma(P, p)$, or in other words, we consider only $L_{K\pi} = 0$, in the following sections.

4. – The Σ^- production: $K^- + d \to n + \Sigma^- + \pi^+$.

In this case we have no $\Sigma\Lambda$ conversion. To discuss the momentum spectrum it is clear that the interesting momentum is the relative $\Sigma\pi$ momentum k_Σ and not p_π. Indeed we would like to point out that near the maximum pion momentum, where k_Σ is small, it may be possible to directly measure k_Σ fairly accurately, so that k_Σ is also the most meaningful experimental quantity.

([7]) R. H. DALITZ and S. F. TUAN: *Ann. Phys.*, **8**, 100 (1959).
([8]) M. ROSS and G. SHAW: *Phys. Rev.* (to be published).
([9]) A. H. ROSENFELD: *Bull. Am. Phys. Soc.*, **3**, 363 (1958).
([10]) T. B. DAY and G. A. SNOW: *Phys. Rev. Lett.*, **2**, 59 (1959).

We propose the comparison of experiment with the effective range approximation (see (29)):

$$\frac{1}{A_l(k)} = \frac{1}{a_l} - \frac{1}{2} r_l k_\Sigma^2 , \qquad B_l = 0 . \tag{48}$$

We calculate the transition probability from (36), (37), and (40). We will not explicitly show the T-matrix elements, $T_i(k^2_{Y\pi})$. These are approximately multiplicative factors which will not affect the spectrum shape very much (because p_π, (11), is almost constant in the region of interest), except for strongly energy dependent $Y\pi$ interactions which will be discussed in the concluding section. Omitting all constant factors we find:

$$\frac{\mathrm{d}\Gamma(L_{Kd}, s)}{\mathrm{d}k_\Sigma} \sim I^a(L_{Kd}) + \Sigma_l[- A_l I_l^b(L) + A_l^2 I_l^d(L)]/\Delta_l . \tag{49}$$

Here Δ_l is defined in (32). The first term represents production into the plane wave final state, the second, interference between plane wave and scattered $\Sigma\mathcal{N}$ wave, and the third term includes both interference and pure scattered wave contributions.

First consider S Bohr orbit capture ($L_{Kd} = 0$), $\Gamma(S, s)$. The angular momentum l of the $\Sigma\mathcal{N}$ system should be the same as that of the pion, since the K has spin 0 (38). We have the following expression for $I(0)$:

$$I^a(0) = \frac{1}{4\pi} w_\Sigma \int \mathrm{d}\Omega_{qk} \left| \frac{1}{\alpha^2 + (\boldsymbol{k}_\Sigma + \boldsymbol{q})^2} - (\alpha \Rightarrow \beta) \right|^2 , \tag{50}$$

$$I_l^b(0) = -2(2l+1) W_\Sigma k_\Sigma^{2l+1} J^0_{l,l} N^0_{l,l} , \tag{51}$$

$$I_l^d(0) = (2l+1) W_\Sigma k_\Sigma^{4l+2} [(N^0_{l,l})^2 - (J^0_{l,l})^2] , \tag{52}$$

where

$$W_\Sigma = q\omega_\pi k_\Sigma^2 (M_{\mathcal{N}} + M_Y + \omega_\pi)^{-1} , \tag{53}$$

$$J^L_{l,l'} = \int \mathrm{d}r r^{2+L} j_l(k_\Sigma r) j_{l'}(qr) \varphi_d(r), \tag{54}$$

$$N^L_{l,l'} = \int \mathrm{d}r r^{2+L} n_l(k_\Sigma r) j_{l'}(qr) \varphi_d(r) . \tag{55}$$

In capture from the P Bohr orbit ($L_{Kd} = 1$) through the s wave $K\mathcal{N}$ channel ($L_{K\mathcal{N}} = 0$), $\Gamma(P, s)$, the $l = 0$ and $l = 1$ waves of the final $\Sigma\mathcal{N}$ system are associated with p and s pion waves respectively (39). We see this in the expres-

sions for $I(1)$:

$$(56)\quad I^a(1) = \frac{1}{4\pi} W_\Sigma \int \mathrm{d}\Omega_{qk} \left| \frac{(\boldsymbol{k}_\Sigma^+ + \boldsymbol{q})\cdot \boldsymbol{l}_i}{[\alpha^2 + (\boldsymbol{q} + \boldsymbol{k}_\Sigma)^2]^2} - (\alpha \Rightarrow \beta) \right|^2,$$

$$(57)\quad I_l^b(1) = -\tfrac{1}{2} W_\Sigma k_\Sigma^{2l+1} [l J^1_{l,l-1} N^1_{l,l-1} + (l+1) J^1_{l,l+1} N^1_{l,l+1}],$$

$$(58)\quad I_l^d(1) = \tfrac{1}{4} W_\Sigma k_\Sigma^{4l+1} \{ l[(N^1_{l,l-1})^2 - (J^1_{l,l-1})^2] + (l+1)[(N^1_{l,l+1})^2 - (J^1_{l,l+1})^2] \}.$$

We wish to consider relatively small k_Σ where effective range theory (48) may be valid. We see that the transition probability has the k_Σ dependence: k_Σ^2 from the density of states with respect to k_Σ, and k_Σ^{2l} (at least) from the square of the matrix element. For capture from the S Bohr orbit ($L_{\mathrm{Kd}} = 0$), this k_Σ^{2l+2} centrifugal barrier dependence suffices to make the s wave final state interaction dominate over an interesting region. We show $I^b(0)$ and $I^d(0)$ for $l = 0$ in Fig. 1*a*. Typical results for $\mathrm{d}\Gamma(S, s)/\mathrm{d}k_\Sigma$ are shown in Fig. 1*b*.

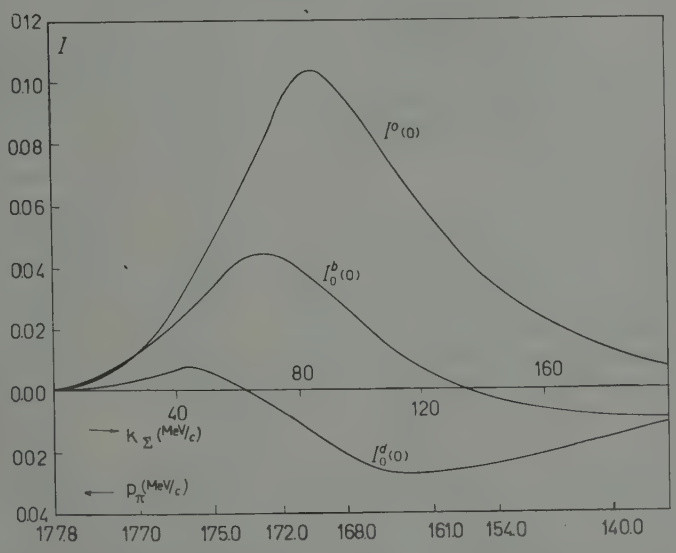

Fig. 1*a*. - Phase shift independent factors $I(0)$ occurring in $\Gamma(S, s)$ for Σ^- production. See eq. (49) and eqs. (50)-(52). The numerical values of I are shown in pion mass units.

The omission of the β term in the deuteron wave function (12) ($\beta \to \infty$) changes the final state interaction significantly, as shown in Fig. 1*b*. The contribution from the ε term, like (24), is not important, *i.e.* about 5% in the rate. Hereafter, we will include the β term, but omit the ε term. For capture from the P Bohr orbit ($L_{\mathrm{Kd}} = 1$), in addition to the k_Σ^{2l+2} dependence, the strong preference for small pion angular momentum becomes important. One finds that the $l = 0$ and $l = 1$ final state interactions are depressed and

enhanced respectively (compared to the S Bohr orbit case), such that both are rather insignificant. Thus, the final state interaction does not modify the spectrum importantly in this case. This is shown in Figs. 2*a* and 2*b*. Both s and p wave final state interaction effects are shown. The amplitude associated with the deuteron D-state was calculated at $k_\Sigma = 0$ in this case and found to be about 10% of that associated with the deuteron S-state. It is the total rate which is principally affected. We neglect this effect.

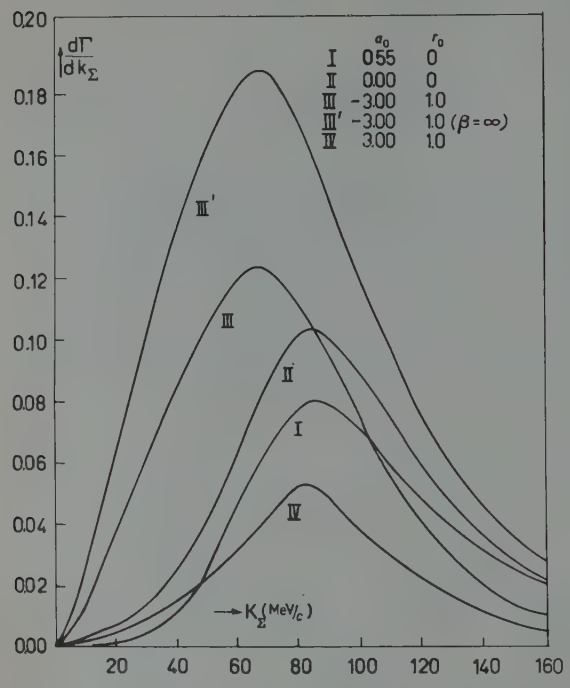

Fig. 1*b*. – The $\Sigma^-n\pi^+$ momentum spectrum $\Gamma(S, s)$ with respect to k_Σ for various scattering lengths and effective ranges of the final state interaction. The latter are given in pion mass units. The relative normalization of the curves is meaningful.

We may conclude that if (and only if) S wave Bohr orbit capture dominates, it is a reasonable experimental possibility to learn something about the (s-wave) Σ^-n interaction. From Figs. 1*b* and 2*b* we see how the spectrum shape changes from the plane wave (case II) to typical attractive (III), repulsive (I), and bound state (IV) cases. These spec-

TABLE I. – *The ratio* $\Gamma_{0-85}/\Gamma_{85-140}$ *for the* Σ^- *production process for various values of scattering length and effective range.* Γ_{i-j} is the number of events from $k_\Sigma = i$ to j (MeV/c). Only the s wave final state interaction is taken into account. a_0 and r_0 are given in units of 10^{-13} cm. E_B is the binding energy. All values are calculated for $\beta = 6.2\alpha$, (14), except the parenthesis which is given for $\beta = \infty$.

a_0	r_0	$\frac{\Gamma(S, s)_{0-85}}{\Gamma(S, s)_{85-140}}$	$\frac{\Gamma(P, s)_{0-85}}{\Gamma(P, s)_{85-140}}$	Note
0.78	0	0.71	0.80	repulsive
0		0.88 (0.82)	0.85	no interaction
— 0.78	3.82	1.09	0.89	attractive no bound state
— 4.14	1.41	2.08 (1.87)	0.85	attractive no bound state
— 14.1	1.41	2.83	0.84	attractive no bound state
+ 7.07	1.41	1.61	0.63	$E_B = 0.94$ MeV
+ 4.24	1.41	1.09	0.59	$E_B = 3.31$ MeV

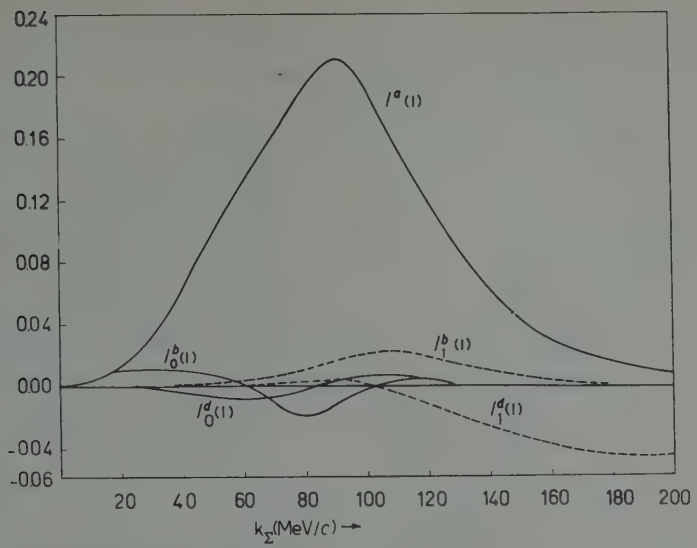

Fig. 2*a*. – Phase shift independent factors $I^a(1)$, $I_0(1)$, and $I_1(1)$ occurring in $\Gamma(P, s)$ for Σ^- production, associated with the plane wave and s and p wave final state interaction contributions, respectively. See eq. (49) and eqs. (56)-(58). The numerical values of I are shown in pion mass units.

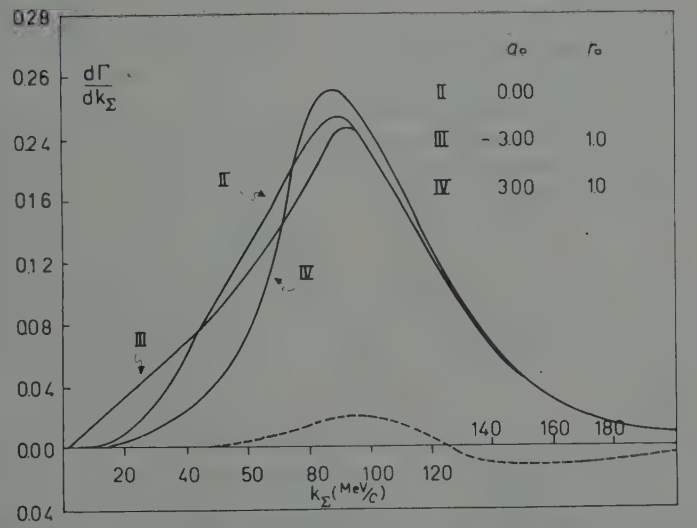

Fig. 2*b*. – The $\Sigma^-n\pi^+$ momentum spectrum $\Gamma(P, s)$ with respect to k_Σ for various scattering lengths and effective ranges of the final state s wave interactions and zero p wave scattering length. The dashed curve should be added to any solid curve to obtain the effects of p wave final state scattering with $a_1 = -1.0$ and $r_1 = 0$ (*i.e.*, the dashed curve represents the $l=1$ contribution of the second term on the r.h.s. of (49)). The a's and r's are given in pion mass units. The relative normalization of the curves is meaningful.

trum changes can also be described by comparing the areas under the curves in given regions of k_Σ. As an example, the ratio of probabilities in the region $0 < k_\Sigma < 85$ MeV/c and $85 < k_\Sigma < 140$ MeV/c is given in Table I.

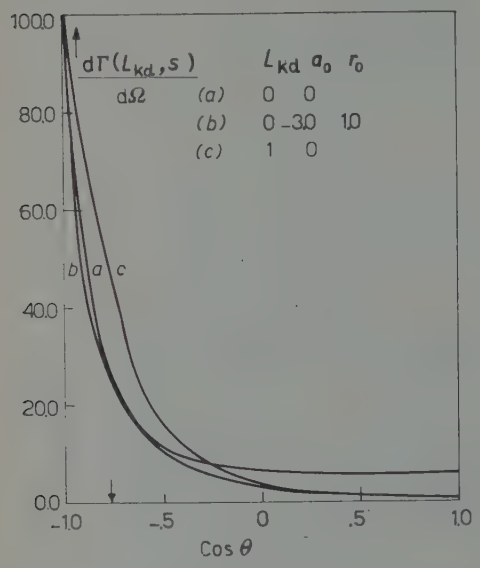

Fig. 3. – The angular correlation between the pion momentum $\boldsymbol{p}_\pi$ and relative Σ^-n momentum $\boldsymbol{k}_\Sigma$ for absorption from S and P Bohr orbits. The scattering length and effective range (in pion mass units) refer to the s wave final state interaction. The curves are normalized at $\theta = 180°$.

Finally we consider the angular correlation after integration over energy. Consider the angle θ between $\boldsymbol{p}_\pi$ and the relative Σn momentum $\boldsymbol{k}_\Sigma$. The correlation is strongly peaked for π and Σ moving in opposite directions, as shown in Fig. 3. They are rather similar for $\Gamma(P, s)$ and $\Gamma(S, s)$. This is also shown in Table II where possibilities for distinguishing these cases by considering the ratio of events for $\theta < j$ and $\theta > j$ are shown (j being a conveniently chosen angle). The change in the distribution $\Gamma(S, s)$ due to a strong attractive final state interaction is also shown in Fig. 3 and Table II. If this angle can be measured accurately in the region near 180° this measurement should be valuable in distinguishing $\Gamma(S, s)$ as a function of the final state interaction. This is the same type of information that is available in the momentum spectrum, if S orbit capture dominates. It appears difficult however to distinguish $\Gamma(P, s)$ from $\Gamma(S, s)$. We again expect, of course, that the $\Gamma(P, s)$ angular distribution is not sensitive to final state interaction.

TABLE II. – *The ratio $\Gamma_{0-j}/\Gamma_{j-180}$ for Σ^- production, where Γ_{i-j} is the number of events from $\theta = i°$ to $\theta = j°$, θ being the angle between $\boldsymbol{k}_\Sigma$ and $\boldsymbol{p}_\pi$.* The s state final state interaction with $a_0 = -4.14$ and $r_0 = 1.41$ in units of 10^{-13} cm is included for the case of $\Gamma(S, s)$.

	$L_{Kd} = 0,\ L_{K\eta} = 0$		$L_{Kd} = 1,\ L_{K\eta} = 0$
	no final int.	S-wave final int.	no final interaction
$\Gamma_{0°-140°}/\Gamma_{140°-180°}$	0.72	1.36	0.79
$\Gamma_{0°-120°}/\Gamma_{120°-180°}$	0.27	.65	.22

5. – The Λ production: $K^- + d \to p + \Lambda + \pi^-$.

5·1. *Direct* Λ *production.* – At very high pion momenta, the Λ's are produced directly in the K^- absorption, and the final $\Lambda\mathcal{N}$ interaction involves no hyperon conversion. The discussion corresponds exactly to that of the previous section on production of the $\Sigma^- n$ system. In Fig. 4, we present the data and curves for $\Gamma(S, s)$ and $\Gamma(P, s)$ with no final state interaction. These curves do not agree with experiment. Also shown is a curve for $\Gamma(S, s)$ with an attractive interaction. It provides a fit to the data. This can be compared with hyperfragment data. The interaction proposed in Fig. 4 is satisfactory in that it is not strong enough for binding, in agreement with the observation that the Λp system probably has no bound state. The interaction is slightly stronger than the triplet interactions proposed in connection with hyperfragment analysis ([11,12]). It is the singlet interaction which is rather strong in the preferred interpretation of hyperfragments. We have a pure triplet Λp system in the S orbit capture of a pseudoscalar K^- and $\frac{2}{3}$ triplet plus $\frac{1}{3}$ singlet for a scalar K^-. The possibility of agreement with hyperfragment data for S orbit capture is thus fairly good. The objection is, of course, that, according to the rough estimation in Section 3·2, we expect the P orbit capture, $\Gamma(P, s)$, and not $\Gamma(S, s)$ or $\Gamma(P, p)$ to dominate. In the case of $\Gamma(p, s)$ we have already seen (Fig. 2*b*) that the final state interactions cannot lead to an important change in the spectrum shape. We will consider the possibility that the dependence of the absorption T-matrix on the $\Lambda\pi$ energy may provide a satisfactory explanation of this spectrum shape in Section **6**.

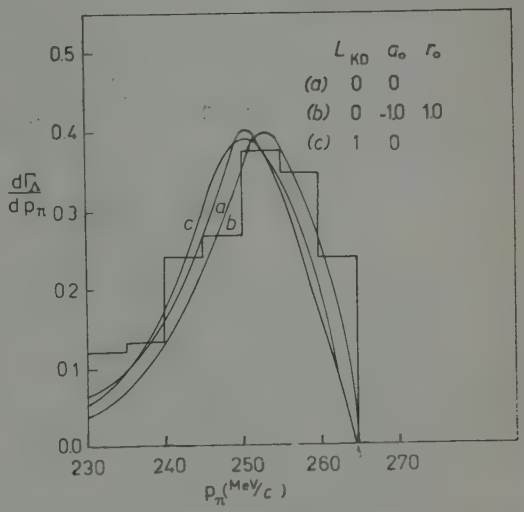

Fig. 4. – The pion momentum spectrum associated with direct Λ production for absorption from S and P Bohr orbits. The scattering length and effective range in the final s state interaction are given in pion mass units. The histogram represents the experimental data in arbitrary units. The curves are also arbitrarily normalized.

(11) R. H. Dalitz and B. W. Downs: *Phys. Rev.*, **111**, 967 (1958); M. H. Ross and D. B. Lichtenberg: *Phys. Rev.*, **110**, 737 (1958).

(12) D. B. Lichtenberg and M. H. Ross: *Phys. Rev.*, **107**, 1714 (1957).

5·2. *The* $\Sigma\Lambda$ *conversion process.* – In this case we will consider the pion momentum spectrum instead of the spectrum with respect to k_Σ or k_Λ. We find for converted Λ's (omitting the same constant factor as in (49)):

$$\frac{\mathrm{d}\Gamma_\Lambda(L_{\mathrm{Kd}})}{\mathrm{d}p_\pi} \sim \left(\frac{M_\Sigma}{M_\Sigma + M_{\mathcal{N}}}\right) \Sigma_l B_l K_l(L_{\mathrm{Kd}})/\Delta_l , \tag{59}$$

where

$$K_l(0) = (2l+1)q^2 |k_\Sigma|^{2l+2} |H^0_{l,l}|^2 , \tag{60}$$

$$K_l(1) = \tfrac{1}{4}q^2 |k_\Sigma|^{2l+2} [l |H^1_{l,l-1}|^2 + (l+1) |H^1_{l\,l+1}|^2] , \tag{61}$$

with

$$H^L_{l,\nu} = \int \mathrm{d}r r^{2+L} h''_l(k_\Sigma r) j_\nu(qr) \varphi_{\mathrm{d}} . \tag{62}$$

Here l, it is recalled, is the $\Sigma\mathcal{N}$ orbital angular momentum. For imaginary k_Σ, we replace: $k_\Sigma \to ix$ and $\Delta_l \to \Delta'_l$ (33).

In contrast with the $\Sigma\mathcal{N}$ scattering case above, the conversion transition probability, $K_l(L)$, is independent of k_Σ for small k_Σ. In other words, both the density of states and matrix element are independent of k_Σ. This can be explained simply. There is no centrifugal barrier in the intermediate state (*i.e.* the $\Sigma\mathcal{N}$ system before interaction). The k_Σ dependence is then associated with the final wave function only, *i.e.* $g_{\Sigma\Lambda}$ (22) with $|f_{\Lambda,l}|^2$ (32), so the matrix element for the conversion is independent of (small) k_Σ, while the matrix element for Σ production goes as k^l_Σ, as seen in $g_{\Sigma\Sigma}$ like (21). An interesting feature of this unusual behavior is that the convergence of the sum over l in

TABLE III. *The comparison of contributions from higher partial wave for* $\Sigma\Lambda$ *conversion in the* $\Gamma(P, s)$ *case,* (59) *and* (63). The ratio is calculated at the Σ threshold, *i.e.* $k_\Sigma = 0$, and in pion mass units.

l	$K_{l+1}(1)/K_l(1)$
0	0.61
1	1.01
2	0.55
3	0.42
	0.32

(59) must come mainly from the imaginary scattering length B_l. The situation is particularly striking for P Bohr orbit capture. We show in Table III the ratio $K_{l+1}(1)/K_l(1)$ at the point $k_\Sigma = 0$. Analytically this can be shown to be

$$K_{l+1}(1)/K_l(1) = q^2(1 + l^{-1})(1 + 1/2l)^2 C_{l+1}/C_l , \tag{63}$$

for $l > 0$, where $q^2 = 0.35$ and $C_{l+1}/C_l \approx 0.8$ for small k_Σ in the units of pion mass. It is seen that the partial wave expansion converges slowly. This is again shown for K_l in Fig. 6*a*. Actually for potentials that are not extremely strong, we can expect the B's to go to zero rapidly with l.

We can conclude that the expansion (59) in partial waves of the final state includes perhaps three important terms ($l = 0$, 1, and 2) for P orbit capture $\Gamma(P, s)$. On the other hand, the dominant term in the S orbit capture case, $\Gamma(S, s)$, in the s wave final state interaction, as shown in Fig. 5*a*. In the latter case we can expect a roughly isotropic angular distribution and a simple spectrum. In the former case, the analysis of the angular correlation will be very complex. A very detailed analysis of the momentum spectrum in the $\Gamma(P, s)$ case is also unpromising. The qualitative features are interesting, however.

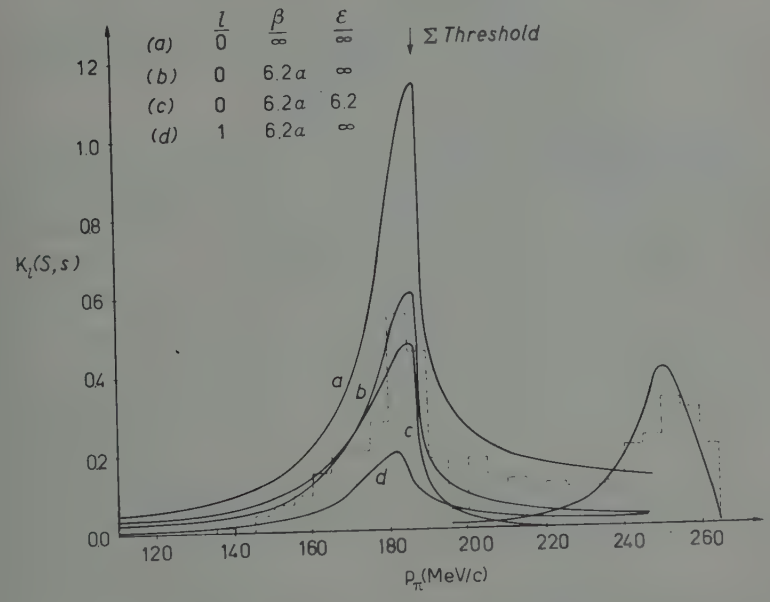

Fig. 5*a*. – The phase shift independent factor $K_l(0)$ occurring in the (pion) momentum spectrum $\Gamma_\Lambda(S, s)$ associated with $\Sigma\pi$ conversion in s and p states. See eqs. (59) and (60). The dependence of the conversion rate and shape on the β and ε terms, (12) and (24), in the initial and final baryon wave function used, is shown. K is given in pion mass units. The histogram represents the experimental data for the transition probability (not directly comparable with K_l) in arbitrary units. The curve at high momentum is the plane wave spectrum $\Gamma(S, s)$ associated with directly produced Σ's (arbitrarily normalized).

In Figs. 5*a* and 6*a*, the quantity K_l which is independent of the scattering length, is plotted for the cases of S and P Bohr orbit capture, respectively. One of the most prominent features is the infinite derivative in $K_0(I_c)$ as

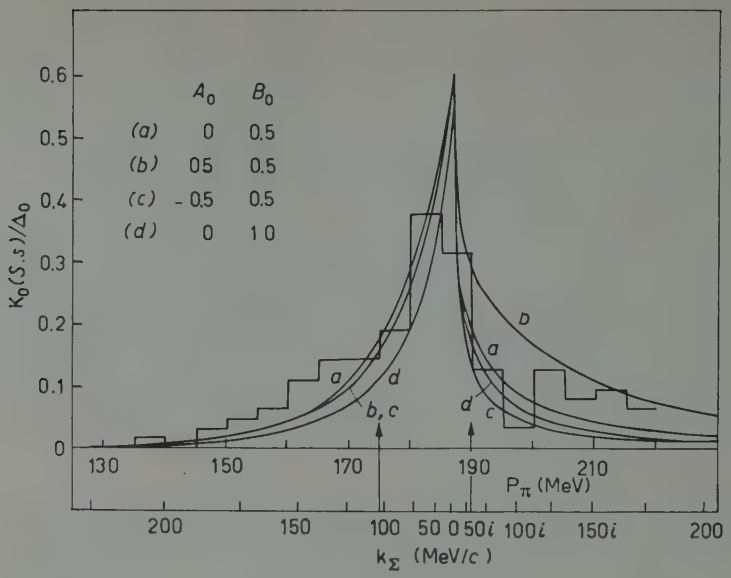

Fig. 5*b*. – The pion momentum spectrum $K_l(S, s)/\Delta_l$ (59) for converted Λ's. The curves are automatically normalized at $k_\Sigma = 0$. The real and imaginary S wave scattering lengths determining the conversion are given in pion mass units. The special region (64) considered for the conversion ratio is indicated. The histogram represents the (arbitrarily normalized) data.

$k_\Sigma = 0$. Taking into account the factor $1/\Delta_0$ we find cusps at this point in the transition probability with respect to p_π (Figs. 5*b* and 6*b*). To see the size and origin of these cusps we present in Table IV an expansion of $\mathrm{d}\Gamma/\mathrm{d}p_\pi$ with respect to k_Σ at small k_Σ. Since $\mathrm{d}k_\Sigma/\mathrm{d}p_\pi \sim p_\pi/k_\Sigma$ the cusps are associated with terms linear in k_Σ. As in the cases of two particle channels the cusp only occurs in association

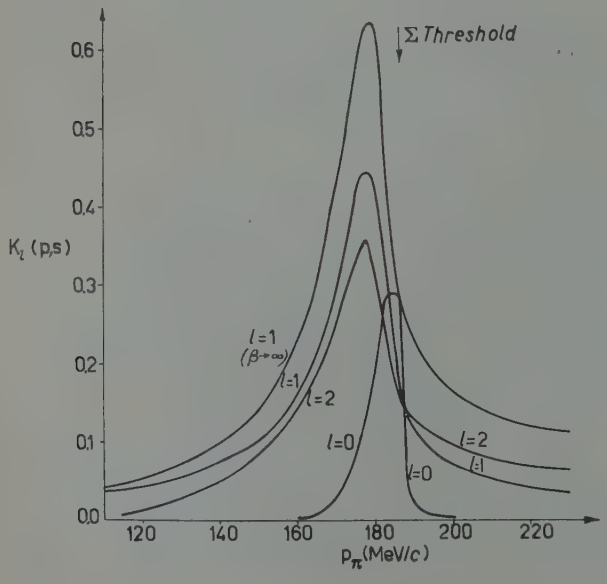

Fig. 6*a*. – The phase shift independent factor K_l occurring in the (pion) momentum spectrum $\Gamma(P, s)$ of converted Σ's for s, p, and d wave conversion.

with a new $l = 0$ channel (*i.e.* the $\Sigma\mathcal{N}$ channel for $k_\Sigma > 0$). Thus for $\Gamma(S, s)$ the spectrum peak is the cusp at $k_\Sigma = 0$. For $\Gamma(P, s)$ the peak may have a

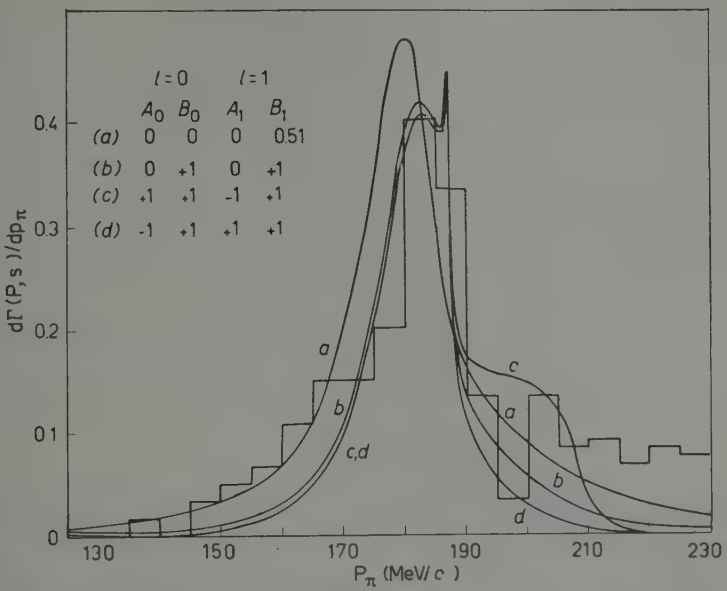

Fig. 6*b*. - The momentum spectrum $K_l(P, s)/\Lambda_l$ (59) for converted Λ's. Real and imaginary s and p wave scattering lengths determining the conversion are given in pion mass units. The normalization is arbitrary.

complex form with a cusp at $k_\Sigma = 0$ and a broader peak shifted to lower pion momenta associated with the higher partial waves (particularly $l = 1$).

TABLE IV. - *The k_Σ dependence of* $(K_l(L)/\Lambda_l)$ (see eq. (59)) *for small* $|k_\Sigma|$. All numerical values are given in pion mass units.

L_{Kd}	l	Real k_Σ	Imaginary $k_\Sigma = i\varkappa$
$L_{Kd} = 0$	0	$0.61 - 1.22B_0k_\Sigma +$ $+[-0.11 + 0.61(3B_0^2 - A_0^2)]k_\Sigma^2$	$0.61 - [1.82 - 1.22A_0]\varkappa +$ $+[2.72 - 3.64A_0 + 0.61(3A_0^2 - B_0^2)]\varkappa^2$
$K_l(0)/\Lambda_l$	1	$0.11 + 0.61k_\Sigma^2$	$0.11 - 0.61\varkappa^2$
$L_{Kd} = 1$			
$K_l(1)/\Lambda_l$	0	$0.28 - 0.56B_0k_\Sigma$	$0.11 - [1.77 - 0.56A_0]\varkappa$
	1	$0.17 + 0.69k_\Sigma^2$	$0.17 - 0.69\varkappa^2$
	2	$0.17 + 0.32k_\Sigma^2$	$0.17 - 0.32\varkappa^2$

More detailed analysis of the spectrum shape will, in principle, give information on the scattering lengths. The number of parameters available is so

large that we would like to discuss only the zero range approximation:

$$A_l(k_\Sigma) - iB_l(k_\Sigma) = A_l - iB_l \,.$$

We should limit ourselves to small $|k_\Sigma|$ in this discussion. We see from the form of Δ_l and Δ_l', (32) and (33), that for $k_\Sigma > 0$ (p_π below the Σ threshold) the spectrum is *somewhat sensitive* to B_l (note $B_l > 0$) and for imaginary k_Σ (p_π above) it is *very sensitive* to A_l. For large positive A_0 we may expect a peak in the spectrum for p_π just above the Σ threshold. This corresponds to a « virtual » bound s state in the ΣN system (*). We shall limit our quantitative considerations of the $\Sigma\Lambda$ conversion spectrum to the region:

$$\text{(64)} \qquad \begin{cases} 175 \text{ MeV/c} < p_\pi < 190 \text{ MeV/c} \,, \\ \quad \text{or} \\ k_\Sigma < 103 \text{ MeV/c} \quad \text{and} \quad \varkappa < 56 \text{ MeV/c} \,. \end{cases}$$

It is also important to limit our analysis to the region (64) of the spectrum peak to minimize effects of production mechanism neglected in this paper (*i.e.* the 3 body absorption and $\pi\mathcal{N}$ scattering processes should both have broad spectra, of minimum relative importance at the peak). The present experimental results do not allow a detailed shape analysis. We do however observe in Figs. 5*b* and 6*b* that the experimental peak seems to be below the point $k_\Sigma = 0$. This favors the case $\Gamma(P, s)$, which seems to be also favored by the arguments of Section 3. Somewhat better resolution and statistics (and especially the actual observation of the cusp) should resolve whether $\Gamma(P, s)$ is the dominant process. Referring to Fig. 6*b*, we see that we will not easily determine A_l or B_l from the spectrum shapes, even if the data are

(*) For $l=1$ and imaginary k_Σ the situation is somewhat complicated. Consider a real scattering length a_1. If there is a very shallow bound state, it will occur at the momentum $i\varkappa$ given by

$$\varkappa^3 = -\frac{1}{a_1} - \frac{1}{2} r_1 \varkappa^2 \,.$$

It is clear that the effective range term is essential. As in the S state a very shallow bound state is associated with positive a, r_1 turns out to be negative. ($r_1 = -\frac{1}{2}R$ for a square well of radius R with a shallow bound state.) We conclude that we cannot describe a shallow « virtual » bound $\Sigma\mathcal{N}$ p state in the zero range approximation. In the zero range approximation, we must limit ourselves to repulsion, *i.e.* small positive A_1, or attraction not strong enough for a bound p state, *i.e.* negative A_1. In the latter case, we must not consider large $\varkappa$ such that the $(1+\varkappa^3 A_1)$ term in Δ_1' (33) becomes small. (If this term goes to zero it corresponds to a deep « virtual » bound state. For a weaker attraction the effective range would take over at such large $\varkappa$.)

considerably improved. Actual observation of the cusp might, however, lead to a rough determination of the ratio B_0/B_1.

We can learn more about the scattering lengths by examining the competition between $\Sigma \to \Lambda$ conversion and $\Sigma \to \Sigma$ scattering. The transition rate for Σ production is, (omitting the same constant factor as in (49)):

$$\Gamma_\Sigma(L_{Kd}) \sim \int dk_\Sigma \{I^a + \Sigma_l [-A_l I_l^b - B_l I_l^c + (A_l^2 + B_l^2) I_l^d]/\Delta_l\} , \tag{65}$$

where

$$I_l^c(0) = 2(2l+1) W_\Sigma k_\Sigma^{2l+1} (J_{l,l}^0)^2 , \tag{66}$$

$$I_l^c(1) = \tfrac{1}{2} W_\pi k_\Sigma^{2l+1} [l (J_{l,l-1}^1)^2 + (l+1)(J_{l,l+1}^1)^2] , \tag{67}$$

and the other I's are defined in (51) to (58).

We define the ratio,

$$R = \frac{\Gamma'_\Lambda(L_{Kd})}{\Gamma_\Sigma(L_{Kd})} , \tag{68}$$

where the denominator includes Σ's associated with the $I = \frac{1}{2}$ $\Sigma\pi$ system. Also only a certain portion of the momentum spectrum, *i.e.* the region (64), will be integrated to obtain Γ'_Λ. Meanwhile since the production of Σ's is relatively insensitive to the final state interaction, we consider the total transition rate Γ_Σ. The shape of the Σ spectrum that goes into Γ_Σ may be of passing interest. The pion momentum p_π spectrum is given in Fig. 7 for various cases (for $\Gamma(S, s)$). We can test here the simple equality between suppression of Σ production and conversion of Σ's to Λ's as would be true if the intermediate state were free. Comparing Figs. 7 and 5*b* we see that indeed there is a rough inverse relationship of Γ_Σ and Γ_Λ as functions of B, for fixed A. If A is varied there is no such relationship, however. This can be seen especially by

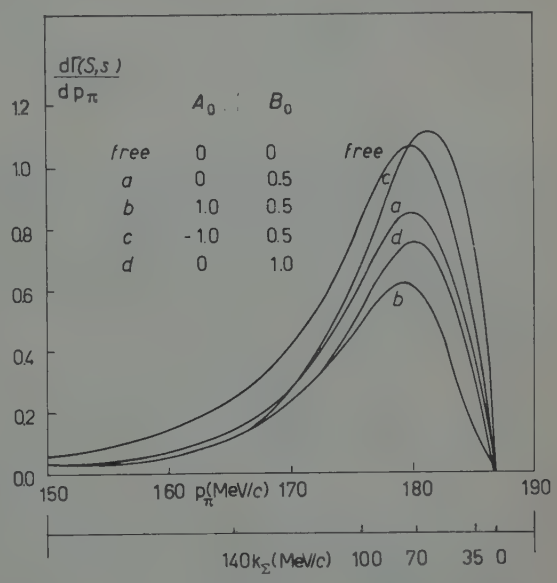

Fig. 7. – The momentum spectrum $d\Gamma_\Sigma(S, s)/dp_\pi$ (59) for unconverted ($T = \frac{1}{2}$ $\Sigma\pi$ production) Σ's. The relative normalization of the curves is meaningful. The scattering lengths of the s wave final state interaction considered are given in pion mass units.

comparing the widely different rates of Σ production given by the cases of a, b, and c of Fig. 7 with the corresponding conversion rates (indicated in Fig. 5b). These conversion rates, in the vicinity of the peak of the production, are all essentially equal (about $\frac{1}{6}$ of the Σ production rate with no final state interaction).

It is found experimentally that the conversion ratio (68) is [1]

$$R = 0.26 . \tag{69}$$

Some calculated values of R are listed in Tables V and VI for various scattering lengths, assuming s wave final state interaction in the case of $\Gamma(S, s)$

TABLE V. – *The ratio,* $R(S, s)$ (eq. (68)) *of* Σ-Λ *conversion to* Σ *production in the state of* $I_{\Sigma\mathcal{N}} = \frac{1}{2}$. Only the s wave ($l=0$) interaction in the $\Sigma\mathcal{N}$ system is taken into account. The scattering length ($A_0 - iB_0$) is measured in units of 10^{-13} cm. All values are given for $\varepsilon=\infty$ (24) and $\beta=6.2\alpha$ (14), except the value in the parenthesis which is calculated for $\varepsilon=6.2\alpha$.

B_0 \ A_0	-1.41	-0.71	0	$+0.71$	$+1.41$
0			$0.43B_0$		
0.14			0.042		
0.28	0.062		0.084 (0.064)		0.13
0.71	0.15	0.17	0.20	0.23	0.29
1.41	0.27		0.37		0.47

TABLE VI-a. – *The ratio,* $R(P, s)$ (68) *of* Σ-$\mathcal{N}$ *conversion to* Σ *production for* $I_{\Sigma\mathcal{N}}=\frac{1}{2}$. The s and p wave interactions in the $\Sigma\mathcal{N}$ system are included. The scattering length ($A_l - iB_l$) is measured in units of $(10^{-13}\text{ cm})^{2l+1}$. All values are given for $\varepsilon=\infty$ (24). We set $A_0=A_1=0$ in Table VI-a.

$(B_1)^{\frac{1}{3}}$ \ B_0	0	0.71	1.41	2.12
0	$0.081B_0 + 0.144B_1$			
1.13	0.07	0.11	0.13	0.14
1.41	0.13	0.17	0.19	0.20
1.70	0.20	0.23	0.26	0.27

TABLE VI-b. – *The conversion ratio* $R(P, s)$. *See heading for Table* VI-a.

$(A_1)^{\frac{1}{3}}$	$(B_1)^{\frac{1}{3}}$ \ A_0 / B_0	-1.41 / 1.41	0 / 1.41	1.41 / 1.41
1.41	1.41	0.21	0.20	0.21
0	1.41	0.19	0.19	0.19
-1.41	1.41	0.17	0.117	0.17

and s and p wave final state interactions in the case of $\Gamma(P, s)$. The large experimental value of R requires a large imaginary scattering length. For $\Gamma(S, s)$ we see that $B_0 \approx 1 \cdot 10^{-13}$ cm For $\Gamma(P, s)$ we see that $B_1^{\frac{1}{2}} \geqslant 1.5 \cdot 10^{-13}$ cm. The latter is certainly a *disturbingly large* p wave scattering length. Further discussion of this result will be given in the final section. Since the ratio we are considering involves mainly B/A, it is insensitive to the real parts of the scattering length A. The ratio is also insensitive to the s wave scattering length B in the $\Gamma(P, s)$ case.

We note that omission of the β term in the deuteron wave function (12) greatly changes the magnitude of the conversion (Figs. 5*a* and 6*a*). The conversion *ratio* would also be exaggerated by omission of this term, though the error would not be large (see curve III′ of Fig. 1*b* for an indication of the dependence of Σ production on this approximation). The importance of a well behaved final $\Sigma\pi$ wave function is shown in Fig. 5*a*, where the ε term of (24) is omitted in all but one curve. The $\Sigma\pi$ conversion is exaggerated much more by omission of the ε term than the production. For simplicity of computation we nevertheless omit the term in our consideration. The calculated conversion ratios are then probably about 10 % too large.

6. – Conclusions.

Our basic assumptions of no $\pi\pi$ scattering and no K-2π absorption mechanism, and the technical assumptions involving use of asymptotic final state wave functions and the zero range approximation, have been discussed in the text. We have concentrated our attention to the peaks in the spectra in order to minimize the resulting errors. We feel that the spectrum shapes, conversion ratios, and to a lesser extent the angular correlations are sufficiently accurate to be of use. The spectrum peaks should be accurately placed. The conversion ratios should be correct to about $\pm 50\%$.

Before drawing conclusions we should discuss the further theoretical uncertainty of the relative importance of the various initial states. We have seen that, on the basis of predicted total transition rates, capture from the P Bohr orbit through the s wave Kπ channel, $\Gamma(P, s)$ is expected to dominate. The only other information we found on this point came from the spectrum shape and conversion ratio, R, of the $\Sigma\Lambda$ conversion. The experimental position of the conversion peak may favor $\Gamma(P, s)$. We feel that more data on this spectrum would be quite valuable. The cusp predicted at the Σ threshold (*i.e.* at the maximum pion momentum associated with Σ production) might be observed. The size and position of this peak compared to the whole peak very easily distinguishes the importance of $\Gamma(P, s)$ compared to $\Gamma(S, s)$ and

$\Gamma(P, p)$ (*e.g.* see Figs. 5*b* and 6*b*) (*). Meanwhile, the conversion ratio is disturbingly large for the $\Gamma(P, s)$ case. We will discuss this below. In the following we will assume the case of dominant $\Gamma(P, s)$ unless otherwise specified.

Let us first consider direct Λ production (*i.e.* the higher pion momentum peak). The spectrum shape and angular correlation are predictable in the sense that they are insensitive to the final $\Sigma\mathcal{N}$ interaction. Nevertheless it is seen (Fig. 4) that the experimental spectrum shape disagrees with the prediction. The most reasonable explanation of this disagreement probably lies in the dependence of the T-matrix element for

$$\mathrm{K}^{-} + \mathcal{N} \to \Lambda + \pi \tag{70}$$

on the $\Lambda\pi$ energy. We saw from (9), (11), and (34) that the transition probability has the form

$$\frac{\mathrm{d}\Gamma}{\mathrm{d}k_{\Lambda}} \sim |T_0(k^2_{Y\pi})|^2 \left(\frac{\mathrm{d}\Gamma}{\mathrm{d}k_{\Lambda}}\right)_1, \tag{71}$$

where T_0 is the (s wave) T-matrix element in question and $(\mathrm{d}\Gamma/\mathrm{d}k)_1$ is the transition probability with $T_0 = 1$, as represented by (49) or Fig. 4. In the spirit of (11) we write to a good approximation:

$$k_{Y\pi} = 0.95\, p_{\pi}\,,$$

in the vicinity of this Λ peak. We want to discuss the energy dependence in a region just below the $\mathrm{K}\mathcal{N}$ threshold of width about 25 MeV. The zero range approximation ([13]) (*i.e.* expansion above the $\mathrm{K}\mathcal{N}$ threshold) should be satisfactory. We can show that T_0 above threshold on the energy shell has the form

$$T_0 \sim \sqrt{-}\,\mathrm{Im}\, a(1 + c^2)/(1 - ic)(1 + iak_{\mathrm{K}\mathcal{N}})\,, \tag{72}$$

(*) A mechanism has been suggested by Day, Snow and Sucher: *Phys. Rev. Lett.*, **3**, 61 (1959), which could lead to S Bohr orbit capture $\Gamma(S, s)$ and essentially no P orbit capture $\Gamma(P, s)$. We feel the converted Λ spectrum shape is one good means of testing this possibility empirically. If indeed $\Gamma(S, s)$ is the dominant mode, we have shown that the present data for the direct Λ spectrum is probably consistent with hyperfragment data without consideration of a strong energy dependence of the $\mathrm{K}\mathcal{N}$ T-matrix (see below), and that the conversion ratio R can be explained by a moderately small imaginary part of the s wave scattering length. The latter result would not be in qualitative disagreement with the predictions of the universal pion baryon interaction (see below).

where a is the complex $(I=1)$ $\overline{K}\mathcal{N}$ scattering lenght, and c is the tangent of the phase shift in the $\Lambda\pi$ channel at the $K\mathcal{N}$ threshold. To go off the energy shell we recall that the T-matrix element in question has the form

$$(\overline{\Psi}^{(-)}_{\Lambda\pi}, H\Phi_{K\mathcal{N}}),$$

where $\overline{\Psi}$ and Φ are complete and plane wave functions, respectively. In the zero range approximation all the energy dependence is in $\overline{\Psi}_{\Lambda\pi}$. To go below the threshold we take

$$k_{K\mathcal{N}} \to i\varkappa_K, \qquad \varkappa_K > 0.$$

Then

$$(73)\quad |T_0|^2 \sim 1/[(1-\varkappa_K \operatorname{Re} a)^2 + (\varkappa_K \operatorname{Im} a)^2].$$

The result (73) is inserted into (71) to obtain the spectrum. A favorable result using an acceptable $\overline{K}\mathcal{N}$ scattering length is shown in Fig. 8 ([13]). This comparison with experiment may be useful to reduce the large ambiguity in $\overline{K}\mathcal{N}$ scattering length solutions. It is disappointing, however, that (73) does not depend explicitly on the $\Lambda\pi$ channel (*e.g.* on c).

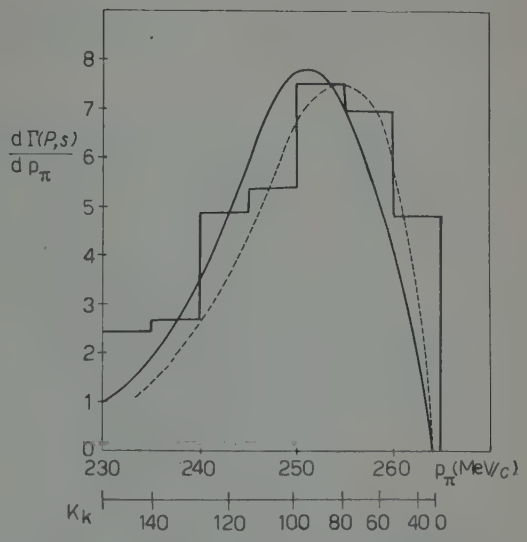

Fig. 8. – The pion momentum spectrum $\Gamma(P, s)$ for direct Λ production. The solid curve corresponds to an energy independent T matrix for the $K^-\mathcal{N}$ absorption. The dashed curve shows the spectrum shape for the $K^-\mathcal{N}$ T matrix (73) corresponding to $(I=1)$ $K^-\mathcal{N}$ scattering lengths $\operatorname{Re} a = -1.7$ and $\operatorname{Im} a = -0.6 \cdot 10^{-13}$ cm. Large negative real a is favored by this analysis (*). The true relative area under the dashed curve is about $\frac{1}{3}$ that of the solid curve.

It would be of interest to experimentally investigate the spectrum of $\Sigma^- n\pi^+$ production (1) accurately enough to make the same type of analysis as above. Meanwhile examination of the angular correlations for the direct Λ's and $\Sigma^- n$ system would serve as a check of the theory.

The $\Sigma\Lambda$ conversion ratio leads to a certain minimum value of the imaginary part of the p wave scattering length B_1. This value is somewhat larger than

([13]) J. C. JACKSON, D. G. RAVENHALL and H. W. WYLD jr.: *Nuovo Cimento*, **9**, 834 (1958).

(*) Our result of a large negative real part in the isotopic spin one, scattering length must be regarded as very preliminary. This sign disagrees with that found by J. D. JACKSON and H. W. WYLD jr.: *Phys. Rev. Lett.*, **2**, 355 (1959).

the range of force, a very surprising result. One can show that B is essentially given by

$$\frac{B}{R} \approx \frac{\bar{V}_{\Lambda\Sigma}^2}{[(1+\bar{V}_{\Lambda\Lambda})(1+\bar{V}_{\Sigma\Sigma})-\bar{V}_{\Lambda\Sigma}]^2+(1+\bar{V}_{\Sigma\Sigma})^2}, \tag{74}$$

where the $\bar{V}_{\Lambda\Lambda}$, $\bar{V}_{\Sigma\Sigma}$, and $\bar{V}_{\Lambda\Sigma}$ are certain matrix elements, linear in the coupling $\Lambda+\mathcal{N}$ to $\Lambda+\mathcal{N}$, and so on ([14]). $\bar{V}_{\Sigma\Sigma}$ is, for example, defined so that in the absence of $\Lambda\Sigma$ coupling, a virtual bound state in the Σ channel at zero energy corresponds to $\bar{V}_{\Sigma\Sigma}=-1$. We see from (74) that B compared to R (a measure of the range of force) is greater than one usually only for the case $\bar{V}_{\Sigma\Sigma}\approx -1$. In other words, large imaginary scattering length will occur only if the diagonal potential in the initial state is approximately strong enough for zero energy binding.

It would indeed be surprising if the potential for the ($I=\frac{1}{2}$) process of

$$\Sigma+\mathcal{N}\to\Sigma+\mathcal{N}, \tag{75}$$

were approximately of the strength needed to bind a *p state*. We believe that consideration of a variety of small contributions to the conversion process, for example, from final state scattering in higher partial waves and from interference between the conversion amplitude and direct amplitude (the direct amplitude should have a contribution at these momenta due to the 3 body absorption mechanism) might reduce the hyperon nucleon p wave scattering length B_1 to a somewhat more reasonable value. It is clear however that the p wave potential for the $\Sigma\Lambda$ scattering process (75) and for the potential for the $\Sigma\Lambda$ conversion process (74) must be comparable with or stronger than the strongest $\mathcal{N}\mathcal{N}$ potentials.

We can compare this result with the pion potential ([12]) predicted by the universal pion baryon interaction ([15]). A relatively weak potential for the $\Sigma\Sigma$ scattering process (76) and a very weak potential for the conversion process (4) are indicated. The latter prediction may depend to some extent on the method of deducing the potential. In spite of doubts about the ability to predict these potentials theoretically, we must recognize that there is no qualitative indication of the very strong potentials needed for the conversion process. We can probably conclude that the universal pion baryon interaction is incorrect, or that effects are greatly modified by very strong K-particle forces.

([14]) M. Ross and G. Shaw: *Ann. Phys.* (to be published).
([15]) M. Gell-Mann: *Phys. Rev.*, **106**, 1296 (1957).

* * *

The authors wish to thank Dr. NAHMIN HORWITZ for kindly informing them of the data before publication, and Professor ROGER G. NEWTON for discussions.

RIASSUNTO (*)

Abbiamo preso in esame da un punto di vista teorico la cattura K^- a riposo da parte del deuterio principalmente in funzione delle interazioni $Y\pi$ dello stato finale. Abbiamo calcolato in particolare i rapporti totali, gli spettri dell'impulso associati alla produzione di $\Sigma^- + n + \pi^-$ e di $\Lambda^0 + p + \pi^-$ e la correlazione angolare corrispondente (non si è riscontrata l'utilità di quest'ultima se non forse come controllo). In base ai rapporti totali si riscontra che la cattura da parte dell'orbita P di Bohr attraverso il canale $K\pi$ dell'onda s risulta con ogni probabilità predominante. Tale ipotesi è rafforzata dallo spettro del picco delle Λ di basso impulso (Λ convertite da Σ). Si può compiere un controllo definitivo quando si misuri lo spettro delle Λ un po' meglio convertito, in quanto, se tale ipotesi è esatta, si osserverebbe un doppio picco (con una cuspide nell'impulso pionico massimo associato alla produzione). L'analisi del picco delle Λ di alti impulsi pionici (Λ prodotte direttamente) che faccia uso di questa ipotesi, rivela che lo spettro è insensibile alle interazioni $Y\pi$ e che non sembra ancora essere in accordo con i dati. Tale forma dello spettro (e quello per le $\Sigma^- n \pi^+$) dipende in modo significativo dal processo di assorbimento $K\pi \to Y\pi$ all'esterno dello strato di energia, il quale a sua volta dipende dalle lunghezze di scattering $K\pi$. Un confronto preliminare fra i dati e la teoria indica un'ampia parte reale negativa per la lunghezza dello scattering $K\pi$ dello spin isotopico uno. Dal rapporto relativo alla conversione delle Σ in Λ, deduciamo infine un valore minimo per la parte immaginaria della lunghezza di scattering $\Sigma\pi$ dell'onda dello spin isotopico $\frac{1}{2}$ p. Il risultato, maggiore della lunghezza d'onda Compton del pione, indica un potenziale molto forte nel canale $\Sigma\pi$ e, se si accoppiano i canali $\Sigma\pi$ e $\Lambda\pi$, un potenziale molto più forte di quello indicato dall'interazione universale pione-barione. Si discute estesamente anche la cattura dall'orbita S di Bohr. In questo caso gli spettri associati alla produzione diretta di Σ^- e Λ sono influenzati dall'interazione $Y\pi$ finale.

(*) *Traduzione a cura della Redazione.*

IL NUOVO CIMENTO Vol. XIV, N. 6 16 Dicembre 1959

The $\mu \to e + \gamma$ Decay and the Intermediate Charged Vector Boson Theory.

PH. MEYER (*) and G. SALZMAN (**)

CERN - Geneva

(ricevuto il 1° Settembre 1959)

Summary. — The μ-e-γ vertex is calculated in the intermediate charged vector boson theory, as a function of the square of the four momentum of the photon. Consistency arguments show that the boson anomalous magnetic moment should be taken equal to zero. The result is then specialized to a real photon. The experimental branching ratio

$$\varrho = (\mu \to e + \gamma)/(\mu \to e + \nu + \bar{\nu}) = (1.2 \pm 1.5) \cdot 10^{-8}$$

fixes the cut-off value at less than one fifth the intermediate boson mass. It is concluded that this theory does not reasonably account for the experimental data, no matter how massive the boson is assumed to be.

1. – Introduction.

The universal V-A interaction among ordinary (non-strange) fermions and the non-observation of certain processes, *e.g.* $\mu^+ \to 2e^+ + e^-$ and $K^0 \to \mu^+ + \mu^-$, has led FEYNMAN and GELL-MANN [1] to postulate that a heavy charged vector boson serves as the intermediary connecting the two fermion lines. Such a structure of the four fermion interaction would lead, barring additional selection rules, to the decay of a free μ-meson into an electron and a photon,

$$\mu \to e + \gamma ,$$

(*) On leave from Ecole Normale Supérieure, Paris.

(**) Ford Foundation Fellow, on leave from University of Colorado, Boulder, Colorado.

(1) R. P. FEYNMAN and M. GELL-MANN: *Phys. Rev.*, **109**, 193 (1958).

at a rate proportional to the same power of the weak interaction coupling constant as the rate for ordinary β-decay. Several calculations of the branching ratio

$$\varrho = \frac{w(\mu \to e + \gamma)}{w(\mu \to e + \nu + \bar{\nu})},$$

given by this theory have been reported ([2-4]), and recently several experimental teams searched again for $\mu \to e + \gamma$ decay ([5]) with the result that

$$\varrho_{\text{experimental}} = (1.2 \pm 1.5) \cdot 10^{-6}.$$

In trying to determine whether the theory is consistent with this small branching ratio, it should be borne in mind that the theory is not renormalizable, and in a strict sense is undefined. However, the usual point vertex assumed for the four fermion interaction is itself non-renormalizable, and yet, in lowest order perturbation theory it is in excellent agreement with β-decay experiments. One may hope that in lowest order, the intermediate boson theory is also satisfactory. However, it is divergent in lowest order for the process $\mu \to e + \gamma$ decay. The predicted branching ratio depends on the boson's assumed anomalous ([6]) magnetic moment, $\lambda(e\hbar/2m_B c)$, where m_B is the boson mass, and on the ratio Λ of the cut-off to the boson mass,

$$\varrho_{\text{theoretical}} = \varrho(\lambda, \Lambda).$$

Our main contention is that λ should be taken equal to zero. There are two reasons for this. First, the boson is assumed not to have strong interactions. Any anomalous moment is thus due to the weak and electromagnetic couplings, and can arise only by higher order corrections to the process under

---

([2]) R. P. FEYNMAN and M. GELL-MANN: 1958 *Annual International Conference on High Energy Physics at CERN*.

([3]) G. FEINBERG: *Phys. Rev.*, **110**, 1482 (1958).

([4]) M. E. EBEL and F. J. ERNST: to be published. These authors find a larger branching ratio than that obtained by FEINBERG. The present authors also find the larger value.

([5]) J. ASHKIN, T. FAZZINI, G. FIDECARO, N. H. LIPMAN, A. W. MERRISON and H. PAUL: *Nuovo Cimento*, **14**, 1266 (1959).

([6]) By «normal» magnetic moment we mean a moment of magnitude $e\hbar/2m_B c$, (*i.e.* one boson magneton) which one obtains from the free Lagrangian.

$$\mathscr{L} = -\tfrac{1}{2} \sum_{\mu,\nu} (\partial\varphi_\mu^*/\partial\chi_\nu - \partial\varphi_\nu^*/\partial\chi_\mu)(\partial\varphi_\mu/\partial\chi_\nu - \partial\varphi_\nu/\partial\chi_\mu) - m_B^2 \sum_\mu \varphi_\mu^* \varphi_\mu$$

by assuming the minimal electrodynamic interaction.

consideration. Therefore, in any lowest order process there is no anomalous moment.

The other, perhaps not as compelling reason why λ should be set equal to zero, is not manifest if one calculates only the $\mu \to e + \gamma$ decay, but is evident from the more general case in which the photon is not real, as occurs for example in the closely related process in which a μ-meson bound in the Coulomb field of a nucleus converts into an electron ([7])

$$\mu^-_{\text{bound}} + \text{nucleus} \to e^- + \text{recoil nucleus} .$$

In both processes the same vertex is involved, the only difference being that in one case the emitted photon is real, and in the other it is virtual. The difficulty with $\lambda \neq 0$ comes from the presence in the matrix element of a term of the form

$$\lambda(k^2 \underline{A} - k \cdot A \underline{k}) C ,$$

where k is the four momentum carried off by the photon, A is the k-th component of the Fourier transform of the electromagnetic field, and C is a quadratically divergent constant. This is the only quadratically divergent term. For the special case of a real photon, the k-dependent factor is zero, so that if one specializes to this case immediately, as is natural if one is considering the $\mu \to e + \gamma$ decay, this term never appears and the result is apparently only logarithmically divergent ([3,4]). If, however, the matrix element is calculated for a momentum k even only slightly off the light cone, the result is quadratically divergent. This ambiguity in the order of divergence of the matrix element on the light cone seems to us to be physically inadmissible. In order to eliminate this ill-behaved term, we must take λ equal to zero ([8]).

The problem is then to determine whether a value of ϱ consistent with experiment can be obtained with a reasonable choice of the single remaining parameter Λ.

In Section 2, a sketch of the calculation is given, and in Section 3 are a brief resumé and our conclusions.

([7]) A general phenomenological treatment of this process has been given recently by S. WEINBERG and G. FEINBERG: *Phys. Rev. Lett.*, **3**, 111 (1959), and by N. CABIBBO and R. GATTO, to be published. Our results obtained with the intermediate charged vector boson theory will be reported in a subsequent paper.

([8]) A similar situation occurs in the closely related process, the scattering of vector bosons by a Coulomb field. If $\lambda \neq 0$ one obtains a physically unreasonable cross-section which increases indefinitely as the squqare of the boson energy. See W. PAULI: *Rev. Mod. Phys.*, **13**, 203 (1941), Table I.

2. – Calculation.

It is convenient to calculate the matrix element for both $\mu \to e + \gamma$ decay and $\mu \to e$ conversion together and to specialize later. Consider the three lowest order graphs for the $\mu \to e + \gamma$ decay, which are shown in Fig. 1. The four-momenta are indicated by arrows and labels. The momentum k carried out of the process by the photon is on the light cone, *i.e.* $k^2 = 0$. In the $\mu \to e$ conversion process the lowest order approximation for the matrix element consists of precisely the three graphs of Fig. 1, with the sole difference that in place of a real photon being emitted, the external Coulomb field of the nucleus acts (9). In this case, of course, the momentum k carried off by the electromagnetic field, that is, the recoil four-momentum of the nucleus, is not on the light cone; $k^2 \neq 0$. The « natural » units, $\hbar = c = 1$ are used. The boson-fermion vertex is taken to be

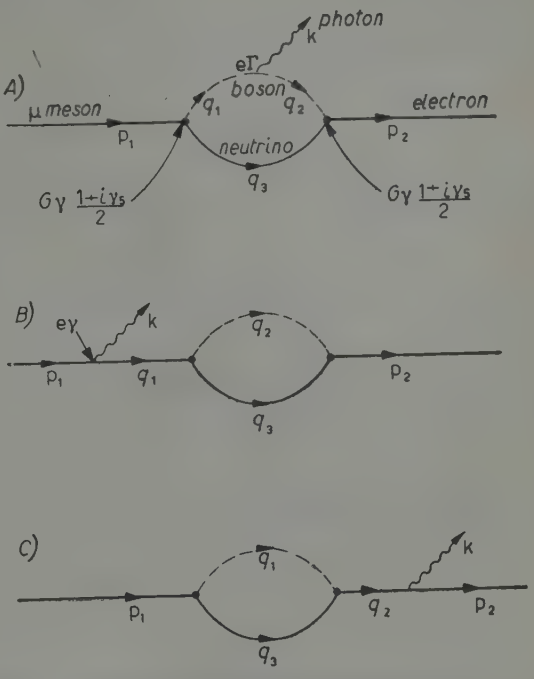

Fig. 1. – The three lowest order graphs for the $\mu \to e + \gamma$ decay in the intermediate charged vector boson theory. They differ only in that the photon is emitted by the charged boson in *A*, by the μ-meson in *B*, and by the electron in *C*.

$$G\gamma_\sigma \tfrac{1}{2}(1 + i\gamma_5) .$$

For the part of the boson-electromagnetic vertex that is linear in the electromagnetic field, we take

$$e(\Gamma_\mu)_{\varrho\sigma} \equiv e\{-(q_{1\mu} + q_{2\mu})\delta_{\varrho\sigma} + q_{1\varrho}\delta_{\mu\sigma} + q_{2\sigma}\delta_{\mu\varrho} + \lambda[(q_{1\varrho} - q_{2\varrho})\delta_{\mu\sigma} - (q_{1\sigma} - q_{2\sigma})\delta_{\mu\varrho}]\} ,$$

(9) Actually the finite size of the nuclear charge distribution should be taken into account, as well as the incoherent process in which the nucleus is left in an excited state.

where a boson with four momentum q_1 and index σ emits or absorbs a photon with index μ and becomes a boson with four momentum q_2 and index ϱ. The boson propagator is

$$\frac{-i}{(2\pi)^4}\frac{1}{q^2-m_{\mathrm{B}}^2}\left(\delta_{\mu\nu}-\frac{1}{m_{\mathrm{B}}^2}q_\mu q_\nu\right).$$

The electromagnetic field operator is

$$A_\mu(x)=(2\pi)^{-\frac{3}{2}}\int \mathrm{d}^4k\,A_\mu(k)\exp\left[ik\cdot x\right],$$

and in the case that a real photon is involved is

$$A_\mu(x)=(2\pi)^{-\frac{3}{2}}\int \mathrm{d}^3k\,\varepsilon_\mu(\vec{k})(2k_0)^{-\frac{1}{2}}\left(a_k\exp\left[ik\cdot x\right]+a_k^+\exp\left[-ik\cdot x\right]\right),$$

where the polarization index is omitted from the polarization four vector $\varepsilon_\mu(\vec{k})$. According to the usual rules ([10]), we then obtain for the graphs of Fig. 1

$$A=K\bar{u}(2)\int\frac{\mathrm{d}^4q_1\,\mathrm{d}^4q_2\,\mathrm{d}^4q_3}{q_3^2(q_1^2-m_{\mathrm{B}}^2)(q_2^2-m_{\mathrm{B}}^2)}\,\delta^4(p_1-q_1-q_3)\,\delta^4(q_1-k-q_2)\,\delta^4(q_2+q_3-p_2)\cdot$$
$$\cdot\frac{1}{m_{\mathrm{B}}^2}\gamma_\mu\boldsymbol{q}_3\gamma_\nu(m_{\mathrm{B}}^2\delta_{\mu\sigma}-q_{2\mu}q_{2\sigma})(\Gamma_\tau)_{\sigma\varrho}A_\tau(m_{\mathrm{B}}^2\delta_{\varrho\nu}-q_{1\varrho}q_{1\nu})(1+i\gamma_5)u(1),$$

$$B=-K\bar{u}(2)\int\frac{\mathrm{d}^4q_1\,\mathrm{d}^4q_2\,\mathrm{d}^4q_3}{q_3^2(q_1^2-m_\mu^2)\,(q_2^2-m_{\mathrm{B}}^2)}\,\delta^4(p_1-k-q_1)\,\delta^4(q_1-q_2-q_3)\,\delta^4(q_2+q_3-p_2)\cdot$$
$$\cdot\gamma_\mu\boldsymbol{q}_3\gamma_\nu(m_{\mathrm{B}}^2\delta_{\mu\nu}-q_{2\mu}q_{2\nu})(1+i\gamma_5)(\boldsymbol{q}_1+m_\mu)\underline{A}u(1),$$

$$C=-K\bar{u}(2)\int\frac{\mathrm{d}^4q_1\,\mathrm{d}^4q_2\,\mathrm{d}^4q_3}{q_3^2(q_1^2-m_{\mathrm{B}}^2)(q_2^2-m_e^2)}\,\delta^4(p_1-q_1-q_3)\delta^4(q_1+q_3-q_2)\delta^4(q_2-k-p_2)\cdot$$
$$\cdot\underline{A}(\boldsymbol{q}_2+\ldots m_e)\gamma_\mu\,\boldsymbol{q}_3\gamma_\nu(m_{\mathrm{B}}^2\delta_{\mu\nu}-q_{1\mu}q_{1\nu})(1+i\gamma_5)u(1),$$

where

$$K=\frac{e}{2(2\pi)^{\frac{3}{2}}}\left(\frac{G}{m_{\mathrm{B}}}\right)^2\sqrt{\frac{m_\mu m_e}{E(1)E(2)}},$$

and $u(1)$ and $\bar{u}(2)$ are the μ-meson and electron spinors. Each of these three terms is in fact quadratically divergent, and the result depends on which of

---

([10]) As for example in S. S. Schweber, H. A. Bethe and F. de Hoffman: *Mesons and Fields*, Vol. I (Evanston, Ill., 1955). The notation $\boldsymbol{q}=q_\mu\gamma_\mu$ is used.

the integrations are carried out with the aid of the δ functions. The most reasonable prescription is to use the δ functions to eliminate those integration variables that describe the propagation of charged particles. This gives a gauge invariant result which corresponds to the answer that would be given by the insertion of a cut-off on the propagator of the neutral particle. Also, no translations of the origins of the integration variables are allowed, because of the degree of the divergence. With this prescription we obtain

$$A = K\delta^4(p_1 - p_2 - k)\,\bar{u}(2)\int \frac{\mathrm{d}^4q}{q^2 D_1 D_2}\,\frac{1}{m_B^2}\,(m_B^2\gamma_\sigma - \underline{q}_2 q_{2\sigma})\underline{q}(m_B^2\gamma_\varrho - \underline{q}_1 q_{1\varrho})\cdot$$

$$\cdot(I_\tau)_{\sigma\varrho} A_\tau(1 + i\gamma_5)u(1)\,,$$

$$B = K\delta^4(p_1 - p_2 - k)\bar{u}(2)$$

$$\int \frac{\mathrm{d}^4q}{q^2(m_e^2 - m_\mu^2)D_2}\,(2m_B^2\underline{q} + \underline{q}_2\underline{q}\,\underline{q}_2)(\underline{A}\,\underline{k} + 2p_2\cdot A)\cdot(1 + i\gamma_5)u(1),$$

$$C = K\delta^4(p_1 - p_2 - k)\,\bar{u}(2)\cdot$$

$$\cdot\int \frac{\mathrm{d}^4q}{q^2 D_1(m_\mu^2 - m_e^2)}\,(-\underline{k}\,\underline{A} + 2p_1\cdot A)(2m_B^2\,\underline{q} + \underline{q}_1\underline{q}\,\underline{q}_1)\cdot(1 + i\gamma_5)u(1),$$

where the subscript 3 has been omitted from the remaining integration variable, $D_1 = q_1^2 - m_B^2$, $D_2 = q_2^2 - m_B^2$, $q_1 = p_1 - q$ and $q_2 = p_2 - q$. Now A, B, and C each have the factor

$$K\delta^4(p_1 - p_2 - k)\,\bar{u}(2)$$

at the left and the factor

$$(1 + i\gamma_5)u(1)$$

at the right. Let the operator (in the spinor space) A' be defined by $A = K\delta^4(p_1 - p_2 - k)\bar{u}(2)A'(1 + i\gamma_5)u(1)$, and similarly for B' and C'. The sum $A' + B' + C'$ may be put into manifestly gauge invariant form by introducing a gauge invariant vector. It is convenient to define, in addition to the vector $k = p_1 - p_2$, the vector $p = \frac{1}{2}(p_1 + p_2)$, and to note that $2k\cdot p = p_1^2 - p_2^2 = m_\mu^2 - m_e^2 \neq 0$. The most general gauge invariant vector that is linear in the four vector potential A and that can be constructed with the vector k, p, and A, is easily seen to be

$$\alpha Q + \beta k\cdot Q\,k + \delta k\cdot Q\,p\,,$$

where

$$Q = A - \frac{p\cdot A}{k\cdot p}\,k\,,$$

and α, β, δ are arbitrary invariant functions of k^2.

Actually we need only the gauge invariant vector Q and the gauge invariant scalar $k\cdot Q$. Note that $p\cdot Q=0$. In A' replace A_τ by $Q_\tau+(p\cdot A/k\cdot p)k_\tau$; in B' replace $\underline{\boldsymbol{A}}\,\underline{\boldsymbol{k}}+2p_2\cdot A$ by $\underline{\boldsymbol{Q}}\,\underline{\boldsymbol{k}}-k\cdot Q+2p\cdot A$; and in C' replace $-\underline{\boldsymbol{k}}\,\underline{\boldsymbol{A}}+2p_1\cdot A$ by $-\underline{\boldsymbol{k}}\,\underline{\boldsymbol{Q}}+k\cdot Q+2p\cdot A$. All terms linear in Q are manifestly gauge invariant. The sum of the other terms of $A'+B'+C'$ vanishes identically algebraically, that is, without doing the integrations. The remaining terms, which are gauge invariant, are

$$(A')=\int\frac{\mathrm{d}^4q}{q^2D_1D_2}\,\frac{1}{m_\mathrm{B}^2}\,(m_\mathrm{B}^2\gamma_\sigma-\underline{\boldsymbol{q}}_2\underline{q}_{2\sigma})\underline{\boldsymbol{q}}(m_\mathrm{B}^2\gamma_\varrho-\underline{\boldsymbol{q}}_1\underline{q}_{1\varrho})\cdot$$
$$\cdot\{-\delta_{\sigma\varrho}(q_1+q_2)\cdot Q+q_{1\sigma}Q_\varrho+q_{2\varrho}Q_\sigma+\lambda(k_\sigma Q_\varrho-k_\varrho Q_\sigma)\}\,,$$

$$(B')=\int\frac{\mathrm{d}^4q}{q^2D_2}\,\frac{1}{2k\cdot p}\,(2m_\mathrm{B}^2\underline{\boldsymbol{q}}+\underline{\boldsymbol{q}}_2\underline{\boldsymbol{q}}\,\underline{\boldsymbol{q}}_2)(-\underline{\boldsymbol{Q}}\,\underline{\boldsymbol{k}}+k\cdot Q)$$

$$(C')=\int\frac{\mathrm{d}^4q}{q^2D_1}\,\frac{1}{2k\cdot p}\,(-\underline{\boldsymbol{k}}\,\underline{\boldsymbol{Q}}+k\cdot Q)(2m_\mathrm{B}^2\,\underline{\boldsymbol{q}}+\underline{\boldsymbol{q}}_1\underline{\boldsymbol{q}}\,\underline{\boldsymbol{q}}_1)\,,$$

where (A') stands for the part of A' linear in Q, and likewise for (B') and (C').

It may be noted that (A') appears to contain a quartically divergent λ-independent part. This, however, is illusory because of the identity

$$q_{2\sigma}q_{1\varrho}\{-\delta_{\sigma\varrho}(q_1+q_2)\cdot Q+q_{1\sigma}Q_\varrho+q_{2\varrho}Q_\sigma\}\equiv 0\,,$$

which causes it to vanish. Evaluation of (A'), (B'), and (C') is carried out by applying the identity

$$[a-b]^{-1}=a^{-1}+a^{-1}b[a-b]^{-1}$$

to the factors $D_1^{-1}=[(q^2-m_\mathrm{B}^2)-(2p_1\cdot q-p_1^2)]^{-1}$ and $D_2^{-1}=[(q^2-m_\mathrm{B}^2)-(2p_2\cdot q-p_2^2)]^{-1}$. Explicitly,

$$D_1^{-1}=D^{-1}+P_1D^{-2}+P_1^2D^{-3}+P_1^3D^{-4}+P_1^4D^{-4}D_1^{-1}\,,$$

and likewise for D_2^{-1}, where D stands for the spherically symmetric expression $q^2-m_\mathrm{B}^2$, $P_1=2p_1\cdot q-p_1^2$, and $P_2=2p_2\cdot q-p_2^2$. This identity permits the angular dependence to be removed from the integrand term by term, except for the last term. It also has the advantage that each term has at least one power of q less than the preceding, and is thus more convergent. The infinite terms are evaluated exactly, that is, formally. In the finite terms, we keep only those that have the lowest power of (Fermion mass/m_B)^2, where the Fermion mass may by either m_μ or m_e. This is the only approximation made

in evaluating the matrix element. We then obtain (it is convenient to write the integrals in dimensionless form, so that henceforth q means q/m_B),

$$A' + B' + C' = \frac{\lambda}{4}(k^2 \underline{Q} - k\cdot Q \underline{k}) \int d^4q (q^2 - 1)^{-1} +$$

$$+ \left\{ \left[(1-\lambda)\frac{1}{2}(\underline{k}\underline{p} - \underline{p}\underline{k}) + \left(\frac{1}{6} - \frac{5}{4}\lambda\right) k^2 \right] \underline{Q} + \left[\left(\frac{1}{3} + \frac{5}{4}\lambda\right)\underline{k} + (1-\lambda)\underline{p} \right] k\cdot Q + \right.$$

$$\left. + \frac{\lambda}{4m_B^2} \left(\left[\frac{1}{2}(\underline{k}\underline{p} - \underline{p}\underline{k}) - \frac{1}{12} k^2 - p^2 \right] k^2 \underline{Q} + \left[\left(\frac{1}{12} k^2 + p^2 \right) \underline{k} + (k^2 - 2k\cdot p)\underline{p} \right] k\cdot Q \right) \right\} \cdot$$

$$\cdot \int d^4q (q^2 - 1)^{-2} + \left\{ \left[(1+2\lambda)\frac{1}{2}(\underline{k}\underline{p} - \underline{p}\underline{k}) + \frac{1}{6} k^2 \right] \underline{Q} + \left[-\frac{1}{6}\underline{k} + (1+2\lambda)\underline{p} \right] k\cdot Q \right\} \cdot$$

$$\cdot \int d^4q (q^2 - 1)^{-3} + \left\{ \left[(3)\frac{1}{2}(\underline{k}\underline{p} - \underline{p}\underline{k}) + 2k^2 \right] \underline{Q} + [-2\underline{k} + 3\underline{p}] k\cdot Q \right\} \int d^4q (q^2 - 1)^{-4} .$$

If one sets k^2 and $k\cdot Q$ equal to zero, one obtains for the real photon matrix element

$$A + B + C = K \delta^4(p_1 - p_2 - k)\, \overline{u}(2) \left[\frac{\lambda}{4} \times \text{zero} \times \int d^4q (q^2 - 1)^{-1} + \right.$$

$$\left. + \frac{1}{2}(\underline{k}\underline{p} - \underline{p}\underline{k}) \underline{Q} \{ - i\pi^2 N \} \right] (1 + i\gamma_5) u(1)$$

where

$$\{ - i\pi^2 N \} = (1-\lambda) \int d^4q (q^2 - 1)^{-2} + (1+2\lambda) \int d^4q (q^2 - 1)^{-3} + 3 \int d^4q (q^2 - 1)^{-4} .$$

The first of the two terms in the square bracket is indeterminate, as it consists of zero multiplied by a quadratically divergent integral. For a virtual photon the factor zero is replaced by the finite expression $k^2 \underline{A} - k\cdot A \underline{k}$, in which case this term is without question quadratically divergent [11]. It is

---

[11] The factor $k^2 \underline{A} - k\cdot A \underline{k}$ is the matrix element, in momentum space, that corresponds to a contact interaction of the form

$$j_\nu^{\text{ext}}(x)\, \overline{\psi}^{(e)}(x)\, \gamma_\nu\, \psi^{(\mu)}(x) ,$$

where $j_\nu^{\text{ext}}(x)$ is the « external » source of the electromagnetic field. On the one hand the $\mu \to e + \gamma$ decay occurs in the absence of any external field and this term does not contribute. On the other hand, the $\mu \to e$ conversion requires an external source, *e.g.* the charge of the nucleus, and this term does not vanish.

[12] If λ were equal to 1 there would be, in addition to the ambiguity with the quadratically divergent term, a similar ambiguity with the logarithmically divergent term.

the presence of this term which causes the previously mentioned ambiguity on the light cone if λ is different from zero. The second term in the square bracket is well behaved as concerns the neighbourhood of the light cone because λ is taken different from 1 ([12]).

We will continue to use the symbol N for the expression given above, although henceforth it will mean this expression evaluated with $\lambda = 0$. With this understanding, the matrix element is

$$(A+B+C)_{\mu\to e,\gamma} = \frac{e}{2(2\pi)^{\frac{9}{2}}}\left(\frac{G}{m_B}\right)^2 \cdot$$

$$\cdot\sqrt{\frac{m_\mu m_e}{E(1)E(2)}}\,\delta^4(p_1-p_2-k)\,\bar{u}(2)\,\frac{1}{2}\,(\underline{k}\,\underline{p}-\underline{p}\,\underline{k})\underline{Q}(1+i\gamma_5)u(1)\{-i\pi^2 N\}\,.$$

Since we want the $\mu\to e+\gamma$ decay rate in the μ-meson's rest system, $E(1)=m_\mu$. Also $p\cdot\varepsilon = p_1\cdot\varepsilon = 0$ because p_1 has only a time component and ε has only space components. If we use the fact that $m_\mu \gg m_e$, then $\bar{u}(2)\frac{1}{2}(\underline{k}\,\underline{p})-\underline{p}\,\underline{k}) \approx \frac{1}{2}m_\mu^2\bar{u}(2)$. The S-matrix element is then

$$S_{\mu\to e,\gamma} = \frac{e}{4(2\pi)^{\frac{9}{2}}}\left(\frac{G}{m_B}\right)^2\cdot\sqrt{\frac{m_e}{E(2)}}\,m_\mu^2\,\delta^4(p_1-p_2-k)\,\bar{u}(2)\,\frac{1}{\sqrt{2k_0}}\,\epsilon(1+i\gamma_5)u(1)\{-i\pi^2 N\}\,,$$

which gives the transition rate

$$w(\mu\to e+\gamma) = 2^{-14}\pi^{-5}e^2(G/m_B)^4 m_\mu^5 N^2\,.$$

The same theory gives for the normal decay mode of the μ-meson the rate

$$w(\mu\to e+\nu+\bar{\nu}) = \tfrac{1}{3}2^{-9}\pi^{-3}(G/m_B)^4 m_\mu^5\,,$$

and therefore the predicted branching ratio is

$$\varrho = \frac{3\alpha}{8\pi}N^2 = 0.87\cdot 10^{-3}N^2\,.$$

Because N is itself logarithmically divergent, a numerical value for ϱ can only be obtained by introducing a cut-off. The Feynman cut-off, $-\Lambda^2(q^2-\Lambda^2)^{-1}$ is sufficiently strong to give finite results. The above expression for N is thus replaced by (recall that $\lambda=0$)

$$i(\pi/\Lambda)^2 N = \int d^4q\,(q^2-1)^{-2}(q^2-\Lambda^2)^{-1} +$$

$$+\int d^4q\,(q^2-1)^{-3}(q^2-\Lambda^2)^{-1} + 3\int d^4q\,(q^2-1)^{-4}(q^2-\Lambda^2)^{-1}.$$

Evaluation of the integrals by the standard technique of Feynman gives

$$N = \frac{-\Lambda^2}{2(1-\Lambda^2)^4}\{2\Lambda^2(\Lambda^4 - \\ -\Lambda^2+3)\ln\Lambda^2 + (1- \\ -\Lambda^2)(2\Lambda^4+\Lambda^2+3)\}\,.$$

The values of ϱ thus obtained, in the range, $0.1 \leqslant \Lambda \leqslant 0.9$, are shown in Fig. 2, where the experimental upper limit on ϱ, which we take to be $2.7 \cdot 10^{-6}$, is indicated by the dotted horizontal line. From this one sees that the cut-off would have to be at least 5 times smaller than m_B.

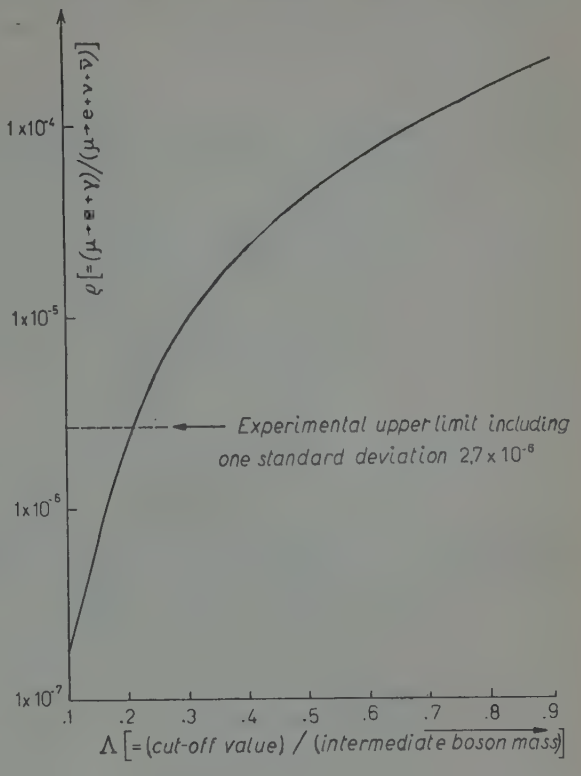

Fig. 2. – The branching ratio, $\varrho = w(\mu \to e + \gamma)/w(\mu \to e + \nu + \bar{\nu})$, as a function of the ratio of the cut-off value to the intermediate boson mass.

3. – Summary and conclusions.

Because the intermediate charged vector boson theory with electromagnetic interaction is non-renormalizable and because the Fermi point interaction theory which it is supposed to replace is itself non-renormalizable, we have adopted the viewpoint that only lowest order perturbation is to be considered. The boson is assumed to have no strong interactions, and therefore, in lowest order in the weak and electromagnetic interactions it has no anomalous moment, *i.e.* $\lambda = 0$. In addition we have imposed the criterion that the order of divergence of the perturbation theory matrix element for a physical process involving a photon must be a continuous function of the photon four momentum. Fulfilment of this condition also requires that in lowest order $\lambda = 0$ [13]. With $\lambda = 0$, and with the Feynman cut-off function, it then fol-

[13] If both these arguments are rejected, one can take instead the point of view that since a cut-off must in fact be inserted into the integrals, it may as well be inserted at the beginning of the calculation. In this case all terms are finite. The « quadratic »

lows that the cut-off must be less than $m_B/5$ in order that $\varrho_{\text{theoretical}}$ be consistent with the upper limit on $\varrho_{\text{experimental}}$.

We reject the theory because $\Lambda \leqslant \frac{1}{5}$ seems to us to be unreasonable. There is the practical objection that the answer is highly cut-off dependent, because of the steepness of the logarithmic function between 0 and 1. A change in Λ from 0.1 to 0.2 produces a 13-fold change in the branching ratio. In this region the logarithmic term is far more Λ-dependent than would be a quadratically divergent term.

There is also a theoretical objection. Of course nothing in the formalism of field theory excludes the possibility of a cut-off much smaller than the rest mass of the associated virtual quantum. However, since a cut-off is inserted *ad hoc* in order to damp out the otherwise infinite contribution of high virtual four momenta, and represents therefore a « domain of ignorance » whose size is measured by the inverse of the cut-off value, it seems unreasonable to attribute meaning to a « theory » for which the domain of ignorance far exceeds the size of the quantum involved, in this case the boson. In other words, the need for a cut-off at small virtual momentum transfer means that the prediction of the vector boson theory for the fermion-neutrino-boson vertex is incorrect even for small virtual momenta. The boson propagator is badly mutilated for almost all momenta. Since only the ratio of the cut-off to m_B is involved in the branching ratio, the difficulty of a large domain of ignorance cannot be overcome by taking m_B very large.

The original reason for introducing an intermediate charged vector boson is that it gives in a natural way the V-A interaction and the charge exchange character of the four fermion vertex. It should be borne in mind that the $\mu \to e + \gamma$ decay can be forbidden even if the Fermi interaction is mediated by an intermediate charged vector boson. For example, if there are two kinds of neutrinos ([14]), those coupled to the electron-boson vertex, and those coupled to the μ-meson-boson vertex, then the $\mu \to e + \gamma$ decay is forbidden. It may also be that the lowest order perturbation result is not correct in such a non-renormalizable theory. Our conclusion is solely that in lowest order, the form of the intermediate boson theory that has been used is not consistent with experiment unless it is so badly mutilated by the cut-off function that

---

terms proportional to λ no longer cause an ambiguity in the neighbourhood of the light cone. Everything is « well defined » even with λ different from zero. However, one would still require on physical grounds that the transition amplitude be a smooth function of k^2 in the neighbourhood of the light cone. Therefore one would be obliged to use instead of the Feynman cut-off function, $-\Lambda^2(q^2 - \Lambda^2)^{-1}$, which was used by FEINBERG and by EBEL and ERNST, a stronger function, such as $\Lambda^4(q^2 - \Lambda^2)^{-2}$, which would be needed to make the quadratically divergent term finite.

([14]) J. SCHWINGER: *Ann. Phys.*, **2**, 407 (1957).

it is in fact no longer the theory with which one starts. We therefore think that it is still necessary to search experimentally for evidence of a structure in the four fermion interaction.

* * *

One of us (G.S.) wishes to thank CERN for the grant of a Ford Foundation Fellowship, which made his visit possible. We thank CERN for the cordial hospitality extended to us. We are particularly indebted to Dr. Y. YAMAGUCHI for several helpful discussions, and to Professor FIERZ for valuable comments.

RIASSUNTO (*)

Nella teoria del bosone vettoriale di carica intermedia, si calcola il vertice μ-e-γ come funzione del quadrato del tetraimpulso del fotone. Coerenti argomentazioni dimostrano che il momento magnetico anomalo del bosone dovrebbe essere assunto uguale a zero. Tale risultato è particolarizzato al caso di un fotone reale. Il rapporto sperimentale di « branching »

$$\varrho = (\mu \to e + \gamma)/(\mu \to e + \nu + \bar{\nu}) = (1.2 \pm 1.5) \cdot 10^{-6}$$

fissa il valore del taglio a meno di un quinto della massa del bosone intermedio. Si conclude che questa teoria non tiene conto in modo ragionevole dei dati sperimentali, comunque compatto si consideri il bosone.

(*) *Traduzione a cura della Redazione.*

IL NUOVO CIMENTO Vol. XIV, N. 6 16 Dicembre 1959

The K_{e4} and $K_{\mu 4}$ Modes of K-Mesons Decay (*).

V. S. Mathur

The Enrico Fermi Institute for Nuclear Studies, Department of Physics, The University of Chicago - Chicago (Ill.)

(ricevuto il 3 Settembre 1959)

Summary. — The characteristics of the K_{e4} and $K_{\mu 4}$ modes of K-meson decay have been studied. Isotopic spin relationships following from the hypothesis of a $T=\frac{1}{2}$ strangeness-nonconserving current are discussed. The decay rates have been estimated in several ways, which agree in predicting a K^+_{e4}/K^+_{e3} branching ratio between 10^{-3} and 10^{-4}, so that the observation of K^+_{e4} events may be expected in the near future. The $K^+_{\mu 4}$ rate is expected to be at least an order of magnitude smaller than that for K^+_{e4} mode of decay.

1. – Introduction.

To present several thousand τ^+-decay events have been reported. These events are distinguished by the emission of three coplanar charged particles whereas the most probable of the other K^+-decay modes give only one charged particle. There are several modes known for K^+-decay which do give rise to three charged particles, although generally non-coplanar, and which have been observed a number of times (1):

$$\text{(A)} \qquad \begin{cases} K^+_{\pi 2} \to \pi^+ + \pi^0\,, & \pi^0 \to \gamma + e^+ + e^-\,, \\ K^+_{L3} \to L^+ + \nu + \pi^0\,, & \pi^0 \to \gamma + e^+ + e^-\,, \end{cases}$$

where L stands for the lepton μ or e.

(*) Work done under the auspices of the U. S. Atomic Energy Commission.

(1) G. Harris, J. Orear and S. Taylor: *Phys. Rev.*, **106**, 327 (1957).

Another K^+ decay process which would give three charged secondaries but whose observation has not yet been reported is the K^+_{L4} mode of decay,

$$\text{(B)} \qquad K^+_{L4} \to L^+ + \nu + \pi^+ + \pi^- ,$$

for which both K^+_{e4} and $K^+_{\mu 4}$ decays are possible. In this note we will investigate what rate it is reasonable to expect for these events on the basis of the (V-A) theory [2]. Several estimates of the relative probability for these modes will be made, and the distributions to be expected for the final particles will be discussed. In Section **2**, the phase space calculations will be reported and the isotopic spin relationships discussed. In Section **3**, the pion spectra and the probability of decay will be discussed on a phenomenological basis, using the (V-A) theory. For illustration, the matrix element has been calculated for a particular model in Section **4**.

2. – Calculation of phase space and isotopic spin considerations.

The phase space $\varrho_{L,n+2}$ for decay of a kaon to L+ν and n pions is given by

$$\text{(1)} \qquad \varrho_{L,n+2} = \frac{1}{(2\pi)^{3n+2}} \int \delta^4(k - p_L - p_\nu - p_1 \dots - p_n) \frac{d^3p_L}{E_L} \frac{d^3p_\nu}{E_\nu} \frac{d^3p_1}{2\omega_1} \dots \frac{d^3p_n}{2\omega_n} ,$$

where k, p_L, p, $p_1 \dots p_n$ are the 4-momenta of the kaon, lepton, neutrino and the n pions. First consider integration over p_L and p_ν. Let

$$\text{(2)} \qquad \begin{cases} Q = p_L + p_\nu , \\ R = p_L - p_\nu . \end{cases}$$

Then with $K = k - p_1 \dots - p_n$, the integration over p_L and p_ν may be written as

$$\int \delta^4(K - p_L - p_\nu) \frac{d^3p_L}{E_L} \frac{d^3p_\nu}{E_\nu} = 4 \int \delta^4(K_L - p_L - p_\nu)\, \delta(p_L^2 - m_L^2)\, \delta(p_\nu^2)\, d^4p_L\, d^4p_\nu =$$

$$= \int \delta^4(K - Q)\, \delta(Q^2 + R^2 - 2m_L^2)\, \delta(Q \cdot R - m_L^2)\, d^4Q\, d^4R ,$$

---

[2] R. P. FEYNMAN and M. GELL-MANN: *Phys. Rev.*, **109**, 193 (1958); E. C. G. SUDARHSAN and R. E. MARSHAK: *Suppl. Nuovo Cimento* (to be published); J. J. SAKURAI: *Nuovo Cimento*, **7**, 649 (1958).

where m_L is the rest mass of the lepton. Integrating over R and Q, this becomes

$$2\pi(1 - m_L^2/K^2) \tag{3}$$

with the restriction

$$K^2 \geqslant m_L^2 . \tag{4}$$

In the case of electron modes of decay, we shall generally make the approximation $m_e = 0$.

For the $K_{\mu 2}$ decay, $K^2 = \varkappa^2$, where $\varkappa$ is the rest mass of the kaon, so that

$$\varrho_{\mu 2} = \frac{1}{2\pi}(1 - m_\mu^2/\varkappa^2) . \tag{5}$$

For the K_{e3} decay, $K^2 = (k - p_1)^2$ so that (4) restricts the upper limit of integration over the pion energy ω_1 to $(\varkappa^2 + m^2)/2\varkappa$, where m denotes the rest mass of the pion. With the non-relativistic approximation for the pion momentum, the final phase space integral leads to the result

$$\varrho_{e3} = \frac{2}{3(2\pi)^3}\frac{(2m)^{\frac{1}{2}}}{(2\varkappa)^{\frac{3}{2}}}(\varkappa - m)^3 . \tag{6}$$

For the K_{e4} and $K_{\mu 4}$ decays, in the non-relativistic approximaiton for the pion momenta,

$$K^2 = (\varkappa - 2m)^2 - 2(t_1 + t_2)(\varkappa - m) - 4m(t_1 t_2)^{\frac{1}{2}} \cos\theta \tag{7}$$

where t_1 and t_2 are the kinetic energies of the two pions, and θ is the angle between their directions of motion. The inequality (4) then imposes the following restriction on angular integration

$$\cos\theta \leqslant \frac{(\varkappa - 2m)^2 - 2(t_1 + t_2)(\varkappa - m) - m_L^2}{4m(t_1 t_2)^{\frac{1}{2}}} = \varphi(t_1, t_2) , \tag{8}$$

the phase space integral becomes

$$\varrho_{L4} = \frac{m}{(2\pi)^5}\int (t_1 t_2)^{\frac{1}{2}}\, dt_1\, dt_2\, d(\cos\theta)(1 - m_L^2/K^2) , \tag{9}$$

where the integration has to be performed in the domain allowed by (8). This domain can be split into two regions:

i) When $\varphi(t_1, t_2) \geqslant 1$, the upper limit in the $\cos\theta$ integration is 1. The t_2-integration has then to be performed between the limits 0 and the value of t_2 given by the solution of the equation $\varphi(t_1, t_2) = 1$ for a fixed t_1, while t_1 goes from 0 to

$$\frac{(\varkappa - 2m)^2 - m_L^2}{2(\varkappa - m)} .$$

ii) When $-1 \leqslant \varphi(t_1, t_2) \leqslant 1$, the upper limit in the $\cos\theta$ integration has to be taken as $\varphi(t_1, t_2)$. Then t_2 goes between the values obtained by solving the equations $\varphi(t_1, t_2) = 1$ and $\varphi(t_1, t_2) = -1$ for a given t_1, while t_1 takes values between 0 and

$$\frac{(\varkappa - m)\{(\varkappa - 2m)^2 - m_L^2\}}{2\varkappa(\varkappa - 2m)} .$$

This upper limit of t_1 is obtained from the condition that the equation $\varphi^2(t_1, t_2) = 1$ for t_2 has real solutions. These integrations have been carried out numerically. The final results for the K_{e4} and $K_{\mu 4}$ modes of decay are

$$\varrho_{e4} = 1.83 \cdot 10^{-4}\, \varkappa^4/(2\pi)^5 , \tag{10}$$

$$\varrho_{\mu 4} = 0.25 \cdot 10^{-4}\, \varkappa^4/(2\pi)^5 . \tag{11}$$

Taking the matrix elements to be momentum independent, from Eqs. (5), (6), (10) and (11), the ratios of the rates of decay are given by

$$R_{e3}/R_{\mu 2} = 2.1 \cdot 10^{-2}(\varkappa L)^2/4\pi , \tag{12}$$

$$R_{e4}/R_{e3} = 8.9 \cdot 10^{-4}(\varkappa L)^2/4\pi , \tag{13}$$

$$R_{\mu 4}/R_{e4} = 1/7.3 , \tag{14}$$

where L is a length characteristic of the decay processes considered. It should be noted that the matrix elements for 2, 3 and 4 particle decays have different dimensions and this is the reason for the appearance of the lenght L. Choosing L to be such that the ratio $R_{e3}/R_{\mu 2}$ is equal to the experimental value [3] of about 1/15, the use of the same value of L in (13) leads to the ratio of K_{e4} the K_{e3} decay to be

$$R_{e4}/R_{e3} \simeq 1/350 . \tag{15}$$

---

[3] R. H. DALITZ: *Rep. on Progr. in Phys.*, **20**, 163 (1957); M. GELL-MANN and A. H. ROSENFELD: *Ann. Rev. of Nucl. Sci.*, **7**, 407 (1957).

It has been suggested [4] that the strangeness-changing currents responsible for strange particle decay processes are spinors in charge space. This means that the total isotopic spin of the final strongly interacting particles should differ by no more than $\Delta T = \frac{1}{2}$ from the initial isotopic spin. For K_{L4}^{+} decay, the isotopic spin of the two final pions is limited to $T = 0$ and $T = 1$. With $T = 0$ the relative motion of the two pions must have even orbital angular momentum, and so s-wave motion is allowed in their c.m. system. With $T = 1$, their relative motion must have odd angular momentum and must be p-wave or higher. As a result of the low energies of the final pions, it is likely that the $T = 0$ final state will be favored relative to the $T = 1$ state. If there exists a strong π-π force, it would modify the decay characteristics a good deal, especially if it involved a resonance in the low energy region under consideration. This possibility has been ignored in this discussion.

For the K_{L4} modes of K_1^0 or K_2^0 decay, the final state of two pions must have $T_3 = \pm 1$ and therefore $T = 0$ is not permitted. Since the $T = 1$ final state involves relative p-wave motion between the two pions, the K_{L4} modes of neutral K decay may be expected to be much rarer than for charged K decay.

It may be noted that the forbiddenness of $T = 2$ is the main consequence of this $T = \frac{1}{2}$ current rule . It is this fact which leads to our remark above concerning the rarity of K_{L4} modes for neutral K decay. This also forbids the decay process

$$\text{(C)} \qquad K^{+} \to \pi^{+} + \pi^{+} + e^{-} + \bar{\nu}\,,$$

although this is also excluded by the $\Delta Q/\Delta S = +1$ rule of Feynman and Gell-Mann [5].

3. – Phenomenological discussion.

The K_{L4} decay can be analysed from invariance principles and the assumption of the (V-A) theory as follows: The emission of pions must be the result of strong interactions whose effect we cannot reliably estimate. The decay process can be depicted as in Fig. 1.

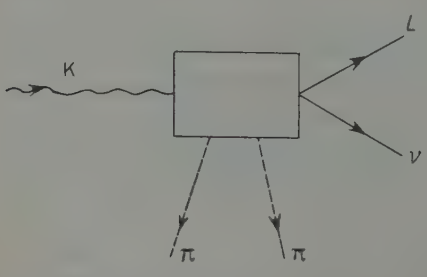

Fig. 1. – The K_{L4} mode of K-meson decay. The effect of strongly interacting intermediate particles is represented by the « black box ».

[4] S. Okubo, R. E. Marshak, E. C. G. Sudarshan, W. B. Teutsch and S. Weinberg: *Phys. Rev.*, **112**, 665 (1958).

[5] R. P. Feynman and M. Gell-Mann: *Phys. Rev.*, **109**, 193 (1958).

The « black box » represents the effect of intermediate particles which are coupled strongly to kaons and pions, and weakly to the lepton-neutrino current.

The matrix element must have the form

$$M_{e4} = \frac{G_K(\sqrt{2}G)^2 g}{(2\varkappa)^{\frac{1}{2}}} F_\mu(p_1, p_2, p)\{\overline{\psi}_L \gamma_\mu(1+\gamma_5)\psi_\nu\}, \tag{16}$$

where $p = p_L + p_\nu$ and $p = p_1 + p_2 = k$. Here $\sqrt{2}G$ denotes the coupling between charged pions and baryons and G_K that between kaons and baryons. From invariance requirements, the function F_μ has the general form

$$F_\mu = A\frac{(p_1+p_2)_\mu}{M} + B\frac{(p_1-p_2)_\mu}{M} + C\frac{p_\mu}{M} + D\varepsilon_{\mu\alpha\beta\gamma}\frac{p_\alpha (p_1)_\beta (p_2)_\gamma}{M^3}, \tag{17}$$

where $\varepsilon_{\mu\alpha\beta\gamma}$ is the alternating symbol, M has been taken to be the nucleon mass, and the dimensionless coefficients A, B, C and D are slowly varying functions of $k\cdot p_1/M^2$, $k\cdot p_2/M^2$ and $p_1\cdot p_2/M^2$. Since the intermediate particles represented in the « black box » of Fig. 1, are massive (mass of the order of M), it is reasonable to neglect the energy dependence of A, B, C, D, the momenta involved being small relative to M. We ignore here the final state π-π interaction. The D term is two orders of magnitude smaller than the others, and will therefore be omitted.

As already seen from the phase space considerations in Section 2, the $K_{\mu 4}$ decay is expected to be rarer than the K_{e4} decay. In this Section we will, therefore, not consider the $K_{\mu 4}$ decay mode. In Eq. (16) the C term reduces to

$$C(m_L/M)\overline{\psi}_L(1+\gamma_5)\psi_\nu .$$

For K_{e4} decay this term is negligible and will be omitted. The remaining terms A and B have opposite symmetry for interchange of the two pions. The A term is even with respect to an interchange of their momenta, and corresponds to an even isotopic spin state, the $T=0$ state alone being permitted according to the theory of a $T=\frac{1}{2}$ strangeness-nonconserving current. The B term is odd with respect to the interchange of pion momenta, and corresponds to the $T=1$ state.

As already stated the existence of a resonance in π-π interaction could modify our results substantially. If we denote the π-π scattering phase shifts by δ_0 and δ_1 for the $T=0$, $j=0$ and $T=1$, $j=1$ states, and assume that the final π-π states are limited to the lowest possible angular momenta states then A and C will have phases δ_0 due to the final scattering, and B and D will have phases δ_1. In general therefore A, B, C and D are complex quantities, and have an energy dependence due to the final state π-π scattering.

The c.m. kinetic energy T of π-π system is given by $(2m_\pi+T)^2=(p_1+p_2)^2$ so that δ_0 and δ_1 will be functions only of $(p_1+p_2)^2$. The parameters A, B, C and D will have energy dependence proportional to $\sin\delta_l \exp[i\delta_l]/k_\pi^{2l+1}$, so that evidence concerning the phase shifts could be obtained from a comparison with experimental data. However, in view of the fact that the K_{L4} event has not yet been reported experimentally, we have not carried out these calculations explicitly.

In the rest frame of the kaon, the K_{e4} decay rate is

$$(18)\qquad R_{e4}=\frac{4}{3\pi^2}g^2\frac{G_K^2}{4\pi}\left(\frac{G^2}{4\pi}\right)^2\frac{1}{M^2\varkappa}\int\frac{p_1^2p_2^2}{\omega_1\omega_2}\,dp_1\,dp_2\,d(\cos\theta)\cdot$$
$$\cdot[|A|^2\varkappa^2\{(\omega_1+\omega_2)^2-2(m^2+p_1\cdot p_2)\}+|B|^2\{\varkappa^2(\omega_1-\omega_2)^2-2\varkappa^2(m^2-p_1\cdot p_2)-$$
$$-4(m^4-(p_1\cdot p_2)^2)+4\varkappa(\omega_1+\omega_2)(m^2-p_1\cdot p_2)\}]\,.$$

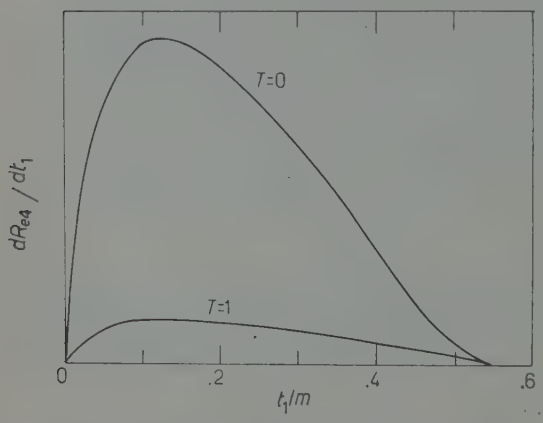

Fig. 2. - The differential pion-energy spectrum in K_{e4} decay.

The integrations over p_1, p_2 and $\cos\theta$ have to be carried out under the restriction imposed by the inequality (8). This has been done numerically, taking the non-relativistic approximation for the pion momenta. The differential pion energy spectrum is plotted in Fig. 2, separately for the $T=0$ and $T=1$ final states. It is evident that if A and B are of the same order of magnitude, the decay goes mainly through the channel $T=0$. The most probable energy for a pion from K_{e4} is about 34 MeV for the $T=0$ channel, and about 23 MeV for the $T=1$ channel.

The total rate of decay is

$$(19)\qquad R_{e4}=\frac{8}{3\pi^2}g^2(G_K^2/4\pi)(G^2/4\pi)^2\frac{m^8}{M^2\varkappa}\,(0.24\,|A|^2+0.034\,|B|^2)\,.$$

For K_{e3} decay, the matrix element has a unique form if the electron mass is neglected, and is given ([6]) in terms of a dimensionless parameter I:

$$(20)\qquad \mathcal{M}_{e3}=G_K\bar{G}gI\frac{p_\alpha}{(2\varkappa)^{\frac{1}{2}}}\{\overline{\psi}_e\gamma_\alpha(1+\gamma_5)\psi_\nu\}\,,$$

([6]) A. Fujii and M. Kawaguchi: *Phys. Rev.*, **113**, 1156 (1959).

where p is the 4-momentum of the neutral pion. The total decay rate for K_{e3} is analytically obtained as

$$R_{e3} = \frac{1}{6\pi} g^2 (G_K^2/4\pi)(G^2/4\pi) |I|^2 \varkappa \left[\frac{(\varkappa^2 + m^2)(\varkappa^2 - m^2)}{(2\varkappa)^4} \cdot \right. \tag{21}$$

$$\left. \cdot \{(\varkappa^2 - m^2)^2 - 6\varkappa^2 m^2\} + \frac{3}{2} m^4 \cosh^{-1}\left(\frac{\varkappa^2 + m^2}{2\varkappa m}\right) \right] .$$

For $K_{\mu 2}$, the matrix element is

$$\mathcal{M}_{\mu 2} = G_K g M J \frac{(p_L)_\alpha}{(2\varkappa)^{\frac{1}{2}}} \{\overline{\psi}_L \gamma_\alpha (1 + \gamma_5) \psi_\nu\} , \tag{22}$$

where J is a dimensionless coefficient. The rate of decay is

$$R_{\mu 2} = g^2 (G_K^2/4\pi) |J|^2 M^2 m_\mu^2 \left(\frac{\varkappa^2 - m_\mu^2}{\varkappa^2}\right)^2 . \tag{23}$$

To estimate the relative magnitudes of the various rates of decay, we take $A \approx B \approx I \approx J$. The ratio $R_{e3}/R_{\mu 2}$ is then about $(G^2/4\pi) \cdot 0.012$ which is to be compared with the observed branching ratio of 1/15. This corresponds to a value $G^2/4\pi \sim 5.5$, which appears reasonable. From Eq. (19) and (21), then

$$R_{e4}/R_{e3} \simeq 4.6 \cdot 10^{-4} \left(\frac{G^2}{4\pi}\right) , \tag{24}$$

which has a value of about 1/400 for the same value of $G^2/4\pi$.

4. – Perturbation theory.

In this Section we shall evaluate the decay rates for a particular model by means of the lowest order perturbation theory. In our model we choose the virtual baryon-antibaryon pair as $(N, \bar{\Lambda})$, and consider the pions to be emitted only by the nucleon. We also neglect the final state π-π interaction. The Feynman diagrams for the decays K_{e4}, K_{e3}, and $K_{\mu 2}$ in this model are shown in Figs. 3*a*, 3*b*, 3*c*.

For the coefficients introduced phenomenologically in Section 3, the following values are obtained:

$$A = B = 2\pi^2 i , \tag{25}$$

$$I = J = -4\pi^2 i \left\{1 - \ln\left(\frac{\lambda^2 + M^2}{M^2}\right)\right\} , \tag{26}$$

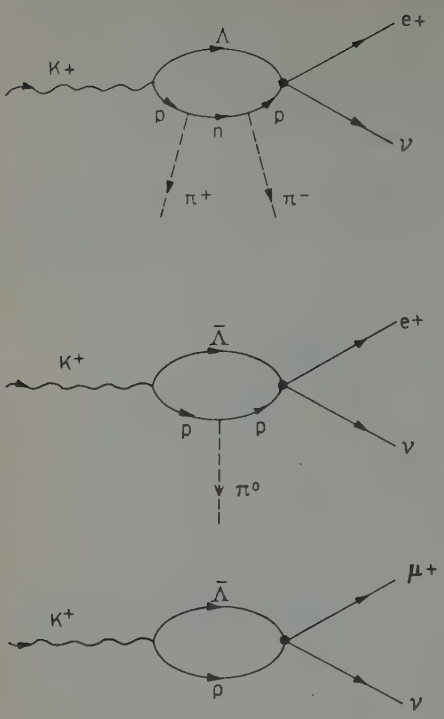

a) b) c) Fig. 3. – Decay diagrams of (*a*) K^+_{e4}, (*b*) K^+_{e3}, and (*c*) $K^+_{\mu 2}$.

where λ denotes a cut-off momentum large relative to M. Since $I = J$, we have as before the ratio $R_{e3}/R_{\mu 2}$ in reasonable accord with the observed value. The ratio R_{e4}/R_{e3} is uncertain because of the logarithmic dependence on the cut-off. Taking $\lambda^2 = 5M^2$, and $G^2/4\pi = 15$, we get, for example,

$$R_{e4}/R_{e3} \simeq \frac{1}{4\,000} . \tag{27}$$

This result clearly has considerable sensitivity to the choice of the cut-off λ, and is only to be regarded as an order of magnitude result.

5. – Conclusion.

An estimate of the ratio of rates of K_{e4} and K_{e3} decay processes has been made in three ways; from phase space considerations in Section **2**, from phenomenological (V-A) theory in Section **3**, and finally from a particular perturbation theoretic model in Section **4**. In the phase space and phenomenological calculations, the unknown parameters have been chosen so as to fit the observed $R_{e3}/R_{\mu 2}$ ratio. The results obtained for the R_{e4}/R_{e3} ratio are then comparable and about 1/400. The calculations of the phenomenological coefficients on the basis of a particular model in Section **4** gave smaller constants for the K_{e4} matrix elements than the above procedure indicated, and led to a R_{e4}/R_{e3} ratio nearer 1/4 000. This value, however, is subject to uncertainty depending on the choice of cut-off for the divergent integrals in the K_{e3} calculation with this model. The experimental detection of the K_{e3} decay is more difficult than, for example, the τ-decay. Since the rates of K^+_{e3} and τ modes of decay are comparable, and because several thousand τ events have already been observed, we conclude that it is reasonable to expect the observation of K^-_{e4} decays of the type (B) in the near future. On the other hand, the K^+_{e4} decays of the type (C) are strictly forbidden on the hypothesis of $T = \frac{1}{2}$ strangeness-

non-conserving currents, or the $\Delta Q/\Delta S = +1$ rule. From phase space considerations the ratio $R_{\mu 4}/R_{e4}$ is found to be $\frac{1}{7}$, so that $K^+_{\mu 4}$ mode of decay is expected to be less frequent by an order of magnitude than the K^+_{e4} decay mode.

* * *

The author is deeply indebted to Professor R. H. DALITZ for suggesting the problem and for helpful discussions, and would like to thankfully acknowledge a fellowship from the Government of India.

RIASSUNTO (*)

Si sono studiate le caratteristiche dei modi K_{e4} e $K_{\mu 4}$ di decadimento dei mesoni K. Si discutono le relazioni dello spin isotopico che discendono dall'ipotesi di una corrente non-conservante la stranezza $T=\frac{1}{2}$. Si sono stimate le velocità di decadimento in molti modi, i quali si accordano nel predire un rapporto di branching K^+_{e4}/K^+_{e3} fra 10^{-3} e 10^{-4}, cosicchè ci si può aspettare nel prossimo futuro l'osservazione di eventi K^-_{e4}. Si prevede che la frequenza del modo $K^+_{\mu 4}$ sia di almeno un ordine di grandezza inferiore a quella del modo K^+_{e4}.

(*) *Traduzione a cura della Redazione.*

IL NUOVO CIMENTO Vol. XIV, N. 6 16 Dicembre 1959

An Experiment to Investigate the Existence of Charged Particles of Mass $\sim 550\ m_e$.

N. Durga Prasad, M. G. K. Menon and O. P. Sharma

Tata Institute of Fundamental Research - Bombay

(ricevuto il 22 Settembre 1959)

Summary. — Evidence suggesting the existence of charged particles of mass $\sim 550\ m_e$ has been reported by Alikhanian, Šostakovič, Dadaian, Fedorov and Deriagin. A search has been made for these particles in a photographic emulsion stack exposed for five months at an altitude of 11000 ft, $\lambda = 24°$ N at Khillanmarg (Kashmir). The central plate of the stack was scanned for all tracks, with dip angles $< 45°$, due to particles brought to rest within it. A total of 5790 tracks was obtained in this scan. Of these tracks, 2613 were due to particles, with ranges < 5 mm, emerging from nuclear disintegrations; these were not considered further. Mass measurements were carried out on the remaining 3177 tracks by the grain density vs. residual range method; the range interval involved is $(3 \div 40)$ g/cm^2. The 3177 tracks investigated were found to be due to 1018 μ-mesons, 168 π-mesons and 1991 particles of mass $\geqslant 850\ m_e$. No particle with a mass estimated to be between 390 m_e and 850 m_e has been observed. Five such particles are to be expected on the abundance of $\sim \frac{1}{2}\%$ compared to μ-mesons (in the same range interval) quoted by Alikhanian *et al.* The question of the existence of such particles is discussed in the light of this and other experiments.

1. – Introduction.

Alikhanian, Šostakovič, Dadaian, Fedorov and Deriagin [1] have reported evidence suggesting the existence of particles of mass $\sim 550\ m_e$ amongst the slow cosmic ray particles observed in an experiment at Mt. Alagez (geomagnetic latitude $\lambda = 35°$ N and height 3200 m). The experimental arrangement consisted of a hodoscoped magnetic spectrometer and two multiplate cloud chambers, one placed above and one below the spectrometer.

[1] A. I. Alikhanian, N. V. Šostakovič, A. T. Dadaian, V. N. Fedorov and B. N. Deriagin: *Žurn. Éksp. Teor. Fiz.*, **31**, 955 (1956).

The triggering system selected all events in which a single charged particle was arrested in the lower chamber. The mass of each particle was estimated with an accuracy of $\sim 50\ m_e$ from a measurement of momentum, (by determining the curvature of the trajectory in the magnetic spectrometer), and from the residual range in the lower cloud chamber. In the observed mass spectrum of slow cosmic ray particles entering the apparatus, there were eleven particles at a mass value of $550\ m_e$. This peak was observed *only* in the mass spectrum of slow particles entering the apparatus from the cosmic ray beam; it was absent in the mass spectrum of slow particles arising from nuclear interactions in the multiplate cloud chamber above the magnetic spectrometer. It must be pointed out that there is a discrimination against the latter group, since, in general, they will be accompanied by fast charged particles and thus be rejected by the triggering system; this is particularly so for the high energy interactions.

On the basis of the observations reported by ALIKHANIAN *et al.* [1] the following properties may be ascribed to these particles, if they exist:

a) Mass: $\sim 550\ m_e$.

b) Abundance: $\sim \frac{1}{2}\%$ compared to μ-mesons in the same range interval (of $(2 \div 5)$ cm of lead).

c) Lifetime: $> 10^{-6}$ seconds. (Since these particles traversed path-lengths comparable with those of the μ-mesons, their lifetime is, perhaps, approximate to that of μ-mesons or greater, unless their abundance is much larger than that observed).

d) Nature: Probably μ-mesonic. (None was seen to be produced in nuclear interactions; further, each of them traversed more than $65\ g/cm^2$ of matter in the apparatus).

e) Charge: Predominantly negative. (The observed ratio of negative to positive particles was 9:2).

f) Decay: A doubtful example was seen of a small electronic shower associated with the point of arrest of one of the positive particles.

Such particles would differ completely from the so-called charged zeta-mesons, reported in earlier literature [2-4].

[2] R. R. DANIEL, J. H. DAVIES, J. H. MULVEY and D. H. PERKINS: *Phil. Mag.*, **43**, 753 (1952).

[3] R. R. DANIEL and D. H. PERKINS: *Proc. Roy. Soc. London*, A **221**, 351 (1954).

[4] M. M. SHAPIRO: *Proc. of the Third Annual Rochester Conference on High Energy Nuclear Physics* (1952), p. 69.

The mass spectrum of slow cosmic ray particles has been measured on previous occasions at sea level and mountain altitudes ([5-8]) and individual mass values of $\sim 550\ m_e$ have been reported in some of these. However, because of the small statistics and the limited reliability of the mass determinations, these observations have never been given great weight.

With properties as listed above, it is unlikely that these particles would have been detected in cloud chamber experiments in which the triggering systems were designed to select nuclear interactions and for particles arising from these interactions. There is, of course, the possibility that they would have been detected in the course of scanning for the decay or capture of K-mesons. However, it is clear that in a systematic and careful survey of the mass spectrum of slow cosmic ray particles there is a reasonable probability of detecting them and thus of being able to set an upper limit to their abundance. A definite need for an independent estimate of abundance arises because of the fairly strong evidence reported by ALIKHANIAN *et al.*, and the evidence, *a priori*, is indeed strong when one considers the well-resolved group of particles at a mass value of 550 m_e and the predominantly negative character of the particles as observed by these workers.

It was, therefore, decided to investigate the existence of particles of this mass in the mass spectrum of slow cosmic ray particles, using nuclear research emulsions as detector. The results obtained are reported in the present paper.

2. – Experimental details.

2·1. *Exposure.* – A stack of 18 Ilford G-5 emulsions, each of dimensions 8in.×6in.×600 μm, was exposed at Khillanmarg (Kashmir), at geomagnetic latitude $\lambda = 24°$ N and altitude 11000 ft, during the period from November 1956 to April 1957. The stack was maintained at an average temperature of $\sim -10\ °C$; there was no detectable fading in grain density; fluctuations in grain density due to variation of development with depth in the emulsion and any possible fading were less than 5%. The grain density on tracks with the minimum value of ionization loss was ~ 17 grains/100 μm.

The stack was aligned ([9]) by placing grids of nylon fibres, soaked in po-

([5]) R. B. BRODE: *Rev. Mod. Phys.*, **21**, 37 (1949).
([6]) C. FRANZINETTI: *Phil. Mag.*, **41**, 86 (1950).
([7]) G. ASCOLI: *Phys. Rev.*, **90**, 1079 (1953).
([8]) M. INOKI, T. YASAKI, M. MACHIDA and Y. MATSUKAWA: *Phys. Rev.*, **105**, 1872 (1957).
([9]) R. R. DANIEL, G. FRIEDMANN, D. LAL, Y. PAL and B. PETERS: *Proc. Ind. Acad. Sci.*, A **40**, 151 (1954).

lonium solution (free from β-activity), between pairs of emulsions. The accuracy of alignment was about 20 μm.

2·2. *Selection criteria.* – The central plate of the stack was scanned for all stopping particles with dip angles less than 45°, as judged from two successive plates; no account was taken of their behaviour at the end of their range. The scanning was restricted to the region of the emulsion 1 cm away from the processed edges.

5 790 tracks were obtained in the scan. Out of these, 2 613 tracks were due to particles emerging from nuclear interactions, with values of residual range less than 5 mm, a range corresponding to an energy of 36 MeV for protons. Mass measurements have not been carried out in these cases since the particles come from nuclear interactions, and are not part of the slow cosmic ray beam whose mass spectrum is being measured. Further, mass measurements for residual ranges less than 5 mm cannot be made very accurately.

Measurements of residual range and grain density were carried out on the remaining 3177 tracks.

2·3. *Calibration curve.* – A calibration curve of grain density versus range in our emulsions was obtained from measurements of grain density at various residual ranges on 81 flat tracks due to stopping π^+-mesons which suffered μ-decay; about 400 grains were counted at each value of residual range. That all of these were indeed π-mesons can be seen from the following two considerations:

i) The range distribution of the decay μ-mesons corresponds to that well-known for the π-μ-decay; the mean range obtained was 596 μm and no tracks had values less than 533 μm or greater than 680 μm.

ii) Direct mass measurements were made by the residual range versus grain density method on all 81 π^+-meson tracks; the calibration curve already obtained was used for mass estimation. The resultant mass distribution can be fitted by a gaussian distribution; the mean mass value is $(271^{+5.5}_{-4.5})\ m_e$; these errors are consistent with the expected values.

The range *vs.* grain density curve for protons was derived from the calibration curve obtained for π^+-mesons; it has been extended to lower ranges by measurements on flat tracks due to stopping protons. The mass distribution of 162 stopping tracks due to protons is consistent with the expected spectrum.

2·4. *Mass determinations.* – The 3177 particle tracks that have been accepted for mass measurement can be split up as in Table I.

TABLE I.

Total number of tracks	Particles that give rise to μ-mesons	Particles that give rise to capture stars	Particles that do not give rise to any visible decay or interaction
3177	91	84	3002

About 400 grains were counted on each of the 3177 tracks over a region of residual range of 6 to 16 mm for protons and 4 to 8 mm for L-mesons. The personal consistency of the observers in grain counting was better than 3% as compared to the statistical error of 5%. Using these measurements, rough mass estimates were obtained from the grain density-range calibration curve. If the rough mass estimate clearly indicated that the particle had a mass greater than 1200 m_e (approximately one standard deviation on the higher side of the K-meson mass) no attempt was made to calculate the mass accurately, though all needful measurements had been made, since for the purpose of this experiment it is not of great interest. There were 1871 such tracks.

Mass values of the remaining 1306 particles were calculated accurately.

3. – Results.

The mass spectrum of these 1306 particles is shown in Fig. 1. There are 1186 estimated mass values less than 390 m_e and 120 above 850 m_e. There is no track for which the estimate of mass lies between 390 m_e and 850 m_e.

Out of the 1186 particles with estimated mass values less than 390 m_e, 91 show the characteristic π-μ-decay and 84 produce capture stars with visible prongs greater than 10 μm. In 1011 cases there is no visible indication of interaction and in many cases no visible decay electron at the point of arrest of the particle. These are predominantly μ-mesons. The efficiency for detection of electrons from μ-e decay was low because of the low value for minimum grain density and the high background; furthermore, no detailed search was made at the point of arrest of each particle to look for the decay electron. Amongst the 1011 tracks, it is estimated that there should be 23 cases of π-ρ events and correcting also for capture stars produced by μ^--mesons (~3%), the total number of μ-mesons is calculated to be 1018.

To strengthen our conclusion that particles with mass values lying between 390 m_e and 850 m_e are absent in our sample, ten tracks which gave mass

values within two standard deviations of 550 m_e were re-examined; grain counting was carried out at higher values of residual range in these cases. The refined mass estimates are shown in Table II.

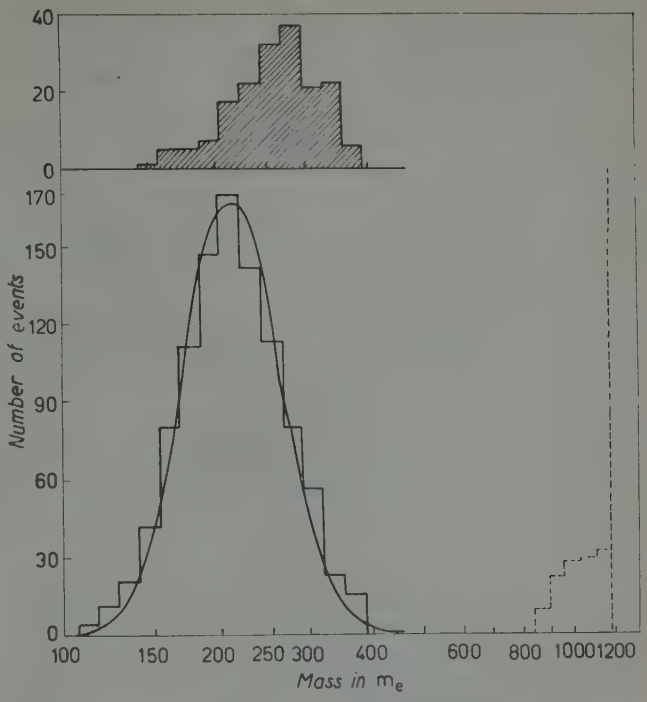

Fig. 1. – Mass spectrum obtained from measurements on 1306 tracks. The spectrum indicated by the solid line represents μ-mesons and some π-mesons (which produce π-ϱ events). Using the left half of the spectrum, where the contamination due to π-ϱ events should be quite small, a gaussian was fitted and folded over. The mean mass value obtained from this is $(213.8^{+1.6}_{1.3})$ m_e. The mean errors (standard deviations) on the individual mass values are +52 m_e and — 42 m_e. The shaded histogram refers to particles which give rise to π-μ-decays (91) and capture stars (84) and the dotted one to 120 cases with mass values less than 1200 m_e.

TABLE II.

S. No.	Mass in m_e		Characteristic at the stopping end
	1st measurement	2nd measurement	
1	389	278	—
2	369	249	—
3	366	336	—
4	382	285	—
5	366	236	—
6	363	243	—
7	362	229	—
8	362	264	π-μ-decay
9	387	253	π-μ-decay
10	374	270	π-μ-decay

There is no track which can be attributed to a particle of mass 550 m_e. On the basis of the relative abundance of ½% (compared to μ-mesons in

the same range interval) quoted by ALIKHANIAN *et al.* the number of particles of mass $\sim 550\ m_e$ expected in this sample is 5; the probability of observing none is 0.7%.

4. – Discussion.

4·1. *Comparison with the experiment of Alikhanian et al.* – This experiment is similar to that of ALIKHANIAN *et al.* but differs in the following three features:

i) Photographic emulsion was used as detector. As the lifetime of these particles is fairly long (comparable to that of the μ-mesons), our experiment, in which all stopping particles have been examined, should certainly detect these particles, if they exist.

ii) The mass spectrum was measured at geomagnetic latitude $\lambda = 24°$ N whilst the experiment of ALIKHANIAN *et al.* was carried out at $\lambda = 35°$ N; this is not expected to make any difference to the slow particles in the cosmic ray beam.

iii) In the present work, the mass spectrum of slow charged cosmic ray particles was measured over a range interval of $(3 \div 40)$ g/cm² of emulsion. ALIKHANIAN *et al.* quote a range interval of $(2 \div 5)$ cm of lead, but the particles in their experiments also traversed about 70 g/cm² of matter in the upper chamber.

4·2. *Detection of* K*-mesons in this experiment.* – The experimental mass spectrum of protons extends as low as $850\ m_e$ on the lower mass side and thus K-mesons cannot be resolved in this mass spectrum. Further, because of the low value of grain density for minimum ionization and due to the high background, it is not possible to recognize with ease tracks due to fast particles arising in decay processes; because of this feature, the efficiency for the detection of μ-e decays has also been quite small. Only those $K_{\pi 3}$, $K_{\mu 3}$ and K_{e3} decays involving slow secondary charged particles, and K^- capture stars could be detected efficiently; but these together constitute about one-fifth of the total number of events associated with stopping K-mesons. For the 168 π-mesons detected in the search, the expected number of such events is $\leqslant 1$.

4·3. *Other experiments.* – A number of other experiments have been carried out to look for these particles. The search may, in principle, be made in different ways as listed below:

i) By measurements of the mass spectrum of slow cosmic ray particles at sea level or mountain altitude.

ii) By looking for such particles as decay products of heavier unstable particles, such as, K-mesons or hyperons.

iii) By scanning across a range of lifetimes for all possible modes by which such a particle might ultimately decay, assuming that it is unstable.

The majority of experiments carried out to date are of type i). The work of ALIKHANIAN *et al.* ([1]), the experiment described herein and similar attempts by BIERMAN *et al.* ([10]), FAZIO ([11]), and FAZIO and WIDGOFF ([12]), the earlier emulsion work of FRANZINETTI ([6]), and cloud chamber experiments by BRODE ([5]), ASCOLI ([7]), INOKI *et al.* ([8]), BASU *et al.* ([13]), CONVERSI *et al.* ([14]) and by PIROUE and HENDEL ([15]) all fall into this category. Individual events which could constitute evidence for the existence of particles of 550 m_e have been reported by BRODE, ASCOLI, INOKI *et al.* and by BASU *et al.* The first three of these are old experiments, prior to that of ALIKHANIAN *et al.* None of these has the accuracy of mass determination or the statistical weight of the experiment of ALIKHANIAN *et al.* The large scale systematic experiments, *e.g.*, the emulsion work of FRANZINETTI, of BIERMAN *et al.*, of FAZIO, of FAZIO and WIDGOFF and this work, and the cloud chamber work of PIROUE and HENDEL and CONVERSI *et al.* have all yielded negative results.

An experiment of type ii) has been attempted by HARRIS *et al.* ([16]) and by BOSGRA and BRUIN ([17]). From an examination of the decay of 7 000 K^+-mesons in these two experiments they conclude that the abundance of charged 550 m_e particles originating from the decay of K^+-mesons is less than 0.1 %.

An experiment by KEUFELL *et al.* ([18]), where the mass spectrum of particles which decay to secondaries of long lifetime was measured, gave an abundance of less than 0.1% for these particles.

BOLDT *et al.* ([19]) have carried out an experiment of type iii). They measured the lifetime spectrum from 1 μs to 20 ms of slow cosmic ray particles stopped in large scintillator blocks and looked for all possible decay modes for which the dynamics would be consistent with the decay of a particle of mass 550 m_e. This experiment was built on the hypothesis that particles of this type are

---

([10]) E. BIERMAN, R. LEA, J. OREAR and S. ROSENDORFF: *Phys. Rev.*, **113**, 710 (1959).

([11]) G. G. FAZIO: *Proc. of Annual International Conference on High Energy Physics at CERN* (1958), p. 153.

([12]) Letter from G. G. FAZIO.

([13]) N. BASU and M. S. SINHA: *Ind. Journ. Phys.*, **32**, 259 (1958).

([14]) M. CONVERSI, G. M. DE' MUNARI, A. EGIDI, E. FIORINI, S. RATTI, C. RUBBIA C. SUCCI and G. TORELLI: *Nuovo Cimento*, **12**, 148, (1959); *Phys. Rev.*, **114**, 1150 (1959).

([15]) P. PIROUE and A. HENDEL: *Proc. of the Annual International Conference on High Energy Physics at CERN*, (1958) p. 153.

([16]) G. HARRIS, J. OREAR and S. TAYLOR: *Nuovo Cimento*, **6**, 1232 (1957).

([17]) S. J. BOSGRA and F. BRUIN: *Nuovo Cimento*, **10**, 551 (1958).

([18]) J. W. KEUFFEL, R. L. CALL, W. H. SANDMANN and M. O. LARSON: *Phys. Rev. Lett.*, **1**, 203 (1958).

([19]) E. BOLDT, J. HERSIL, YASH PAL and J. RUSSEL: private communication from YASH PAL.

unstable and ultimately decay, with lifetimes comparable to or longer than that of μ-mesons. They concluded that the abundance of such particles compared to μ-mesons is much less than hitherto assumed or that they have a lifetime greatly in excess of 20 ms or less than 10^{-6} s. A similar experiment by FAZIO and RITSON [12] also gave a negative result.

The mass determination in the experiment of ALIKHANIAN *et al.* is based on a measurement of residual range; it is assumed therefore that the particle was brought to rest by ionization loss only, which was established qualitatively from the rate of increase of track density. Thus in this experiment it is possible to overestimate the mass of a particle, if, in addition to ionization loss, the particle also lost energy in nuclear encounters. This feature has been pointed out by the Russian authors themselves (*e.g.*, Table II in the paper of ALIKHANIAN *et al.*). They conclude that it is also necessary to make accurate specific ionization measurements to settle this point and have proposed new measurements to be carried out using multi-layer proportional counters. MEŠKOVSKJ and SOKOLOV [20], working with scintillation counters at Mt. Alagez (3250 m), have studied the ionization spectrum of cosmic rays and find a considerable number of particles in the interval corresponding to the most probable ionization by mesons of mass 550 m_e. Nevertheless, they find that almost all these particles can be explained as due to protons which have lost energy in processes other than that of ionization.

Further, a point regarding the relative abundance of these particles may be made. The ratio quoted by ALIKHANIAN *et al.* of K-mesons to π-mesons amongst the slow particles is 0.08, which increases to 0.14 when corrected for the different lifetimes of the K and π-mesons [10]. This figure is higher than any obtained by other workers. For example, HORNBOSTEL *et al.* [21] quote a value of about 0.0016 for the ratio K^+/π^+ in reactions involving primary protons of 2.95 GeV — this, of course, is very close to the threshold for production of K-mesons; cloud chamber [22] and counter [23] experiments done at mountain altitude yield a ratio of $K^+/\pi^\pm \sim 0.01$ to 0.03. Higher values have been quoted for this ratio in the case of jets, but as stated before, the triggering system employed in the experiment of ALIKHANIAN *et al.* discriminates against particles produced in high energy nuclear interactions. It is therefore relevant to compare the production ratio of K-mesons to π-mesons in low energy disintegrations ($\sim$ tens of GeV) with the abundance quoted by the Russian workers. In all of what has been said above, the values refer to slow particles. It thus appears that the number of π-mesons in the sample has been underestimated by ALIKHANIAN *et al.* and if so, the number of

[20] A. G. MEŠKOVSKJ and L. I. SOKOLOV: *Soviet Physics JETP*, **4**, 629 (1957).
[21] J. HORNBOSTEL, E. O. SALANT and G. T. ZORN: *Phys. Rev.*, **112**, 1311 (1958).
[22] H. S. BRIDGE, CH. PEYROU, B. ROSSI and R. SAFFORD: *Phys. Rev.*, **90**, 921(1953).
[23] L. MEZZETTI and J. W. KEUFFEL: *Nuovo Cimento*, **4**, 1096 (1956).

μ-mesons would also be underestimated. The loss factor for μ-mesons would be even higher than for π-mesons as they are the lighter particles. This argument indicates that the relative abundance of particles of mass 550 m_e in the experiment of ALIHANIAN *et al.*, compared to μ-mesons in the same range interval, is probably $\leqslant 10^{-3}$. From the paper of ALIHANIAN *et al.* it is not clear how the aperture corrections necessary for arriving at the value of relative abundance have been made.

5. – Conclusion.

It is concluded therefore that if such particles exist, they do so with a relative abundance much less than that quoted by ALIKHANIAN *et al.* The care taken in the present experiment is sufficient to ensure that these particles with a relative abundance of $\frac{1}{2}\%$ would have been detected with a high probability. The abundance is likely to be of the order of 10^{-3} or lower, and if so, it would be difficult to use the photographic emulsion technique to discover them. For this reason an attempt to increase the statistics quoted in this paper is not considered worthwhile.

* * *

We are very grateful to Professor B. PETERS and to Dr. R. R. DANIEL for valuable discussions and helpful suggestions during the progress of the work. We are also thankful to Dr. M. S. SWAMI, who participated in this work for a short time, to Mrs. T. M. UPADHAYAY who did the scanning of the plates and to Mr. B. S. AMIN for the exposure of the stack.

RIASSUNTO (*)

Indizi che suggeriscono l'esistenza di particelle cariche di massa $\sim 550\ m_e$ sono stati riferiti da ALIHANIAN, ŠOSTAKOVIČ, DADAIAN, FEDOROV e DERIAGIN. Queste particelle sono state ricercate in una pila di lastre esposte per cinque mesi ad un'altezza di 11000 ft., $\lambda = 24°$ N a Khillanmarg (Kashmir). Nella lastra di centro della pila sono state esaminate tutte le tracce, con angoli di dip $< 45°$, dovute a particelle venute a fermarsi nel suo interno. In questa ricerca si sono trovate in totale 5790 tracce. Di queste tracce 2613 erano dovute a particelle, con percorsi < 5 mm, che derivavano da disintegrazioni nucleari; queste non vennero ulteriormente prese in considerazione. Sulle rimanenti 3177 tracce furono eseguite misure di massa col metodo del rapporto fra densità di grani e percorso residuo; l'intervallo di percorso considerato è $(3 \div 40)\ g/cm^2$. Si trovò che le 3177 tracce esaminate erano dovute a 1018 mesoni μ, 168 mesoni π e 1991 particelle di massa $\geqslant 850\ m_e$. Non si è osservata alcuna particella di massa stimata fra 380 m_e e 850 m_e. Sulla base di una percentuale del $\frac{1}{2}\%$ rispetto ai mesoni μ (nello stesso intervallo di percorso) riportato ALIHANIAN *et al.*, ci si dovrebbero aspettare 5 di queste particelle. La questione dell'esistenza di tali particelle viene discussa alla luce di questa ed altre prove.

(*) *Traduzione a cura della Redazione.*

IL NUOVO CIMENTO Vol. XIV, N. 6 16 Dicembre 1959

Size-Spectrum of Extensive Air Showers of the Cosmic Radiation.

I. – Response of a Single Scintillator to Extensive Air Showers (*).

J. R. Green

University of New Mexico - Albuquerque (New Mexico)

(ricevuto il 29 Settembre 1959)

Summary. — Previously determined experimental and theoretical expressions for the lateral distribution of particles in extensive air showers are used to predict the response of a single scintillator to these showers. The integral rate of particles traversing the scintillator is found in terms of the integral rate of showers; the average size of shower resulting in a given number of particles through the scintillator is calculated; the effect of the zenith-angle distribution of the shower axes is also investigated.

1. – Introduction.

The extensive air showers of the cosmic radiation are of two-fold interest. First, there is the intrinsic value of the showers themselves in their complicated structure and development. Secondly, there is the expectation of deducing knowledge of the primary cosmic radiation, as it is incident upon the outer atmosphere of the earth, from the behavior and occurrence of the extensive air showers; such knowledge can then be used as a basis for speculations of cosmological importance. One of the more important and basic characteristics of the extensive air showers is the frequency of occurrence of the showers as a function of the total number of particles in the shower. A size-spectrum of this kind is of obvious importance because there must be a monotonic relation between increasing size of showers and increasing energy of the primary cosmic radiation.

(*) Supported by the United States Air Force Office of Scientific Research.

Investigations of extensive air showers have been largely characterized by widespread arrays of Geiger-Müller tubes in trays or of scintillators. In addition to the obvious necessity of such dispersal if any knowledge of the lateral structure of the showers about their cores is to be obtained, there is the practical consideration of obtaining reasonably high counting rates. Because of the rapid decrease in particle density as one leaves the shower core and because of the fairly rapid decrease in the rates of the showers with increasing size, appreciable counting rates could be obtained with detectors of practicable size only by employing many such detectors and by distributing them over a very large area. Now, however, good experimental evidence of the lateral structure has become available together with theory that closely approximates the observed distribution; also, improved techniques in the manufacture of photomultiplier tubes has made it possible to construct scintillators of very large acceptance area. These circumstances made it appear desirable to investigate the behavior of extensive air showers using but a single large scintillator in place of many smaller ones. This paper is concerned with developing the expected response of such a scintillator to the extensive air showers. The following paper presents the results of the experiment as they apply to the size-spectrum of the showers.

2. – Properties of extensive air showers.

In order to calculate the response of a single scintillator to the extensive air showers, it is necessary to know something of the structure of the air showers. The particular properties that are most pertinent are the lateral structure, the form of the number-spectrum, and the angular distribution of the shower axes.

It has generally been observed that the lateral distribution of the electronic particles comprising an extensive air shower has the same form regardless of size (*i.e.*, total number of particles) of the shower and regardless also of the height of the point of observation in the lower atmosphere ([1-4]). The distributions will therefore be treated in the form

$$F_i(x) = Nf_i(x)\,, \tag{1}$$

([1]) V. I. Zatsepin: *Žurn. Èksp. Teor. Fiz.*, **33**, 190 (1957); *Soviet Physics J.E.T.P.* (*U.S.S.R.*) **6**, 150 (1958). This paper contains references to recent Russian experimental work.

([2]) H. L. Kasnitz and K. Sitte: *Phys. Rev.*, **94**, 977 (1954).

([3]) G. Clark, J. Earl, W. Kraushaar, J. Linsley, B. Rossi and F. Sherb: *Nature*, **180**, 353 (1957).

([4]) E. W. Kellermann, T. Shaw and G. O. Walker: *Proc. Phys. Soc.*, **71**, 491 (1958).

where $f_i(x)$ is the fractional density of the particles of the shower occuring at x units from the shower axis. The first distribution to be used was found empirically by Rossi and his coworkers ([3]) and is given by

$$f_1(x) = \frac{1}{2\pi r_1^2} \frac{\exp[-x]}{x}, \tag{2}$$

where $x = r/r_1$; r is the radial distance from the axis of the shower, and r_1 is 79 m at an altitude of 183 m s.l. At the elevation of Albuquerque, where the present experiment was performed (1575 m s.l.) the appropriate length for r_1 is 94 m. This will be referred to as the « exponential distribution ». The second distribution that will be used is that derived by Nishimura and Kamata, although for ease in calculation an approximate form due to Greisen will actually be used. This distribution is

$$f_2(x) = (1/r_2^2)c(s)x^{s-2}(x+1)^{s-4.5}. \tag{3}$$

Here $x = r/r_2$, where r_2 is the length corresponding to the scattering unit of 9.5 g/cm² of air evaluated for a point two radiation lengths above the point of observation; s is the parameter called the shower age, and $c(s)$ is a normalization constant. The Nishimura-Kamata distribution function has been found to describe the experimentally observed distribution of shower particles satisfactorily for values of the shower age from 1.2 to 1.4 ([1-3,7]). At 1575 m s.l. the value of the characteristic length is $r_2 = 97$ m.

The number spectrum of extensive air showers has been found to be well approximated by a power law ([6])

$$K(N) = K_0 N^{-\gamma}, \tag{4}$$

where $K(N)$ is the number of showers containing N or more particles whose axes pass through a unit horizontal area in unit time; all showers are counted without regard to the inclination of the shower axes. The parameter γ varies slowly with the size of the shower; for the showers to be considered, the value of γ lies in the range 1.5 to 1.9. The differential distribution giving the frequency of showers whose size lies between N and $N+\mathrm{d}N$ is

$$k(N)\,\mathrm{d}N = B N^{-\gamma-1}\mathrm{d}N, \tag{5}$$

where $B = -\gamma K_0$.

([5]) J. Nishimura and K. Kamata: *Progr. Theor. Phys.*, **5**, 899 (1950); **6**, 628 (1951); **7**, 185 (1952).

([6]) K. Greisen: *Progress in Cosmic Ray Physics*, vol. **3** (Amsterdam, 1956), chap. 1.

([7]) T. E. Cranshaw, W. Galbraith and N. A. Porter: *Phil. Mag.*, **2**, 891 (1957).

Also of importance is the angular distribution of the shower axes. Unfortunately the zenith angle distribution of the axes of extensive air showers does not display any simple functional form; however, in the lower half of the atmosphere an approximate representation can be obtained in the form ([6])

$$R(\theta) = R(0)\cos^m\theta\,, \tag{6}$$

where $R(\theta)$ is the frequency of showers whose axes are inclined at an angle θ to $\theta+\mathrm{d}\theta$ with the zenith direction, $R(0)$ is the frequency of showers directed vertically, and m is a parameter that varies slightly with angle and rather strongly with elevation. At 1575 m s.l. the value of m varies from 5.6 for small angles to 7.4 at 45°; an average value of 6.5 affords a satisfactory representation over the entire range.

As will be described later, when a single scintillator is exposed to the extensive air showers, it is found that the frequency with which p or more particles traverse the scintillator can be expressed as a function of the size p in the form

$$Q(p) = Q_0 p^{-\gamma}\,, \tag{7}$$

where Q_0 and γ can be determined from the observed rates. It will now be shown that this functional form is reasonable and that the exponent is the same as that involved in the number spectrum of the extensive air showers.

3. – Vertical approximation.

The expected rate at which p or more particles traverse the scintillator will first be calculated as if all of the showers were directed vertically. It will also be assumed that the size of the scintillator is small enough relative to the characteristic length describing the lateral distribution of the shower particles so that variations in the particle density occurring over the dimensions of the scintillator can be ignored.

In order that p or more particles traverse the scintillator of area A because of a shower having a total of N particles and occurring with its axis at x units from the scintillator, the shower must be of a minimum size

$$N_{\min} = p/f_i(x)A\,. \tag{8}$$

The total rate of occurrence of p or more particles is obtained by integrating the differential shower frequency from $N_{\min}$ to $N=\infty$ to include showers of the required size at a given distance, and then by integrating over all distances

from the scintillator:

$$Q(p) = \int_0^\infty 2\pi r_i^2 x \, \mathrm{d}x \int_{N_{\min}}^\infty k(N) \, \mathrm{d}N \,. \tag{9}$$

This then gives

$$Q(p) = \frac{2\pi r_i^2 A^\gamma B}{\gamma} I_i(\gamma) p^{-\gamma} \,, \tag{10}$$

where

$$I_i(\gamma) = \int_0^\infty x f_i^\gamma(x) \, \mathrm{d}x \,. \tag{11}$$

Since it is desired to calculate the shower frequencies from the observed scintillator rates, a relation of the form

$$B = g_i(\gamma) Q_0 \tag{12}$$

is required. Comparison of (5), (7) and (10) then gives

$$g_i(\gamma) = \frac{\gamma}{2\pi r_i^2 A^\gamma I_i(\gamma)} \,. \tag{13}$$

For the exponential distribution function the integral in (11) is readily evaluated in terms of the Γ-function to give

$$I_i(\gamma) = \frac{1}{(2\pi r_i^2)^\gamma} \gamma^{\gamma-2} \Gamma(2-\gamma) \,, \tag{14}$$

consequently,

$$g_i(\gamma) = \frac{1}{2\pi r_i^2} \left(\frac{2\pi r_i^2}{A} \right)^\gamma \frac{\gamma^{3-\gamma}}{\Gamma(2-\gamma)} \,. \tag{15}$$

Values of $g_1(\gamma)$ will be found in Table I. These and other values of functions are calculated with regard to the experimental arrangement at Albuquerque, namely, an elevation of 1575 m s.l. and for a scintillator area of 7.3 m².

It will be noticed that I_1 becomes infinite as γ approaches 2. This is a consequence of the fact that the particle density at a point was used to obtain the number of particles passing through a scintillator of finite area, together with the fact that the distribution is singular at the origin. Such behavior must be expected also for the approximate Nishimura-Kamata distribution,

TABLE I. – *Quantities relating the shower-rate constant to the scintillator rates for the exponential distribution.*

γ	g_1	$I_1'(\gamma)/I_1(\gamma)$	$g_1'(\gamma)$
1.4	5.67 m^{-2}	0.924	6.14 m^{-2}
1.5	12.4	0.876	14.1
1.6	25.4	0.802	31.6
1.7	47.5	0.693	68.6
1.8	76.8	0.535	143
1.9	91.0	0.310	293

although the singularity will be found to be less pronounced. This singularity in the constant relating the rate of occurrence of the scintillator events to the intensity of the extensive air showers themselves is actually not new, but was tacitly inherent in earlier work, particularly in connection with extended trays of Geiger-Müller counters that are used to observe the same phenomenon.

In the case of the exponential distribution function, it is relatively easy to make a better approximation using the following argument. In the double integral (9), $N_{\min}$, as defined by equation (8), approaches zero as x approaches zero because of the singularity in $f_1(x)$. Actually, the smallest shower capable of producing p particles in the tank is one whose axis passes through the center of the tank and whose total number of particles $N'_{\min}$ is given by the integral

$$(16) \qquad p = N'_{\min}\int_0^{r_t} F(r)\,2\pi r\,\mathrm{d}r = N'_{\min}\int_0^{x_t} \exp[-x]\,\mathrm{d}x = N'_{\min}(1-\exp[-x_t])\,,$$

where r_t is the radius of the detector and $x_t = r_t/r_1$. In all practicable experiments, the value of x_t will be small; in the particular case with which we are concerned, the value is $1.62\cdot10^{-2}$. As a result, we make the approximation $p = N'_{\min}\,x_t$. The resulting value of $N'_{\min} = (1/x_t)p = 612p$ will be of interest in interpreting the experimental data. What we can now do is to select a minimum value x'_t for the variable x in integral (9) so that the value $N_{\min}$ as determined by equation (8) will correspond to the true minimum value just found. Because of the smallness of the quantities involved, approximations can be used to obtain the result that

$$(17) \qquad x'_t = \frac{1}{x_t}\frac{A}{2\pi r_1^2}.$$

In the experimental arrangement with which we are concerned $x'_t = 8.13\cdot10^{-3}$. Inserting x'_t as the lower limit of x in (9), we obtain the same result as in (13)

except that $I_1(\gamma)$ is replaced by

$$I_1'(\gamma) = \int_{x_i'}^{\infty} x f_1^{\gamma}(x)\, \mathrm{d}x \,. \tag{18}$$

The integral is evaluated in terms of the incomplete Γ-function ([8]):

$$I_1'(\gamma) = I_1(\gamma)\left[1 - I\left(\frac{\gamma x_i'}{\sqrt{2-\gamma}}, 1-\gamma\right)\right]. \tag{19}$$

In Table I will be found values of $I_1'(\gamma)/I_1(\gamma)$ as well as the corrected values $g_1'(\gamma) = g_1(k) I_1(\gamma)/I_1'(\gamma)$ that are to be used to compute the shower-rate constant B from the observed scintillator rates.

If we ask what scintillator rates should be expected from the naturally occurring air showers, we see from (12) that $Q_0 = (1/g_1')B$. Examination of (15) shows that the scintillator rates are proportional to $(A/2\pi r_1^2)^{\gamma}$; other expressions to be derived later display the same dependency on the size of the scintillator area. This is of great importance because the value of γ is 1.5 or more, so that increasing the area has a greater effect in increasing the scintillator rates than might be expected.

Substitution of the approximate Nishimura-Kamata distribution function in (11) leads to the results

$$I_2(\gamma, s) = \frac{c^{\gamma}(s)}{r_2^{2\gamma}} \frac{\Gamma(s\gamma - 2\gamma + 2)\,\Gamma(6.5\gamma - 2s\gamma - 2)}{\Gamma(4.5\gamma - s\gamma)}, \tag{20}$$

and

$$g_2(\gamma, s) = \frac{1}{2\pi r_2^2}\left(\frac{r_2^2}{A}\right)^{\gamma} \frac{\gamma}{c^{\gamma}(s)} \frac{\Gamma[(4.5-s)\gamma]}{\Gamma[2-(2-s)\gamma]\,\Gamma[(6.5-2s)\gamma - 2]}. \tag{21}$$

Values of $g_2(\gamma, s)$ for $r_2 = 97$ m and for $A = 7.3$ m^2 are given in Table II. It will be noticed that $g_1'(\gamma)$ corresponds very closely with $g_2(\gamma, 1.3)$. A somewhat more generous range is allowed for the parameter γ than in the preceding case; for the range $1 < s < 1.5$, it is necessary only that $0.57 < \gamma < 2$.

It would be possible to make a better approximation for this distribution, just as in the case of the exponential distribution, by introducing x_i' as the lower limit in (9). In such a case, one would obtain expressions involving the incomplete β-function in exact analogy to the incomplete Γ-functions obtained

([8]) K. PEARSON: *Tables of the Incomplete Gamma-Function* (Cambridge, 1934).

TABLE II. – $g_2(\gamma, s)$ *for the approximate Nishimura-Kamata distribution* (*in* m^{-2}).

γ	$s = 1.0$	1.1	1.2	1.3	1.4	1.5
1.4	3.04	3.87	4.81	5.92	7.30	9.18
1.5	5.59	7.78	10.4	13.6	17.7	23.5
1.6	9.52	14.8	21.4	30.0	41.6	58.4
1.7	14.7	26.8	42.6	64.4	94.9	142
1.8	19.5	45.2	81.5	134	211	335
1.9	18.9	56.7	149	270	459	778

in the other case. However, the singularity in the case of the approximate Nishimura-Kamata function is not so violent as in the case of the exponential function; as a result there would be only a relatively small correction that would not justify the large amount of labor necessary to evaluate the terms.

4. – Average shower response.

It is of interest to determine the average size of showers responsible for producing a given number of particles in the scintillator. To obtain this, we start with the number of particles p traversing the scintillator area A because a shower of N particles passes with its axis at x units from the scintillator, namely, $p = Nf(x)A$. For a given size of shower N there is a maximum x_m for which p or more particles will traverse the scintillator. This maximum value is obtained as a solution of the equation $f(x_m) = (1/A)(p/N)$; consequently we would have $x_m = x_m(N/p)$. Now all showers of size N to $N + \mathrm{d}N$ within a radial distance x_m from the scintillator will contribute to the counting rate of p or more particles; the rate at which these counts occur is

$$q(N, p)\,\mathrm{d}N = \pi r_i^2 x_m^2 B N^{-\gamma-1}\,\mathrm{d}N\,. \tag{22}$$

But the total rate for which p or more particles traverse the scintillator is $Q(p) = Bp^{-\gamma}/g_i(\gamma)$. Since the fraction of the rate of p or more particles in the scintillator due to showers of size N to $N + \mathrm{d}N$ must be given by $w(N, p) = q(N, p)/Q(p)$, we then have

$$w(N, p) = \pi r_i^2 x_m^2 g_i(\gamma)\,\frac{1}{N}\left(\frac{N}{p}\right)^{-\gamma}. \tag{23}$$

The fraction $w(N, p)$ is a normalized distribution function for showers of N particles to give p or more particles in the scintillator; therefore, the average number of particles in the shower that gives rise to p or more particles in the

scintillator can be calculated from

$$\overline{N}(p) = \int_{N_{\min}}^{\infty} N w(N, p)\, \mathrm{d}N\,, \tag{24}$$

or

$$\overline{N}_i(p) = \pi r_i^2 g_i(\gamma) \int_{N_{\min}}^{\infty} x_m^2 \left(\frac{N}{p}\right)^{-\gamma} \mathrm{d}N\,. \tag{25}$$

The assignment of $N_{\min}$ will be discussed shortly. First, however, we change the variable of integration to x_m using the functional relationship between x_m and (N/p). The result of the transformation is

$$\overline{N}_i(p) = -\pi r_i^2 p g_i(\gamma) A^{\gamma-1} \int_{x_m(N_{\min}/p)}^{x_m(\infty)} x_m^2 [f_i(x_m)]^{\gamma-2} \frac{\mathrm{d}f_i(x_m)}{\mathrm{d}x_m}\, \mathrm{d}x_m\,. \tag{26}$$

If we choose to define $N_{\min}$ through the obvious relation $N_{\min} = p/f(0)A$, then it is clear that $N_{\min} = 0$ because of the singularity in $f(x)$; it also follows that $x_m(N_{\min}/p) = 0$. A better approximation would be obtained by evaluating $N_{\min}$ as was done in the preceding section, and then calculating the x_m corresponding to this. Fortunately this proves to be an unnecessary refinement.

Insertion of the exponential distribution function in (26) gives

$$\overline{N}_1(p) = \pi r_1^2 p g_1(\gamma) \left(\frac{A}{2\pi r_1}\right)^{\gamma-1} \frac{2\Gamma(3-\gamma)}{(\gamma-1)^{4-\gamma}}\,. \tag{27}$$

We can now express the size of the average shower contributing to the rate of p or more particles in the scintillator in the form $N_i(p) = h_i(\gamma)p$. Substitution of the previously found expression for $g_1(\gamma)$ then gives

$$h_1(\gamma) = \frac{2\pi r_1^2}{A} \frac{(2-\gamma)\gamma^{3-\gamma}}{(\gamma-1)^{4-\gamma}}\,. \tag{28}$$

Substitution of the lower limit given by (17) in place of the lower limit of zero in the integral results in an entirely negligible correction; more serious, however is the use of $g_1(\gamma)$ in place of $g_1'(\gamma)$. Using the better approximation $g_1'(\gamma)$ results in the similarly better approximation $h_1'(\gamma) = h_1(\gamma)I_1(\gamma)/I_1'(\gamma)$. Values of $h_1(\gamma)$ and $h_1'(\gamma)$ are given in Table III for the values $r_1 = 94$ m and $A = 7.3$ m^2.

Substitution of the approximate Nishimura-Kamata distribution function

in (26) leads to the function

$$(29) \qquad h_2(\gamma, s) = \frac{r_2^2}{c(s)A}\,\frac{\gamma}{\gamma-1}\,\frac{\Gamma[(4.5-s)\gamma]\,\Gamma[2-(2-s)(\gamma-1)]\,\Gamma[(6.5-2s)(\gamma-1)-2]}{\Gamma[(4.5-s)(\gamma-1)]\,\Gamma[2-(2-s)\gamma]\,\Gamma[(6.5-2s)\gamma-2]}.$$

Values of $h_2(\gamma, s)$ for $r_2 = 97$ m and $A = 7.3$ m^2 are listed in Table IV. Again, there is reasonable agreement between $h_1'(\gamma)$ and $h_2(\gamma, 1.3)$.

TABLE III. – $h_1(\gamma)$ *and* $h_1'(\gamma)$ *for the exponential distribution.*

γ	$h_1(\gamma)$	$h_1'(\gamma)$
1.4	$8.54 \cdot 10^4$	$9.25 \cdot 10^4$
1.5	$3.94 \cdot 10^4$	$4.50 \cdot 10^4$
1.6	$2.01 \cdot 10^4$	$2.51 \cdot 10^4$
1.7	$1.03 \cdot 10^4$	$1.49 \cdot 10^4$
1.8	$5.02 \cdot 10^3$	$9.38 \cdot 10^3$
1.9	$1.92 \cdot 10^3$	$6.19 \cdot 10^3$

TABLE IV. – $h_2(\gamma, s)$ *for the approximate Nishimura-Kamata distribution.*

γ	$s = 1.0$	1.1	1.2	1.3	1.4	1.5
1.5	$3.77 \cdot 10^4$	$1.10 \cdot 10^5$	$4.43 \cdot 10^5$	—	—	—
1.6	$8.14 \cdot 10^3$	$1.60 \cdot 10^4$	$3.08 \cdot 10^4$	$6.07 \cdot 10^4$	$1.34 \cdot 10^5$	$4.12 \cdot 10^5$
1.7	$2.84 \cdot 10^3$	$6.01 \cdot 10^3$	$1.14 \cdot 10^4$	$2.06 \cdot 10^4$	$3.77 \cdot 10^4$	$6.97 \cdot 10^4$
1.8	$1.32 \cdot 10^3$	$2.81 \cdot 10^3$	$5.64 \cdot 10^3$	$1.02 \cdot 10^4$	$1.82 \cdot 10^4$	$3.19 \cdot 10^4$
1.9	$3.62 \cdot 10^2$	$1.40 \cdot 10^3$	$3.18 \cdot 10^3$	$6.04 \cdot 10^3$	$1.08 \cdot 10^4$	$1.87 \cdot 10^4$

It will be noticed that the permissible range of values for γ has been seriously curtailed. From (28) we see that $1 < \gamma < 2$. Similar but more complicated restrictions result from (29).

5. – Spread in average shower response.

When we attempt to calculate $\bar{N}^2$ in a manner similar to that of the preceding Section, we find that the integrals will diverge unless $\gamma > 2$; consequently, some other means must be found to estimate the spread in the

average. An idea as to the behavior of the system can be obtained from the distribution function $w(N, p)$ in (23) and the weighted values $Nw(N, p)$ that form the integrand of (24). To plot these functions, it is necessary to introduce values of N, p, and of γ approximating the actual experimental conditions; we shall take $p = 10^3$ particles. In Fig. 1 there is plotted the functions $w(N, 10^3)$ for $\gamma = 1.5$ and 1.8; in Fig. 2 there is plotted the functions

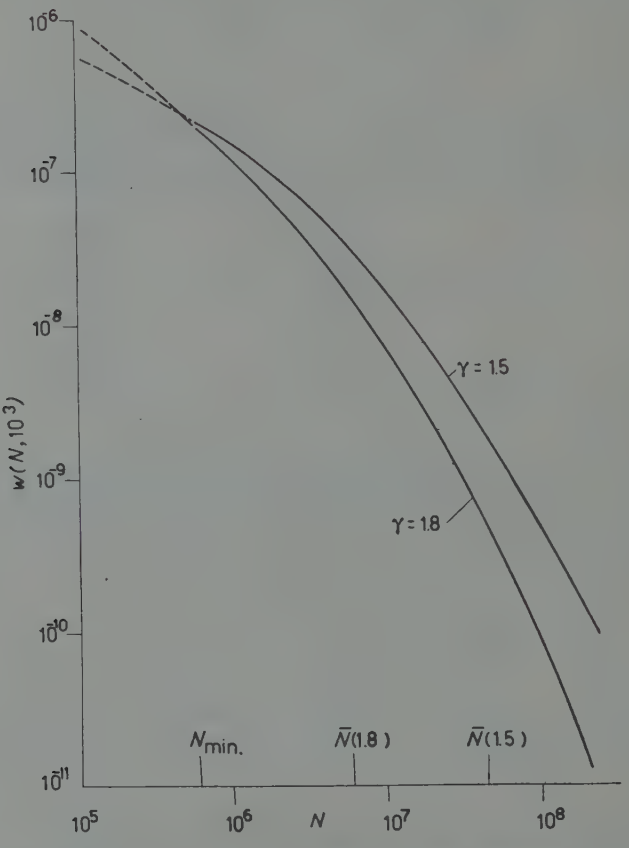

Fig. 1. – Fraction of the counting rate of 10^3 or more particles in the scintillator as a function of the shower size N for $\gamma = 1.5$, 1.8.

$Nw(N, 10^3)$ for the same values of γ. In both graphs indication is made of the average values and of the minimum values of N. It is clear from these graphs that the data obtained from the single scintillator are more useful in obtaining general aspects of the spectrum of the extensive air showers, such as the constant B and the power exponent γ, rather than specific details of

the spectrum. Still, the graphs can be used to find the range of showers involved in producing the responses of the scintillator.

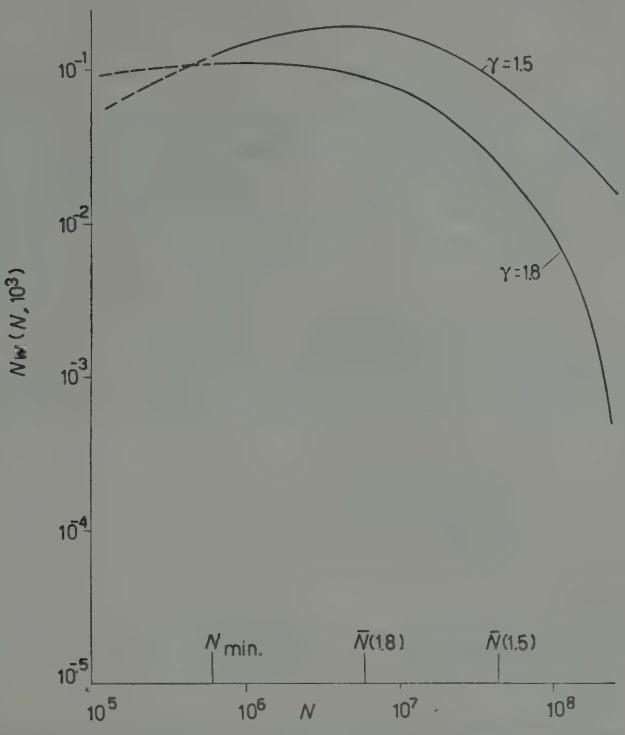

Fig. 2. – Contribution of showers of size N to the average value $\bar{N}$ for 10^3 or more particles in the scintillator and for $\gamma=1.5$, 1.8.

6. – Effect of angular distribution of showers.

Particles traversing the material of the scintillator at an angle θ to the vertical will pass through a thickness $t/\cos\theta$ and will therefore produce a light pulse greater than that produced by a particle traveling vertically by the factor $1/\cos\theta$. Fortunately, however, the projected area of the tank is given by $A\cos\theta$ for the showers of inclined axes, so that the angular factor from these two causes will cancel. This still leaves a difference because of the change in the radial variable. As can be seen from Fig. 3, the horizontal distance r of the axis of the shower core from the scintillator tank must be replaced by the true radial distance ϱ if the shower axis is inclined at the usual angles θ and φ. From the figure we can obtain the relations

$$(30) \quad \varrho^2 = r^2\cos^2\alpha = r^2[\sin^2\alpha\sin^2\theta\cos^2\varphi + \sin^2\alpha\cos^2\theta + (1-\sin\alpha\sin\theta\sin\varphi)^2].$$

From this we obtain $\sin\alpha = \sin\theta\sin\varphi$, so that

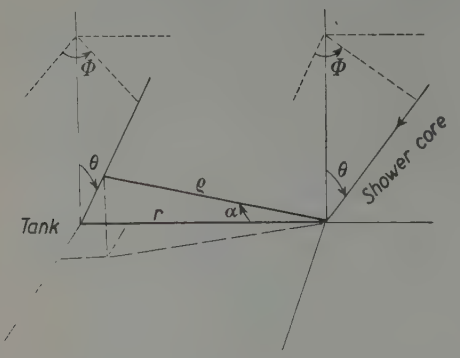

Fig. 3. – A shower core at polar angles θ and φ strikes the ground at a distance r from the scintillator; the true radial distance of the scintillator from the core is ϱ.

$$(31)\qquad \varrho = r(1-\sin^2\theta\sin^2\varphi)^{\frac{1}{2}} \doteq$$

$$\doteq r(1-\tfrac{1}{2}\sin^2\theta\sin^2\varphi-\tfrac{1}{8}\sin^4\theta\sin^4\varphi).$$

The approximation in terms of small angles is made because of the rapid decrease in rate with zenith angle θ. Assuming now that the showers occur at the rate of $B_v\cos^m\theta\,N^{-\gamma}\cdot\mathrm{d}N\ \mathrm{s}^{-1}\,\mathrm{m}^{-2}\,\mathrm{sr}^{-1}$, we obtain the expression giving the total rate of occurrence of p or more particles in the scintillator by modifying equation (9) to give

$$(32)\qquad Q(p) = 2\pi r_i^2\int_0^\infty x\,\mathrm{d}x\int_0^{2\pi}\mathrm{d}\varphi\int_0^{\pi/2}\sin\theta\,\mathrm{d}\theta\int_{N_{\min}}^\infty\cos^m\theta\,B_v N^{-\gamma-1}\,\mathrm{d}N\,.$$

Substitution of $N_{\min} = p/f_i(x)A$, and integration over the variable N gives

$$(33)\qquad Q(p) = \frac{2\pi r_i^2 B_v}{\gamma}\int_0^\infty x\,\mathrm{d}x\int_0^{2\pi}\mathrm{d}\varphi\int_0^1\cos^m\theta\,\mathrm{d}(\cos\theta)\,A^\gamma f^\gamma(x)\,p^{-\gamma}\,.$$

Replacement of the variable x by $(x+\delta x)$, where

$$\delta x = -x(\tfrac{1}{2}\sin^2\theta\sin^2\varphi+\tfrac{1}{8}\sin^2\theta\sin^2\varphi)\,,$$

allows the replacement of $f^\gamma(x)$ by an expansion: $[f(x+\delta x)]^\gamma$. The binomial expansion and Taylor's expansion are used to obtain the approximation

$$(34)\qquad f^\gamma(x)\to f^\gamma(x+\delta x)\doteq f^\gamma(x)\{1-(\gamma x/f)\sin^2\theta\sin^2\varphi\,\mathrm{d}f/\mathrm{d}x+$$

$$+\tfrac{1}{8}(\gamma x/f)\sin^4\theta\sin^4\varphi[-\mathrm{d}f/\mathrm{d}x+x\,\mathrm{d}^2f/\mathrm{d}x^2+(\gamma-1)(x/f)(\mathrm{d}f/\mathrm{d}x)^2]+\ldots\}.$$

The angular integrations can now be performed at once.

Integration over x can be performed using partial integration. Assuming suitable cut-offs so that the expressions $x^2f^\gamma(x)$ and $x^3f^{\gamma-1}(x)\,\mathrm{d}f(x)/\mathrm{d}x$ vanish at

both upper and lower limits leads to the expression

$$(35) \qquad Q(p) = \frac{2\pi r_i^2}{\gamma} B_v A^\gamma p^{-\gamma} I_i \frac{2\pi}{m+1}\left[1 + \frac{1}{m+3} + \frac{3}{(m+3)(m+5)} + \cdots\right],$$

where $I_i = \int_0^\infty x f_i^\gamma(x)\,\mathrm{d}x$ as before. It is thus seen that to these approximations the only effect of the distribution of shower axes about the vertical direction is to introduce a multiplicative factor that depends only on the angular distribution and not on the other variables. Thus the rate of occurrence of p or more particles in the scintillator is given by the expression

$$(36) \qquad Q(p) = \frac{k(m)}{g_i(\gamma)} B_v p^{-\gamma},$$

where $g_i(\gamma)$ are any of the appropriate functions obtained previously, and where

$$(37) \qquad k(m) = 2\pi\left[\frac{1}{m+1} + \frac{1}{(m+1)(m+3)} + \frac{3}{(m+1)(m+3)(m+5)}\right].$$

Values of $k(m)$ are given in Table V.

TABLE V. – *Values of the factor $k(m)$ giving angular dependence.*

m	$k(m)$	m	$k(m)$
5.0	1.22	6.5	0.95
5.5	1.11	7.0	0.88
6.0	1.02	7.5	0.83

RIASSUNTO (*)

Espressioni teoriche e sperimentali per la distribuzione laterale delle particelle in estesi sciami dell'aria, determinate in precedenza, vengono usate per predire la risposta di un unico scintillatore a questi sciami. Il numero complessivo di particelle che traversano lo scintillatore si trova in funzione del numero complessivo di sciami; si determina la grandezza media dello sciame che provoca il passaggio di un dato numero di particelle attraverso lo scintillatore; si analizza l'effetto della distribuzione secondo gli angoli zenitali degli assi dello sciame.

(*) *Traduzione a cura della Redazione.*

IL NUOVO CIMENTO Vol. XIV, N. 6 16 Dicembre 1959

Size-Spectrum of Extensive Air Showers of the Cosmic Radiation.

II. – Experimental Results from a Single Scintillator (*).

J. R. Green and J. R. Barcus

University of New Mexico - Albuquerque (New Mexico)

(ricevuto il 29 Settembre 1959)

Summary. — The operation and calibration of a single scintillator of area 7.3 m^2 is discussed. The integral spectrum of particles passing through the scintillator at 1575 m.s.l. has a logarithmic slope of $-(1.514 \pm 0.022)$; from this it is deduced that the integral spectrum of extensive air showers whose sizes lie in the range from 10^5 to 10^8 particles is given by $K(\geqslant N) = 3.2 \cdot 10^{-7} (N/10^6)^{-1.514}$ m^{-2} s^{-1} sr^{-1}. Smaller events are identified with stars produced locally in the toluene of the scintillator; the integral spectrum of such events dissipating E MeV in the scintillator is given by $R(\geqslant E) = 4.5 \cdot 10^2 E^{-2.76}$ min^{-1}/g of toluene.

---

1. – Apparatus.

The apparatus has been described in some detail in an earlier paper (1). Briefly, it consists of a liquid scintillator 10 ft. in diameter and about 5 in. deep, the light output of which is viewed by a 15 in. diameter photomultiplier tube placed about $2\frac{1}{2}$ ft above the surface of the liquid. The output of the photomultiplier tube is passed through separate cathode follower circuits to separate analyzing channels. The first of these consists of a linear amplifier whose maximum gain is about 10^4 followed by a discriminating circuit and a counting circuit. This is referred to as the «rate channel». The second

(*) Supported by the United States Air Force Office of Scientific Research.

(1) J. R. Green: *Rev. Sci. Instr.*, **29**, 10 (1958).

channel consists of a circuit that produces a pulse of fixed height but whose length is approximately proportional to the logarithm of the amplitude of the input pulse to the circuit; this is followed by a timing circuit that measures the length of the converted pulse. This is called the « logarithmic channel ». Both channels are connected through a data conversion unit to an IBM card punch. The rate channel counts events greater than a predeterminated size occurring during a 9 min interval and records this count every ten minutes. These events are smaller and occur at a much higher rate than those analyzed by the logarithmic circuit. The larger events which do activate the logarithmic circuit are recorded individually as they happen. Under usual operating conditions these occur at a rate of from 0.1 to 1.2 per min depending on the range of events being investigated. Also recorded by both channels are the day, solar time, sidereal time, barometric pressure, and temperature. The scintillator and the analyzing circuits are maintained at a temperature of about 70 °F with fluctuations of about 1°. The high voltage supply to the photomultiplier tube is periodically monitored and can be reset to 1 part in 10^5 by means of a potentiometric comparison with a standard cell. The apparatus is located at Albuquerque, New Mexico, at an elevation of 1575 m.s.l.

2. – Calibration.

Calibrations are effected using a DuMont Type 404 Pulse Generator and a Radiation Instruments Development Laboratory Model 47-1 Mercury Relay Pulse Generator that is itself calibrated against a Tektronix Type 515A Oscilloscope. Pulses from these instruments can be introduced at the point where the output from the photomultiplier enters the cathode follower circuit; thus, the entire train of circuits is calibrated at once, excluding only the photomultiplier itself. Since, as will result, these external calibrating instruments are used only as comparison devices to connect different regions of operation of the scintillator and its associated circuits, absolute calibration is fortunately unnecessary. The DuMont Pulse Generator is the most convenient to use and is stable in its operation; it is used in calibrating the rate channel, which has a wide band, and for daily comparison calibrations of the logarithmic channel. For actual calibrations of the logarithmic channel, which necessarily includes non-linear circuits, the RIDL Pulser is used because it can be set to simulate very closely the shape of the output pulse of the photomultiplier.

The first basic calibration of the scintillator is that for the « single » particle. This is the average response generated by a single, minimum-ionizing particle passing through the tank of the scintillator randomly. The preliminary calibration of this quantity was accomplished by means of counter trays run in coincidence with the scintillator as described in the earlier paper. Now

that the general region has been found, the scintillator is calibrated as a whole by obtaining first the integral spectrum by taking successive three to nine-minute counts from the rate channel for different settings of the discriminator, and then deriving the differential spectrum from these data. The differential spectrum obtained in this way displays a rather broad peak corresponding to the single particle as shown in Fig. 1. Many calibrations performed with

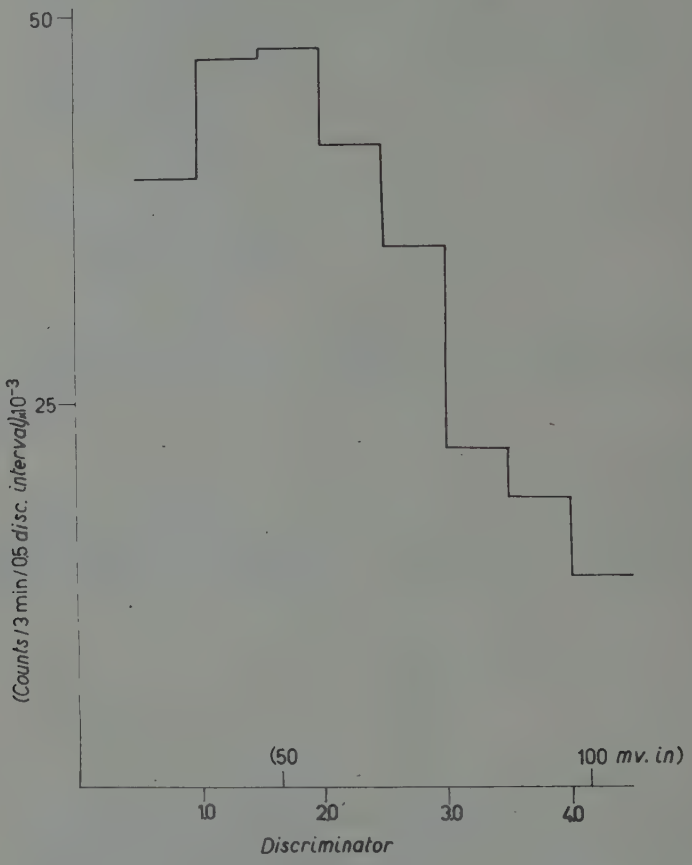

Fig. 1. – Differential spectrum used to obtain single particle calibration.

different supply voltages to the photomultiplier, with widely varying circuit components in the photomultiplier circuit, and with entirely different circuits in the rate channel, have consistently produced a single particle occurring at a setting of the discriminator which results in an integral rate of about $7 \cdot 10^4$ counts/min. Actually, this fact is used to find the new region in which the single particle occurs after large changes in circuit parameters have been made. In the single particle calibration shown in Fig. 1, the supply voltage

of the photomultiplier was 1400 V; the single particle is taken to be at a discriminator setting of 1.60 which, from the rate channel calibration, corresponds to 49 mV. The particular calibration shown is typical in form but happens to be one for the data to be discussed later.

The single particle calibration is carried out at a supply potential of 1400 V in order to get these small pulses out of the noise region of the photomultiplier. When the scintillator is used to examine the larger air showers, however, there may be 10^3 or more patricles passing through the tank of the scintillator associated with one event. Since this would produce a pulse far beyond the region of saturation of the photomultiplier, it is necessary that the tube be operated at much lower voltages, namely, at 900 V. At this voltage, the logarithmic circuit gives pulses covering the range of 10^2 to a few times 10^3 particles in the tank; saturation of the photomultiplier circuit prevents satisfactory recording of events much larger than this. At the same time, although the single particle is far in the region of noise, the rate channel can be used to obtain rates for the occurrence of events giving 10 to 10^2 or more particles in the tank. The problem arises of correctly identifying the number of particles represented by a given size pulse from the photomultiplier, or, assuming linearity of response, of deducing what the single particle pulse size would be if it could be measured. This gives rise to the second basic calibration that has been named the « phototube gain ». It is possible to obtain this calibration by proceeding in 100 V steps from 1400 V, where the single particle pulse height is obtained, to 900 V, where the tube is actually operated, and finding the change in amplification for each step. The cosmic radiation itself is used to accomplish this. At a given supply voltage, say 1000 V, and with the discriminator set at 1.00, the counting rate is 4630 per 10 s; with the supply now set at 1100 V, it is found that the discriminator must be set at 3.75 to obtain the same counting rate. From the calibration of the rate channel, it is found that 1.00 corresponds to 3.7 mV at the photomultiplier cathode follower and that 3.75 corresponds to 9.0 mV; consequently, it follows that the ratio of the photomultiplier gain at 1100 V to that at 1000 V is 2.43. Proceeding in this way, we find that the ratio of the gain 1400 V to that at 900 V is 57.6 for the particular values used in the photomultiplier circuit to obtain some of the results given below. A graph showing the logarithm of the ratio of the pulse height at a given supply voltage to that at 900 V as a function of the logarithm of the ratio of the value of the supply voltage to 900 V is shown in Fig. 2. The line drawn through the data points on the double logarithmic plot has a slope of 9.2, *i.e.*, $v_E = v_{900}(E/900)^{9.2}$, where v refers to the output pulse height from the photomultiplier and E is the supply voltage. The gain factor of 57.6 from 900 V to 1400 V then means that the single particle pulse of 49 mV at 1400 V becomes a single particle pulse of 0.85 mV at 900 V.

Because of the great sensitivity of parts of the circuitry, various kinds of electrical noise have proved to be a plague that could be eliminated only with great difficulty. For example, if was found that paper-oil coupling capac-

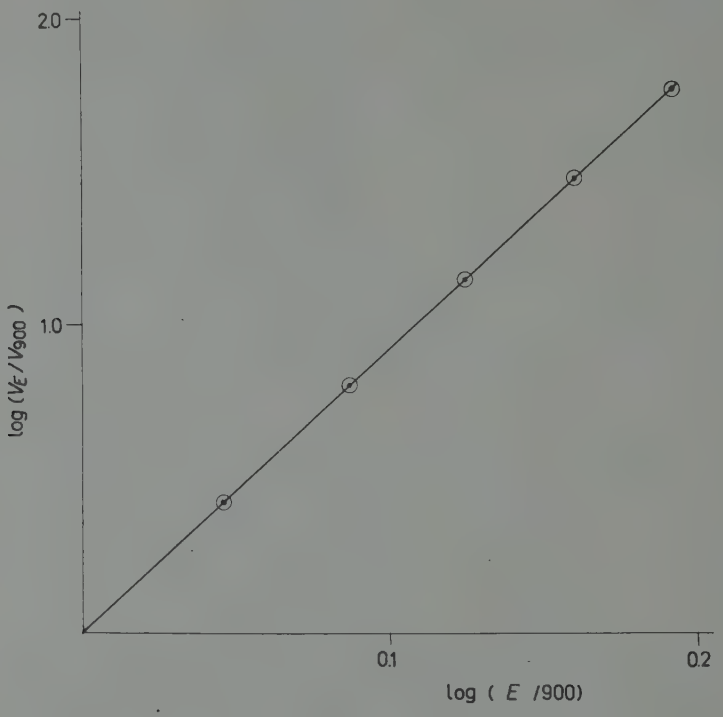

Fig. 2. – Variation in output pulse from photomultiplier as a function of supply voltage.

itors rated at 1600 V had small breakdowns even at only 900 V to produce pulses of several tens of millivolts; as a result, it was necessary to employ mica capacitors rated at 6000 V for the photomultiplier cathode follower circuits. It is also necessary to isolate all sensitive circuits from the power line which supplies the calibrating equipment and the controls for the air conditioning equipment.

3. – Results.

The results obtained are shown in Fig. 3, where the integral counting rate is displayed as a function of the number of particles produced in the tank of the scintillator. Three different runs are used to obtain the complete graph. For smaller numbers of particles, the rates are obtained using the linear ampli-

fier and discriminator of the rate channel; these are the points indicated by an « x ». The larger events were obtained using the logarithmic channel. The points indicated with double circles were obtained with the circuits in their regular condition; the points with the single circles were obtained with a reduced gain of the photomultiplier. The gain was reduced by connecting together two adjacent dynodes of the photomultiplier by shorting out the connecting resistor; an equal resistor was inserted at the end of the dynode chain, however, to maintain the same potential difference between the dynodes as before. The statistical errors of the data points in Fig. 3 have been indicated where feasible; the double circle points have the same error as the single circle points at the same counting rates.

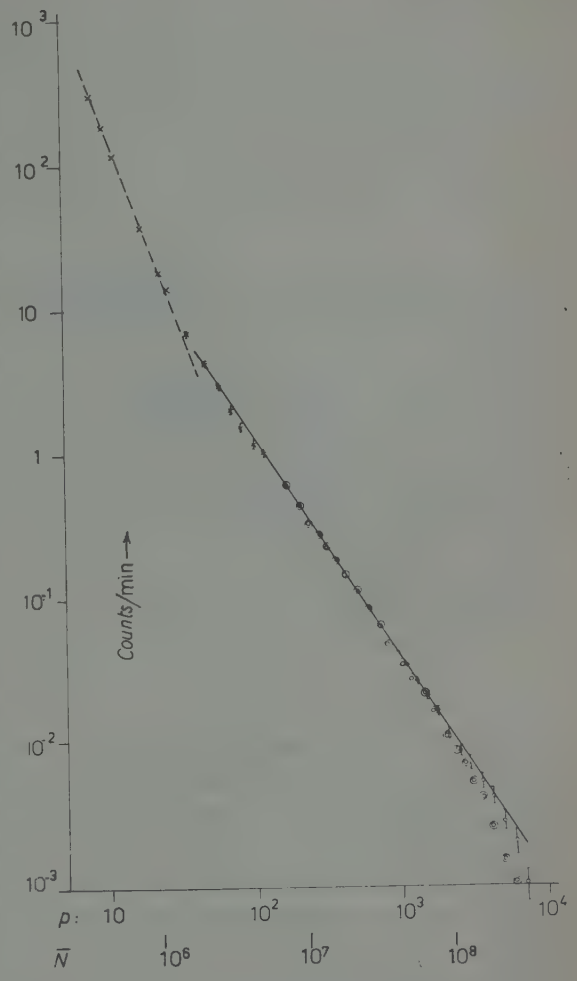

Fig. 3. – Integral spectrum of particles in the scintillator. $\bar{N}$ is the average size of the shower that will produce p particles in the scintillator.

3·1. *Saturation.* – The run at reduced amplification of the photomultiplier was made to check the fall-off of the integral spectrum for the larger events to decide if this is due to an actual change in the spectrum of the pulses occurring in the scintillator or if it is due to a saturation effect in the circuitry. The latter is found to be the case. Reducing the gain of the photomultiplier, but keeping the dynode voltages the same, means that the saturation effect (which would be effective only across the last dynode pair) should appear at the same output pulse sizes as before but at correspondingly larger particle numbers. When the counting rates obtained in the two runs are plotted as a function of the size of the output pulse from the last dynode of the photomultiplier,

they are found to coincide exactly. Plotting the data as a function of particle number, as is done in Fig. 3, results in an extension of the range of useful results.

3·2. *Spectrum of extensive air showers.* – The solid straight line drawn through the group of points corresponding to $3 \cdot 10^1$ to $3 \cdot 10^3$ particles in the scintillator is representative of the response of the scintillator to extensive air showers. The equation of this straight line is

$$Q(\geqslant p) = 22.0 p^{-(1.514 \pm 0.022)} \text{ s}^{-1} , \tag{1}$$

where p is the number of particles in the scintillator. The error of the exponent was estimated by finding the different straight lines that could reasonably be passed through the data points with the effect of saturation for the larger events being allowed for. The constancy of the slope of the integral counting rate of particles in the scintillator strongly suggests that it is possible to apply the theory developed in Part I of this paper and to deduce that the exponent of the integral spectrum of extensive air showers is also constant over a certain range in sizes and is equal to the exponent just obtained, namely, $-(1.514 \pm 0.022)$. The theory of Part I can be further applied to deduce the integral spectrum of the extensive air showers. If we use the functions $g_1'(1.514)$ and $k(6.5)$, we obtain the result:

$$K(\geqslant N) = (3.2^{+2.6}_{-1.4}) \cdot 10^{-7} (N/10^6)^{-(1.514 \pm 0.022)} \text{ m}^{-2} \text{ s}^{-1} \text{ sr}^{-1} . \tag{2}$$

Knowledge of the exponent enables us also to use the theory to calculate the average size of shower corresponding to a given number of particles in the scintillator. Using the function $h_1'(1.514)$ gives $\bar{N} = 4.1 \cdot 10^1 p$. From the values of $\bar{N}$ so obtained and indicated in Fig. 3, it would appear that the spectrum (2) is valid for a range of average sizes $10^6 < N < 10^8$. From the shapes of the response curves $w(N, p)$ and $Nw(N, p)$ for the single scintillator, it would perhaps be best to extend particularly the lower limit. We can accomplish this by saying that, at a given region of integral spectrum of scintillator pulses, the counting rate is due to air showers extending over a range in size from somewhat less than 1/10 the average shower size to somewhat less than 10 times the average shower size, the overall range being somewhat more than 100.

The value obtained for the exponent is low compared to the results of earlier experiments involving counter trays [2] which seem to indicate a change in the value of the exponent from about 1.5 for the smaller showers to about

[2] K. GREISEN: *Progress in Cosmic Ray Physics*, vol. **3** (Amsterdam, 1956).

1.8 for the larger showers. Also the results of CLARK *et al.* (3), were such as to be fitted by an exponent of value 1.85 for showers in the range from 10^6 to 10^8 particles. On the other hand, in the region of 10^5 to 10^6 particle, KULIKOV and KHRISTIANSEN (4) have reported an exponent of 1.5 ± 0.1. Furthermore, they have proposed that the data obtained by CLARK *et al.*, are better fitted if two values are assumed for the exponent, namely, 2.2 ± 0.3 in the region $8 \cdot 10^5 < N < 3 \cdot 10^6$ and 1.5 ± 0.2 in the region $10^7 < N < 10^8$. Because of the broad response of the single scintillator, it would be impossible to detect the change in slope over a limited region in the vicinity of 10^6 particles that is postulated by KULIKOV and KHRISTIANSEN. The exponent obtained in the present experiment is also not in disagreement with the underground experiments of the Cornell group (5).

Even though the response of the single scintillator to extensive air showers is such that it is impossible to detect details in the spectrum of the showers, still the high statistical accuracy of the present results combined with the high degree of regularity of the integral spectrum of pulses obtained in the scintillator lead one to conclude that the integral spectrum of the extensive air showers themselves must be on the average very regular over the range of about 10^5 to 10^8 particles and that the average logarithmic slope in this region is (1.514 ± 0.022). If we assume that each particle represents about 10^{10} eV of energy in the primary particle causing the shower (2), then the larger showers investigated must have been produced by primary particles of over 10^{18} eV. It has been pointed out that particles of such energy can scarcely be confined to our galaxy if its structure is that of a disc whose thickness is of the order of 10^3 light years and in which the confining magnetic fields are of the order of 10^{-5} gauss. Two of the possible answers are (1) that the galaxy contains turbulent gas clouds containing magnetic fields that result in a more nearly spherical shape for the galaxy with a radius of the order of 10^5 light years (3) and (2) that particles of such energies and higher do escape from the galaxy but are compensated for by a flux of particles of similar energies but of metagalactic origin (1). The extreme regularity of the spectrum obtained in this experiment would seem to favor the first explanation.

3·3. *Local interactions.* – The abrupt change in the slope of the spectrum of Fig. 3 for the lower particle numbers indicates that a different phenomenon

(3) G. CLARK, J. EARL, W. KRAUSHAAR, J. LINSLEY, B. ROSSI and F. SCHERB: *Nature*, **180**, 406 (1957).

(4) G. V. KULIKOV and G. B. KHRISTIANSEN: *Žurn. Éksper. Teor. Fiz.*, **35** (8), 441 (1959).

(5) P. H. BARRETT, L. M. BOLLINGER, G. COCCONI, Y. EISENBERG and K. GREISEN: *Rev. Mod. Phys.*, **24**, 133 (1952).

is involved. The counts in this region are due to nuclear interactions produced within the volume of the scintillating liquid. The dotted line drawn through the points corresponding to these interactions is given by

$$R(\geqslant p) = 1.01 \cdot 10^5 \, p^{-2.76} \text{ min}^{-1} . \tag{3}$$

In terms of absolute rate, comparison can be made with the data obtained by TEUCHER (6) concerning the rate of production of stars in nuclear emulsions. At an elevation corresponding to that of Albuquerque, TEUCHER finds that three-pronged stars are produced at the rate of 5.9 ± 0.7 per day per cm^3 of emulsion. To make a comparison with the rates in the scintillating liquid, touluene, we assume that the rates will be proportional simply to the geometrical cross-sections and so obtain the ratio: (Rate per cm^3 emulsion)/(Rate per g toluene) = 2.47. Using the fact that the scintillator tank contains approximately $8.7 \cdot 10^5$ g toluene enables us to calculate that events in the scintillator tank corresponding to three-pronged stars in emulsion should occur at the rate of 1500 per min. From the spectrum (3), we find that this corresponds to a number of particles p = 4.5. It must be remembered, however, that the calibration in terms of number of particles was for minimum-ionizing particles passing through the scintillator, so that it is better to make the comparison in terms of the energy lost to the scintillator liquid. The minimum-ionizing particles lose approximately 20 MeV in passing through the liquid; consequently, the 4.5 particles just found actually represents a loss of energy of 90 MeV. Now according to CAMERINI *et al.* (7), stars of three prongs are produced by primaries whose kinetic energy is 100 MeV. The agreement between these numbers is such that we conclude that the counting rate for $p \leqslant 10$ is indeed due to the production of « stars » by local nuclear interactions. A further confirmation is the fact that the logarithmic slope corresponds closely to that found by CAMERINI *et al.* (7), for the rate of star production as a function of size.

Since a single particle is equivalent to 20 MeV energy loss, the spectrum (3) can be converted into a more useful form giving the rate at which local events dissipating more than the energy E MeV in the scintillator are produced in the toluene of the scintillator:

$$R(\geqslant E) = 4.5 \cdot 10^2 \, E^{-2.76} \text{ min}^{-1} \text{ (g toluene)}^{-1} . \tag{4}$$

(6) M. TEUCHER: *Zeits. f. Naturfor.*, **7a**, 61 (1952).

(7) U. CAMERINI, J. H. DAVIES, P. H. FOWLER, C. FRANZINETTI, H. MUIRHEAD, W. O. LOCK, D. H. PERKINS and G. YEKUTIELI: *Phil. Mag.*, **42**, 1241 (1951).

RIASSUNTO (*)

Si discute l'uso e la taratura di uno scintillatore di 7.3 m^2 di area. Lo spettro integrale di particelle passanti attraverso lo scintillatore a 1575 m s.l.m. ha una inclinazione logaritmica di $-(1.514 \pm 0.022)$; da questo si deduce che lo spettro integrale dei sciami estesi dell'aria, le cui dimensioni sono comprese fra 10^6 e 10^8 particelle, è dato da $K(\geqslant N) = 3.2 \cdot 10^{-7} (N/10^6)^{-1.514}$ m^{-2} s^{-1} sr^{-1}. Eventi minori vengono indicati da stelle prodotte localmente nel toluene dello scintillatore: lo spettro integrale di tali eventi, che dissipano E MeV nello scintillatore, è dato da $R(\geqslant E) = 4.5 \cdot 10^2 E^{-2,76}$ min^{-1}/g di toluene.

(*) *Traduzione a cura della Redazione.*

IL NUOVO CIMENTO Vol. XIV, N. 6 16 Dicembre 1959

Zur Frage der bei Elementarteilchen möglichen Spins.

F. Engelmann

Institut für Theoretische Physik der Technischen Hochschule - München

(ricevuto l'8 Ottobre 1959)

Summary. — It is shown that it is possible to formulate the phenomenological description of elementary particles in a way which allows the existence of particles of the spins 0, $\frac{1}{2}$ and 1 only. This restriction appears as a consequence of the fact that space-time is 4-dimensional.

1. – Einleitung.

In der phänomenologischen Theorie der Elementarteilchen führt man für jede auftretende Teilchensorte eine eigene Feldfunktion ein und formuliert für sie eine Wellengleichung. Die physikalischen Eigenschaften des beschriebenen Elementarteilchens werden dabei wesentlich durch die Transformationseigenschaften des zugehörigen Feldes bestimmt. So ist der Spin eines Teilchens durch das Transformationsverhalten seines Feldes gegenüber Drehungen des 3-dimensionalen Ortsraums gegeben. In diesem Sinn ist die Frage nach den möglichen Spins der Elementarteilchen identisch mit der Frage nach den irreduziblen Darstellungen der 3-dimensionalen Drehgruppe und die bekannte Antwort lautet, daß im Prinzip jeder ganz- und halbzahlige Spin denkbar ist. Andererseits sind jedoch experimentell bisher nur Elementarteilchen mit den Spins 0, $\frac{1}{2}$ und 1 bekannt. Die reale Elementarteilchen beschreibenden Feldfunktionen haben also im 3-dimensionalen Ortsraum nur skalares, spinorielles oder vektorielles Transformationsverhalten. Alle übrigen Darstellungen der 3-dimensionalen Drehgruppe kommen nicht vor, ohne daß dafür ein plausibler Grund zu sehen ist.

Im folgenden soll nun eine Prinzip formuliert werden, aus dem diese Einschränkung der Spins der Elementarteilchen folgt und das gleichzeitig alle

auftretenden Feldgleichungen freier Elementarteilchen unter einem einheitlichen Gesichtspunkt zu behandeln gestattet. Man erhält auf diese Weise eine geschlossenere Form für die phänomenologische Theorie der Elementarteilchen.

2. – Das Ausgangsprinzip.

Als grundlegendes Prinzip einer phänomenologischen Theorie der Elementarteilchen werde postuliert:

Die Felder aller Elementarteilchen sind im Rahmen einer Clifford-Algebra beschreibbar. Sie genügen, solange von Wechselwirkungen abgesehen wird, der einfachsten gegenüber Lorentztransformationen forminvarianten linearen homogenen Differentialgleichung 1. *Ordnung mit einem willkürlichen, die Masse definierenden skalaren Parameter.*

Die darin enthaltenen Forderungen nach Lorentzinvarianz und größtmöglicher Einfachheit der Theorie sind üblicherweise getroffene Grundannahmen. Wesentliche spezielle Voraussetzung ist somit die Formulierbarkeit der Theorie in einer Clifford-Algebra. Da jedoch die Clifford-Algebren einfache hyperkomplexe Systeme sind, die metrischen Räumen zugeordnet werden können [1], kommen hierin die genannten Grundannahmen nur in spezifischer Weise zum Ausdruck.

3. – Folgerungen.

Die Forderung nach der Gültigkeit einer möglichst einfachen lorentzinvarianten Differentialgleichung 1. Ordnung für die freien Feldfunktionen führt auf eine Formulierung der Theorie im Rahmen der 16-gliedrigen Clifford-Algebra $\mathfrak{C}_4$, die von den 4 Größen γ_1, γ_2, γ_3, γ_4 mit den Relationen

$$\gamma_\mu \gamma_\nu + \gamma_\nu \gamma_\mu = 2\delta_{\mu\nu}\,, \tag{1}$$

erzeugt wird. Denn gerade diese Algebra $\mathfrak{C}_4$ ist einem 4-dimensionalen, euklidischen Raum zugeordnet [1], so daß sie mit dem Raum-Zeit-Kontinuum in Zusammenhang gebracht werden kann. Die erzeugenden Elemente γ_μ der Algebra entsprechen dabei speziell einem Orthogonalsystem von Grundvektoren e_μ, das die 4-dimensionale Raum-Zeit aufspannt. Die hierin ausgeführten Lorentztransformationen können in $\mathfrak{C}_4$ als innere Automorphismen dargestellt

---

[1] Siehe z.B.: M. Eichler: *Quadratische Formen und Orthogonale Gruppen* (Berlin-Göttingen-Heidelberg, 1952), S. 22 ff. und M. Lagally: *Vorlesungen über Vektorrechnung*, 6. Aufl. (bearbeitet von W. Franz) (Leipzig, 1959), S. 362 ff.

werden, d.h. alle Elemente X von $\mathfrak{C}_4$ werden dabei einer Transformation

$$X' = \Lambda X \Lambda^{-1} \tag{2}$$

unterworfen, wobei Λ selbst ein Element von $\mathfrak{C}_4$ ist, das nur von der ausgeführten Lorentztransformation abhängt. Speziell für die den Grundvektoren entsprechenden erzeugenden Elemente gilt

$$c_{\nu\mu}\gamma_\nu = \Lambda \gamma_\mu \Lambda^{-1}, \tag{3}$$

woraus sich Λ bis auf einen normalen Zahlenfaktor aus der Transformationsmatrix $c_{\mu\nu}$ der Komponenten eines Vierervektors berechnen läßt. Man verifiziert nun leicht, daß sich in dem allgemeinen Element

$$X = \chi^S + \chi^V_\mu \gamma_\mu + \tfrac{1}{2}\chi^T_{\mu\nu}\gamma_{\mu\nu} + \chi^{PV}_\mu \gamma_\mu \gamma_5 + \chi^{PS}\gamma_5, \tag{4}$$

mit $\gamma_{\mu\nu} = \gamma_{[\mu}\gamma_{\nu]} = \frac{1}{2}(\gamma_\mu\gamma_\nu - \gamma_\nu\gamma_\mu)$; $\gamma_5 = \gamma_1\gamma_2\gamma_3\gamma_4$ der Algebra $\mathfrak{C}_4$ bei Lorentztransformationen

$$\left|\begin{array}{ll} \chi^S & \text{wie ein Skalar,} \\ \chi^V_\mu & \text{wie die Komponenten eines Vierervektors,} \\ \chi^T_{\mu\nu} & \text{wie die Komponenten eines Tensors,} \\ \chi^{PV}_\mu & \text{wie die Komponenten eines Vierer-Pseudovektors,} \\ \chi^{PS} & \text{wie ein Pseudoskalar} \end{array}\right. \tag{5}$$

transformiert, wenn das System der Grundvektoren festgehalten wird. $\gamma^T_{\mu\nu}$ ist außerdem antimetrisch anzunehmen, da die Antimetrie von $\gamma_{\mu\nu}$ einen symmetrischen Anteil gegenstandslos macht. Da wegen (2) jede als Produkt von Elementen von $\mathfrak{C}_4$ schreibbare Beziehung lorentzinvariant ist, lautet somit die einfachste einparametrige, lineare, homogene, lorentzinvariante Differentialgleichung 1. Ordnung in $\mathfrak{C}_4$

$$(\gamma_\mu \partial_\mu + \varkappa)\Phi = 0, \tag{6}$$

wobei Φ analog zu (4) ein allgemeines Element von $\mathfrak{C}_4$ ist, dessen Koeffizienten φ^S, φ^V_μ, $\varphi^T_{\mu\nu}$, φ^{PV}_μ und φ^{PS} Funktionen von Ort und Zeit sind, und $\varkappa$ den freien Parameter bedeutet. Man erhält also die in $\mathfrak{C}_4$ formulierte Dirac-Gleichung, der dem eingangs postulierten Prinzip gemäß alle freien Elementarteilchenfelder genügen müssen.

Als physikalische Folgerung aus der Formulierung der Feldfunktionen der

Elementarteilchen als Elemente Φ von $\mathfrak{C}_4$ mit dem Transformationsverhalten (2), d.h. $\Phi' = A\Phi A^{-1}$, bei Lorentztransformationen ergibt sich unmittelbar, daß nur Teilchen mit den Spins 0 und 1 auftreten. Denn aus dem Transformationsverhalten (5) der Koeffizienten eines Elementes von $\mathfrak{C}_4$ gegenüber Lorentztransformationen sieht man, daß bei Drehungen des 3-dimensionalen Ortsraums nur skalares und vektorielles Transformationsverhalten vorkommt, da sich für diese Drehungen bekanntlich die Vierervektoren φ^V_μ und φ^{PV}_μ zu je einem Skalar und einem Dreiervektor, der antimetrische Tensor $\varphi^T_{\mu\nu}$ aber allgemein zu zwei Dreiervektoren ausreduzieren läßt.

Die Gleichungen, denen die in Φ enthaltenen Felder genügen, ergeben sich explizit durch Zerlegung von (6) nach den Basiselementen $1, \gamma_\mu, \gamma_{\mu\nu}, \gamma_\mu\gamma_5, \gamma_5$. Für nicht verschwindenden Massenparameter $\varkappa$ hat dies bereits FIUTAK [2] behandelt. Man erhält zunächst die kovarianten Beziehungen

$$
(7)\qquad \begin{cases} \partial_\mu \varphi^V_\mu + \varkappa\varphi^S = 0\,, \\ \partial_\mu \varphi^T_{\mu\nu} + \partial_\nu \varphi^S + \varkappa\varphi^V_\nu = 0\,, \\ 2\varepsilon_{\mu\nu\varrho\sigma}\partial_\mu \varphi^{PV}_\nu + \partial_\varrho \varphi^V_\sigma - \partial_\sigma \varphi^V_\varrho + \varkappa\varphi^T_{\varrho\sigma} = 0\,, \\ \varepsilon_{\mu\nu\varrho\sigma}\partial_\varrho \varphi^T_{\mu\nu} + \partial_\sigma \varphi^{PS} + \varkappa\varphi^{PV}_\sigma = 0\,, \\ \partial_\mu \varphi^{PV}_\mu + \varkappa\varphi^{PS} = 0\,. \end{cases}
$$

Hierbei ist $\varepsilon_{\mu\nu\varrho\sigma}$ der durch

$$
(8)\qquad \gamma_{\mu\nu}\gamma_5 = \varepsilon_{\mu\nu\varrho\sigma}\gamma_{\varrho\sigma}\,,
$$

definierte totalantimetrische Tensor mit dem Bestimmungsstück

$$
(9)\qquad \varepsilon_{1234} = -\tfrac{1}{2}\,.
$$

Für $\varkappa \neq 0$ läßt sich das Gleichungssystem (7) auf die Form

$$
(10)\qquad \begin{cases} (\partial_\mu\partial_\mu - \varkappa^2)\varphi^S = 0\,, \\ (\partial_\mu\partial_\mu - \varkappa^2)\varphi^{PS} = 0\,, \\ (\partial_\mu\partial_\mu - \varkappa^2)\pi^V_\nu = 0\,, \qquad \partial_\mu \pi^V_\mu = 0\,, \\ (\partial_\mu\partial_\mu - \varkappa^2)\pi^{PV}_\nu = 0\,, \qquad \partial_\mu \pi^{PV}_\mu = 0\,, \\ \varphi^V_\mu = \pi^V_\mu - \dfrac{1}{\varkappa}\partial_\mu\varphi^S\,, \qquad \varphi^{PV}_\mu = \pi^{PV}_\mu - \dfrac{1}{\varkappa}\partial_\mu\varphi^{PS}\,, \\ \varphi^T_{\varrho\sigma} = -\dfrac{1}{\varkappa}\{2\varepsilon_{\mu\nu\varrho\sigma}\partial_\mu\varphi^{PV}_\nu + \partial_\varrho\varphi^V_\sigma - \partial_\sigma\varphi^V_\varrho\} \end{cases}
$$

---

[2] J. FIUTAK: *Nuovo Cimento*, **10**, 292 (1958).

bringen. Man hat also vier Klein-Gordon-Felder, ein skalares φ^S, ein pseudoskalares φ^{PS}, ein vektorielles π^V_μ und ein pseudovektorielles π^{PV}_μ, wobei die beiden letzten durch die Lorentz-Konvention eingeschränkt sind. Die übrigen hier eingehenden Felder sind aus diesen berechenbar.

Für verschwindenden Massenparameter $\varkappa$ zerfällt das Gleichungssystem (7) in zwei voneinander unabhängige Gruppen. In die Gleichungen

$$\begin{cases} \partial_\mu \varphi^T_{\mu\nu} + \partial_\nu \varphi^S = 0 \,, \\ \varepsilon_{\mu\nu\varrho\sigma} \partial_\varrho \varphi^T_{\mu\nu} + \partial_\sigma \varphi^{PS} = 0 \end{cases} \tag{11}$$

gehen nur φ^S, φ^{PS} und $\varphi^T_{\mu\nu}$, in die Gleichungen

$$\begin{cases} \partial_\mu \varphi^V_\mu = 0 \,, \\ \partial_\mu \varphi^{PV}_\mu = 0 \,, \\ 2\varepsilon_{\mu\nu\varrho\sigma} \partial_\mu \varphi^{PV}_\nu + \partial_\varrho \varphi^V_\sigma - \partial_\sigma \varphi^V_\varrho = 0 \end{cases} \tag{12}$$

nur φ^V_μ und φ^{PV}_μ ein. Daraus lassen sich Wellengleichungen für φ^S, φ^{PS}, φ^V_μ und φ^{PV}_μ gewinnen, doch scheint diesen Möglichkeiten keine physikalische Bedeutung zuzukommen. Für den speziellen Fall $\varphi^S = 0$, $\varphi^{PS} = 0$ folgt jedoch aus (11)

$$\begin{cases} \partial_\mu \varphi^T_{\mu\nu} = 0 \,, \\ \partial_\varrho \varepsilon_{\varrho\sigma\mu\nu} \varphi^T_{\mu\nu} = 0 \,. \end{cases} \tag{13}$$

Das sind genau die Maxwellschen Gleichungen.

Die bisher behandelten Feldtypen erschöpfen die durch das am Anfang formulierte Prinzip gegebenen Möglichkeiten noch nicht vollständig. Man kann nämlich für die hyperkomplexe Feldfunktion Φ die Beschreibung der Lorentztransformationen durch die Transformationen (2) aufgeben und durch

$$\Phi' = \Lambda \Phi \tag{14}$$

ersetzen. Die Invarianzeigenschaften der Feldgleichung (6) bleiben dadurch offensichtlich erhalten. Der Übergang zu dem Transformationsverhalten (14) bedeutet eine Ausnützung der durch (2) gegebenen Darstellung der Lorentztransformationen durch Elemente Λ von $\mathfrak{C}_1$. Dabei steht für Φ nun nicht mehr die ursprüngliche geometrische Bedeutung der Elemente von $\mathfrak{C}_4$ im Vordergrund, sondern es wird abstrakt als Element des regulären Darstellungsraums von $\mathfrak{C}_4$ aufgefaßt (1).

Bei Zugrundelegung des Transformationsverhaltens (14) ist eine Zerlegung von Φ analog zu (4) unzweckmäßig, da das Transformationsverhalten der so

auftretenden Koeffizienten nun nicht mehr einfach ist. Angemessen ist nun vielmehr die Zerlegung nach Elementen der in $\mathfrak{C}_1$ enthaltenen vier 4-dimensionalen minimalen Linksideale [3]. Jedes solche minimale Linksideal wird von einer Basis $s_\mu^{(\lambda)}$ aufgespannt, wobei $\lambda = 1, 2, 3, 4$ die verschiedenen Linksideale numerieren möge und μ von 1 bis 4 läuft. Alle 16 Basiselemente $s_\mu^{(\lambda)}$ sind wiederum eine Basis von $\mathfrak{C}_1$, die aus der in (4) benutzten durch Linearkombination hervorgeht. Damit läßt sich schreiben

$$\Phi = \sum_\lambda \psi_\mu^{(\lambda)} s_\mu^{(\lambda)} \quad (*). \tag{15}$$

Die $\psi_\mu^{(\lambda)}$ sind dabei Funktionen von Ort und Zeit, die sich bei Lorentztransformationen nach

$$\psi_\mu^{(\lambda)'} = d_{\mu\nu}^{(\lambda)} \psi_\nu^{(\lambda)}, \tag{16}$$

transformieren, wobei die Matrix $d_{\mu\nu}^{(\lambda)}$ durch

$$A s_\nu^{(\lambda)} = d_{\mu\nu}^{(\lambda)} s_\mu^{(\lambda)}, \tag{17}$$

gegeben ist. Dies sind bekanntlich unabhängig von λ die Transformationseigenschaften eines Viererspinors [1,3,4]. Man kommt also auf diese Weise zur Beschreibung von Elementarteilchen mit dem Spin $\frac{1}{2}$.

Die Zerlegung der Feldgleichung (6) nach den minimalen Linksidealen liefert nun die Dirac-Gleichungen

$$(\gamma_\mu \partial_\mu + \varkappa)\psi^{(\lambda)} = 0, \tag{18}$$

für die vier Viererspinorfelder $\psi^{(\lambda)} = \psi_\mu^{(\lambda)} s_\mu^{(\lambda)}$ als kovariante Feldgleichungen. Die auftretende Vierfachheit ist physikalisch bedeutungslos, da der Index λ zueinander isomorphe Fälle unterscheidet. Sie kann durch rechtsseitige Multiplikation von Φ mit einem Nullteiler vom Reduktionsgrad $\frac{1}{4}$ beseitigt werden [4].

Damit ist gezeigt, daß das eingangs formulierte Prinzip gerade Felder von Elementarteilchen mit dem Spin 0 und 1, die der Klein-Gordon-Gleichung genügen, sowie mit dem Spin $\frac{1}{2}$, die der Dirac-Gleichung genügen, liefert. Der Spezialfall verschwindenden Massenparameters enthält auch die Maxwellschen

---

[3] Vgl. z.B.: G. Falk: *Handb. d. Phys.* (S. Flügge), Bd. 2 (Berlin-Göttingen-Heidelberg, 1955), S. 85 ff.

[4] Siehe hierzu auch A. Sommerfeld: *Atombau und Spektrallinien*, Bd. 2 (Braunschweig, 1939), S. 209 ff.

(*) Über eingeklammerte Indizes soll nur summiert werden, wenn die Summe explizit angeschrieben ist.

Gleichungen. Während also alle bekannten Elementarteilchenfelder inbegriffen sind, werden Felder mit einem Spin größer als 1 ausgeschlossen. Der formale Grund für diesen Umstand liegt in der Tatsache, daß mit der Darstellung der Lorentzgruppe gerade in $\mathfrak{C}_4$ eine entsprechende Einschränkung ihrer darin enthaltenen irreduziblen Darstellungen verbunden ist. Da aber das Auftreten von $\mathfrak{C}_4$ mit der *Vier*dimensionalität des Raum-Zeit-Kontinuums zusammenhängt, kann man sagen, daß hierin der eigentliche Grund für das Nichtauftreten von Elementarteilchenspins größer als 1 liegt. Der Rahmen der möglichen Elementarteilchen ist damit in, wie es scheint, vernünftiger Weise eingeschränkt, wenn auch noch viele, in der Natur nicht ausgenützte Möglichkeiten offen bleiben. Um diese vollständig auszuschließen, muß man jedoch über eine rein phänomenologische Behandlung der Elementarteilchen hinausgehen.

RIASSUNTO (*)

Si dimostra che è possibile formulare una descrizione fenomenologica delle particelle elementari che consente l'esistenza di sole particelle con spin 0, $\frac{1}{2}$ ed 1. Questa restrizione consegue dal fatto che lo spazio è quadridimensionale.

(*) *Traduzione a cura della Redazione.*

IL NUOVO CIMENTO Vol. XIV, N. 6 16 Dicembre 1959

Self Diffusion in Liquid In-Sn Alloys.

M. Vicentini

Istituto di Fisica dell'Università - Roma

A. Paoletti

C.N.R.N., Divisione Studi e Ricerche - Roma

(ricevuto il 12 Ottobre 1959)

Summary. — Further self diffusion experiments in In-1% Sn and Sn-1% In alloys, using as tracers ^{114}In and ^{113}Sn, confirme the results previously obtained in the In-Pb system. Within the experimental errors the activation energy is indipendent of the tracer. A « wall effect » already found in pure Indium and in In-Pb alloy affects the In-Sn results too. This effect is discussed and it is shown that it cannot be due to turbulent diffusion.

1. – Introduction.

The self-diffusion measurements in liquid alloys might be very useful in the study of the transport properties of liquids. Our previous investigation (1) has been then extended to the Indium-Tin system.

In this research we have measured the self-diffusion coefficients of Indium and Tin for the alloy In-1 atomic pct Tin and the self-diffusion coefficient of Indium for the alloy Tin-1% In in the temperature range 250 °C — 470 °C.

2. – Experimental.

The experimental technique consists in allowing two half rods of radioactive and inert metal to follow a thermal cycle in a mullite capillary under vacuum.

During this cycle the diffusion in liquid phase takes place and the diffusion coefficient is then evaluated from the penetration curve of the active component.

(1) A. Paoletti and M. Vicentini: *Nuovo Cimento*, **14**, 748 (1959).

A detailed report on the apparatus and experimental procedure was given in previous papers ([1-3]).

All the experiments were performed with capillaries of two different diameters (1.6 mm and 0.8 mm) in order to check whether a « wall effect » is present as it was found in pure Indium and In-0.5% Pb (tracer Pb) self-diffusion ([1,3]).

The metals (*) were of the highest purity; ^{114}In (**) and ^{113}Sn were used as tracers. Some precautions had to be taken in the analysis of the Sn concentration. ^{113}Sn decays in ^{113}In with a half-life $T_1 = 112$ d emitting a β_1^* of 0.05 MeV and a γ_1 of about 0.09 MeV, and further decays in ^{113}In with $T_2 = 1.73$ h and a γ of 0.39 MeV. Because of the thickness of the the counter's window it was the second disintegration that we detected and not the first one. However, since the samples were left for at least one day after the diffusion experiment before being counted, we were sure to follow the diffusion of the Tin atoms and not of the Indium ones.

3. – Results.

TABLE I. – *Self-diffusion in* In-1% Sn (*Tracer* ^{114}In).

Run	T (°C)	$10^3/T$ (°K)$^{-1}$	Time	$D \cdot 10^5$ (cm^2/s)
		$\Phi = 0.83$ mm		
6*c*	330	1.660	5^h 52′ 00″	3.50 ± 0.16
6*d*	330	1.660	5^h 52′ 00″	3.57 ± 0.16
7*c*	238	1.957	7^h 20′ 30″	2.55 ± 0.15
8*c*	284	1.793	6^h 08′ 00″	3.20 ± 0.15
8*d*	284	1.793	6^h 08′ 00″	3.14 ± 0.15
9*c*	417	1.449	4^h 02′ 30″	5.13 ± 0.24
9*d*	417	1.449	4^h 02′ 30″	5.03 ± 0.22
11*d*	283	1.779	3^h 00′ 00″	3.03 ± 0.18
12*c*	460	1.365	2^h 56′ 30″	6.03 ± 0.20
		$\Phi = 1.60$ mm		
6*a*	330	1.660	5^h 52′ 00″	3.57 ± 0.15
6*b*	330	1.660	5^h 52′ 00″	3.83 ± 0.26
7*a*	238	1.957	7^h 20′ 30″	2.56 ± 0.10
8*a*	284	1.793	6^h 08′ 00″	3.24 ± 0.13
9*a*	417	1.449	4^h 02′ 30″	4.70 ± 0.22
11*a*	283	1.779	3^h 00′ 00″	3.29 ± 0.18

([2]) G. CARERI, A. PAOLETTI and F. L. SALVETTI: *Nuovo Cimento*, **2**, 399 (1954).
([3]) G. CARERI, A. PAOLETTI and M. VICENTINI: *Nuovo Cimento*, **10**, 1088 (1958).
(*) From Johnson, Matthey and Co.
(**) Supplied by A.E.R.E., Harwell (England).

TABLE II. – *Self-diffusion in* In-1% Sn (*Tracer* ^{113}Sn).

Run	T (°C)	$10^3/T$ (°K)$^{-1}$	Time	$D \cdot 10^5$ (cm^2/s)
		$\Phi = 0.83$ mm		
14*c*	237	1.960	7^h 04′ 00″	2.57 ± 0.14
15*d*	314	1.702	3^h 00′ 00″	3.23 ± 0.26
17*c*	371	1.552	5^h 53′ 00″	4.15 ± 0.21
17*d*	371	1.552	5^h 53′ 00″	3.92 ± 0.21
18*c*	464	1.357	3^h 25′ 00″	5.30 ± 0.30
18*d*	464	1.357	3^h 25′ 00″	5.06 ± 0.35
		$\Phi = 1.60$ mm		
14*a*	237	1.960	7^h 04′ 00″	2.83 ± 0.11
14*b*	237	1.960	7^h 04′ 00″	2.71 ± 0.18
15*a*	314	1.702	3^h 00′ 00″	3.75 ± 0.38
15*b*	314	1.702	3^h 00′ 00″	3.62 ± 0.28
17*a*	371	1.552	5^h 53′ 00″	4.82 ± 0.33
18*a*	464	1.357	3^h 25′ 00″	6.12 ± 0.30
18*b*	464	1.357	3^h 25′ 00″	5.80 ± 0.30

TABLE III. – *Self-diffusion in* Sn-1% In (*Tracer* ^{113}Sn).

Run	T (°C)	$10^3/T$ (°K)$^{-1}$	Time	$D \cdot 10^5$ (cm^2/s)
		$\Phi = 0.83$ mm		
19*d*	356	1.590	2^h 46′ 30″	3.73 ± 0.17
20*c*	355	1.592	2^h 09′ 00″	3.47 ± 0.16
20*d*	355	1.592	2^h 09′ 00″	3.65 ± 0.16
21*c*	297	1.756	2^h 59′ 30″	2.75 ± 0.13
21*d*	297	1.756	2^h 59′ 30″	2.62 ± 0.10
22*d*	298	1.752	6^h 12′ 15″	2.60 ± 0.11
29*c*	263	1.866	5^h 36′ 30″	2.53 ± 0.11
29*d*	263	1.866	5^h 36′ 30″	2.52 ± 0.11
30*c*	467	1.354	3^h 00′ 30″	5.14 ± 0.24
		$\Phi = 1.60$ mm		
19*a*	356	1.590	2^h 46′ 30″	3.81 ± 0.17
19*b*	356	1.590	2^h 46′ 30″	3.46 ± 0.18
20*a*	355	1.592	2^h 09′ 00″	3.75 ± 0.18
20*b*	355	1.592	2^h 09′ 00″	3.57 ± 0.15
21*b*	297	1.756	2^h 59′ 30″	2.83 ± 0.17
22*a*	298	1.752	6^h 12′ 15″	2.80 ± 0.11

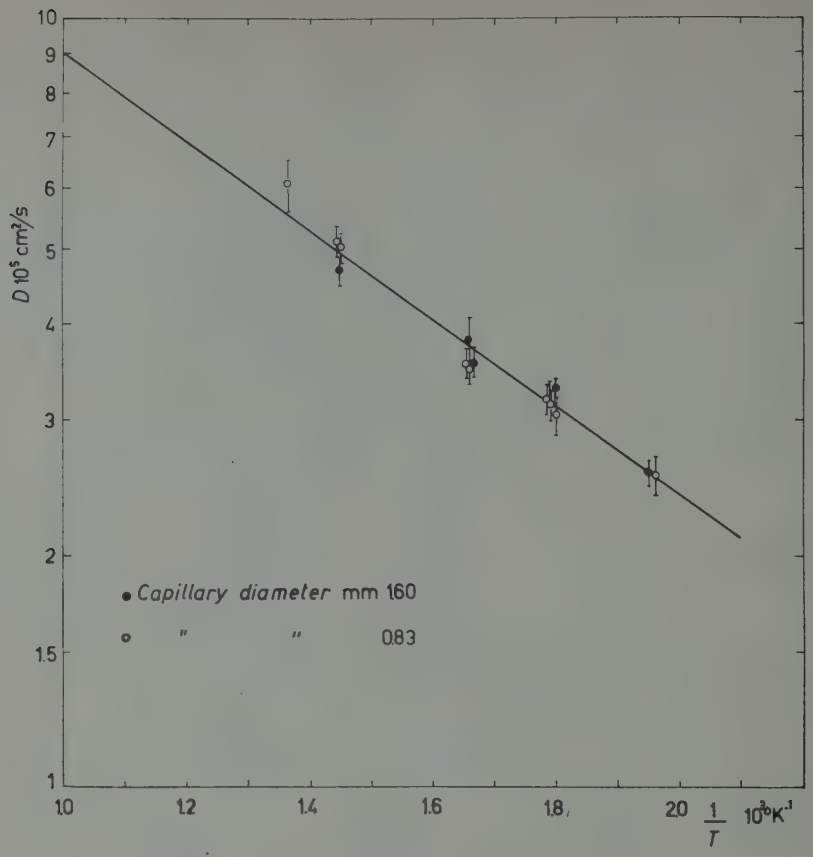

Fig. 1. – Self-diffusion of ^{114}Sn in In-1% Sn.

TABLE IV. – *Experimental D_0 and Q.*

System	Tracer	Φ (mm)	$D_0 \cdot 10^5$ (cm²/s)	Q (cal/mol)
In	^{114}In	1.6	33.4 ± 2.1	2 554 ± 79
In	^{114}In	0.8	30.2 ± 2.0	2 580 ± 83
Sn	^{113}Sn	1.6	32.4 ± 1.2	2 768 ± 80
Sn	^{113}Sn	0.8	32.4 ± 1.2	2 768 ± 80
In - 1% Sn	^{114}In	1.6	33.5 ± 3.6	2 606 ± 127
In - 1% Sn	^{114}In	0.8	33.5 ± 3.6	2 606 ± 127
In - 1% Sn	^{113}Sn	1.6	31.9 ± 3.5	2 473 ± 129
In - 1% Sn	^{113}Sn	0.8	25.7 ± 3.6	2 356 ± 176
Sn - 1% In	^{113}Sn	1.6	37.4 ± 5.4	2 909 ± 172
Sn - 1% In	^{113}Sn	0.8	37.4 ± 5.4	2 909 ± 172

The results of the self-diffusion of Indium and Tin in the In-1 % Tin alloy are given in Table I and II. In the Fig. 1 and 2, ln D is plotted as a function of $1/T$ respectively for Indium and Tin: in both cases the Arrhenius equation

$$D = D_0 \exp[-Q/RT]$$

is fairly well verified. The experimental D_0 and Q values are given in Table IV together with the D_0 and Q values for pure Indium and pure Tin self-diffusion.

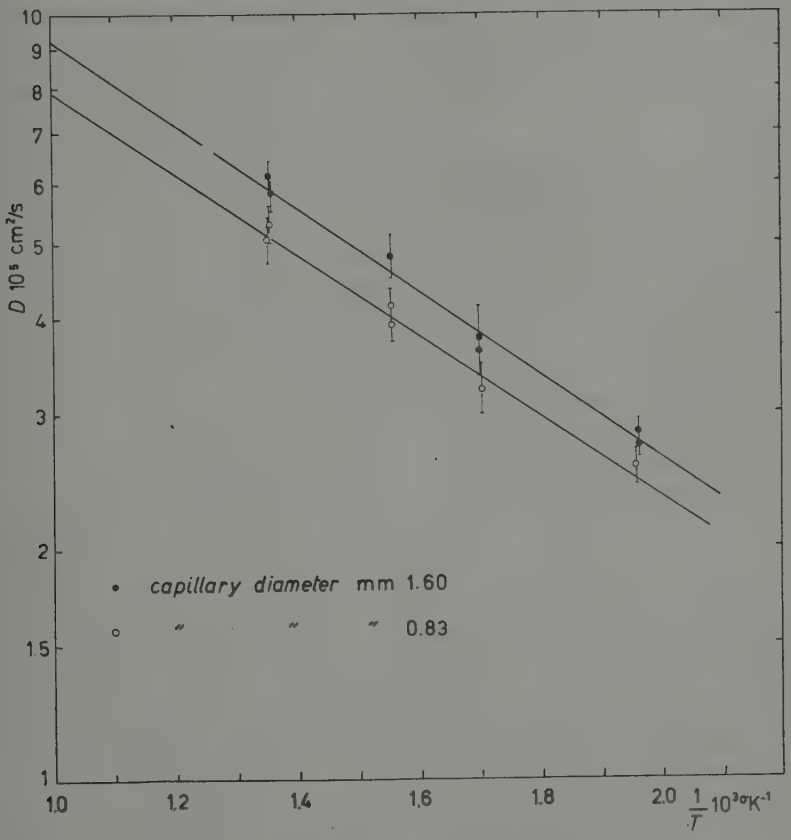

Fig. 2. – Self-diffusion of ^{113}Sn in In-1% Sn.

The experimental results for self-diffusion of Indium in the Tin-1 % In are given in Table III and Fig. 3. In this case too, the Arrhenius equation is verified with D_0 and Q values given in Table IV.

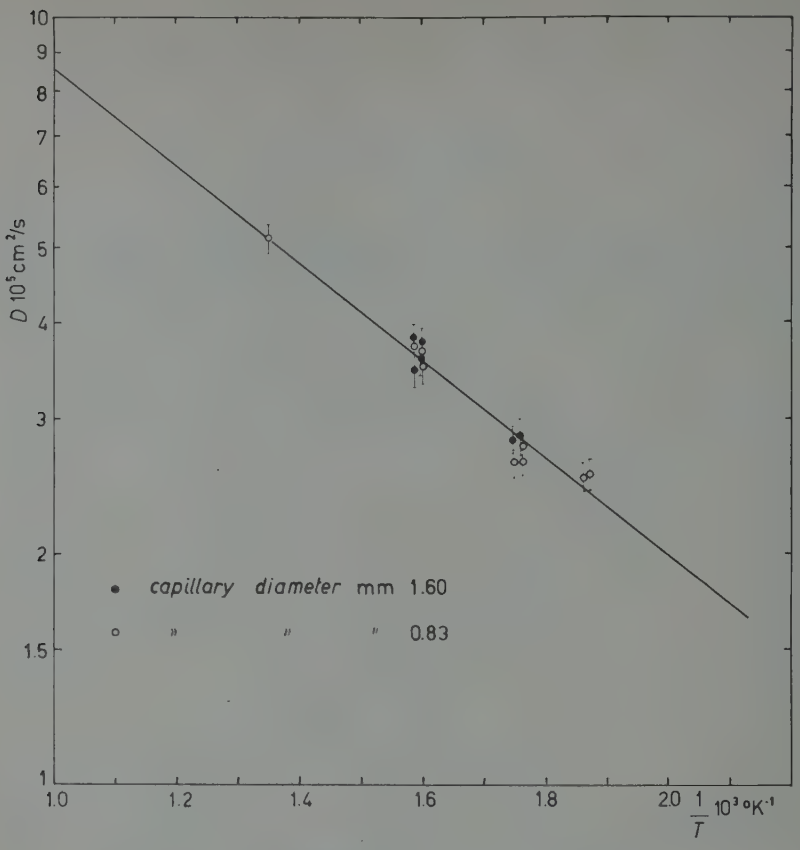

Fig. 3. – Self-diffusion of ^{113}Sn in Sn-1% In.

4. – Discussion.

The results obtained for Indium and Tin self-diffusion in the alloy In-1% Tin show a small change in the diffusivity in respect to the pure Indium self-diffusion, but the activation energies are equal within the experimental errors and very close to the activation energy for the pure metal. The Tin-1% In alloy has the same behaviour: the activation energy is very close to the one of the pure Tin. For this alloy the unfavourable phase diagram of the Indium-Tin system prevented the measure of the self-diffusion coefficient for Indium.

All these experiments agree completely with the previous results obtained for the In-Pb system [1]. They can be then interpreted as an indication that the introduction of small impurity concentrations in a liquid metal, would affect only slightly and of the same amount the energy barrier for both the solvent and solute atoms.

It is also interesting to notice that for diffusion of Tin in the In-1% Sn

alloy the experimental ln D values, if plotted as a function of $1/T$ lie on two different straight lines according to the diameter of the capillaries used in the runs.

The two straight lines are, within the experimental errors, parallel: the lower one is relative to the runs in which capillaries of 0.8 mm diameter were used, the other one to the runs with capillaries of 1.6 mm. Needless to say that all the precautions were taken in order to check the consistency of the data.

We recall that the same behaviour was found by us in the pure Indium [3] and in the self-diffusion of Lead in an alloy In-0.5% Pb [1].

On the contrary, for self-diffusion of pure Tin [3], of Indium in the In-0.5% Pb [1], In-1.5% Pb [1], In-1% Sn alloys and of Sn in the Sn-1% In alloy, the results were completely independent of the capillaries diameter.

Till now we have not been able to explain this fact. Our analysis of the experimental data allows us to refuse on the basis of the penetration curve the runs where some convection was present. The objection that the higher values for the runs with larger diameter capillaries is due to turbulent diffusion which would be absent when smaller diameter capillaries are used, can be ruled out.

We notice that it is true that if some conditions are verified, molecular and turbulent diffusion can overlap without affecting the general shape of the penetration curve [4,5] which will still obey the equation

$$c(x) = \frac{1}{2}\left(1 - \operatorname{erf} \frac{x}{2(Dt)^{\frac{1}{2}}}\right),$$

where D is the sum of the molecular and « eddy » diffusion coefficients. This has been also experimentally verified [6], but no reproducibility of the data has been found.

We must point out, that on the contrary, the reproducibility of our data has been checked for very different time lengths of diffusion. Furthermore, it is very difficult, just on the basis of turbulence effect caused by the capillary diameter, to explain the different behaviour of different tracers in the same alloy. Both In-0.5% Pb and In-1% Sn alloys, show a change of D with the diameter of the capillary only when one component is used as tracer (respectively Pb and Sn); no change is found when the tracer is the other component of the alloy (In).

It is obvious that any turbulence should show up independently of the tracer used.

---

(4) G. I. Taylor: *Proc. London Math. Soc.*, A **20**, 196 (1921).
(5) F. N. Frenkiel: *Advances in Applied Mechanics*, vol. **3**, p. 61 (New York).
(6) A. Paoletti and M. Vicentini: *Physics of Fluids*, **1**, 454 (1958).

We conclude that after these last experiments, our considerations previously published ([3]) about the so called « wall effect » are still valid, namely that the molecules which are near the wall of the capillary do not seem to participate to the diffusion in the same way as the molecules of the core do. In a recent paper M. FIXMAN ([7]), on the basis of a model previously proposed for moment transport in fluids, calculates the hindering effect of a wall on diffusion. In his model, momentum and energy are carried by dipole density waves centered on the molecule of interest and both specular and diffuse reflection of the density waves by the wall are considered. M. FIXMAN gets formulas for calculating the ratio of the diffusion constant at a distance l from the wall, to the bulk fluid diffusion constant.

However, according his results, it is impossible to explain, for instance, the different behaviour found in Indium self-diffusion compared to Tin and moreover the dependence of the « wall effect » upon the material of the capillary is not considered. In order to say something quantitative about the variation of D within the liquid, to be compared with diffusion experiments, it would be mainly necessary to solve first the Fick equation with a variable D, which has not yet been done.

From the other side, more investigations of different substances should be performed to be used as an experimental basis for interpreting this effect.

([7]) M. FIXMAN: *Journ. Chem. Phys.*, **29**, 540 (1958).

RIASSUNTO

Ulteriori esperimenti di autodiffusione in leghe In-1% Sn e Sn-1% In confermano i risultati ottenuti precedentemente nel sistema In-Pb. Entro gli errori sperimentali, l'energia di attivazione risulta indipendente dal tracciante. Un « effetto parate » già trovato nell'Indio puro e nella lega In-Pb, è presente anche nelle leghe In-Sn. Questo effetto viene discusso e viene dimostrato che esso non può essere dovuto a diffusione turbolenta.

Electromagnetic Mass Shift for Spinless Particles.

H. KATSUMORI

Department of Physics, Osaka Gakugei University - Osaka

(ricevuto il 24 Agosto 1959)

The electromagnetic mass shift for the spinless particle was discussed by several authors [1-3], in order to explain the observed $\pi^{\pm}$-π^0 mass difference (9 m_e). The numerical estimate of the π-meson mass difference suggested the validity of the attractive viewpoint that the observed mass splitting between the members of the same charge multiplet is purely electromagnetic. In the meantime, the K^0-K^+ and K^0-K^- mass excesses have been recently detected at Berkeley [4,5]. The observed $K^{\pm}$-$K^0(\bar{K}^0)$ mass difference ($-$ 9 m_e), however, has the opposite sign and seems difficult to understand in the same manner [6].

The purpose of the present report is to point out that the K^0 may happen to be heavier than the $K^{\pm}$ while the π^0 must be lighter than the $\pi^{\pm}$, in the e^2-order calculation of the electromagnetic self energy, if the isospace transformation property of the electromagnetic form factor is taken into account, following the Nishijima and Gell-Mann rule for the strangeness assignment.

The electromagnetic form factors for the π and K-mesons can be written, as functions of the invariant momentum transfer k, as follows

$$(1) \qquad F^{(\pi)}(k) = I_3 F_V^{(\pi)}(k) ,$$

$$(2) \qquad F^{(K)}(k) = F_S^{(K)}(k) + \tau_3 F_V^{(K)}(k) , \qquad F^{(\bar{K})}(k) = - F_S^{(K)}(k) + \tau_3 F_V^{(K)}(k) ,$$

where

$$I_3 = \begin{pmatrix} 1 & 0 & 0 \\ 0 & 0 & 0 \\ 0 & 0 & -1 \end{pmatrix} \quad \text{and} \quad \tau_3 = \begin{pmatrix} 1 & 0 \\ 0 & -1 \end{pmatrix} .$$

(1) R. P. FEYNMAN: *International Conference in Theoretical Physics* (Paris, 1950).
(2) Y. OISHI: *Soryushiron Kenkyu* (mimeographed circular in Japanese), **6**, 975 (1954).
(3) A. PETERMANN: *Helv. Phys. Acta*, **27**, 441 (1954).
(4) A. H. ROSENFELD *et al.*: *Phys. Rev. Lett.*, **2**, 110 (1959).
(5) F. S. CRAWFORD *et al.*: *Phys. Rev. Lett.*, **2**, 112 (1959).
(6) S. GASIOROWICZ and A. PETERMANN: *Phys. Rev. Lett.*, **1**, 457 (1958).

F_S and F_V stand for the isoscalar and isovector parts of the form factor respectively and they satisfy the conditions

$$F_V^{(\pi)}(0) = 1\,, \qquad F_S^{(K)}(0) = F_V^{(K)}(0) = \tfrac{1}{2}\,. \tag{3}$$

The vanishing of $F_S^{(\pi)}$ for the π-meson is due to the fact that the strangeness quantum number of the π is assigned to be zero and the charge conjugate π^+ and π^--mesons belong to the same charge triplet, as commonly assumed. This is not the case for the K-meson, because the charge conjugate K^+ and K^- mesons do not belong to the same charge doublet but have the strangeness quantum numbers of opposite sign.

Introducing these form factors into the electromagnetic interaction of a spinless boson, we obtain the mass difference between charged and neutral members of the same charge multiplet, in the e^2-approximation, for the π and K-mesons

$$m(\pi^{\pm}) - m(\pi^0) = (\delta m_\pi)_{I_3=\pm 1} - (\delta m_\pi)_{I_3=0} = \frac{1}{2m_\pi}\cdot\frac{1}{\pi}\left(\frac{e^2}{4\pi}\right)\int [F_V^{(\pi)}(k)]^2 I^{(\pi)}(k)\,\mathrm{d}^4k\,, \tag{4}$$

$$m(K^{\pm}) - m(K^0 \text{ or } \overline{K}^0) = (\delta m_K)_{\tau_3=1} - (\delta m_K)_{\tau_3=-1} = (\delta m_{\overline{K}})_{\tau_3=-1} - (\delta m_{\overline{K}})_{\tau_3=1} =$$

$$= \frac{1}{2m_K}\cdot\frac{1}{\pi}\left(\frac{e^2}{4\pi}\right)\int 4F_S^{(K)}(k)\,F_V^{(K)}(k)\,I^{(K)}(k)\,\mathrm{d}^4k\,. \tag{5}$$

If we treat the boson field by Klein and Gordon's formalism, the electromagnetic interaction,

$$-ie(\varphi^*\cdot\partial_\mu\varphi - \partial_\mu\varphi^*\cdot\varphi)A_\mu - e^2\varphi^*\varphi A_\mu A_\mu\,, \tag{6}$$

leads to $I(k)$ as a sum of the contributions from the two diagrams (a) and (b) in Fig. 1

$$I(k) = \frac{1}{4i\pi^2}\left[-\delta_{\mu\mu} + (2q-k)_\mu\,\frac{1}{(q-k)^2 - m^2}\,(2q-k)_\mu\right]\frac{1}{k^2}\,. \tag{7}$$

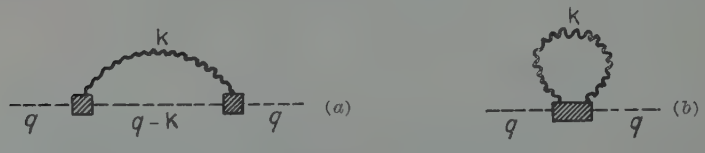

Fig. 1.

For simplicity we are going to consider the form factor which works essentially as a cutoff factor for the space like part of k^2. The inclusion of the time like part of k^2 does not change the main features of the following discussion. Now the integration of $I(k)$ over k_4 is carried out independently of the form factor,

$$\int I(k)\,\mathrm{d}\boldsymbol{k}\,\mathrm{d}k_4 = m^2\int_0^\infty\left[2l + \sqrt{1+l^2} + \frac{1}{\sqrt{1+l^2}}\right]\mathrm{d}l\,, \tag{8}$$

where $l = |\boldsymbol{k}|/m$. As this integral is clearly positive definite, eq. (4) tells us that $m(\pi^{\pm}) - m(\pi^0)$ is also positive definite without respect to the explicit behavior of the form factor. Consequently the charged π-meson ought to be heavier than the neutral one in agreement with the experimental data.

On the other hand, eq. (5) indicates that the sign of the $K^{\pm}$-$K^0(\overline{K}^0)$ mass difference is indefinite, because the integrand contains the product of the isoscalar and isovector parts, $F_S^{(K)}F_V^{(K)}$, in contrast with $[F_V^{(\pi)}]^2$ in eq. (4). Since the integral (8) is quadratically divergent, the sign of the K-meson mass difference strongly depends upon the sign of the product $F_S^{(K)}F_V^{(K)}$ for the large momentum transfer $|\boldsymbol{k}|$. Thus there is a possibility of understanding the observed mass shift for the K-meson which is opposite to that of the π-meson. In other words, the observed $K^{\pm}$-K^0 mass difference seems to suggest that the electromagnetic form factor of the K-meson behaves as

$$F_S^{(K)}(k)\,F_V^{(K)}(k) < 0 \,, \qquad \text{for large } |\boldsymbol{k}| . \tag{9}$$

It seems quite difficult to examine the validity of this condition (9) at the present stage. Future experimental and theoretical works, which intend to investigate the inner charge distribution of the K-meson, might test this condition.

We can obtain the observed values of the K-meson mass difference as well as of the π-meson mass difference, assuming the suitable form factor. Such a form factor suggests some informations on the inner charge distribution. The somewhat detailed discussion about this problem will be reported in a separate article [7]. In this article similar discussions are also made for the n-p, Σ^--Σ^+, Σ^+-Σ^+ and Ξ^0-Ξ^- mass differences.

Furthermore we have studied the self energy through the strong interaction, which also may largely contribute to the electromagnetic mass shift. This effect of the lowest order in g^2, however, turns out to be regarded as a small correction to the main electromagnetic effect [7].

---

[7] H. KATSUMORI: to be published.

IL NUOVO CIMENTO Vol. XIV, N. 6 16 Dicembre 1959

The K-Absorption Spectrum of Neutron Irradiated Nickel.

D. Bally and L. Benes

The Institute of Atomic Physics - Bucharest

(ricevuto il 14 Settembre 1959)

The modifications of the K-absorption spectra produced by irradiating the absorbers with neutrons have been studied for nickel and a Ni-Cu alloy (1), for germanium and germanium dioxide (2), and for nickel, iron and Ni-Fe alloys (3).

Our purpose was to study the manner in which the K-absorption spectrum of nickel is modified when the integral irradiation flux of the absorber and the spectral composition of the incident beam are varied.

The irradiation was performed in one of the vertical channels of the reactor of the Institute of Atomic Physics in Bucharest, with integral fluxes varying from 10^8 n/cm^2 to 10^{17} n/cm^2. The temperature of the object during the irradiation was less than 80 °C.

In order to find out the contribution of the thermal neutrons to the effect under investigation, an object enclosed in a cadmium container whose walls practically completely absorbed neutrons with energies below 0.7 eV was irradiated by the integral flux of 10^{17} n/cm^2.

The absorption spectra were obtained with an X-ray bent-crystal, Cauchois type spectrometer having a radius of 41.5 cm. A mica crystal (first order reflexion on planes $(\bar{2}\,0\,1)$) was used.

The results obtained are given in Table I, where the following symbols were used: L and l denote the extreme limits of the K-absorption discontinuity of nickel, while K_1 and K_2 are the intermediate stages of this discontinuity; φ_i denotes the integral irradiation flux.

Conclusions.

1) The neutron irradiation of the absorber causes a structure of the K-absorption discontinuity of nickel to appear.

2) The variation of the integral flux within the limits of $(10^{15} \div 10^{17})$ n/cm^2 does not modify the absorption discontinuity.

3) The minimum integral flux at which the modification of stage K_1 begins

(1) Y. Cauchois: *Compt. Rend.*, **241**, 942 (1955).

(2) M. M. Kahana and E. E. Veinstein: *Izv. Akad. Nauk SSSR*, Seria Fizicescaia, **21**, 1459 (1957).

(3) D. Bally and L. Benes: P/1293 (Geneva, 1958).

TABLE I. – *Values of the elements of the structure of K-absorption discontinuity of nickel, in* UX.

	unirradiated	$\varphi_i =$ 10^8 n/cm^2	$\varphi_i =$ 10^{15} n/cm^2	$\varphi_i =$ 10^{16} n/cm^2	$\varphi_i = 10^{17}$ n/cm^2	
					without Cd	with Cd
L	1486.08	1486.08	1486.12	1486.10	1486.12	1486.06
K_1	1485.04	—	1485.60	1485.58	1485.53	1485.52
		1485.39	1485.28	1485.23	1485.25	1485.38
		1485.02	1485.11	1485.10	1485.11	1485.16
K_2	1483.35	1483.80	1483.75	1483.72	—	—
		1483.58	1483.58	1483.54	1483.59	1483.61
		1483.32	1483.42	1483.39	1483.37	1483.32
l	1482.56	1482.37	1482.27	1482.24	1482.26	1482.23

is of the order of 10^8 n/cm^2, while for stage K_2 it is inferior to this value.

4) Comparing the results obtained with absorbers irradiated in the cadmium container and outside it, it is obvious that the modifications observed are caused primarily by the neutrons with energy above 0.7 eV.

5) The modification of the K absorption spectrum of nickel following neutron irradiation of the absorber is similar to that observed after the formation of a solid solution [4].

[4] D. BALLY and L. BENES: *Compt. Rend.*, **248**, 2327 (1959).

IL NUOVO CIMENTO Vol. XIV, N. 6 16 Dicembre 1959

Diffusion cohérente des photons de 2.62 MeV par les électrons de la couche K du mercure.

H. Cornille et M. Chapdelaine

Laboratoire de Physique, Ecole Normale Supérieure - Paris

(ricevuto il 24 Settembre 1959)

Nous nous sommes proposé le calcul théorique [1] de la diffusion Rayleigh par les électrons de la couche K et de la diffusion Thomson nucléaire en vue d'interpréter les résultats expérimentaux [2,3] de la diffusion cohérente des photons de 2.62 MeV par le plomb. Nous ne discuterons pas ici de la différence entre les courbes théoriques et expérimentales. Cependant disons qu'il existe entre 30° et 70° un trop grand écart que ne peuvent expliquer la diffusion parl es électrons L, la résonance nucléaire et les erreurs expérimentales; ceci nous a fait penser qu'un autre effet, l'effet Delbrück, donnait à cette énergie une contribution importante [1].

Résultats numériques de la diffusion Rayleigh par les électrons K.

La méthode utilisée est celle de Brown, Peierls, Woodward, Brenner et Mayers mise au point à Birmingham [4]. Nous rappelons:

$$\frac{\mathrm{d}\sigma}{\mathrm{d}\Omega} = r_0^2 \left[\left| M(1', 1) + M(2', 2) \right|^2 + \left| M(1', 2) + M(2', 1) \right|^2 \right];$$

r_0 étant le rayon classique de l'électron.

$$M(1', 1) + M(2', 2) = a_1(\theta) + i a_2(\theta) , \qquad M(1', 2) + M(2', 1) = b_1(\theta) + i b_2(\theta) ;$$

θ étant l'angle de diffusion; $a_1(\theta)$, $a_2(\theta)$, $b_1(\theta)$, $b_2(\theta)$ sont sans dimension.

---

[1] L. Goldzahl, P. E. Eberhard, H. Cornille and M. Chapdelaine: *Compt. Rend. Acad. Sci.*, **249**, 401 (1959).

[2] P. Eberhard L. Goldzahl and E. Hara: *Journ. Phys.*, **19**, 658 (1958).

[3] A. M. Berstein et A. K. Mann: *Phys. Rev.*, **110**, 805 (1958).

[4] G. E. Brown, R. E. Peierls et J. B. Woodward: *Proc. Roy. Soc.*, A **227**, 51 (1954); S. Brenner, G. E. Brown et J. B. Woodward: *Proc. Roy. Soc.*, A **227**, 59 (1954); G. E. Brown et D. F. Mayers: *Proc. Roy. Soc.*, A **234**, 387 (1955); A **242**, 89 (1957).

$M(i', j)$ étant l'amplitude de diffusion correspondant à des photons initiaux i, finaux j. $i, j = 1, 2$: 1 polarisation circulaire droite, 2 polarisation circulaire gauche.

$$M(i', j) = \sum_{L=0}^{L=s} \alpha_L(i', j) P_L^0(\theta) + \beta_L(i' j) P_L^2(\theta) \quad (5) .$$

La résolution numérique des coefficients complexes α_L et β_L a nécessité l'utilisation d'une machine électronique I.B.M. 704. Nous avons déterminé exactement les 40 premiers termes des développements en polynômes de Legendre donnant $a_1(\theta)$, $a_2(\theta)$, $b_1(\theta)$, $b_2(\theta)$; ce qui a demandé principalement l'intégration de 1000 équations différentielles couplées (5) (équations radiales de Dirac en présence d'un champ coulombien, avec des termes inhomogènes provenant de l'interaction avec le champ électromagnétique des photons) et de 1440 intégrales (5). Nous avons ensuite extrapolé les coefficients α_L et β_L correspondants de $L = 40$ à $L = 60$ ce qui n'a entraîné de modifications que sur $a_1(\theta)$.

Nous avons porté dans la Table I les différentes amplitudes et les résultats donnés par le facteur de forme (6).

BROWN (4) avait déjà remarqué pour des énergies inférieures que le facteur de forme est une assez bonne approximation pour l'amplitude avec changement de polarisation $b_1(\theta) + ib_2(\theta)$. A 5.12 mc² il en est de même entre 0° et 50°. Nous retrouvons également que le facteur de forme est une mauvaise approximation pour $a_1(\theta) + ia_2(\theta)$, amplitude sans changement de polarisation; de plus le facteur de forme ne tient pas compte du changement de signe de $a_1(\theta)$ vers 50°. Ce changement entraîne que les amplitudes Rayleigh et Thomson sont opposées, ce qui diminue la section efficace due à ces deux effets.

Nous avons deux contrôles de nos calculs portant sur l'amplitude de diffusion en avant.

Nous pouvons comparer $a_1(0)/2$ avec un résultat numérique obtenu par LEVINGER (7) à l'aide de relations de dispersion. Il trouve 0.856 ± 0.026 pour le plomb à 5 mc² tandis que notre résultat est 0.865 pour le mercure à 5.12 mc². Comparons la suite des valeurs $a_1(0)/2$ obtenues par Levinger pour le plomb et par la méthode de Brown pour le mercure à des énergies voisines:

LEVINGER (7): 0.978 - 0.913 - 0.870 - 0.851 - 0.856 - 0.860;
pour des énergies des photons de
0.34 mc² - 0.68 mc² - 1.36 mc² - 2.6 mc² - 5 mc² - ∞

BROWN (4): 0.983 - 0.918 - 0.873 - 0.849 - 0.865;
pour des énergies des photons de
0.32 mc² - 0.64 mc² - 1.28 mc² - 2.56 mc² - 5.12 mc².

Ainsi semble se confirmer un résultat donné par LEVINGER (7). L'amplitude réelle de diffusion cohérente en avant (unités r_0) pour un électron lié de la couche K tend vers une constante quand l'énergie du photon croît; cette constante (voisine de

(5) S. BRENNER, G. E. BROWN et J. B. WOODWARD: loc. cit., formules (4'), (5') p. 69; (7') p. 64; (9'), (10'), (11) p. 64.

(6) W. FRANZ: *Zeits. Phys.*, **95**, 652 (1955), **98**, 314 (1956); J. S. LEVINGER: *Phys. Rev.*, **87**, 656 (1952).

(7) J. S. LEVINGER et M. L. RUSGI: *Phys. Rev.*, **103**, 439 (1956).

TABLE I. – *Amplitudes de diffusion (en unités, r_0) pour le mercure à 5.12 mc².*

	$M(1', 1) + M(2', 2)$		$-\{M(1', 2) + M(2', 1)\}$	
θ	$\left.\begin{matrix} a_1(\theta) \\ a_2(\theta) \end{matrix}\right\}$ calculés	facteur de forme	$\left.\begin{matrix} b_1(\theta) \\ b_2(\theta) \end{matrix}\right\}$ calculés	facteur de forme
0	1.7311 — 0.0246	2	— —	—
10	0.7011 — 0.0138	0.9602	0.0081 — 0.0021	0.0073
20	0.1387 — 0.0069	0.2959	0.0086 — 0.0033	0.0092
30	0.0261 — 0.0058	0.1104	0.0063 — 0.0030	0.0079
40	0.0034 — 0.0052	0.0502	0.0046 — 0.0025	0.0066
50	— 0.0011 — 0.0043	0.0261	0.0036 — 0.0021	0.0057
60	— 0.0016 — 0.0034	0.0150	0.0029 — 0.0018	0.0050
70	— 0.0012 — 0.0027	0.0093	0.0024 — 0.0016	0.0046
80	— 0.0008 0.0020	0.0058	0.0020 — 0.0015	0.0041
90	— 0.0005 — 0.0015	0.0038	0.0018 — 0.0014	0.0038
100	— 0.0003 — 0.0011	0.0025	0.0016 — 0.0013	0.0035
110	— 0.0001 — 0.0008	0.0016	0.0015 — 0.0012	0.0033
120	— 0 — 0.0006	0.0011	0.0014 — 0.0012	0.0032
130	— 0 — 0.0004	0.0007	0.0013 — 0.0012	0.0031
140	— 0 — 0.0002	0.0004	0.0012 — 0.0012	0.0030
150	— 0 — 0.0001	0.0002	0.0011 — 0.0011	0.0029
160	— 0 — 0	0.0001	0.0011 — 0.0011	0.0029
170	— 0 — 0	0	0.0011 — 0.0011	0.0029
180	— —	—	0.0011 — 0.0011	0.0029

0.86 pour le plomb) est différente de 1, ce qui serait la valeur trouvée pour un électron libre. Ceci nous entraîne à prévoir que $d\sigma/d\Omega$ ($\theta=0$) pour des énergies plus grandes que 5.12 mc² sera peu différent de notre valeur trouvée à 5.12 mc².

Si nous considérons la partie de $a_2(0)/2$ correspondant au cas où le photon initial est absorbé avant que le photon final soit émis, nous pouvons la relier à la section efficace totale photoélectrique pour un électron de la couche K. Le quotient de

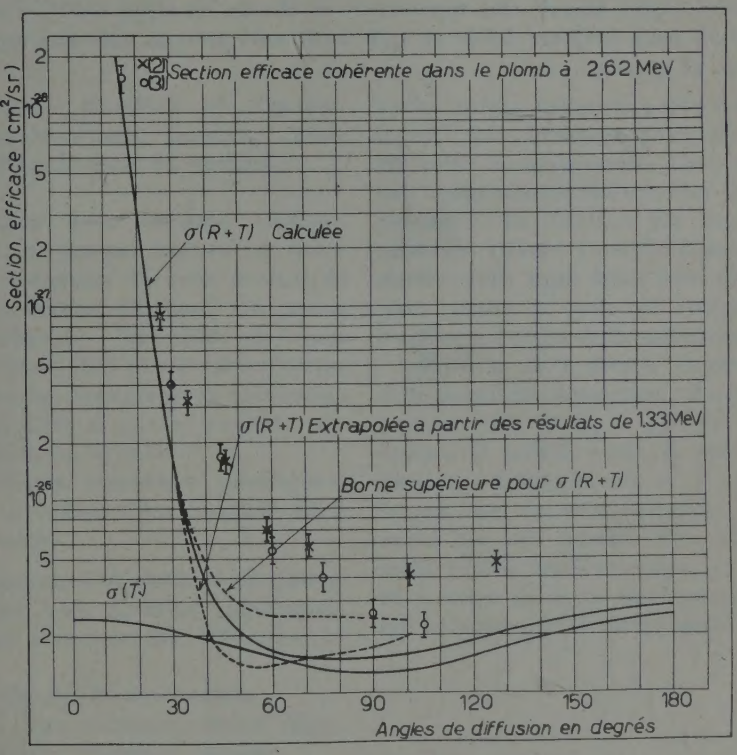

Fig. 1. – $X^{(2)}O^{(3)}$ résultats expérimentaux. —— $\sigma(T)$ section efficace Thomson pour le plomb. —— $\sigma(R+T)$ calculée; $\sigma(R+T)=r_0^2[|a_1'(\theta)+ia_2(\theta)+a_T(\theta)|^2+|b_1'(\theta)+ib_2'(\theta)+b_T(\theta)|^2]$; $a_T(\theta)$ et $b_T(\theta)$ sont les amplitudes Thomson correspondantes; $a_1'(\theta)$, $a_2'(\theta)$, $b_1'(\theta)$, $b_2'(\theta)$, amplitudes Rayleigh des électrons K pour le plomb à 5.12 mc² sont obtenues par extrapolation des résultats donnés pour le mercure dans la table. Cette courbe ne tient pas compte de la résonance nucléaire et de la diffusion par les électrons L [1]. - - - Courbes extrapolées [3] en utilisant les résultats de Brown et Mayers pour le mercure à 2.56 mc²; des extrapolations à partir de cette énergie ont été établies antérieurement à nos calculs [3,11].

notre valeur trouvée à celle donnée par la formule asymptotique de Hall [8,9] est de 1.03 pour le mercure à 5.12 mc². Nous pouvons aussi extrapoler notre résultat pour le plomb 0.48 bar à 5.12 mc² et le comparer au calcul de Hall [9] 0.55 bar à 5.15 mc² et à l'expérience [10] (0.54 ± 0.15) bar à 5.12 mc². Il faut remarquer que

[8] W. HEITLER: *Quantum Theory of Radiation*, 3rd ed., formule (19) p. 210.
[9] H. HALL: *Phys. Rev.*, **45**, 620 (1934); *Rev. Mod. Phys.*, **8**, 358 (1936).
[10] G. D. LATYSHEV: *Rev. Mod. Phys.*, **19**, 132 (1947).
[11] L. GOLDZAHL et J. BANAIGS: *Journ. Phys.*, **19**, 678 (1958).

$a_2(0)$ est environ 1.4% de $a_1(0)$ et que la détermination numérique simultanée des parties réelles et imaginaires des coefficients $\alpha_L(i', j)$ et $\beta_L(i', j)$ donne une meilleure précision pour les termes réels plus grands. Nous n'avons pas tenu compte de l'effet d'écran exercé par les autres électrons, ceci n'entraînant qu'une erreur de 3% à 0.32 mc^2 [4].

Nous voyons sur la figure la prédominance de la contribution Rayleigh jusqu'à 30°, puis de 50° à 180° $\sigma(R+T)$ reste voisin de $\sigma(T)$. En effet, d'une part $a_1(\theta)$ grand aux faibles angles décroît très rapidement et change de signe à 50°, d'autre part, $b_1(\theta)+ib_2(\theta)$ reste toujours faible et $a_1(\theta)$, $a_2(\theta)$ sont presque nuls aux angles intermédiaires et grands.

LIBRI RICEVUTI E RECENSIONI

R. KRONIG – *Textbook of Physics.* Pergamon Press, Londra, 1959, pp. 961. Prezzo 84 scellini.

Si tratta della seconda edizione inglese di un famoso trattato di fisica didattico compilato da nove docenti di diverse università olandesi. La prima edizione olandese è del 1946, ed il successo editoriale oltre che il valore intrinseco ne hanno consigliato la traduzione inglese nel 1954 e questa seconda edizione aggiornata attuale.

Per chi non conoscesse quest'opera, citeremo in ordine i vari capitoli ed il relativo autore

1) R. KRONIG, *Introduzione alla fisica.*
2) P. VAN DER LEEDEN, *Meccanica.*
3) P. VAN DER LEEDEN, *Vibrazioni ed Onde.*
4) G. J. SIZOO, *Elettrodinamica.*
5) P. H. VAN CITTERT, *Ottica fisica.*
6) R. KRONIG, *Struttura atomica.*
7) I. DE BOER, *Teoria atomica del calore.*
8) C. J. GORTER, *Elettricitá atomica.*
9) J. DE BOER, *Termodinamica.*
10) C. J. GORTER, *Strumenti ottici.*
11) A. C. S. VAN HEEL, *Strumenti ottici.*
12) H. C. BURGER, *Fisica medica.*

Segue una serie di note biografiche sui più grandi fisici, ed una raccolta delle costanti naturali, curate entrambe da J. KORRINGA. Il sistema di misure usato è quello di GIORGI razionalizzato. Ogni capitolo è seguito da una serie di problemi con le relative risposte.

Come si vede l'ordine con cui si segnano i diversi capitoli è forse discutibile: prima tutta la parte fenomenologica, poi l'interpretazione atomistica, ed infine le applicazioni. Devo dire che nell'insegnamento della nostra fisica sperimentale, ho trovato più conveniente mostrare appena possibile l'aspetto atomistico delle leggi della fisica macroscopica, anche a costo di rompere così l'ordine e l'unità della esposizione.

Presi a se i diversi capitoli sono delle eccellenti monografie, che potranno tornare utili anche a noi per modernizzare il nostro corso di fisica sperimentale. Naturalmente il materiale è troppo per poterlo insegnare in due anni, per cui questo libro rimane a metà strada tra l'antologia, il trattato ed il corso di fisica sperimentale come noi attualmente lo intendiamo.

G. CARERI

A. F. IOFFE, L. S. STIL'BANS, E. K. IORDANISHVILI and T. S. STAVISKAYA – *Semiconductor Thermoelements and Thermoelectric Cooling.* Infosearch Ltd., Londra, 1957, pp. 184. Prezzo 6 sterline.

Questo libro è stato pubblicato in Russia nel 1956, ed in seguito rivisto e completato per l'edizione inglese dal prof. IOFFE, direttore dell'Istituto per i Semiconduttori della Accademia delle Scienze dell'U.R.S.S., personalità assai nota per la sua opera di ricercatore nella fisica dei solidi e che ha avuto una parte importante nella formazione della scuola russa attuale. Il libro tratta i

fenomeni fisici che hanno permesso in Russia la costruzione di congegni per convertire il calore in elettricità con l'effetto Seebeck o viceversa tramite l'effetto Peltier. Sono riportate delle fotografie piuttosto impressionanti: come quella di una batteria di termoelementi montata su un bruciatore a benzina, che produce l'energia elettrica sufficiente ad azionare una radio, e quella di un normale frigorifero azionato da termoelementi con un consumo di 50 W. Purtroppo non viene indicato il costo di questi congegni.

Il libro è diviso in due parti; la prima tratta la fisica dei semiconduttori che si prestano alla costruzione di convertitori termoelettrici efficienti, e la seconda la tecnologia di questi elementi. Si ha l'impressione di una opera che cerca di sistemare in modo ancora elementare e schematico un campo nuovo ed importante, specialmente per le sue applicazioni.

G. Careri

J. V. Jelley – *Čerenkov Radiation and its Applications*. Pergamon Press, London, 1958, pp. x+304. Prezzo 65 scellini.

Nel campo dei rivelatori di particelle elementari, quelli che utilizzano la radiazione di Čerenkov sono divenuti negli ultimi anni di sempre più largo impiego. Questo volume di Jelley giunge quindi assai opportuno e utile, specialmente per quei fisici sperimentali che intendono impiegare questo tipo di rivelatori.

Nei primi tre capitoli di questo libro vengono dettagliatamente illustrate le attuali conoscenze teoriche e sperimentali sulla natura della radiazione di Čerenkow. Nei successivi capitoli vengono poi presentate le varie applicazioni di questo tipo di radiazione con particolare riguardo ai rivelatori di particelle elementari dei quali vengono discussi in dettaglio i criteri di progettazione a seconda delle diverse possibilità di impiego. Non manca infine una breve ma aggiornata rassegna dei vari problemi la cui indagine sperimentale può essere facilitata dall'utilizzazione della radiazione di Čerenkov. La trattazione è ovunque densa di grafici, tabelle e informazioni che ne rendono assai utile non solo la lettura ma anche la semplice consultazione. Una dettagliata bibliografia completa questo libro di notevole interesse e utilità.

A. Alberigi

G. H. Wannier – *Elements of Solid State Theory*. Cambridge University Press, 1959, pp. 270. Prezzo 31 scellini.

Si tratta di un libretto particolarmente raccomandabile a chi voglia interessarsi di fisica dei solidi avendo già una buona preparazione di fisica teorica. Perciò questo libro non sostituisce il Kittel od altri libri più ampi ed anche più facili, ma rimarrà sempre come una ottima guida per chi voglia entrare in questo campo. Vi sono presentati in sintesi, ma non affrettatamente, solo alcuni argomenti di fisica dei solidi, con riferimenti così bene aggiornati da permettere al lettore un successivo sviluppo. Di particolare rilievo ci è sembrato il capitolo sulla legge di Ohm, in termini della dinamica elettronica con forze di attrito.

G. Careri